Magnetic domain studies in gadolinium

Fathia M. Saad

MAGNETIC DOMAIN STUDIES IN GADOLINIUM

BY

FATHIA M. SAAD, M.Sc.

A thesis submitted to the University of Durham for the Degree of Doctor of Philosophy.

February, 1977.

Department of Physics,
Science Laboratories,
Durham University,
Durham City.

TO MY SONS

ABSTRACT

The domain structure of gadolinium has been observed and investigated. The wet colloid technique has been used for observation at temperatures down to 240K. The dry colloid technique has been used for the observation of the patterns formed at low temperatures below 240K. Various specimens of gadolinium of different sizes have been used to investigate the changes of domain structure with crystal shape and size. All the crystals except one were obtained from the Centre for Materials Science University of Birmingham, and were of high purity.

At 273K patterns on planes containing the c-axis showed parallel 180° walls, with the development of reverse domains. The effect of the crystal thickness on the size of the domain structure has been observed on the basal plane at 273K. This is discussed and found to agree with an expression due to Kaczer. The effect on the patterns of reducing the temperature has been studied.

The domain structure has been observed at 77K, where the easy directions lie on a cone around the c-axis, on all prepared surfaces. The zero field basal plane pattern shows complex wall structure, while planes containing the c-axis show a system of domains parallel to the c-axis. The effect of applying a magnetic field on the domain structure has been observed and is discussed. The lengths of daggers of reverse magnetization and the widths of their bases were found to be in direct

proportion at both temperatures 77K and 216K.

An interpretation of the pattern is given for the two range of temperature, where the c-axis is easy and for the easy cone region. A model is given for the patterns observed at 77K and its limitations discussed. Possible types of walls and magnetization direction are also discussed on the basis of the known magnetic properties of the material.

ACKNOWLEDGEMENTS

I would like to take this opportunity of expressing my appreciation to Dr. W.D.Corner for his encouragement, guidance and help throughout the whole of this work which was carried out under his supervision. My gratitude also goes to Professor A.W.Wolfendale the Head of the Department for accepting me in his department. I would also like to thank Dr. B.K.Tanner sincerely for useful discussion and suggestions.

My wishes to thank all the Physics Department workshop staff and solid state group technicians for technical assistance. Thanks are due also to Mrs. McGough for typing this thesis.

I should also like to record my thanks to the Government of Egypt for a Grant which has enabled me to carry out the work.

CONTENTS

CHAPTER ONE

INTRODUCTION

1.1 Ferromagnetism

A number of different types of material are called ferromagnetic and they are characterized by the following magnetic properties. The most notable property of a ferromagnetic material is that it can be permanently magnetized. Also its magnetization may be saturated by the application of relatively small magnetic fields. At the same time it is possible for the magnetization of the same specimen to be zero in zero applied field.

The fields required to magnetize the ferromagnetic substances are considerably weaker than those required for the paramagnetics. The explanation for this is that the atomic magnetic moments in a ferromagnetic substance interact strongly with one another and tend to align themselves parallel to each other giving a spontaneous magnetization.

The existence of this magnetization in ferromagnetic substances arises from a combination of the presence of a magnetic moment associated either with the spins of unpaired electrons in an unfilled band or with the total angular momentum of an incomplete shell, and the presence of an interaction field aligning the moments parallel to each other. The interaction is such as to correspond to an applied field of the order of magnitude of 10^7 Oe.

On increasing the temperature the alignment is disturbed and the net magnetization decreases until above a critical temperature, the Curie point T_c, the thermal effect is greater than the interaction and the system is disordered. Above T_c the material is paramagnetic.

The presence of a strong inner magnetic field was first postulated by P. Weiss (1907). He called it the Molecular Field and developed a theory of the temperature dependence of the saturation magnetization. In the Weiss theory it is assumed that the molecular field is proportional to the average magnetization. It is more reasonable to assume that a local molecular field is produced by the surrounding moments and that the moments tend to lie parallel to their neighbours rather than to the average magnetization. By using the supposition that the dipole orientation is governed by Boltzmann's Distribution Law, he showed that the magnetic susceptibility becomes infinite at a specific temperature and that below this temperature the saturation magnetization is a definite function of temperature, (figure 1.1). The variation is plotted in reduced units, the form of the curve depends slightly on the J value of the carriers of magnetic moment, but a broadly similar dependence is found for all ferromagnetic materials.

Another attack on the same problem is by the Bloch theory of spin waves (1930). This takes into account an

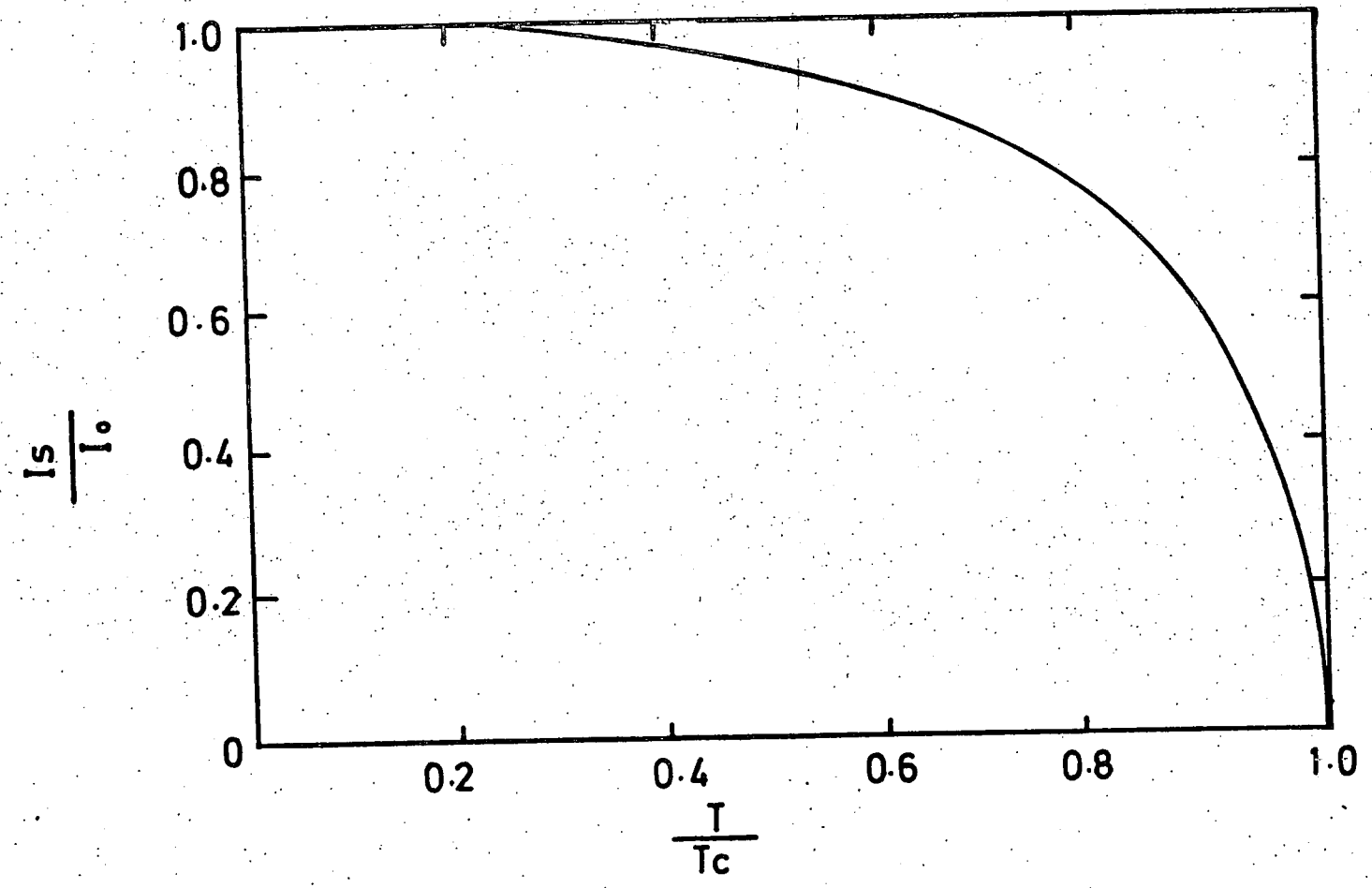

FIG.(1.1)

interaction due to quantum mechanical exchange producing magnetic ordering. The problem is treated by considering the correct expression for this exchange interaction instead of the molecular field, and assuming that the spin reversals are freely propagated with various wave-lengths through the crystal in which there is an almost perfect alignment of spins. It was not possible to decide on the basis of the experimental data which theory was the correct one. Some of the predictions of the molecular field theory were in disagreement with experiment.

Magnetism has its origins in the spin and orbital magnetic moments in an unfilled electron shell. Actually the three ferromagnetic elements Fe, Co, and Ni have an unfilled 3d shell, while the rare earth metals, most of which exhibit ferromagnetism at low temperatures, have an unfilled 4f shell.

The interpretation of the nature of the molecular field was first presented by Heisenberg in (1928) with 3d elements in mind. According to his theory, the force which makes the spins line up is an exchange force of quantum mechanical nature. The potential energy between two atoms having spins S_i and S_j is given by

$$W_{ij} = -2 J \underline{S}_i \cdot \underline{S}_j$$

where J is the exchange integral. If J is positive, the energy is least when S_i is parallel to S_j; if J is negative, the stable state is that in which S_i is

antiparallel to S_j. Two electrons with the same kind of spin cannot approach one another closely, since the Pauli principle permits an orbit to be occupied by one plus and one minus spin electron. The mean distance between two electrons should be different for parallel spins from that for antiparallel spins, and the coulomb energy must be different in the two electrons. Then the exchange energy is the electrostatic energy as it depends on the spin orientation through the Pauli principle.

It has been shown experimentally, from work on the gyromagnetic ratio in 3d metals, that about 90% of the saturation magnetization is due to electron spins, the rest being due to orbital motion. Van Vleck (1945) has shown that the spins responsible for ferromagnetism are not those of valence electrons but of unfilled electron shells. Thus for a substance to be ferromagnetic, it must have an incomplete shell.

There have been two points of view in interpreting the moment configurations in the ferromagnetic substances. One is based on a localized model in which the electrons responsible for ferromagnetism are regarded as localized at their respective atoms. Rare earth metals are good examples to be explained by the localized model, since the electrons responsible for the magnetism of these metals are in the deep inner 4f shells of individual

atoms. Then the atomic moments interact with one another by an exchange interaction through conduction electrons.

The other point of view uses a collective electron model in which the electrons responsible for ferromagnetism are thought of as wandering through the crystal lattice.

The 3d electrons in the transition metals are the most exposed except for the 4s conduction electrons. The 3d shells of individual atoms are thought to be nearly touching or overlapping with those of neighbouring atoms. Then the energy levels of 3d electrons are perturbed and spread to form an energy band. The band theory of ferromagnetism was first proposed by Stoner in (1936) and independently by Slater in (1936).The theory of collective electron ferromagnetism is in better agreement with experiment. Detailed comparison with experimental measurements of magnetic and thermal properties and with neutron diffraction studies show that for Ni the collective electron theory of ferromagnetism is favoured, whereas for Fe and Gd the Heisenberg theory is better.

An intermediate polar model of crystals was also proposed in the works of Slater (1930), Shubin and Vonsovskii (1934). The latter also suggested an s-d exchange model for ferromagnetic metals, and this idea was developed further in the work of Vonsovskii (1946).

1.2 Magnetization Curve

We now return to the problem, that whilst theory predicts that a ferromagnetic material will be spontaneously magnetized to saturation below the Curie temperature, in fact it can appear to have zero magnetization in the absence of an applied field. Further experimental facts must also be considered. When a magnetic field is applied to a

ferromagnetic specimen, the magnetization may vary from zero to the saturation value. The variation of (M_H) the component of the magnetization along the direction of the applied field, with the applied field depends on the material, but frequently the curves have the general appearance of the well-known hysteresis-loop as shown in figure (1 - 2).

It is assumed that the material is initially in a demagnetized state. When a field is applied, the magnetization M_S increases at first slowly and then very rapidly, until the saturation value I_s is reached. After saturation the rise in magnetization is very gradual and nearly linear. This part of the plot is known as the magnetization curve, and the magnetization process up to saturation is called technical magnetization. By performing the sequence of operations of reducing the field to zero, increasing it in the reverse direction, decreasing it to zero, and then increasing it to the original value, a hysteresis curve or loop is obtained. This curve is symmetric about the origin and is usually closely reproducible after a few cycles of magnetization. Since the magnetization lags the applied field, work is performed on taking the material through a cycle. This work is given by the line integral

$$W = \oint H \, dM_S$$

taken along the hysteresis loop and is obviously equal to the area enclosed by the loop. On the hysteresis loop the value of the magnetization for H = 0 is called the residual magnetization or remanence M_r. The value of

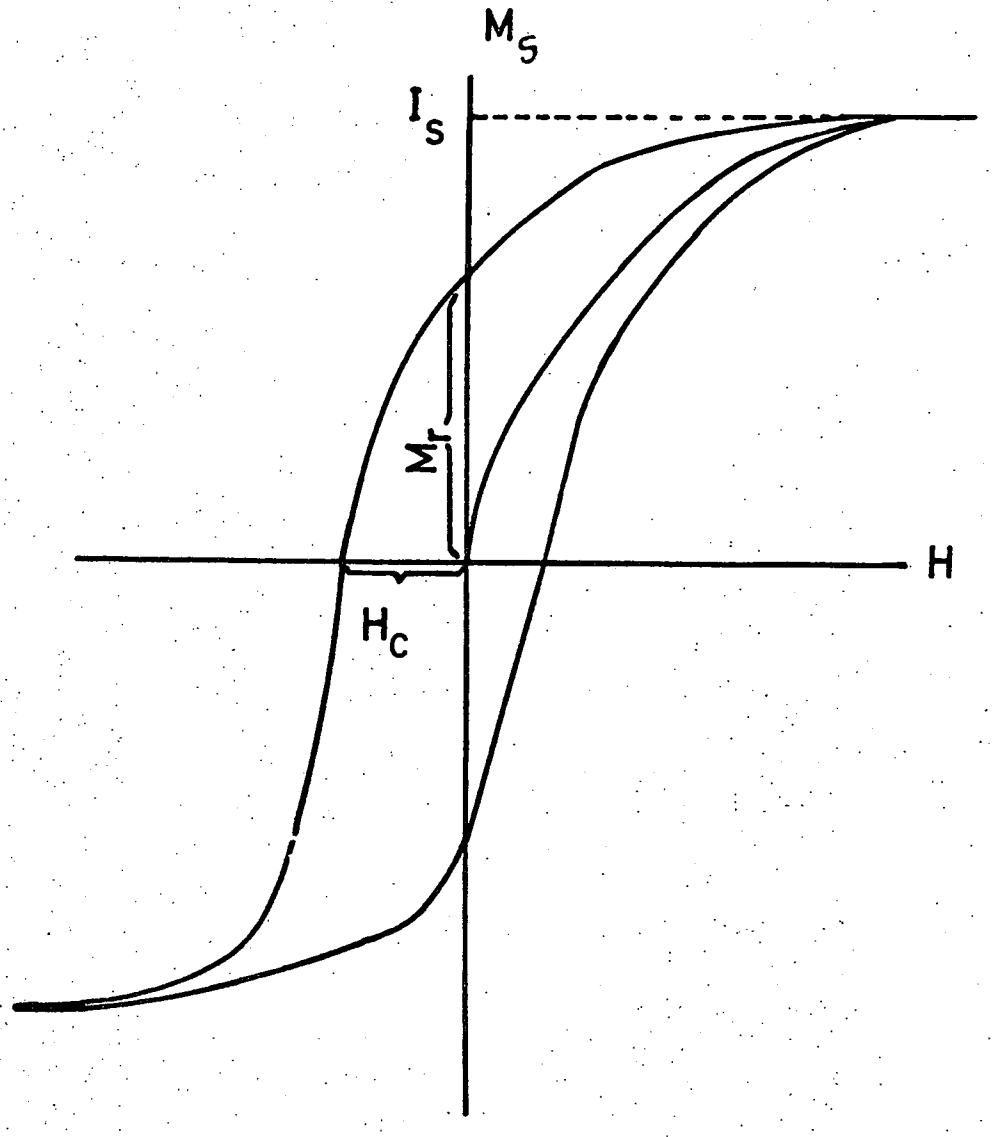

FIG. (1.2)

the field for which $M_H = 0$ is called the coercive force H_c.

The saturation field of a ferromagnet is determined by its magnetic anisotropy (Honda and Kaya 1926). Even in the most perfect ferromagnetic single crystals, saturation is reached in very weak field only for magnetization along a small number of principal symmetry axes of the crystal, known as the axes of easy magnetization. Saturation in other directions requires higher (and sometimes very much higher) fields.

Thus the energy to magnetize is dependent on direction in the crystal and this is known as magnetocrystalline anisotropy energy.

The spontaneous magnetization is independent, at least in the first approximation, of an external magnetic field and is equal in magnitude to the observed magnetic saturation I_s. This magnetization, as we said before, depends considerably on the temperature and it disappears completely above the Curie point.

Changes of magnetization around the hysteresis loop are accompanied by changes in the dimensions of the sample. These changes are described by the general term magnetostriction.

1.3 Domain assumption

Domains were originally postulated by Weiss (1907) in order to account for the observed magnetization and hysteresis curves. In spite of the presence of spontaneous magnetization, a block of ferromagnetic substance, polycrystalline or single crystal, in practice, is usually not spontaneously magnetized

but frequently observed to exist in a state of zero overall magnetization. But in the ferromagnetic state it is possible for the induction and magnetization to be both different from zero ($B = 4\pi I \neq 0$) at zero field, provided that div $B = o$ and div $I = 0$. For the latter to be true in this case, vectors I ($\neq 0$) must be so distributed over the sample volume that no magnetic charges capable of producing a field can appear. This fact led Weiss to suggest further that such crystals are always magnetically saturated throughout small regions, and that when a crystal is in the demagnetized state, the directions of magnetization of these regions, or domains, are randomly oriented so that the resultant magnetization of the crystal along any direction is zero. According to this, the effect of an applied field in such a crystal is, then, not to induce the magnetization at the atomic level, but to align the magnetization vector of the domains.

Now the magnetization of the ferromagnetic specimen changes when a magnetic field is present. The process of magnetization generally consistsof a rearrangement of the structures, as was suggested by R.Becker (1930). It is believed that two main processes may occur. In one the volume of the domains favorably oriented with respect to the applied field grows at the expense of those unfavorably oriented; that is, there is a displacement of the domain walls. In the other process the magnetization of the domain rotates toward the field direction. The two processes may occur either reversibly or irreversibly

depending on the strength of the applied field and on the nature of the specimen.

Landau and Lifshitz (1935) showed that the sub-division of a specimen into domains could result in a considerable reduction in the magnetostatic energy from that of the saturated condition. The separate energy contributions are summed to give the total free energy of the specimen and the sizes of the domains are assumed to be those which lead to a minimum value of the free energy.

Now however, let us see from a simple qualitative argument why domains may be expected to occur. The stable equilibrium state of the specimen's magnetization is sought by minimizing an expression for the free energy. The total free energy of a ferromagnetic specimen in an applied magnetic field may be written as the sum of several free energy terms.

$$F_T = F_H + F_D + F_K + F_\sigma + F_e + F_o \quad .$$

F_H is the energy of the specimen's magnetization in the applied field H.

F_D is the self-energy of the magnetization in its own field

F_K is the crystalline anisotropy energy

F_σ is the magneto-strictive energy

F_e is the exchange free energy

F_o represents any other contributions to the free energy that may be present.

Suppose that the applied field is zero, that there are no stresses, internal or external, and that the specimen has

no imperfections. Then $F_H = F_\sigma = F_o = 0$. Further, suppose that the long edge of the crystal lies along an easy direction of magnetization. Then F_K will be a minimum if all the atomic magnetic moments lie parallel to this long edge. Such a single-domain configuration is shown in figure (1.3a). In addition, the exchange energy F_e will also be a minimum. However, the remaining term, F_D, the demagnetization energy, will not have its minimum value. This large magnetostatic energy will be decreased by introducing a domain structure, although it may be accomplished only at the expense of increasing the other energy terms. For example for the configuration of two antiparallel domains, figure (1.3b), the demagnetizating energy is reduced by a factor of about one half. There is now a boundary or transition region between the two domains in which the atomic moments are not parallel to each other and moreover do not lie along easy directions. Hence F_e and F_K are increased. The boundary region is often called a domain wall. Certain domain arrangements make the demagnetization energy zero figure (1.3c). The triangular or prismatic domains, called closure domains, are most likely to occur if their magnetization lies along an easy direction. Such may be the case for cubic crystals. For uniaxial crystals the magnetization in closure domains would have to lie along a hard direction. However, in both cases, the formation of closure domains involves a certain amount of magneto-elastic energy due to magnetostriction. The demagnatization energy term is primarily responsible for the occurrence

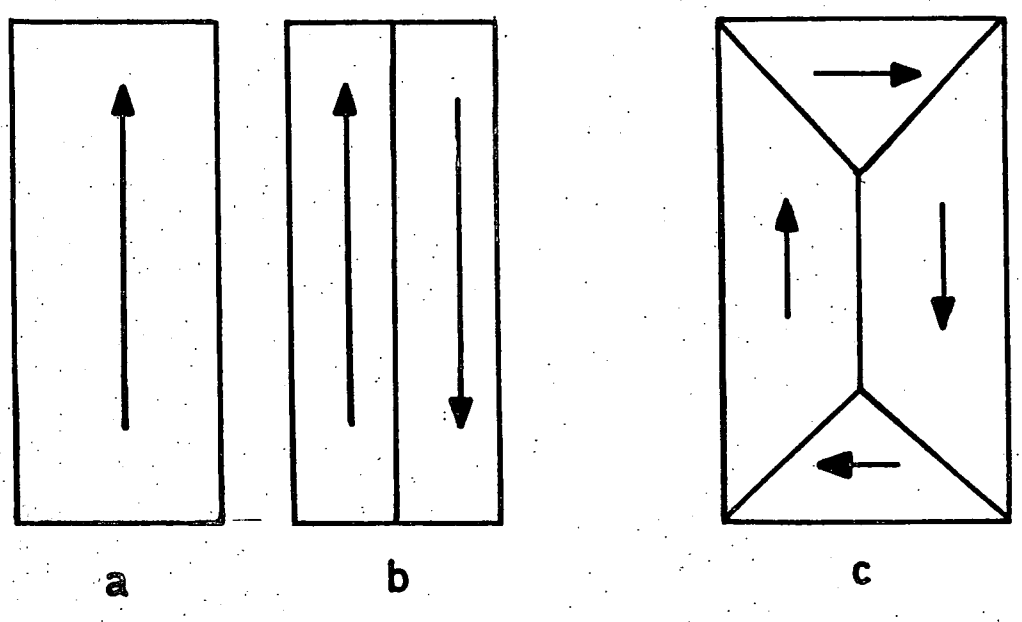

FIG. (1·3)

of domains.

It is known that the origin of the demagnetization energy is the classical dipole-dipole interaction, which is very much smaller than the exchange interaction between adjacent atoms. Hence it may at first appear anomalous that a domain structure rather than a state of uniform magnetization is usually favoured. The reason is that the dipole-dipole forces are long range, dropping off slowly with distance, whereas the exchange forces are short range being limited almost to the nearest neighbours. Thus, overall, a domain structure is to be expected, whereas over short distances, that is within one domain, the magnetization is expected to be uniform.

Therefore, as a general rule, a domain configuration is expected that will reduce, if not remove, the uncompensated poles on the surface of the specimen.

1.4 Domain discovery

The first experimental verification of the presence of ferromagnetic domains was indirect and was made by Barkhausen in (1919). His experiment consists in amplifying the voltage induced in the secondary coil which is wound around the ferromagnetic being magnetized, and observing the noise induced by the changing magnetization. The presence of characteristic noise proved that the magnetization process consists of many small discontinuous flux changes. At the time these were thought to be due to the reversal of magnetization of each small magnetic domain.

The direct observation of ferromagnetic domain structure

was attempted by Bitter in (1931), and independently by Von Hamos and Thiessen in (1932). They applied a drop of a ferromagnetic colloidal suspension, containing fine ferromagnetic particles, to a polished surface of a ferromagnetic specimen and observed the image of the domain. Bitter did not conclude that the image he got was true domain structure, but explained as being due to the inhomogeneity in the substance. He was unable to provide a relationship between the pattern observed on the surface and the internal structure, because the mechanical polishing produced strain on the surface, and the magnetic particles used were not sufficiently responsive to the stray fields at the surface. This technique became known as the Bitter technique.

Several improvements were made by Elmore (1938) in the techniques of the preparation of the ferromagnetic colloidal suspension and also in polishing. By electro-polishing a cobalt specimen he eliminated the strain previously resulting from mechanical polishing and thus observed the true domain structure of cobalt.

In (1934) Kaya made detailed domain patterns of iron and nickel single crystals and showed the maze pattern due to the grinding or the polishing of the crystal surface.

Well defined domain structures were observed by Williams, Bozorth and Shockley in (1949) on Si-Fe crystals. They used the Bitter Technique on the electro-polished surface. These investigators showed that the domain structures are in good agreement with the theoretical predictions of Landau and Lifshitz and also of Néel.

CHAPTER TWO

ENERGY OF MAGNETIC DOMAINS

The purpose of this chapter is to derive expressions for the different types of energy which enter specially into the theory of magnetic domain structures. The most important energies are: exchange energy; anisotropy energy; magnetoelastic energy and magnetostatic energy. In principle the inclusion of all of these terms is necessary and the omission of any one will cause modifications in the nature of the structure of the domains. Thus it is necessary in an examination of domain structure to provide expressions for the energy due to various effects. The expression for the total energy per unit volume of the system is

$$E' = E - \underline{H}.\underline{I} \qquad 2.1$$

H.I represents the potential energy of a magnetized body in the magnetic field, and E is the internal energy which includes magnetocrystalline anisotropy, magnetostriction and energy due to free pole. It is then assumed that, at equilibrium, the sum of the energy terms is a minimum with respect to some parameter ξ, i.e. $dE'/d\xi = 0$. It has not yet been found possible to predict a particular domain structure by calculation from the constants of the material and the dimensions of the specimen, but if reasonable models are proposed they may be analysed to find which has the least energy and is therefore most likely to occur in practice. Structures found by direct observation may be analysed in order to test the validity of the mathematical approach or, to measure one of the parameters where the others are known. The domain structure should correspond to the general solution

for the lowest energy state.

2.1 Exchange Energy

The existence of spontaneous magnetization may be considered as an atomic phenomenon. The ferromagnetism arises by combining two facts, first the presence of magnetic moment associated with an incomplete electron shell and secondly the existence of an interaction field between moments of neighbouring atoms. This interaction, aligning the moments parallel to each other, may be expressed in terms of a magnetic field H_W (the Weiss Field), proportional to the intensity of magnetization I,

$$H_W = N_W I \qquad 2.2$$

So the potential energy corresponding is

$$W' = -\mu H_W \qquad 2.3$$

where μ is the spin moment.

Heisenberg's treatment showed that a positive exchange interaction could have effects similar to those of the Weiss molecular field, when electrons with parallel alignment of their spins have a lower energy than those with antiparallel alignment.

In quantum mechanical terms the parallelism of the spin vector arises from the application of the Pauli exclusion principle, which for a particular electron configuration forbids the antiparallel arrangement of spins. It is usual to employ a model in which, at each lattice point of the crystal, there is situated an atom with total spin quantum number S where S is equal to the number of unpaired electron spins in the atom and is an integer.

The relevant result of the quantum-mechanical treatment

of the many-electron problem may be summarized by saying that there is a term of electro-static origin, which does not enter on classical dynamics, in the energy of interaction between neighbouring atoms, and this term tends to orient the electron moment of the atoms either parallel or anti-parallel to each other according to the algebraic sign of a certain energy integral J, known as the exchange integral.

The effective coupling between spins caused by the exchange effect is equivalent to a potential energy of the form:

$$V_{ij} = -2 J_{ij} \underline{S}_i \cdot \underline{S}_j \qquad 2.4$$

where J_{ij} is the exchange integral connecting atom i and j, and S_i in the spin angular momentum of atom i and S_j that of atom j, measured in multiples of $h/2\pi$. This equation was shown to be a fundamental result of quantum theory by Van Vleck (1945). It turns out that the spin matrices are approximately related to classical vectors, and in this case equation 2.4 may be rewritten as

$$W_{ex} = -\sum 2 J_{ij} S^2 \cos \phi_{ij} \qquad 2.5$$

Where ϕ_{ij} is the angle between the directions of the spin angular momentum vectors, understood in a classical sense; W_{ex} is now the exchange energy.

In domain theory one is often interested in the exchange energy only for configurations in which neighbouring spins make small angles with each other. If it is supposed that only interactions between nearest neighbours are important for the exchange energy and that these interaction are equal, then

$$W_{ex} = -2 J S^2 \sum \cos \phi_{ij} \qquad 2.6$$

$\phi_{ij} \ll 1$ since neighbouring spins make a small angle with each other, then

$$\Delta W_{ex} \simeq J S^2 \sum \phi_{ij}^2 \qquad 2.7$$

and the exchange energy between each pair of spins is

$$\Delta W_{ij} \simeq J S^2 \phi^2 \qquad 2.8$$

We may express equation (2.7) in another form as follows: Suppose that the direction cosines of the spin at lattice point r_j are $\alpha_j^x, \alpha_j^y, \alpha_j^z$. Now the direction cosines $\alpha_i^x, \alpha_i^y, \alpha_i^z$ at the neighbouring lattice point r_i may be expended in a Taylor series

$$\alpha_i^x = \alpha_j^x + \left(x_{ij}(\partial/\partial x_{ij}) + y_{ij}(\partial/\partial y_{ij}) + z_{ij}(\partial/\partial z_{ij}) \right) \alpha_j^x + \tfrac{1}{2} \left(x_{ij}^2 (\partial^2/\partial x_{ij}^2 + y_{ij}^2 (\partial^2/\partial y_{ij}^2 + z_{ij}^2 (\partial^2/\partial z_{ij}^2) \right) \alpha_j^x + - - - - -$$

On summing over nearest neighbours on a body centered cubic lattice with lattice constant a then:

$$\Delta W_{ex} \simeq -2 JS^2 a^2 \sum_j (\alpha_j \cdot \nabla^2 \alpha_j)$$

and by using $\nabla^2(\alpha.\alpha) = 0$,

the equation turns to

$$\Delta W_{ex} = 2 JS^2 a^2 \sum \left[(\nabla \alpha_j^x)^2 + (\nabla \alpha_j^y)^2 + (\nabla \alpha_j^z)^2 \right] \qquad 2.9$$

The energy density of exchange interaction becomes

$$f_{ex} = A \left[(\nabla \alpha_1)^2 + (\nabla \alpha_2)^2 + (\nabla \alpha_3)^2 \right] \qquad 2.10$$

where $A = 2JS^2/a$ is the exchange constant. This form was proposed by Landau and Lifshitz (1935).

The relation between A and the Weiss coefficient N_w is found by equating the exchange energy for the saturated state to the internal energy due to the Weiss field $\frac{1}{2} N_w I_s^2$.

The exchange constant A cannot be measured directly

but may be simply estimated by two different methods. Firstly it may be obtained from the measured value of the Curie temperature where the thermal energy becomes roughly equal to the exchange energy $k T_c$. The second method is by the experimental determination of the constant C in the law, (Bloch 1930).

$$I = I_s (1 - C T^{3/2}) \qquad 2.11$$

for the variation of the saturation magnetization at low temperatures. Here the value of C is related directly to the exchange constant. These estimates are useful since the value of the exchange constant enters into the theoretical calculation for both the width and energy of the domain walls. Seavey and Tannenwald (1959) describe a method which gives the exchange constant A directly from spin wave resonance measurements.

2.2 Anisotropy Energy

Weiss suggested that in a single crystal in a demagnetized state the domain magnetizations could lie in all directions. This would mean that the magnetization curves whatever the direction of the applied field relative to the axes of the crystal, would be the same. Experimental magnetization curves show that much smaller applied fields are required to induce a given level of magnetization in some directions than in others.

The anisotropy energy or the magnetocrystalline anisotropy energy of a ferromagnetic crystal is a function of magnetization direction so that the magnetization tends to

be directed along certain definite crystallographic axes, which accordingly, are called directions of easy magnetization. The directions along which it is most difficult to magnetize the crystal are called hard directions. It is found to require the expenditure of a certain and often considerable amount of energy to magnetize a crystal to saturation in a hard direction. A lower amount of energy is required to saturate the crystal along a direction of easy magnetization. The excess energy needed in the hard direction is the anisotropy energy.

Magnetic anisotropy can be produced by applying mechanical stress to the material. This is called magnetostrictive anisotropy. Magnetic anisotropy can also be controlled by heat treating the material in a magnetic field, and this is called induced magnetic anisotropy.

The simplest form of crystal anisotropy is uniaxial anisotropy. A crystal which exhibits this form of anisotropy has an easy direction parallel to some axis of the crystal. As the internal magnetization rotates away from this axis, the anisotropy energy increases with increase of θ, the angle between the axis and the internal magnetization. It takes its maximum value at $\theta = 90^{\circ}$, and then decreases to its original value at $\theta = 180^{\circ}$. It is natural to expect that the anisotropy energy density f_k may be represented by a series expansion of the powers of $\sin^2\theta$.

$$f_k = \sum_n K_n \sin^{2n}\theta \qquad 2.12$$

Odd powers of $\sin\theta$ have not been included since, by symmetry, the $-\theta$ direction is equivalent magnetically and crystallographically to the $+\theta$ direction. The K_n are

constants independent of θ . It is actually found that a very good representation of the experimental observations is usually given by the first three terms.

$$f_k = K_1 \sin^2\theta + K_2 \sin^4\theta + K_3 \sin^6\theta \qquad 2.13$$

So the anisotropy energy in effect determines the direction of magnetization relative to the crystal axes. This contribution to the total energy will be a minimum when the various domain magnetizations all lie along easy directions.

The quantities K_1,K_2 and K_3 are formal coefficients which may be used to describe accurately the anisotropic properties of ferromagnetic materials. They give no indication of the physical origin of the anisotropy.

The exchange energy by itself does not lead to any anisotropy regardless of the actual geometrical anisotropy of the crystal structure. The magnetic moment dipole-dipole interaction between electronic moments leads to only very small values of the anisotropy constants, much smaller than are observed. The anisotropy constants are found to be very sensitive to temperature changes, and it is not unusual for the sign of the constants to change between low and high temperatures. The origin of the anisotropy energy was believed (Sommerfeld and Bethe 1933, Brooks 1940, Van Vleck 1947) to be the result of the combined effects of the mutual coupling between electron spins and the interaction between the spins and the crystal lattice. The physical origin of the interaction between the electron spins and the crystal lattice was believed to be the result of spin-orbit coupling, but the theory is complex even when simplifications are made.

One result which might be anticipated from any theory of anisotropy is that the magnetic anisotropy energy would tend to be large for crystals whose lattice of magnetic ions is of low symmetry, while the anisotropy energy would be expected on the whole to be low for crystal lattices of high symmetry. This rule is suggested by the fact that the anisotropy energy enters only in higher order approximations in a cubic crystal than in an uniaxial crystal. The data observed support this hypothesis, the anisotropy energies of the cubic crystals F_e and N_i are of the order of 10^5 erg/cc, while for the hexagonal crystal Co it is of the order of 10^7 erg /cc.

Iron is a cubic crystal, and the magnetization curves show that the cube edges [100], [010] and [001] are the directions of easy magnetization, while the body diagonals [111] and equivalent axes are hard directions. In attempting to represent the anisotropy energy of iron in an arbitrary direction with direction cosines $\alpha_1, \alpha_2, \alpha_3$ referred to the cube edges it is found that there are restrictions imposed by cubic symmetry. For example, the expression for the anisotropy energy must contain even powers of each α_i ; and it must be invarient under interchanges of the α_i ; among themselves

$$f_k = k_1 (\alpha_1^2 \alpha_2^2 + \alpha_2^2 \alpha_3^2 + \alpha_3^2 \alpha_1^2) + k_2 \alpha_1^2 \alpha_2^2 \alpha_3^2 \qquad 2.14$$

There are various means for measuring the magnetic anisotropy. The torque magnetometer is an apparatus commonly used for this purpose. The principle of this apparatus is to suspend the specimen by a fine elastic string between the

pole pieces of a rotatable electromagnet. When a strong magnetic field is applied to the specimen, the internal magnetization is forced to line up with the field, and the specimen disk tends to rotate to make an easy direction approach the direction of magnetization. If the magnet is rotated, the torque can be measured as a function of crystallographic direction of magnetization, and the various anisotropy constants may be obtained by analysis of these torque curves.

An alternative method for determining the anisotropy is to measure the magnetization curves for a single crystal in a number of principal crystal directions. Then the constants may be calculated from the area enclosed by the magnetization curve, the ordinate axis, and the line I = Is; that is $W = \int H \, d \, I$. This however, involves an accurate knowledge of the demagnetizing factor.

The magnetic anisotropy can also be measured by means of ferromagnetic resonance. The resonance frequency depends on the external magnetic field, which exerts a torque on the precessing spin system. Since a magnetic anisotropy also causes a torque on a spin system if it points in other than easy directions, the resonance frequency is expected to be dependent on the magnetic anisotropy.

2.3 Magneto-striction energy

The crystal anisotropy energy and the exchange energy are found to depend on the interatomic spacing of the lattice. Consequently any change in the interatomic spacing gives rise

to a further energy contribution to the free energy of a magnetic crystal.

It is found experimentally that there is a change in the dimension of a crystal when its magnetization is varied, and this may cause internal stress if the crystal is not allowed to expand freely. This phenomena is called magnetostriction and observed by Joule (1842). The magnetoelastic energy is that part of the energy of the crystal which arises from the interaction between the magnetization and the mechanical strain of the lattice, which implies that the application of a stress will change the magnetization. The magnetoelastic energy is defined to be zero for unstrained lattice.

In consideration of the energy terms relevant to domain structure problems, the inverse effect is perhaps more important. This means that, if a magnetic crystal is strained by an external force, this additional strain will alter the direction of the intrinsic magnetization. The preferred direction of domain magnetization may be controlled not only by the magnetocrystallin anisostropy but also by the presence of strained regions within the material.

The most extensive investigations have been of the linear magnetostriction λ, defined as the change of length Δ l per unit length, that is $\Delta l/l$, measured in a particular direction. There will be no linear magnetostriction if the anisotropy energy is independent of the state of strain of the crystal. The smallness of the change of length requires the use of sensitive measuring equipment. A variety of techniques have been employed but the resistive strain gauge method has been much used despite problems of bonding and gauge factor

determination.

When the specimen is magnetized to saturation, the magnetostriction approaches a limiting value, λ_s, called the saturation magnetostriction. The magnetostriction is positive or negative, depending on whether there is an expansion or contraction.

Magnetostriction phenomena are treated by macroscopic phenomenogical theory developed by Akulov (1931) and Becker (1930). This theory has been criticized by Brown (1953), though it has provided an interpretation of most of the experimental results. In cubic crystals the assumption was made that the crystal strain depends on the direction of the spontaneous magnetization with respect to the crystal axes, that is on the direction cosines α_1, α_2 and α_3. Hence the change of the length in a certain direction whose direction cosines are β_1, β_2 and β_3 is given by (Becker & Döring (1939).

$$\frac{\Delta l}{l} = \frac{3}{2}\lambda_{[100]}\left(\alpha_1^2\beta_1^2 + \alpha_2^2\beta_2^2 + \alpha_3^2\beta_3^2 - \frac{1}{3}\right) + 3\lambda_{[111]}(\alpha_1\alpha_2\beta_1\beta_2 + \alpha_2\alpha_3\beta_2\beta_3 + \alpha_3\alpha_1\beta_3\beta_1) \qquad 2.15$$

λ_{100} and λ_{111} are the saturation values of the longitudinal magnetostriction constants in [100] and [111] directions respectively. If the magnetostriction is assumed to be isotropic, that is, $\lambda_{[100]} = \lambda_{[111]} = \lambda_s$ then

$$\frac{\Delta l}{l} = \frac{3}{2}\lambda_s\left(\cos^2\theta - \frac{1}{3}\right) \qquad 2.16$$

where $\theta = \cos^{-1}\sum \alpha_i \beta_i$ is the angle between the spontaneous magnetization and the direction in which $\Delta l/l$ is measured. This equation finds some use for polycrystalline specimens.

When a tension σ is applied, an expression for the

contribution to the free energy F_σ per unit volume arises. This free energy will be equal to the work done when the magnetostriction change of length occurs in the presence of the tension.

$$F_\sigma = -\sigma \int d\left(\frac{\Delta l}{l}\right) = -\frac{3}{2}\lambda_s \sigma \cos^2\theta \qquad 2.17$$

For $\lambda_s > o$ the mimimum in F_σ occurs when the direction of magnetization is parallel to the stress axis, while for $\lambda_s < o$ the minimum occurs when M is perpendicular.

2.4 Magnetostatic Energy

The first correct conception of magnetic domain structure was obtained by Landau and Lifshitz (1935), and by Néel (1944), because they took the magnetostatic energy into consideration in the calculation of the size of magnetic domains. Williams, Bozorth and Shockley in (1949) verified this calculation experimentally.

The effect of an applied magnetic field H on a domain magnetized to an intensity I_s in a direction at an angle θ with the field direction is to create on it a couple equal to $I_s H \sin\theta$ per unit volume, tending to rotate the magnetization into the field direction. The potential energy of a magnetic specimen is given by

$$E_H = -\underline{H}.\underline{I} = -HI_s \cos\theta \qquad 2.18$$

The energy according to this expression will be zero at $\theta = \frac{1}{2}\pi$ and as it is sometimes convenient to have the energy equal zero at $\theta = 0$, so the energy expression is written as

$$E_H = HI_s\ (1 - \cos\theta) \qquad 2.19$$

Because of the demagnetizing field of the specimen, this field H will usually differ considerably from the externally applied field H_a.

At the same time, even when no external field is applied a magnetized body of finite size has a certain magnetostatic energy. This is because of the interaction between the magnetic moment of the body and its own field, which may be calculated as the work required to assemble all the dipoles, equal to $E = -\frac{1}{2} I_s H_D$. The factor $\frac{1}{2}$ is introduced since each dipole would otherwise be counted twice. The demagnetizing field H_D is proportional to I and is equal $H_D = -NI$, N is the demagnetizing factor; I and H_D are in opposite directions. So the self energy due to the interaction between the free pole and its own demagnetizing field is $-\frac{1}{2} H_D I = \frac{1}{2} NI^2$.

Demagnetizing factors can be derived for an ellipsoid because its magnetization is uniform. The major demagnetizing factors N_a, N_b and N_c in the direction of the major semi-axes a, b and c were calculated by Stoner (1945) and Osborne (1945). It was found that $N_a + N_b + N_c = 4\pi$ and the effective value of N in a direction with cosines α_1, α_2 and α_3 equal

$$N = N_a \alpha_1^2 + N_b \alpha_2^2 + N_c \alpha_3^2$$

For a cylinder of elliptical cross-section magnetized along the b or c axes ($a = \infty$), $N_b = 4\pi c/(b+c)$ and $N_c = 4\pi b/(b+c)$

For an prolate spheroid with $a/b = q$ and magnetized parallel to a, $N_a = 4\pi (\ln 2q - 1)/q^2 + \pi(3\ln 2q - 5)/q^4 + - - -$

For sheets and rectangular prisms, Rhodes and Rowlands (1954) have derived expressions for the energy, assuming that the two are uniformly magnetized. The value of N for a sphere uniformly magnetized in any direction is $\frac{4}{3}\pi$, this value is

also for N of a cube . For rods of square cross-section magnetized along the axis a

$N_a = 3(3q - 1)/q^2$ where q ratio of length/side and $q \rangle 2$.

The magneto-static energy is reduced as a result of dividing the crystal into magnetic domains. The subdivision is assumed to continue until the energy required for the formation of further domain boundary is greater than the reduction in the magnetostatic energy.

Near the surface under the influence of the demagnetizing field, the magnetization vector may be slightly rotated away from the easy direction. The component of magnetization along the easy direction remains unchanged, while the component of magnetization produced perpendicular to the easy direction is proportional to the demagnetizing field. For a small rotation of the magnetization the material has a constant effective permeability perpendicular to the easy direction.

$$\mu^* = 1 + \frac{2\pi I_s}{K} \qquad 2.20$$

This value was calculated by Williams, Bozorth and Shockley (1949).

CHAPTER THREE

DOMAIN STRUCTURES

3.1 Domains in uniaxial material

The domain structure in a ferromagnetic metal is not uniquely determined by the material. The domain structure which appears at the surface of the magnetic crystal is dependent on a number of factors. It is a function of the dimensions of the sample, and the orientation of the surface of the crystal relative to the crystal structure. Also the structure depends on the shape and state of stress of the crystal. The intrinsic magnetic properties of the material such as spontaneous magnetization and the anisotropy are of great importance for the formation of the domain structure. A most important factor is the demagnetizing field arising at the boundary of the specimen. The structure will also depend on external factors such as the direction and the magnitude of any applied magnetic field. The domain boundaries lie in planes corresponding to the minimum in the total boundary energy.

Uniaxial materials have a relatively low degree of crystal symmetry. According to this a high value of magnetocrystalline anisotropy referred to the one easy axis is found for most such materials. In a uniaxial crystal, boundary walls generally contain the easy axis which is the c-axis for many of these materials. Then the domain structure consists basically of arrays of 180^{o} domains within the body of the material. Differences in structure existing between different material are found in the closure domain formed at basal plane surface. Possible domain

configuration have been suggested by many workers for uniaxial crystals as following.

Landau and Lifshitz (1935) suggested a structure which is found when a large demagnetizing field arise due to any free pole on the basal plane, figure (3.1.1). They proposed the formation of closure structures which have a magneto-crystalline anisotropy energy proportional to their volume. This structure gives a total energy per unit area.

$$E = \frac{\gamma L}{D} + \frac{KD}{2} \qquad (3.1)$$

where D is the width of the domain and L is the length of the crystal as in figure (3.1.1). γ is the wall energy per unit area, and K is the anisotropy constant.

Kittel (1949) gave three models in material where the magneto-crystalline energy is very large compared with the magnetic energy. The structure will be of simple parallel 180° walls with no closure domains because these secondary structure will have a large magnetocrystalline anisotropy energy. Figure (3.1.2) shows a structure which has become known as the Kittel model. Kittel calculated the magneto-static energy W_M for a surface of this structure consisting of equally spaced parallel strips of magnetic poles of alternating sign.

$$W_M = 0.8525\, I_s^2\, D \quad \text{per unit area,} \qquad (3.2)$$

where D is the width of each strip.

The total energy of unit surface area is given by

$$W = 2W_M + W_\gamma \qquad (3.3)$$

where W_γ is the total wall energy. So

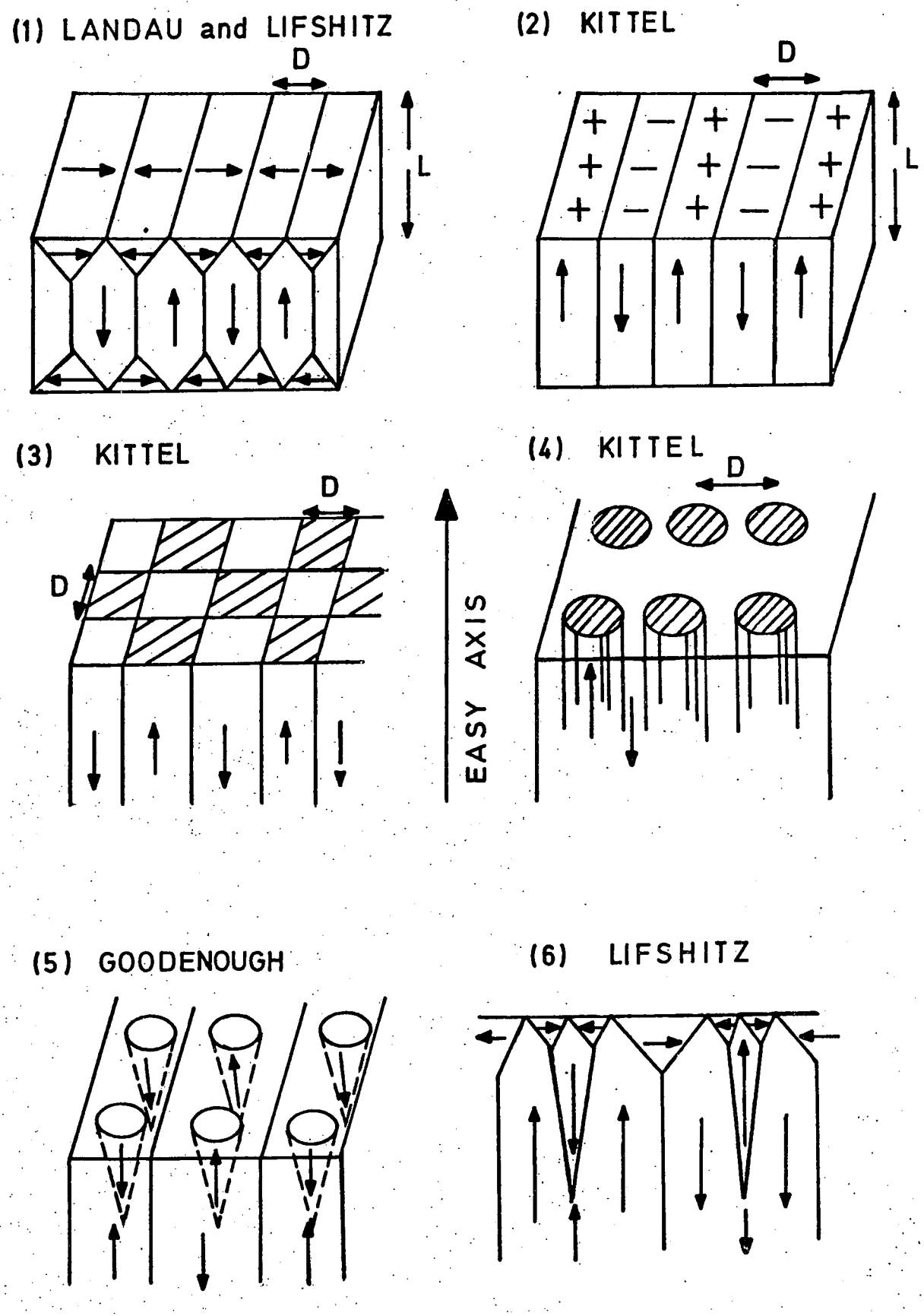
(1) LANDAU and LIFSHITZ
D
L
(2) KITTEL
D
L
(3) KITTEL
D
D
EASY AXIS
(4) KITTEL
D
(5) GOODENOUGH
(6) LIFSHITZ

FIG. (3·1)

$$W = 1.705\ I_s^2\ D + \gamma \frac{L}{D} \qquad (3.4)$$

γ is the wall energy per unit area.

Another model of Kittel is shown in figure (3.1.3) which shows a structure known as chequer board pattern. This structure has a total energy equal

$$W = 0.53\ I_s^2\ D + \gamma \frac{L}{D} \qquad (3.5)$$

Figure (3.1.4) shows a circular pattern which is the third model of Kittel and it has a total energy equal to

$$W = 0.374\ I_s^2\ D + \gamma \frac{L}{D} \qquad (3.6)$$

It is clear that in each case the magneto-static energy is proportional to the domain width. Minimization of these expressions yields values for equilibrium wall spacing and total energy.

Goodenough (1956) proposed the structure shown in figure (3.1.5) in which the magneto-static energy decreases without the formation of closure structures and without greatly increasing the wall energy.

Lifshitz (1944) proposed a structure of more complicated nature for a uniaxial crystal shown in figure (3.1.6). He showed that this structure has lower energy than that of closure structure.

It is reasonable to expect that the structures mentioned before are those which might be found in any homogeneous uniaxial crystal.

The domain wall spacing D on an axial plane varies with the crystal thickness L in the axial direction. For a sheet of thickness below a critical value (12μm for Co) Kittel (1949) showed that D was proportional to

$\sqrt{L}$. For specimens with L more than 12 microns, patterns of undulatory wall are found on basal planes. The undulations increase in both spacing and amplitude as the specimen thickness is increased. With further increase in thickness, the undulatory patterns become gradually more complex, Goodenough (1956).

When high fields are applied along the axial direction differences are also found in the behaviour of the patterns. Patterns of alternate strips or rings become covered by colloid particles according to the emergent flux is parallel or antiparallel to the applied field. This structure has been interpreted simply as one of reverse spikes. Some of the basal plane pattern may remain unchanged throughout a complete magnetization cycle, indicating no normal component of the magnetization. Very high fields are needed to transfer this structure into free pole structure. This structure is thought to be of the Liftshitz type, with small closure domains. The differences in structure may be attributed to the magnitudes of the saturation magnetization and magnetocrystalline anisotropy in particular materials. Unixial material with high I_s & low K exhibits Lifshitz closure structures while material with low I_s & high K possesses reverse spikes.

3.2 Domain wall.

The demagnetizing fields may be responsible for the subdivision of the crystal into domains. There will be a transition layer between adjacent domains which are magnetized in different directions. In

this layer the spins change from one direction to the other. This transition layer is called the magnetic domain wall. A common type of wall is often referred to as the Bloch wall, for its properties were first considered by Bloch (1932). In this wall the magnetization rotates about the wall normal as one proceeds through the wall. Bloch showed that in transition metals the change in moment direction does not occur in one discontinuous jump between one atomic plane and the next, but takes place over a distance of many atomic planes in a gradual manner. So the domain wall has a finite thickness. The reason for the gradual nature of the moment change is that the exchange energy is lower when the change is distributed over many moments, than in abrupt change over a couple of atoms. The origin of the force which lines up the spins is the exchange interaction of quantum mechanical nature. The expression for the exchange energy is given by the equation

$$W_{ex} = -2 J_K S^2 \cos \phi \qquad (3.7)$$

for an angle ϕ between spins. If ϕ is a small angle this may be approximated by

$$W_{ex} = -2 J_K S^2 \left(1 - \frac{\phi^2}{2}\right) \qquad (3.8)$$

where J_K is the exchange integral and S the total spin quantum number of each atom. Thus the change in the exchange energy due to a deviation of ϕ from the parallel position is given by

$$\Delta W_{ex} = J_K S^2 \phi^2 \qquad (3.9)$$

The magnetization in a domain is generally parallel to the easy direction, but in the domain wall this is not

so. In the domain wall, the atomic moments are not parallel to one another, hence there is an increase in the exchange energy W_{ex}. If the change is spread out over a number of lattice planes some of the moments in the wall are not lying along the easy direction of the magnetization. Therefore the anisotropy energy W_K is increased. This means that there will be an anisotropy energy associated with the wall, which will be the greater the thicker the wall. Thus anisotropy energy acts to limit wall thickness and the exchange energy favours the thick wall. The equilibrium width will occur when the decrease in exchange energy is balanced by the increase in anisotropy energy. i.e. the width of the wall is considered to be that which make the sum of the exchange energy and the anisotropy energy a minimum, assuming the magneto-static energy is zero. Moreover if there are any uncompensated poles in the wall, that is, if there is a divergence of the magnetization I, there will also be an increase in the magnetostatic energy. It has usually been assumed that the normal component of the magnetization remains constant throughout the wall.

On this basis we may make an approximate calculation of wall energy and thickness. Assuming that only exchange and anisotropy energy contribute, the wall energy density may be written as following

$$W_w = W_{ex} + W_{anis} \qquad (3.10)$$

If the material has uniaxial symmetry the anisotropy energy W_{anis} is then (taking only the lowest order term)

$$W_{anis} = KV \sin^2\theta \qquad (3.11)$$

where θ is the angle between the moment direction and the reference axis which is taken to be the easy axis of the magnetization. If the total change in spin direction is Φ_o, and takes place in N equal steps, then $\phi = \Phi_o/N$ and

$$\Delta W_{ex} = J_K S^2 \left(\frac{\Phi_o}{N}\right)^2 \qquad (3.12)$$

so that the total change in the exchange energy over N + 1 spins is given by

$$W_{ex} = J_K S^2 \left(\frac{\Phi_o^2}{N}\right) \qquad (3.13)$$

If the total angle $\Phi_o = \pi$ (180^o domain walls), the exchange energy will be

$$W_{ex} = J_K S^2 \left(\frac{\pi}{N}\right)^2 \qquad (3.14)$$

Assuming 180^o domains and a lattice constant a, then

$$W_{ex} = \frac{\pi^2 J_K S^2}{N a^2} \quad \text{per unit area} \qquad (3.15)$$

The anisotropy energy per unit volume is approximately given by the first anisotropy constant K_1. The volume of the wall per unit area will be Na.

Thus,

$$W_{anis} = Na\, K_1 \quad \text{per unit area.} \qquad (3.16)$$

Then the wall energy per unit area will be as following:

$$W_w = \frac{\pi^2 J_K S^2}{N a^2} + Na\, K_1 \,. \qquad (3.17)$$

The wall thickness, which is determined by N, will be such as to minimize the total energy per unit area. Differentiating equation (3.17) with respect to N and equating it to zero we have

$$N = \left(\frac{\pi^2 J_k S^2}{K a^3}\right)^{\frac{1}{2}} \qquad (3.18)$$

The wall thickness $\delta_0 = Na = \left[\frac{\pi^2 J_k S^2}{Ka}\right]^{\frac{1}{2}}$ (3.19)

Substituting for N in equation (3.17), the wall energy per unit area W_w equals:

$$W_w = 2\left(\frac{\pi^2 S^2 K J_k}{a}\right)^{\frac{1}{2}} \qquad (3.20)$$

If the exchange constant A is defined as equal to $\frac{2J_k S^2}{a}$ then

the wall width $\delta_0 = \sqrt{\frac{\pi^2 A}{2K}}$ (3.21)

and the energy per unit area $\gamma = \sqrt{2\pi^2 AK}$ (3.22)

As a simple approximation we may write $2JS^2 = k T_c$

Thus for gadolinium with

$T_c = 292K$, $a = 3.6 \times 10^{-8}$cm and

(at temperature 270K) $K_1 = 0.17 \times 10^6 \text{erg} / \text{cm}^3$

we obtain $\delta_0 = 0.572 \times 10^{-5}\text{cm} = 572A^\circ$

and $\gamma = 1.94 \text{ erg} / \text{cm}^2$.

To consider how the wall width δ_0 and the wall energy per unit area for gadolinium depend on temperature graphs of δ_0 and γ have been calculated using appropriate values for the effective anisotropy K.

The anisotropy constants K_1, K_2, K_3 for gadolinium are functions of the temperature as will be explained further, figure (4.8). The appropriate combination to use for K depends on the temperature range.

For the range of temperature $T > 240K$, the c-axis is the easy direction, so in a 180° wall the moments will rotate through the energy maximum at $\theta = 90^\circ$. The effective anisotropy is given by the difference

between F_k at $\theta = 0^\circ$ and at $\theta = 90^\circ$. As shown in figure (3.2a) it is given by $\Delta F_k = K_1 + K_2 + K_3$ since

$$F_k \text{ (0001)} = K_o$$

$$F_k \text{ (basal)} = K_o + K_1 + K_2 + K_3$$

so $$\Delta F_k = K_1 + K_2 + K_3$$

For the range of temperature $T < 240K$, where the easy direction lies on a cone, the rotation may be over a lower barrier. The anisotropy constant given by the difference of F_k between $\theta = \theta_o$ and $\theta = 90^\circ$ as in figure (3.2b). The differences given by

$$\Delta F_k = F_k(\theta_o) - F_k(90^\circ)$$

$$= -F_k(\theta_o) - (K_1 + K_2 + K_3)$$

The values of θ_o, the cone angle, for different temperature determined from the graph, figure (4.10), of the variation of the easy cone angle with temperature for Gd, also the resultant values for $K_1 + K_2 + K_3$ are measured from figure (4.8), for the variation of the anisotropy constants with temperature for Gd. Graphs of calculated σ and γ values are shown in figure (3.3) and (3.4). These graphs will be discussed later in the next chapter.

3.2.1 Closure domain

It is possible to design a domain arrangement for a rectangular surface, which will have no magnetic poles, Figure (3.1.1). Such an arrangement was first treated by Landau and Lifshitz (1935) for unixial crystals. Close to the surface, the shape of domain becomes such as to diminish the effect of demagnetization energy. Surface closure regions domain have the form of trigonal

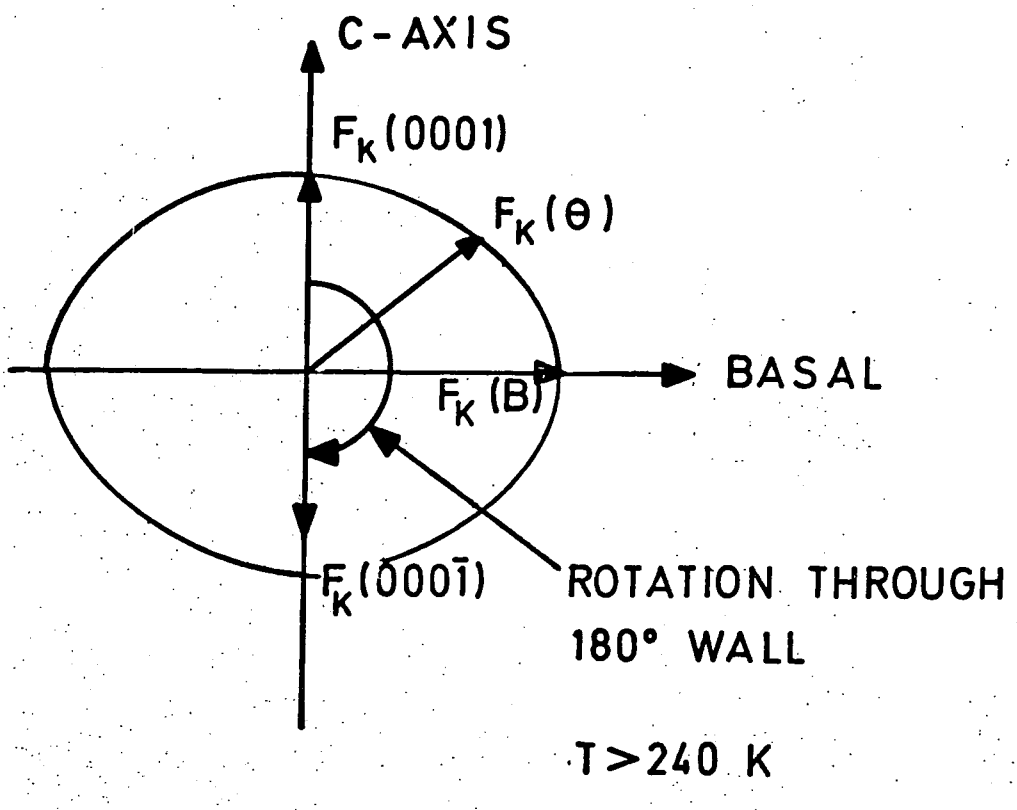

FIG. (3.2 a)

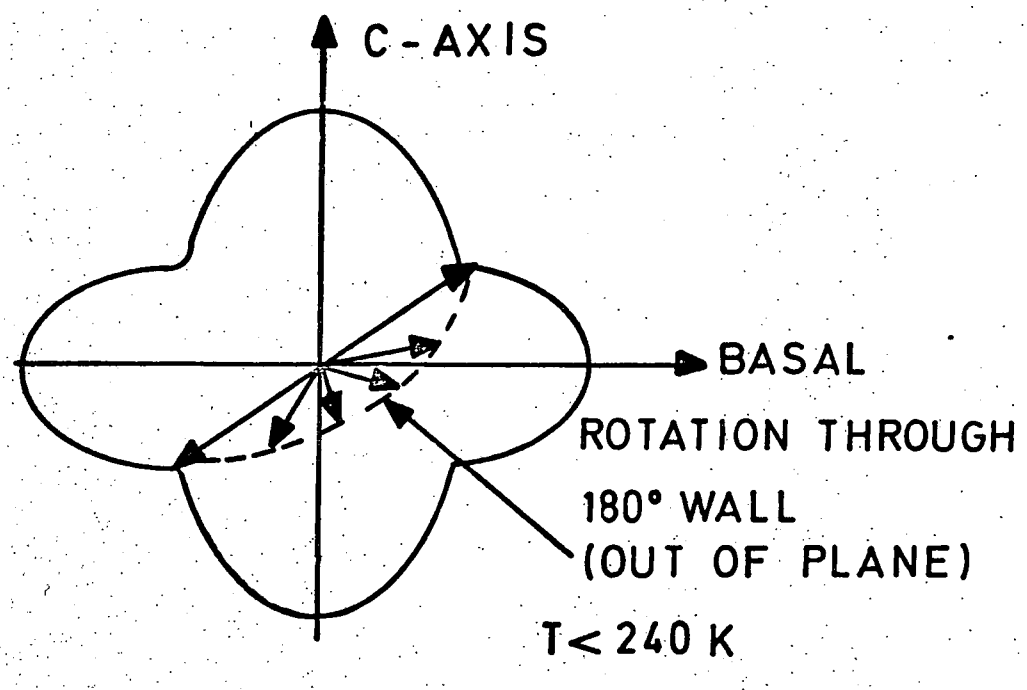

FIG. (3.2 b)

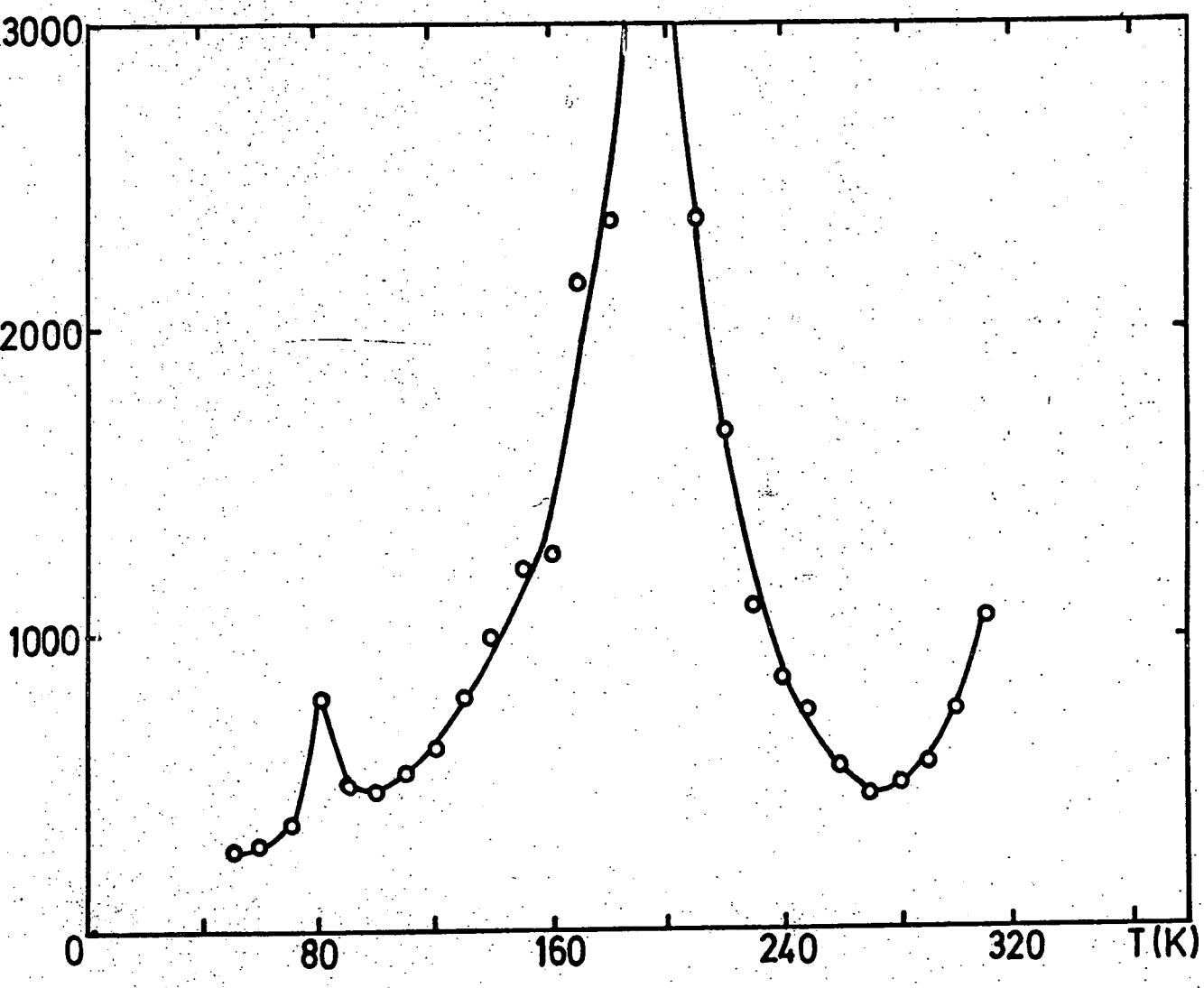

FIG. (3.3)

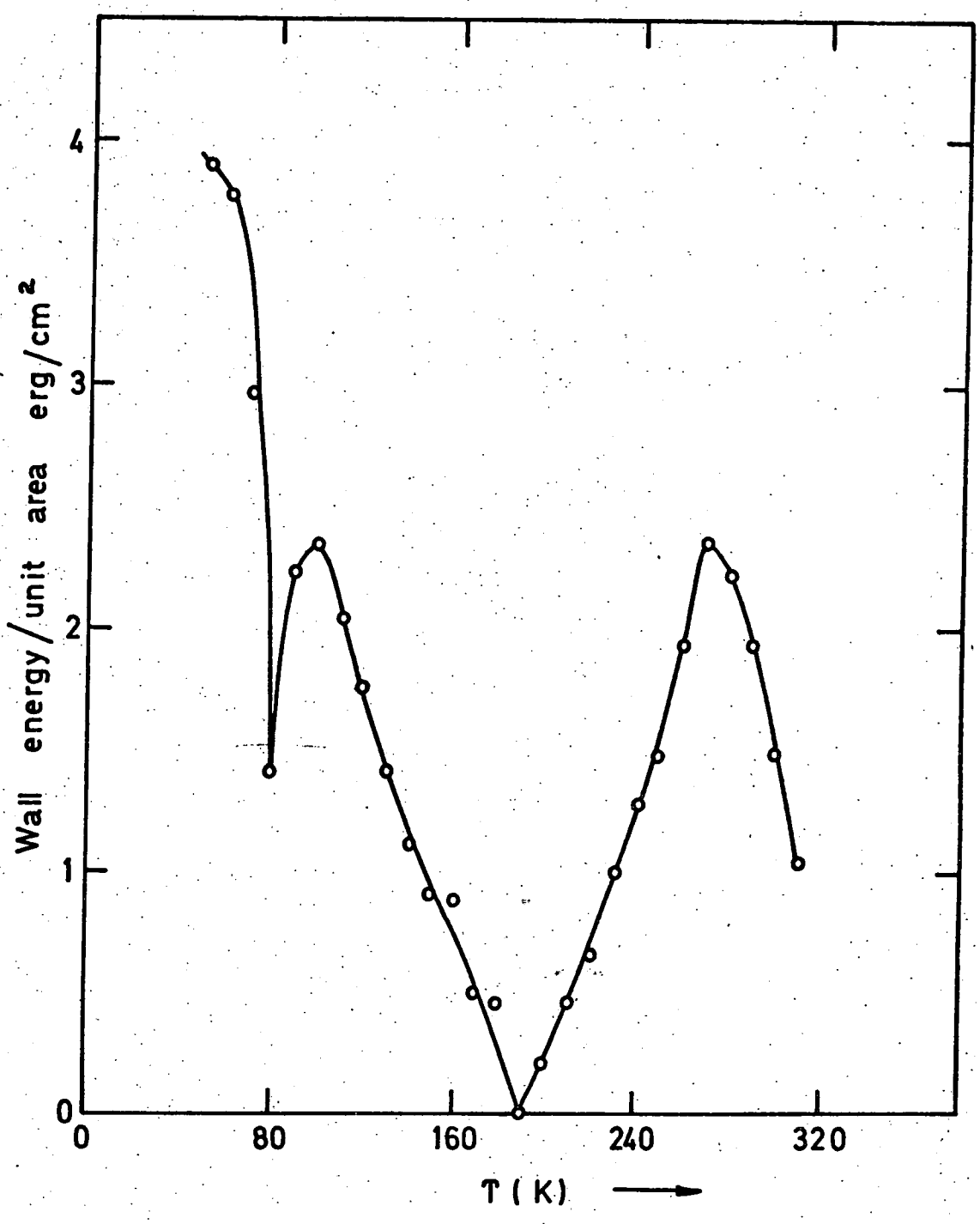

FIG. (3-4)

prisms. In closure domains the magnetization is perpendicular to the easiest axis but parallel to the sample surface.

The flux circuit is completed within the crystal by means of the closure domain on the two parallel surfaces of the crystal. Closure domains transfer the magnetization flux from the forward directed domains to the backward directed domain without formation of any poles. The poles are absent as a result of the continuity across the prism sides of the normal component of magnetization.

The magnetic energy is zero, but the anisotropy energy is not zero in uniaxial crystals. The volume within the domain of closure is magnetized in a hard direction, its anisotropy energy is K per unit volume, where K is the anisotropy constant. The volume of the closure domain is D/2 so that:

$$W_{anis} = KD/_2 \qquad 3.23$$

Using this it is possible to carry out energy minimization calculations to yield domain wall spacings.

If the sample surface is flat but inclined to the easiest axis, the shapes of the wall closure regions will be more complicated. The theory of magnetic domains in uniaxial materials have been considerably developed and applied to a variety of materials. It will not be pursued further at this stage, but attention will now be diverted to the material of particular interest in the present investigations.

3.3 Previous work

Because of the complicated types of ordering found in the heavy rare earths it was anticipated that they would provide domain structures that provided new challenges in interpretation. With its Curie temperature of 292K and its moderate anisotropy gadolinium would appear to be an interesting element on which to begin investigation.

The development of this work has been strongly dependent on the availability of suitable materials. The first observation of domains in gadolinium was by Birss and Wallis (1963) who observed needle-shaped domains at a temperature of about 268K running parallel to the c-axis, using the Bitter technique with a modified colloid. Then in (1964) Bates and Spivey observed a domain structure in gadolinium using the same technique, but with a different suspending medium for the colloid. They found domains of a variety of structure in a range of temperatures between 180K and 210K using polycrystalline samples. Also in (1965) the German workers Schaffer and Helmut observed a domain structure in thin film of Gd using the magneto optic Kerr effect technique, in temperature range from 95K to 273K. The domain structure did not appear to change but was much clearer at 95K.

Then in (1969) Al-Bassam and Corner observed domains in a gadolinium single crystal between 273K and 210K temperature by using the wet colloid technique with solution secondary butyl alcohol. They showed clearly the closure structure near the edge of the plane containing the c-axis. They also saw a domain of

complex type on the basal plane.

Recently an investigation of magnetic domains in Gd foil using the transmission electron microscope technique has been made by Chapman et al (1976). They saw clear Néel walls at temperature 160K.

Previous attempts to extend the temperature range downward have been unsuccessful and it is clearly of interest to know what structures are present when the easy cone is well developed.

3.4 Methods of the observation of magnetic domains

Many methods of direct observation of magnetic domains have been used including the colloid technique, magneto-optic methods; Lorentz microscopy, scanning electron microscopy, and X-ray topography. These methods will now be briefly discussed.

3.4.1 The Colloid Technique

This has been the only important method for direct observation until comparatively recently, leading to a fundamental understanding of many domain structures. The methods of studying ferromagnetic domain by means of tiny magnetic particles free to move over the surface of a sample was first suggested by Bitter (1931). The magnetic powders used earlier consisted of magnetic particles in a true colloidal suspension, this gave smaller particle aggregates of about 1μm in diameter (Elmore1934). Improved colloidal suspensions have been developed with finer particles down to about 0.1μm (Garood 1962). These particles were allowed to set in Celacol whilst on the specimen, subsequently peeled off, and examined with the much higher resolution of the electron microscope (Craik and Griffiths 1958).

The mechanism of the effect is that the tiny magnets (crystallites of magnetite Fe_3O_4) are acted upon by the stray magnetic fields produced at the surface of a ferromagnetic material by the free poles formed on the surface, when a domain boundary terminates there. That is to say that the crystallites collect most densely in the regions of an inhomogeneous magnetic field where the field intensity is highest.

A recent development of this technique is the evaporation of a ferromagnetic material in an atmosphere of inert gas onto the ferromagnetic specimen, where the particles are deposited preferentially in regions of maximum field. The particle size of the deposit depends primarily on the helium pressure. The patterns so formed may be examined optically or may be replicated and examined in the electron microscope (Hutchinson et al 1965).

Quite fine domain boundaries can be studied using the colloid technique, but the technique has certain limitations. Due to the inertia of the magnetic particles it permits only static or quasistatic observations to be made. The gradients of the magnetic fields above the specimen are dependent on the magnetocrystalline anisotropy of the specimen material. The lower the anisotropy the wider is the domain wall producing the field, and consequently the smaller is the field gradient above the wall. Since the forces on the colloid particles are proportional to field gradient a less well defined pattern results from a broad wall.

The first requirement for successful use of the powder pattern method is that the surface under examination should

be strain-free and microscopically smooth. If these conditions are fullfilled the magnetic fields at the surface will be due to the domains and not influenced by the presence of foreign matter or strains.

For wet colloid the temperature range over which observation can be made is somewhat restricted. So the nature of the suspension liquid becomes of dominant importance. By using methylcyclohexane stabilised by sodium oleate Bates and Spivey (1964) were able to reach 180K. Birss and Wallis (1963) had used sodium di-(ethylhexyl) suphasucinate at 268K.

At high temperature liquid evaporation is the difficulty, but by using oil Andrä (1956) has made observations up to 380°C. Clearly colloid technique results are extremely important for high resolution studies.

3.4.2 Magneto Optical Techniques

The interaction of plane polarized light with a magnetized medium can lead to changes in the polarization of the light which can be usefully used to reveal domain structure. Provided that there is a component of the magnetization along the direction of propagation of the light, the plane of polarization will be rotated by an amount dependent on the direction of magnetization.

The plane polarized light is reflected from the surface of a magnetic material as elliptically polarized with the major axis of the ellipse rotated. This change is known as Kerr effect. It can be classified into several types according to the relative orientations of the magnetization, the plane of incidence and the electric-vector of the incident light. The polar Kerr Effect was first used by

Williams, Foster and Woods (1951), to reveal domains in a single crystal of cobalt. The meridional Kerr effect was first employed by Fowler and Fryer (1952) to observe domain structure in a crystal of silicon-iron. The longitudinal Kerr effect shows a maximum for a particular angle of incidence.

A similar effect known as the Faraday effect, when plane polarized light is transmitted through magnetic medium with a component parallel to the direction of propagation, can lead to a rotation of the plane of polarization. This may be used to study domain structures in transparent materials.

The magneto-optic effects are particularly useful for material with low anisotropy and very wide domain boundaries. Domains whose direction of magnetization differ rotate the plane of polarization by different amounts. When the difference in direction of magnetization of adjacent domains is small, the light contrast is so small that observation is difficult. The small rotation by the magneto-optic interaction of the polarized beam, and the need to work with nearly crossed prisms, leads to an image of the domain structure very low in intensity. Techniques have been developed for enhancement of contrast by coating the surface with a dielectric layer.

3.4.3 Lorentz microscopy

When an electron moves in a magnetic field it is deflected by the action of the Lorentz force F, given by:

$$\overline{F} = -\frac{e}{c}(\overline{V}x\overline{B}) \qquad (3.24)$$

where e is the electronic charge, $\overline{V}$ its velocity and $\overline{B}$ the magnetic intensity. The deviations of an electron beam may be used to detect the magnetic variations. Studying the domain structure of thin foils has led to the Lorentz microscopy technique. In this the direct interaction between the electron beam and the specimen magnetization is used to produce a picture of the domain structure.

The first observation of domain walls was in thin evaporated films of nickel-iron alloy by Hale, Fuller and Dubinstein (1959). The electron beam was deflected by transmission through a thin ferromagnetic specimen containing a 180° Néel wall. The electrons passing through the film on either side of the wall will converge or diverge after transmission, this depending on the sense of the domain magnetization relative to the electron beam. Domain walls will be imaged as regions of high and low electron density and appear as alternate bright and dark lines.

3.4.4 Scanning Electron Microscopy

This is the most recent of the methods of direct observation (Banbury J.R. et al, 1967). Experiments have shown that the magnetic contrast may be obtained by two techniques. The first (Type I) uses the Lorentz force suffered by the secondary electrons, as they pass through the stray fields at the specimen surface, after their emission (Joy and Jakubovics, 1968). These fields

reflect the domain structure at the surface and consequently vary in magnitude and direction. Type II contrast is used when the specimen surface has no poles except at the walls. By this technique a large depth-of-focus can be achieved. For small values of magneto-crystalline anisotropy leading to small or even non-existent stray fields at the specimen surface flux-closure domains may be difficult to detect by Type I contrast but may be revealed by Type II contrast with a suitably oriented surface.

3.4.5 X-Ray Topography

This technique allows the internal distribution of magnetic structures to be investigated in specimens as thick as 300 μm. Polcarova and Lang (1962) have shown the feasibility of the method.

The effect depends on magneto-striction and the consequent mis-match between domains puts the crystallographic lattice into a state of strain which is a maximum at the domain wall. This strain gives rise to diffraction contrast since the Bragg angles will be different in the strained and unstrained parts of the lattice. Monochromatic radiation is used in these methods. Also transmission and reflection methods of X-ray topography can be used to reveal domains. Scanning an area of selected reflection plane, in the crystal, can be done by moving the specimen and the photographic plate together.

3.5 Methods used in this work

The wet and dry colloid techniques were used for observation of domain structure. The results of these two methods were very satisfactory for giving nearly a complete picture of the domain structure of gadolinium.

Also the Kerr magneto-optical effect was tried, but for gadolinium the domains are very small in size and problems were encountered with the limited resolving power of the system used. The objective lens had to be situated outside the cryostat containing the sample and this imposed a severe limitation on the numerical aperture. It also proved difficult to prepare a perfect surface and if the surface was slightly irregular the scattering of the incident light destroyed the contrast. After preliminary trials the technique was abandoned in favour of the colloid method.

Scanning electron microscopy has also been tried for gadolinium. Using the Scanning Electron Microscope in the Metallurgy Department of the University of Oxford, it proved impossible to observe a domain structure. The difficulties were the irregularity and contamination of the surface of the crystal which took place rapidly after surface preparation before mounting in the equipment, an operation that took about two minutes. This foreign layer prevented the development of magnetic contrast, and the domain magnetization could not be detected.

In these circumstances the colloid technique will often still give results. It is not possible to use X-ray topography since the magnetostriction of gadolinium

is too low for the development of adequate contrast to reveal domain structures. Lorentz microscopy was not used since we were dealing with bulk crystals.

For these reasons the Kerr effect, Lorentz microscopy, scanning electron microscopy and X-ray topography were not employed for the observation reported in this work.

CHAPTER FOUR

RARE EARTH METALS

The Rare Earth metals consist of fifteen elements all having very similar chemical properties. They are commonly known as the lanthanides after the first member of the series. The initial member of the family of the rare earth elements has atomic number 57, and the final member, lutetium has atomic number 71. The physical properties of the elements show differences and in particular they have very different magnetic properties. The reason lies in their 4f electrons which determine the magnetic properties. The 4f transition series elements are all structurally quite similar and consist of three electrons outside a Xenon core and a partially filled 4f shell. Lanthanum has the electron configuration $(1s^2 2s^2 2p^6 3s^2 3p^6 3d^{10} 4s^2 4p^6 4d^{10} 5s^2 5p^6)\ 4f^o\ 5d^{(1)}\ 6s^{(2)}$ where the configuration within the brackets is that of Xenon. The parentheses for the 5d and 6s states are used to indicate that in many of the elements, once the 4f shell contains electrons, the 5d and 6s electrons are transferred to the 4f shell. The energy of the 4f shell being higher than the 5d state and it is therefore unoccupied. There are 14 available electron states since the 4f shell has an angular momentum quantum number l equal to three and therefore has 2(2l + 1)states (seven orbital states and two spin states for each). The filling of these states up to $4f^{14}$ for lutetium characterises the rare earth series.

There is a decrease in the radius of the 4f wave

function with increasing atomic number. This phenomenon is known as the lanthanide contraction. This arises because an electron added to the 4f shell cannot screen the remaining electron in this shell from the added positive nuclear charge. This contraction has important effects in some of the properties of rare earths.

Unlike the corresponding 3d transition series, the 4f electrons of the rare earths generally remain highly localized in the solid and form the magnetic electrons. The 4f electrons behave, to a first approximation, like those in a free ion.

The outer-lying electron states are essentially unchanged and it is for this reason that the rare earth elements are so chemically alike. The $5d^{(1)}$ and $6s^{(2)}$ electrons are readily removed to become conduction electrons, leaving a trivalent ion. If the 5d electron has transferred to the 4f shell one conduction electron comes from this shell. In the solid state the three outer electrons form bands of mixed 5d-p 6s character, which account for the metallic conductivity of the elements. (Watson (1968)).

It is the unpaired 4f electrons which give the rare earth ion its permanent magnetic moment, and lead to the appearance of ferromagnetism in some elements, the magnitude of which is governed by Hund's Rules. These state that the moment associated with an incomplete ionic shell is given first by the combination of spin moments to give the maximum value of S and then the combination of orbital moments to give the maximum

value of L consistent with this arrangement of the electron spins. Spin and orbital angular momenta are strongly coupled yielding J as a good quantum number. The total moment is then calculated from J = L-S for a less than half-filled shell and J = L+S for a more than half-filled shell. The series is conveniently divided at the point of a half-filled 4f shell into light (La-Eu) and heavy (Gd-Lu) groups.

The Rare Earth metals, in the solid phase, can be observed in many of the normal metallic configurations as body centred cubic, face centre cubic, hexagonal close packed, double hexagonal close packed and samarium structures. At normal temperatures the structures of all the elements, with the exception of europium, are of a close packed nature. These structures may be described in terms of three types of layer. These layers may be defined as A, B and C and are shown in figure (4.3).

4.1 The heavy rare earth metals

4.1.1 Crystal structures

All the heavy rare earth elements, but ytterbium, have at room temperature a hexagonal close packed structure of A3 type. This structure has a form ABAB., and is shown in figure (4.3a).

The lattice spacings decrease on going from Gd to Lu, due to the lanthanide contraction. The axial ratios c/a of the heavy metals vary between 1.59 for gadolinium and 1.586 for lutetium having a lowest value of about 1.571

between holmium and thulium. All these ratios are somewhat less than the ideal value of $2\sqrt{2}/\sqrt{3}$ = 1.633 obtained for the close packing of spheres.

4.1.2 Magnetic properties

In the heavy group the element ytterbium has a full complement of fourteen 4-f electrons and is only weakly paramagnetic. Likewise, the element Lutetium has a full 4-f shell and it too is weakly paramagnetic. Each of the remaining heavy metals exhibits an effective magnetic moment in the paramagnetic state.

As the temperature is reduced below a certain critical temperature there is a transition from the paramagnetic state to an ordered state in which the moments arrange themselves in one or another ordered magnetic configuration. The temperatures at which the order-disorder transitions occur are known by noticeable anomalies or discontinuities in the measured electrical, thermal or magnetic properties of the metals. For all the heavy rare earth metals except Gd, there is evidence at lower temperatures for order-order transformations to other magnetic configurations. For the heavy series the mean radius of the 4f shell is one tenth of the interionic spacing, so that the direct overlap between 4f orbitals on the neighbouring ions is negligible.

The magnetic ordering observed in the heavy rare-earth metals arises from an indirect exchange mechanism between the polarization of the conduction band electrons and the local 4f moments. Such an interaction is

oscillatory in nature and has long range. It is therefore capable of giving rise to a variety of periodic spin structures, such as indeed are observed in the heavy rare earth metals. The application of the theory of exchange interaction for the Rare earth metals is associated with the names of Rudermann and Kittel (1954), Kasuya (1956) and Yosida (1957). It is known as (RKKY) interaction. This interaction has led to a fuller understanding of many of their properties.

The exchange funtion J which appears in the energy is equal $\sum J(r_{ij})\, \underline{S}_i \cdot \underline{S}_j$, and is usually discussed in terms of the Fourier transform function

$$J(q) = \sum_{i \neq j} J(r_{ij}) \quad e^{i\underline{q} \cdot \underline{r}}$$

This function $J(q)$ may indicate a maximum at $q = o$ or at other general value $q = q_{max}$ elsewhere in the Brillouin zone (Keeton and Loucks 1968). In the case of maximum at $q = o$ the initial magnetic ordering is ferromagnetic, while when $J(q)$ exhibits a maximum at a non-zero value of q, a periodic ordering results which is antiferromagnetic with wave vector q_{max} (Evenson and Liu 1969). This condition is found in most of the rare earths. The condition that the exchange functions occurred having maximum at non zero q has been studied by a number of workers. Keeton and Loucks and Evenson and Liu connect this situation to the nesting property in the elements T_b to T_m. The nesting feature is absent in Gd, which shows only ferromagnetism.

The other interactions between ions are assumed small. The most important are the coulomb electrostatic interaction and an interaction between the 4f moment and the crystal field. The effect of the later is to align the magnetic moments of the 4f electrons in some preferred direction relative to the crystal axes. It gives rise to magnetocrystalline anisotropy which is important in determining the spin structures in the ordered state.

The definite form of the exchange interaction has been investigated by the inelastic neutron scattering technique. Koehler et al (1970) using this technique observed the spin-wave relation in Gd, while Nicklow et al (1971) have examined it for Dy. For the elements Tb and Er it was worked out by Bjerrum-Moller et al (1966) and Woods et al (1967) respectively.

The exchange integral between the 4f electron of an ion and a conduction electron is known as the s-f interaction. The conventional exchange energy for the rare earth metals always favours the parallel alignment of the 4f moment and the conduction electrons moments. So that the conductions electron moment adds to the ionic moment. So the conduction electron polarization results in an additional value (μ_c) to the observed magnetization, and this accounts for the excess moment values observed for the heavy rare earth metals.

4.1.3 Magnetic behaviour in ordered states

The magnetic behaviour of the heavy rare earth

metals has been shown by neutron diffraction to result from a variety of different equilibrium magnetic configuration. This variety is shown in figure (4.1). On cooling down the various heavy rare earth metals from the paramagnetic region the appearance of extra lines in the neutron diffraction spectrum can be explained in terms of a model of the magnetic ordering (Koehler 1965). The figure shows the various moment arrangements for successive planes going down the c-axis. The moments lying in a given (0001) plane order ferromagnetically, i.e. parallel to each other. There are two temperature regions of magnetic order, except for Gd. There is observed a transition to an oscillatory antiferromagnetic configuration of a helical or linear oscillatory type for each of the metals Tb, Dy, Ho, Er and Tm. The temperature at which this transition occurs is the Néel temperature T_N. Lowering the temperature a further transition is observed to ferromagnetic ordering at the Curie temperature T_C. Between the two temperatures T_N and T_c a spiral structure has been found for the elements Tb, Dy and Ho. It is holds between 179 and 85K for the element Dy, while it is present between 230 and 221K for the element Tb. The spiral turn angle between the moments of successive hexagonal layers varies with temperature. This angle for Dy changes from 43^o at the Néel temperature to 26^o at the Curie temperature. For Tb the angle is smaller and varies from 20^o to 17^o. The ferromagnetic alignment below T_c is along an a-axis in the hexagonal plane for Dy, and it is along a b-axis

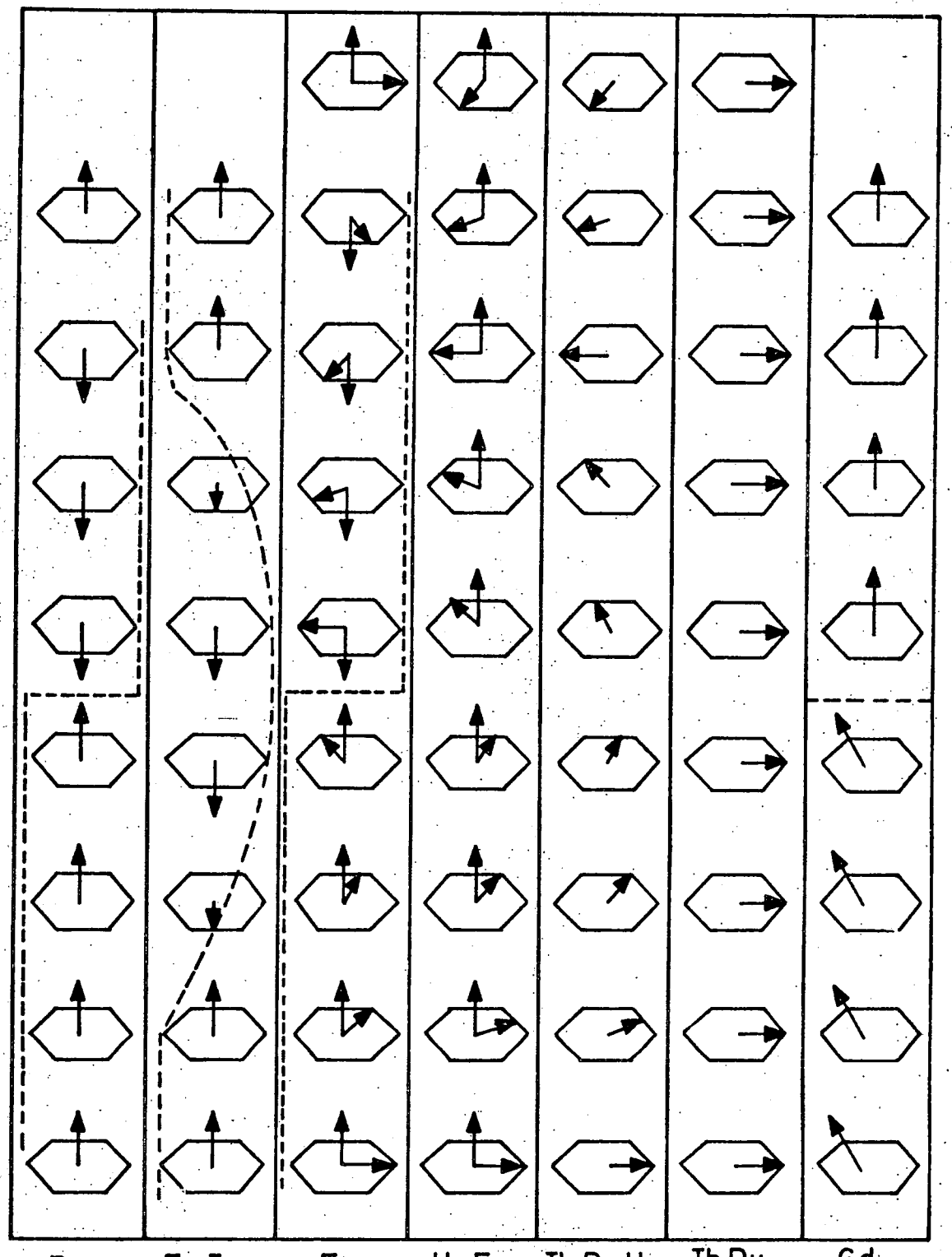

FIG. (4·1)

in the hexagonal plane for Tb. For Ho, the basal plane components retain the helical structure, but below T_c = 20K there exists a small ferromagnetic component in the c-axis direction. The conical or ferromagnetic spiral configuration is illustrated in figure (4.1d), in which the planar and axial components are shown separately. For each plane the total moments lie on the surface of a cone. At low temperature Jordon and Lee (1967) found that Dy also may have a small axial component.

In figure (4.1b) is observed a different type of oscillatory magnetic structure. This structure is found for Er and Tm and is called sinusoidal spin arrangement, linear spin wave type or oscillatory z-component structure. In this structure the z-components of the moment in any layer are parallel to each other but the magnitude of the component varies sinusoidally when going along the c-axis. The sinusoidal spin arrangement is observed for Er and Tm in the temperature range between 85 - 53.5 K and 56 - 40 K respectively.

The structure found for Tm at very low temperatures below 30 K contains three layers with moments pointed down the c-axis followed by four layers with moments pointed up the c-axis as in figure (4.1a). This is a type of antiphase domain structure. Figure (4.1c) shows a type of structure where the components of moment perpendicular to the c-axis order in the helical arrangment, while the parallel components form a type of antiphase domain structure. This structure is observed in Er at temperature 53.5K and below.

As stated earlier, the origin of the magnetization of the ordered state arises from the indirect exchange mechanism in the heavy rare earth metals. Relating to this theory it has been found that the paramagnetic Curie temperatures will be proportional to a factor known as the de Gennes factor and given by the relation

$$G = (g_J - 1)^2 J(J + 1)$$

In practice this is reasonably well obeyed. The Néel points of the heavy metals are discovered also as a function of the de Gennes factor, but are given by the relation $T_N \propto G^{2/3}$. This variation was given by Weinstein et al (1963).

It was found that it is not possible to obtain magnetic saturation in a magnetic field of the order 20 kOe in measurements of polycrystalline samples of the heavy rare earths other than Gd. This is due to the existance of large magnetocrystalline anisotropies, which have been observed in single crystal measurements. This is clear from determination of the magnetization along the different crystallographic axes. Saturation in the hard direction has not been obtained in fields up to 150 kOe (Schieber et al (1968). Yet for erbium this value has been observed to be the saturation field, but it has been difficult to determine the anisotropy constant.

Neutron diffraction work has shown the configuration in the antiferromagnetic phase to be a helical spin structure Applying a magnetic field in the basal plane to the helical configuration distorts the helix until a large value of the magnetic field (the critical field H_c) is enough to rotate

the spins into the general direction of the field making a fan structure. Further increasing the field brings about the collapse of the fan structure and the spins are aligned in the direction of the field. This structure gives saturation as in figure (4.2).

The magnetostriction strains have been found by many workers to be large in the heavy rare earth metals (Corner et al (1960)) and (P. de V.Plessis et al (1965)). As stated before an applied field in excess of the critical field changes the specimen from antiferromagnetic structures to ferromagnetic ordering at higher temperatures. It has been suggested that the transition is driven by enormous magnetostriction associated with the ferromagnetic structure. Clark et al (1962) found all the magnetostriction terms to be proportional to H^2 above the Néel point. It has been found that the magnetostriction is dependent on the temperature. Callen and Callen (1966) have treated the temperature dependence of the magnetostriction.

4.2 The Light Rare Earth Metals

The light rare earth metals have crystal structures that are morecomplicated than those of the second half of the series. These include the double hexagonal structure in which the stacking layers are in the form ABACABAC rather than ABAB figure (4.3.b), the f.c.c. structure with stacking sequence ABCABC figure (4.3d) and a complicated structure in which the sequence of layers is ACACBCBABA known as the Sm-type structure figure (4.3c). Lanthanum, praseodymium and neodymium have the double hexagonal

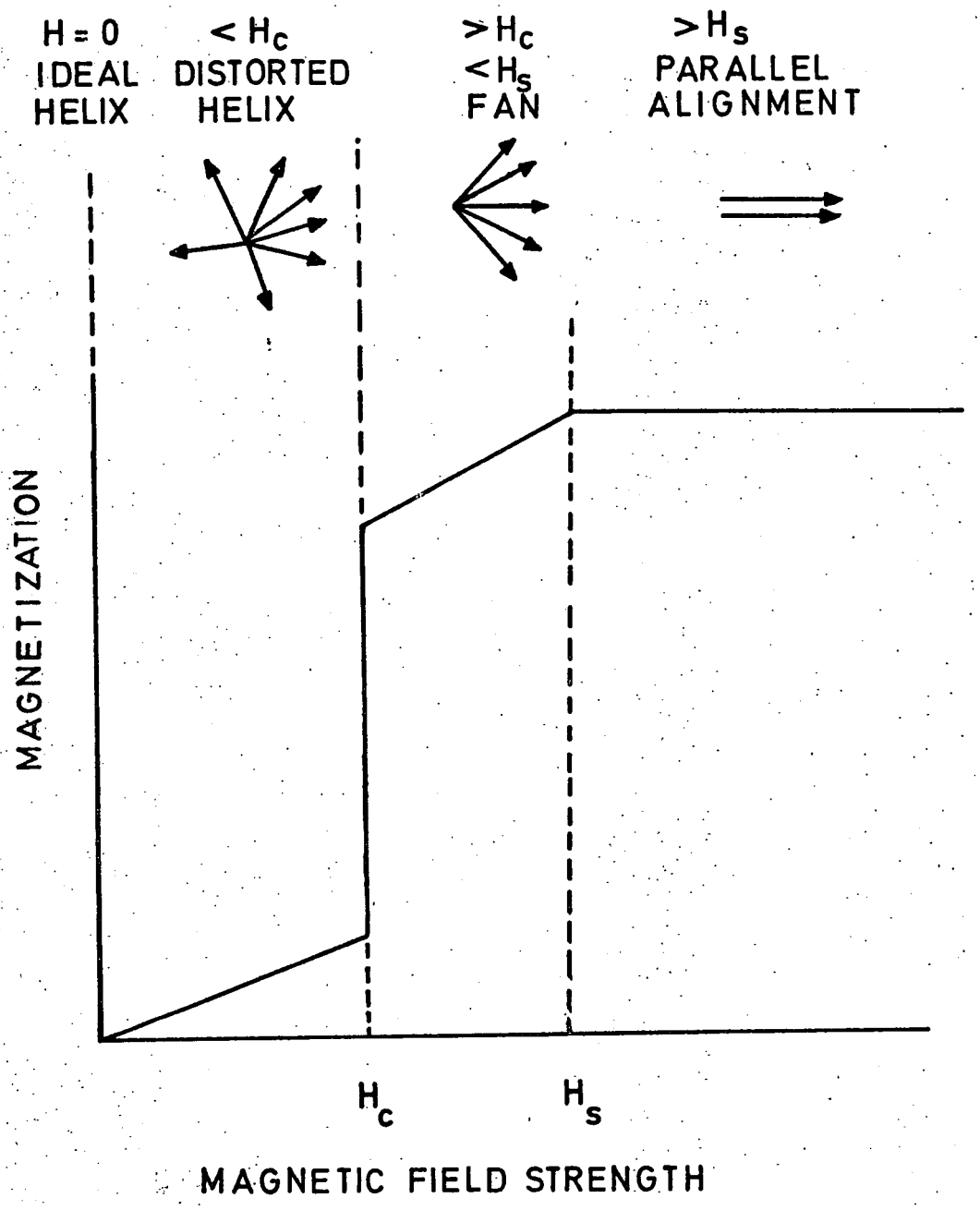
H = 0
IDEAL
HELIX
< Hc
DISTORTED
HELIX
> Hc
< Hs
FAN
> Hs
PARALLEL
ALIGNMENT
MAGNETIZATION
Hc
Hs
MAGNETIC FIELD STRENGTH

FIG.(4.2)

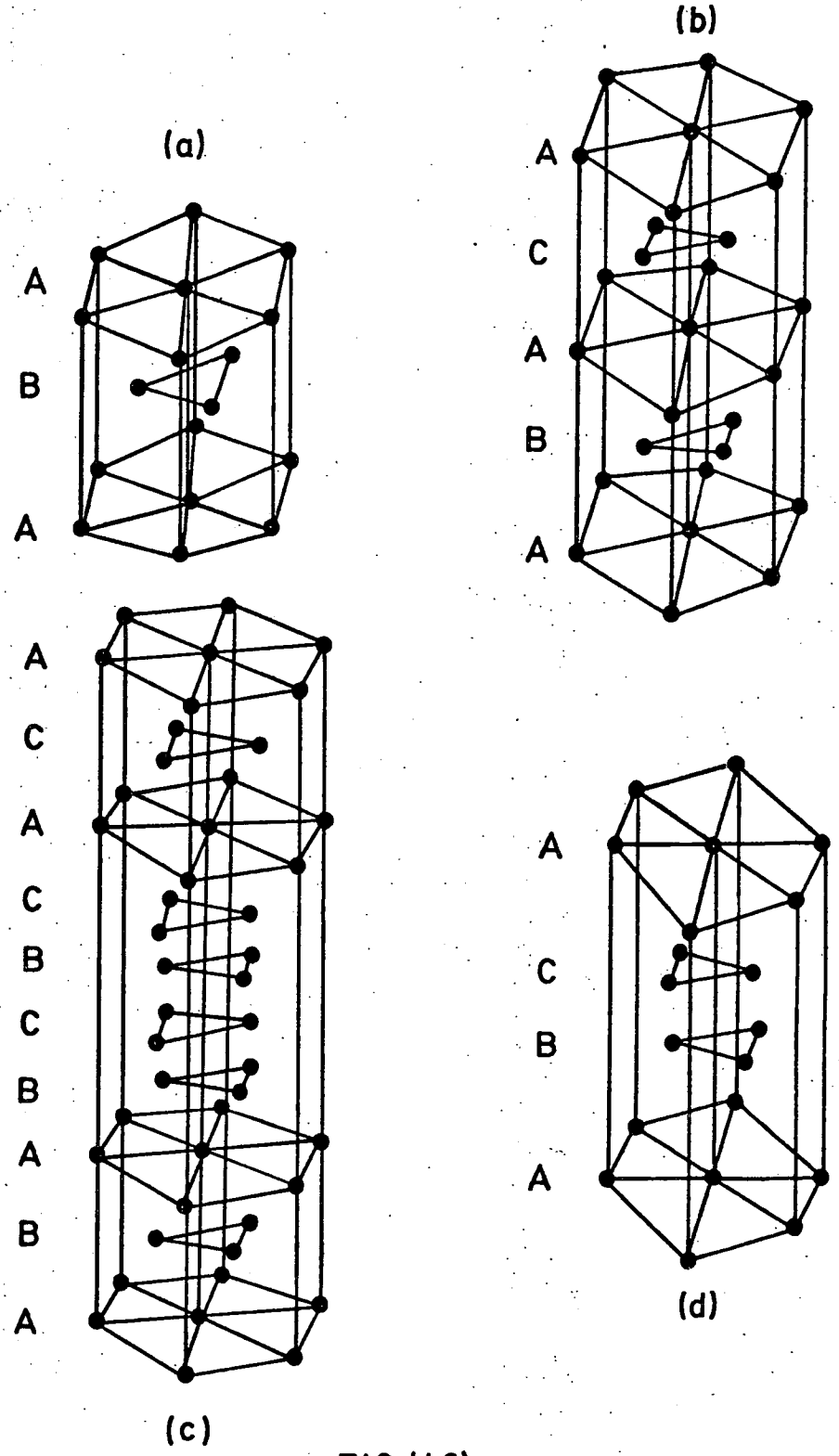

FIG. (4.3)

a) Hexagonal close packed.
b) Double hexagonal.
c) Sm-type.
d) f-c-c.

structure at room temperature, figure (4.3b). Samarium has a rhombohedral structure which is only for this element, figure (4.3c). Europium crystallizes in the body centred cubic structure at room temperature while ytterbium possesses the face centred cubic structure. All the light rare earths have the axial ratios c/a in excess of 1.6 and are closer to the ideal value for close packing than are the heavy rare earths. Anomalies in the specific heat and maxima in the susceptibility have been observed in all the metals except Praseodymiun.

The observed magnetization in the light rare earths is strongly controlled by the crystal field. It has energy splittings comparable to the energy of the exchange interaction. At low temperatures, below 300K, the susceptibilities of most of the elements deviate from the Curie-Weiss behaviour. The light elements exhibit magnetic ordering below some characteristic temperature.

The element Lanthanum is weakly paramagnetic, and this is found to be due to the 5d and 6s conduction electrons with the 4f shell empty. The antiferromagnetic transition for polycrystalline cerium has been observed at 12.5K. The magnetic ordering suggested is that the magnetic moment parallel to the c-axis and having the value $0.62\mu_B$. The measurements of Cable et al (1964), suggested that the metal Pr is antiferromagnetic below 25K. Rainford (1971) confirmed antiferromagnetism in polycrystalline Pr and its absence in single crystals. The magnetic structure of neodymium has been found to be antiferromagnetic in the temperature range 1.6 to 20.0K

for single crystal by neutron diffraction (Moon et al 1964). There are two magnetic transition due to the independent ordering of the hexagonal and cubic sites in the double hexagonal structure of this metal.

Neutron diffraction data from a single crystal of Sm (Koehler et al 1972) show an antiferromagnetic ordering transition at the temperature 100 K and ferromagnetic ordering layers at temperature 14 K. These involve the ordering of moments on the hexagonal and cubic sites respectively.

The magnetic properties at temperature 4.2 K for single crystal Europium are consistent with antiferromagnetic order. The transformation at the Néel point at 90 K, has been shown to be a first order transition (Cohen et al 1969). The interlayer angle varied slightly with temperature.

4.3 Magnetic Properties of Gadolinium

Gadolinium is a non-typical member of the heavy rare earths. It has the usual hexagonal close packed structure with the ratio c/a equal to 1.591, smaller than the value for perfect hcp which equals 1.633.

An ion in a pure s-state has a cloud of completely spherical charge and all multipoles of its moment are zero. According to this case there is no crystal field effect and all the $\alpha_l = 0$. The spin-orbit coupling will modify this result, and then the state is simply one of $J = 7/2$. It requires an extra order of spin-orbit coupling to increase the L value. Perturbation theory suggests that

the effective $\alpha_2 > \alpha_4 > \alpha_6$. This is according to magnetic resonance measurements.

Gd exhibits an effective magnetic moment in the paramagnetic state. The valance electrons $5d^1\ 6s^2$ are lost to conduction bands, then there is left a highly localized moment due to unpaired electrons in the 4f shell. The moment is quite well given by application of Hund's Rules.

As the temperature is reduced below a certain critical temperature it is found that a transition from the paramagnetic state to a ferromagnetic ordered state occurs, in which the moments adopt ordered magnetic configuration.

Gadolinium has no antiferromagnetic phase and transforms directly to the ferromagnetic state. The Curie temperature T_c equal 292K as determined from resistivity measurements. The paramagnetic Curie temperature θ_p is obtained from susceptibility data as $\theta_{\parallel} = \theta_{\perp} = 317K$. The saturation magnetization has been measured for gadolinium parallel to the easy axes, is found to be equal to $7.55 \mu_B$. This measured saturation moment exceeds slightly the predicted value from the Hund's Rules ground state $gJ(\mu_B)=7.0$. The excess is related to polarization of the conduction electrons.

The thermal neutron absorption cross-section for Gd measured by neutron diffraction experiments has been found to be $\sigma_{capt}(\text{barn}) = 46{,}000$. The cross-section of Gd is so large that the ordering of the 4f moments is extremely difficult to study except in certain specialized experiments. Isotopes of gadolinium.....

exist with much more favourable absorption cross-sections and these are being utilized.

Although Gadolinium has been reported to be a ferromagnetic with Curie temperature of 292K, Belov and Pedko (1962) observed anomalies in very low field magnetization curves using polycrystalline gadolinium. These anomalies were above the temperature 210K and they suggested that they were due to the existence of a spiral spin structure. According to their report, a very small field of order one oersted was sufficient to transform the spiral into a ferromagnetic. Graham (1963) has repeated their measurements on a single crystal of gadolinium but he found no such anomalies. After that a number of neutron diffraction studies have been made to look for any evidence of the occurrence of this structure in gadolinium. Will, Nathans and Alperin (1964) studied a single crystal of gadolinium, with naturally occurring isotope content. They were able to conclude that there were no observable satellites and gadolinium is a normal ferromagnet. Also Cable and Wollan (1968) used shorter wavelength neutrons for which the cross-section is smaller, they found no evidence for any satellite structure. There was no field dependence of the intensities in the range 0.1 to 50 Oe. The evidence is that gadolinium is spontaneously ferromagnetic throughout the ordered region.

It is possible that the anomalous behaviour of Belov and Pedko may arise from inhomogeneous or strained samples of gadolinium. It is also possible that these observations

related to the anomalous behaviour of the easy magnetization direction in this metal below 240K. In,a recent investigation by Kuchin et al (1969)a single crystal of Gd was studied at temperatures ranging from 78K to room termperature. They concluded that Gd is a normal ferromagnet below T_c. They observed that the direction of the moment depends strongly on the temperature.

The measurements of the magnetization on single crystal Gd made by Legvold (1963) at Iowa State university remain the essential basic data. Gadolinium has no orbital momentum contribution to the total moment. Magnetization curves are typically characteristic of a ferromagnet of low anisotropy. Small anisotropy effects are seen at low field with a temperature dependant variation in the easy direction of magnetization. The dependence of the magnetization on the temperature is shown in figure (4.4) and it is well defined by the $S = 7/_2$ function. The saturation magnetization is represented by a T^2 dependence from 0 to 150K. The variation of magnetization with temperature for gadolinium was investigated by Nigh, Legvold and Spedding (1963). They measured the magnetic moment of single crystal Gd in fields from 0 to 18k Oe along the $[0001]$, $[10\bar{1}0]$ and $[11\bar{2}0]$ direction at temperatures ranging from 1.4 to 900 K, figure (4.5) and figure (4.6). The c-axis isofield curves show a peak at 220 K and a broad minimum at 160-180 K at low fields, while the b-axis curves show a peak at 120 K. For high fields the curve was shown to exhibit nearly normal Weiss behaviour. The magnetization of gadolinium

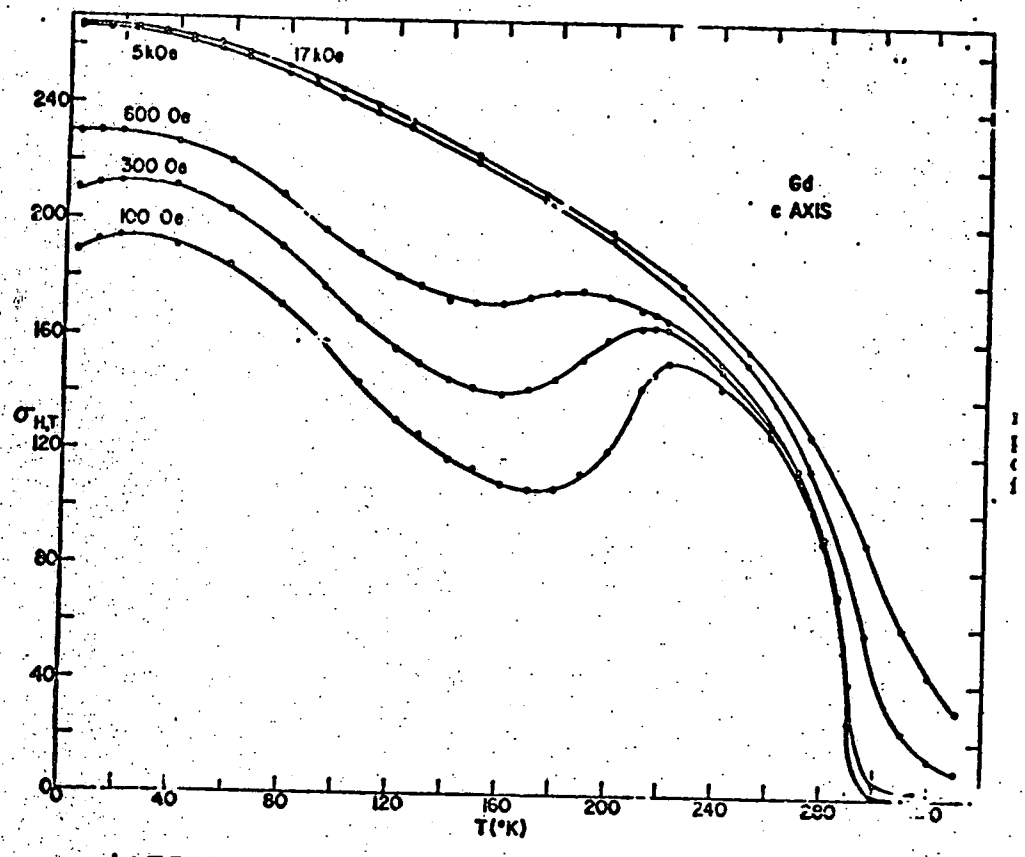

(AFTER NIGH LEGVOLD SPEDDING) FIG. 4.5.

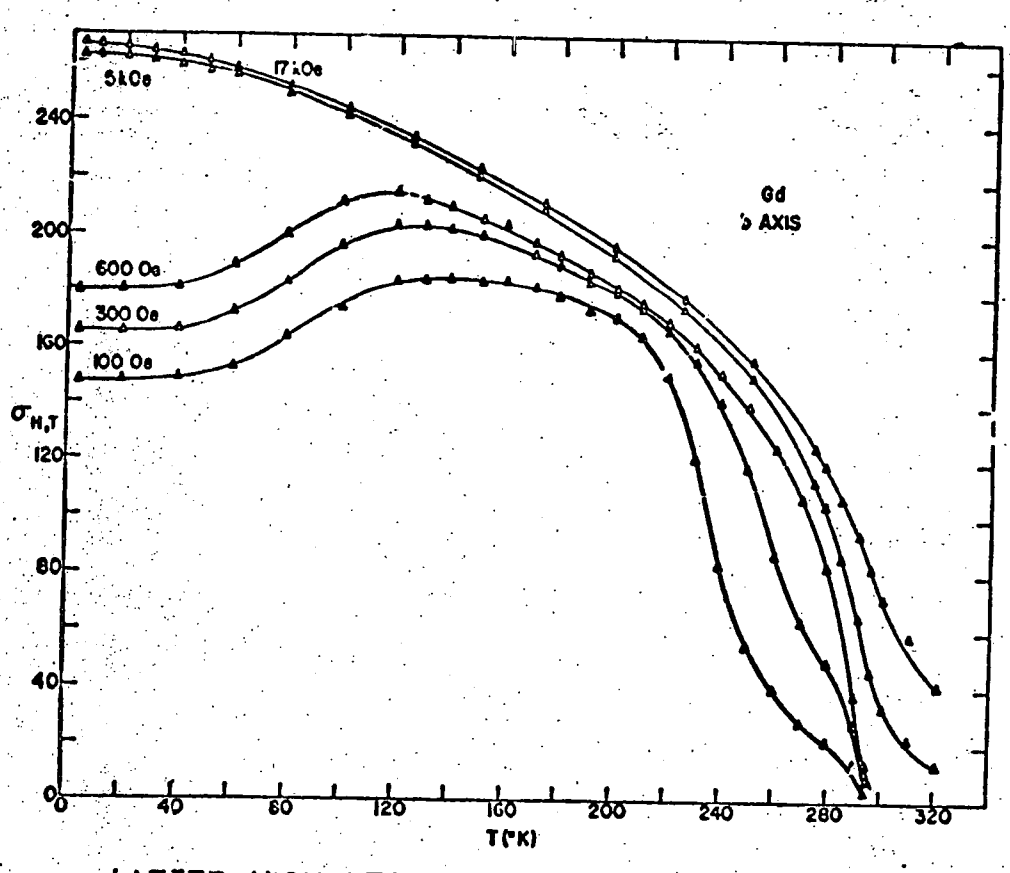

(AFTER NIGH LEGVOLD AND SPEDING 1963)

FIG. 4.6

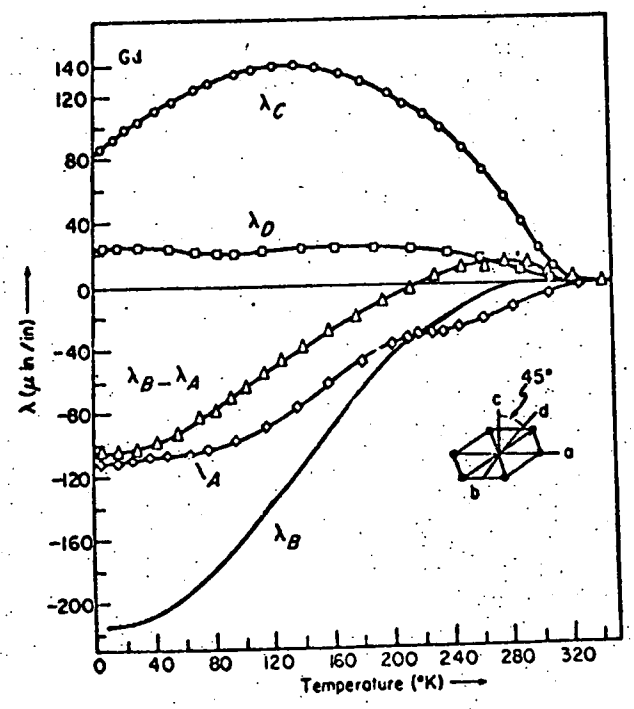

Figure (4.7) after Alstad and Legvold.

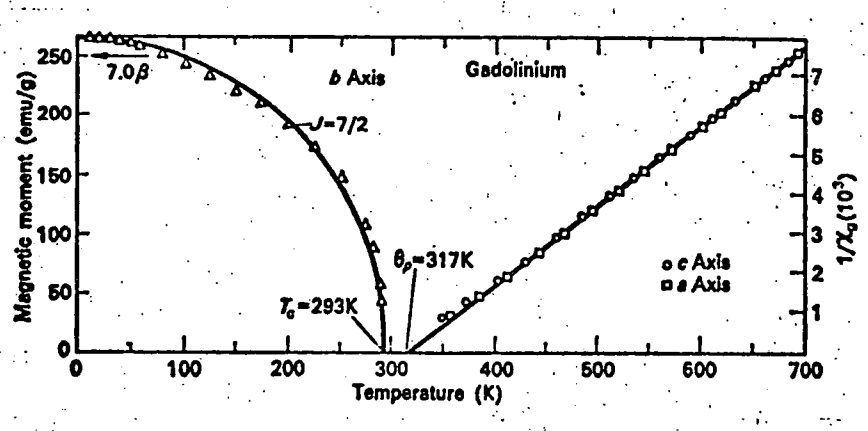

Figure (4.4) after Nigh, Legvold and Spedding

in weak field was found to fall rapidly between temperature 210 K and the Curie point temperature.

The variation of magnetostriction coefficient λ_s for gadolinium with the temperature is shown in figure (4.7). It shows the variation of the magnetostriction constant for a single crystal and polycrystalline samples.

4.4 The anisotropy of gadolinium

The early magnetization measurements of the gadolinium metal were found to show evidence of certain amount of magnetocrystalline anisotropy. Torque measurements of axial anisotropy of gadolinium showed that its magnitude was several times that of the hexagonal transition metal cobalt (Corner 1962).

The variation of the anisotropy constant K_n (n = 1, 2, 3, 4) with temperature for this metal are shown in figure (4.8). It was shown by the measurements of Corner et al (1962) and Graham (1962), that at least three parameters are required to represent the anisotropy of gadolinium. The anisotropy energy E_K is given by the following equation,

$$E_K = K_1 \sin^2\theta + K_2 \sin^4\theta + K_3 \sin^6\theta + K_4 \sin^6\theta \cos 6\phi$$

where θ is the angle between I_s and the hexagonal axis and ϕ the projected angle with one of the a-axes in the basal plane. Below T_c the c-axis is the easy direction but at temperature 240 K there is a change from this alignment of spins to one making a finite angle with the c-axis resulting in a conical alignment of the moments below this temperature. The observed change in sign

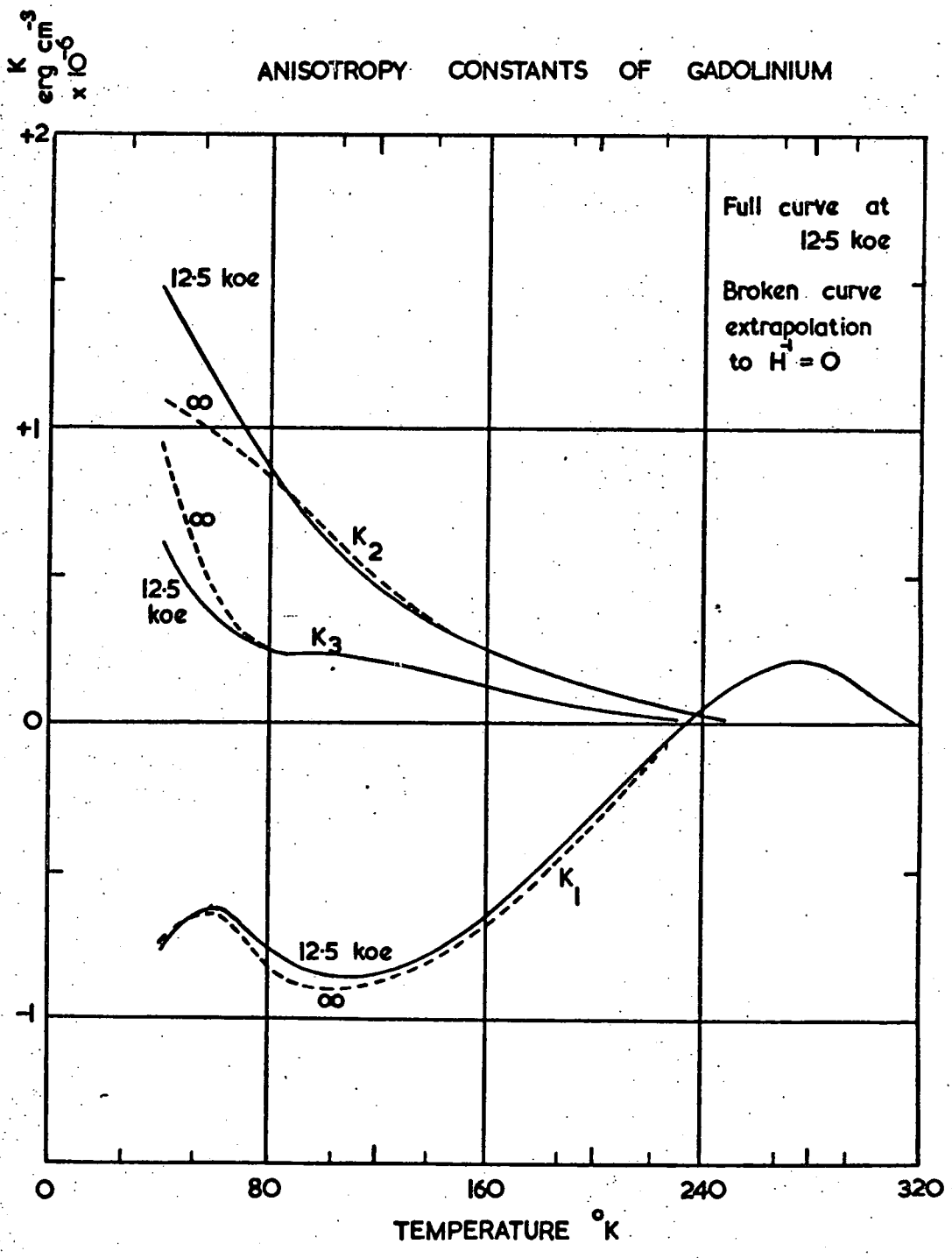

FIG.(4·8) AFTER CORNER et. al.

of the principal axial term K_1 at about 240 K corresponds to sudden change in the moment away from the c-axis. The magnitudes of K_2 and K_3 are such as to prevent the easy direction from reaching the basal plane. The basal plane anisotropy measurements made by torque magnetometer, Taylor and Darby (1964) and Graham (1967), have shown that the K_4 term is relatively small, becoming appreciable only below about 100 K and indicating a preferred a-axis. Combination of these constants with the magnetization results leads to the polar energy diagram shown in figure (4.9). In the figure it may be seen that just below 240 K, the moments are prevented from aligning parallel to the basal plane by a small energy maximum in that direction.

As stated before, at temperature above 240 K, the easy direction is parallel to the c-axis and at lower temperature it lies on the surface of a cone whose axis is the c-axis. The variation of the cone angle of the moment orientation with temperature is given in figure (4.10). In the figure it is seen that the angle between the c-axis and the easy direction has a maximum value of 70° at temperature 220K, while at temperature 37.5K it has a value of 30°. The original results of Graham (1962) indicated that for a small interval of temperature from 232K to 180K, the basal plane was the easy direction. Neutron diffraction studies by(Cable et al 1964) and (Will. Nathansand Alperin 1964) have established that there is no such basal plane easy direction, and their curve was the same as the curve obtained by Corner et al (1976).

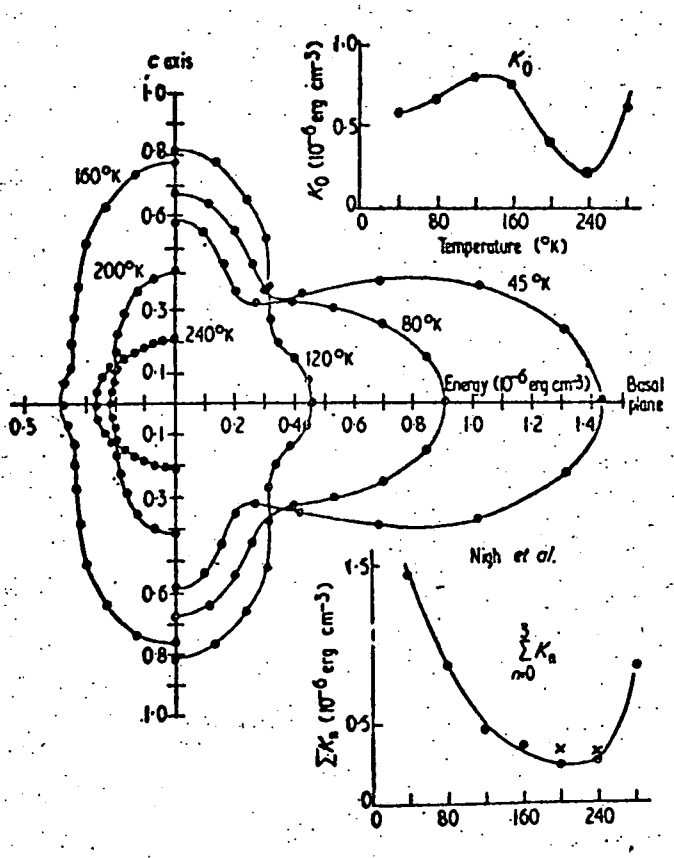

Polar energy diagrams in a plane containing the c axis at various temperatures, and variation of K_0 and $\sum_{n=0}^{3} K_n$ with temperature.

Figure (4.9)(after Darby and Taylor)

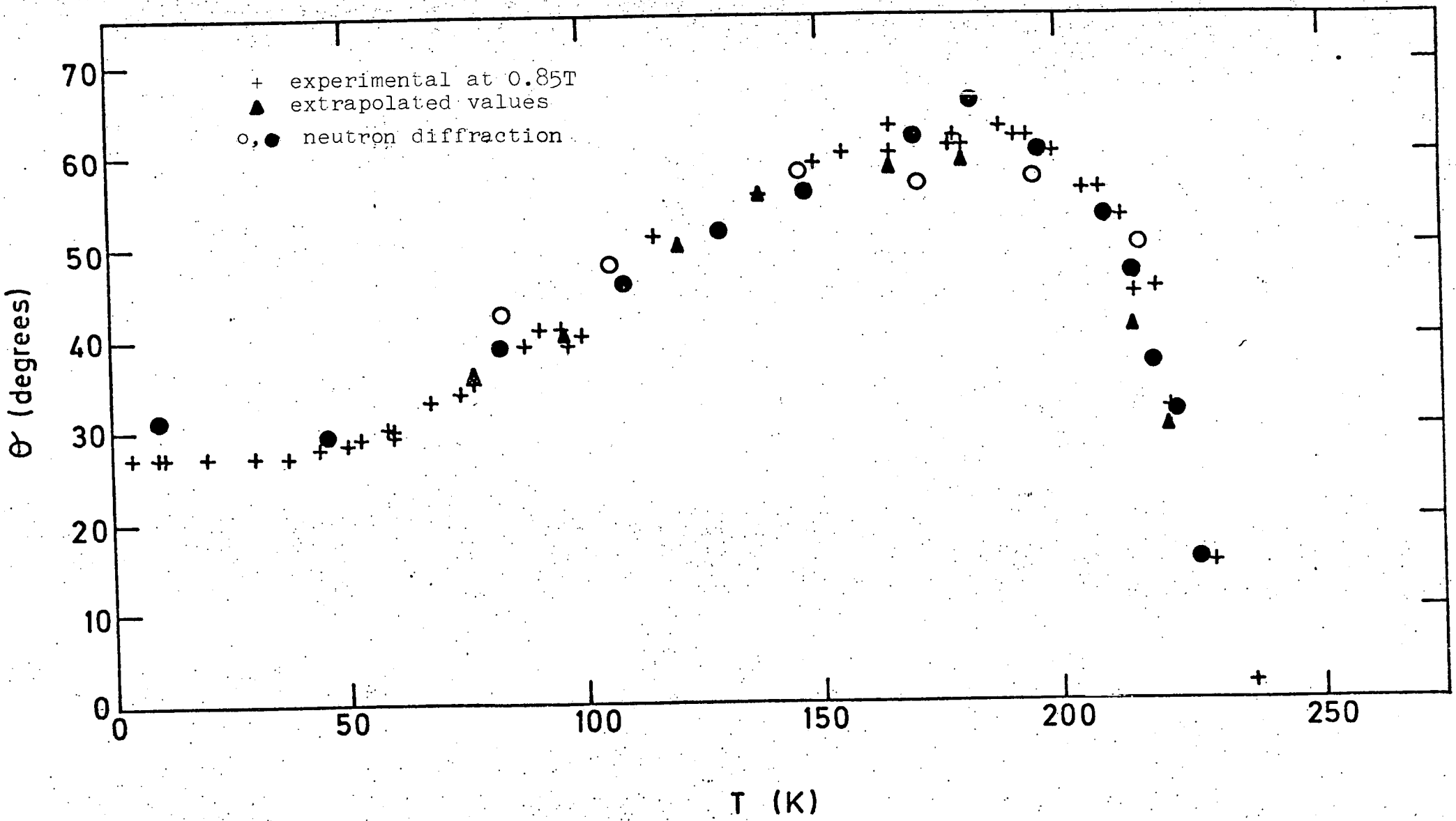

Figure (4.10) after Corner and Tanner.

Near the Curie point there is an appreciable contribution to the anisotropy due to a difference in the paramagnetic susceptibility parallel and the perpendicular to the c-axis. Graham has investigated the field dependence of the anisotropy for gadolinium in the vicinity of the Curie temperature. The data on forced magnetostriction show that for Gd near the Curie temperature, the lattice constants change with the value of applied field in an anisotropic way. Also Corner et al (1976) have shown that the anisotropy constants were functions of the applied field. They related this effect to an increase in spontaneous magnetization due to the field.

CHAPTER FIVE

EXPERIMENTAL

5.1 Origin & Identification of Specimens

A number of single crystals of high purity Gadolinium have been used in the present investigations. All but one were obtained from the Center for MaterialsScience at the University of Birmingham. They had been grown by a solid state electrolysis technique which had improved the overall purity of the material as well as inducing crystal growth. The material was generally of similar purity to that described by Jordan (1974) and had an oxygen content of less than 10^2 p.p.m. (atomic). As a consequence the presence of oxide as a second phase was infrequent. It is convenient to list the specimens as below.

A. This was wedge-shaped with the basal plane as one of the larger faces. This was of length 6 mm and width 4 mm tapering from a thickness of 4 mm to one of 1 mm.

B. A disc of elliptical cross-section with major and minor axes of 7 mm and 5 mm respectively and thickness 6 mm. The surface of the disc was a b-plane, but small sections perpendicular to an a-axis and to the c-axis were later cut on the sides of the disc.

C. A further disc-shaped crystal of thickness 3 mm and diameter 6 mm, the plane surfaces being b-surfaces.

D.E. Two rectangular crystals, with dimensions 1 x 2 x 3 mm, the larger surfaces being b-planes. Specimen E however, was of 99.9% purity material from Metals Research Ltd., Cambridge, and contained appreciable quantities of oxide

as a second phase. All specimens were cut from larger crystals using the spark erosion technique.

5.2 Orientation of the crystals

The crystals were oriented by X-ray technique using a back reflection Laue technique. The specimen was placed on a goniometer facing one beam from the X-ray set. A Polaroid cassette was placed to stand between the goniometer and the X-ray set, and carried both the X-ray film and collimator.

Before mounting the specimen on the goniometer it was well etched to remove any strained layer. Etching the surface continued until clear spots appeared on the film. The etching solution used was the same solution as used for polishing and described later. The specimen was rinsed with absolute alcohol and dried in a stream of warm air. Exposures were made using an X-ray tube with Molybdenum anode. This tube was operated at 30 mA and 30 kV, and the exposure time was about six minutes. Many exposures were made with the X-ray beam incident at different points on the surface in order to make sure that the specimen was a single crystal.

The specimen was set at a fixed distance from the film, 3 cm for convenience. This permitted the use of a Greninger chart constructed for this separation to measure angles of prominent zone intersections. One of these was then chosen and the crystal rotated through appropriate angles to centralize it. This

was done by changing the goniometer to the required angle. The resulting pattern was compared with patterns computed for reflection from the three principal axes of a hexagonal crystal. It was easy, by trial and error, to locate one of these axes. This method is capable of determining the orientation of the crystal to within $\pm \frac{1}{2}^{o}$ with the apparatus used.

5.3 Cutting and shaping the crystals

Next it was necessary to cut certain surfaces parallel to crystallographic planes on the oriented crystals. It is essential that this cutting is as strain-free as possible since this will avoid the need for annealing. Also if the specimen is badly strained then it could possibly show no true domain structure but only maze patterns, due to surface strain.

For the above reasons it was decided to carry out the cutting operations using an electro-spark technique. In this method an electric discharge passing between two electrodes causes erosion of the contacting areas. With the use of a suitable tool the specimen, which forms the anode, wears away at a greater rate than the tool. The tool is a continuously moving tinned copper wire. The cutting head is counterbalanced by an adjustable weight and the cutting is controlled electromagnetically by a small selonoid. When the machine is sparking there is a small current flowing through the selonoid. This is cut off when the distance between the electrodes is too large for a spark to pass and so the tool moves

downwards due to the effect of the weight, until sparking once more takes place.

The specimen is mounted on a twin arc goniometer. The goniometer can rotate about a vertical axis, and can move in a horizontal plane on two slides at right angles. Thus the specimen can be set up at any desired angle with respect to the cutting tool to a very high accuracy. The crystal is fixed on the goniometer by Durofix cement mixed with graphite powder to render it conducting. After cutting this Durofix mixture can be removed by dissolving it in acetone. The anode is mounted in a tank which contains the coolant, transformer oil, chosen for its low viscosity and high dielectric constant. This prevents the electrodes from melting and fusing. A range of charging potentials is available and the rate of cutting is directly proportional to the voltage. The machine used was a commercial model by Metals Research Ltd.

The surface produced was examined under the microscope and found to be pitted to a depth of 10 - 20 microns. The surface so prepared showed very little contamination from the decomposition of oil and cathode material.

In some cases the surface was found to be a degree or so from that desired. This was detected by making an X-ray Laue photograph after cutting and before dissolving the Durofix.

5.4 Specimen preparation

Observation of domain structure requires a plane

strain-free and highly polished surface. Methods of specimen surface preparation are clearly of primary importancein practical investigations. In certain cases no problems arise, for instance, the surface of evaporated films and of crystals which have been grown from the melt without subsequent cutting or grinding.

In the general case a crystal will have been cut to a special shape, or to expose a particular crystal plane. The resulting surface will be strained or deformed by the preliminary cutting and any subsequent grinding. These effects may be minimized by careful treatment, such as choosing the correct rate of cutting when using the spark erosion machine.

5.4.1 Mounting the specimen

First the specimen was mounted, the material being carefully chosen since some mounting materials could produce a high compression during solidification which in turn produces a strain in the sample especially for the rare earth metals which are comparatively soft. Obviously it is necessary to take care to avoid any plastic deformation of possibly fragile specimens.

A cold-mount resin "Trylon CC 303" mixed with a few drops of accelerator and hardener, gave excellent results, but one disadvantage of this mount is that it needs about 24 hours to set at a temperature of 290 K. It is very easy to remove the specimen by cutting and breaking the edges of the mounting material. Also it is easy to dissolve this mount in acetone.

5.4.2 Mechanical polishing

After the specimen had been set, a mechanical polishing was carried out by using successively finer grades of emery paper (G, 0/0, 2/0, 3/0 and 4/0). This was followed by the use of diamond compound paste on a rotating disc. There are three discs, one for each grade of the compound, 6/3, 3/2 and 1/$\frac{1}{4}\mu$m respectively. The discs were covered by a cloth to carry the abrasive. Throughout the process a spray of dry Kerosene was used as a lubricant. Between every stage the specimen was carefully washed with absolute alcohol to prevent the carrying of particles of abrasive from the previous stage.

A suitable pressure should be applied to the specimen to ensure the maximum possible polishing rate. It must be noted that high pressures may result in a significant deterioration in the quality of polish. In the case of Gadolinium high pressures may give rise to heavy scratches.

Cloths such as "Metron" (Metallurgical Services Ltd.) consisting of synthetic rayon fibres bonded to a heavy cotton backing and manufactured as synthetic suedes have proved to be the most satisfactory for this work.

Low rotational speeds are desirable for a polishing disc, about 300 r.p.m. maximum, to enable better control and reduce throw-off losses of abrasive.

For cleaning the specimen, a stream of alcohol was directed on to the surface from a squeeze bottle. The method of drying the washed surface is important since it must be carried out without causing strain. A

standard technique is to warm the specimen under a stream of hot dry air. A hand hair-dryer which conveniently supplies a stream of either hot or cold dry air was used.

When a specimen surface is mechanically polished, an amorphous, glass-like surface layer is formed. The damaged layer present on the surface is always shallow. This layer has associated with it a high strain-induced anisotropy and for most metallic materials, this strain-induced anisotropy overrides the normal magnetocrystalline anisotropy of the specimen. It is essential to remove this damaged layer by a very brief chemical or electrochemical polishing treatment.

5.4.3 Chemical polishing

To remove strain and scratches and also any secondary effects which appeared on the surface of the gadolinium crystals, a technique of chemical polishing was used. This was considered preferable to the alternative of vacuum annealing both from the point of view of convenience and also the avoidance of any further contamination. A technique of chemical polishing suggested by Roman (1965) was adopted in this work using a solution containing the following

20 ml	lactic acid
5 ml	phosphoric acid
10 ml	acetic acid
15 ml	nitric acid
1 ml	sulphuric acid

Water should not enter this solution during the preparation

or in subsequent use and acids should be highly pure.

Polishing was done by using a cotton swab, wrapped around an end of a glass rod, soaked in the above solution and moved gently over the surface of the specimen. This was carried out for a few seconds after which the specimen was rinsed carefully with a stream of alcohol on to the surface from a squeeze bottle. The specimen was then dried in a stream of warm air.

It was then examined under a microscope and the process repeated until a satisfactory surface was obtained. This solution could be stored for a long time. It should be kept in an open container such as a small glass beaker. If the constituent acids are impure the solution may damage the surface so that it needs repolishing mechanically. If the damage is not deep it may require mechanical polishing for only the finer grade ($1/\frac{1}{4}$) and not for a long time.

5.5 Apparatus

5.5.1 For wet colloid technique

The conventional colloid method of studying domain structures on the surface of bulk specimens of ferromagnetic metals relies on the field inhomogeneity at the domain boundaries. These boundaries attract the very small single domain ferromagnetic particles. They are decorated by these small particles which can be observed by an optical microscope. It is obvious that the domain walls will be observed rather than domains. However, if a small field is applied

perpendicular to the surface under examination the small particles will be polarized and in turn attracted and deposit preferentially on domains magnetized in directions such that the free surface has a suitable polarity. This technique is known as the Bitter technique after its originator. It has been applied to the study of domains at room temperature and for many magnetic materials. The wet colloid Bitter technique cannot be applied at very high or very low temperatures. The colloid particles produced by the Elmore method (1934) are of Fe_3O_4 which is ferrimagnetic. They have a diameter of nearly 100 Å and are suitable for the observation of domain walls in Gadolinium. A suitable suspension liquid is secondary butyl alcohol. This liquid does not freeze until it reaches 184 K which is below the Curie temperature of gadolinium. In this work it has been used for temperatures down to 220 K.

The arrangement for observing domains in this range of temperature is shown in figure (5.1). A chamber of brass with two side tubes was used. In a depression on the top side of this brass chamber the specimen was placed. Through a small hole in one side near the top a thermo-couple was joined to measure the temperature of the specimen. The brass block was of cylindrical shape with a diameter of 1.5 cm and the length of its axis was 3 cm. It maintained a fairly constant temperature and was cooled by nitrogen gas passing first through a copper spiral tube immersed

FIG. (5.1)

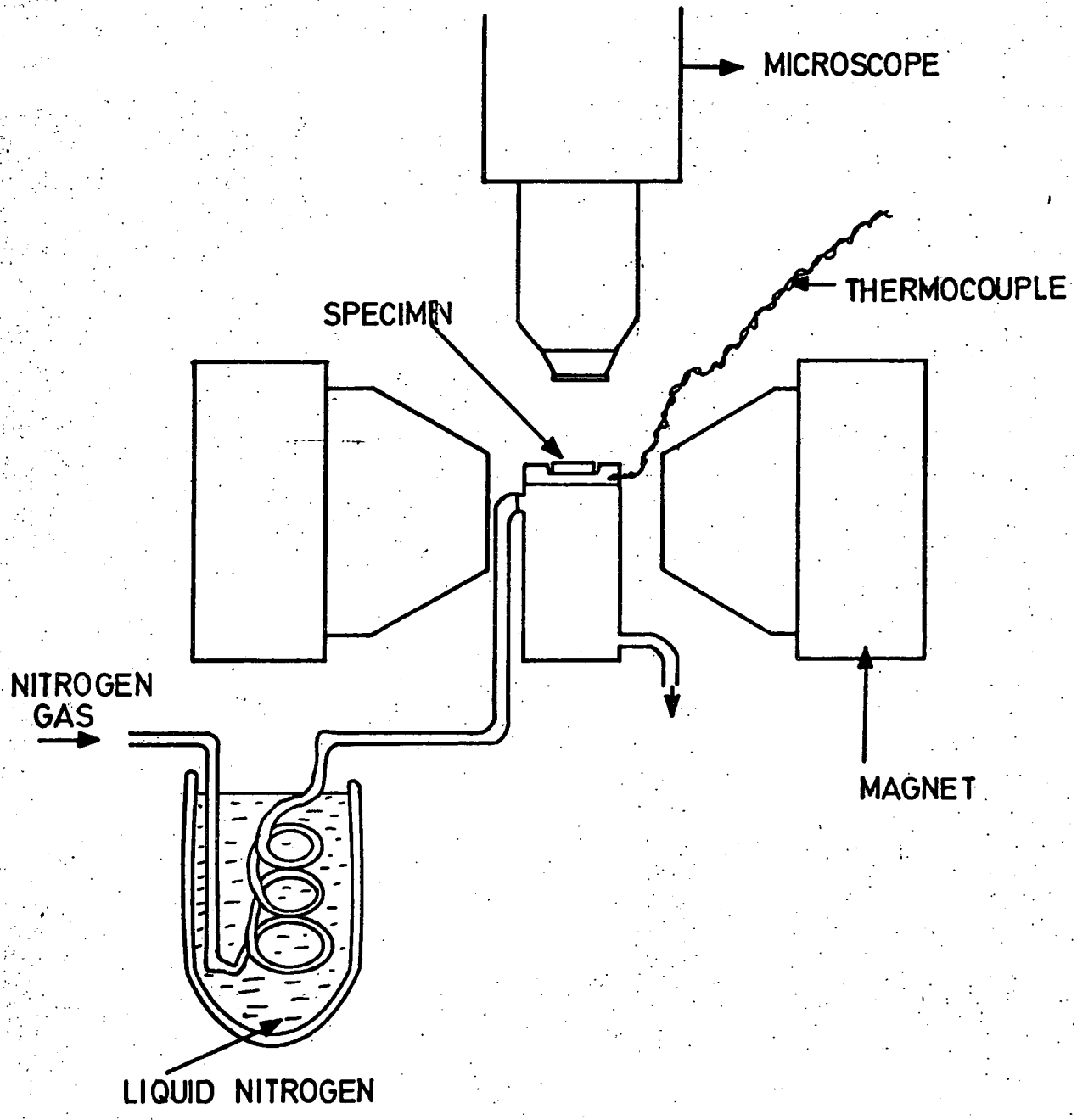

APPARATUS FOR WET COLLIOD TECHNIQUE.

in liquid nitrogen. Alternatively it could be cooled by air passing first through a spiral tube immersed in ice or dry ice. A specific temperature was obtained by controlling the rate of flow of the cooled nitrogen gas or air. The magnetic field used in this case was provided by a permanent magnet for a fixed value and an electro-magnet for variable values of the magnetic fields. The sample on its mounting and the magnet were all mounted on the stage of the microscope. This method can be used for observing the changes in structure or movement of the domain walls according to the variation of the temperature or the value and the direction of the applied field.

The staining of the surface by the colloid was not a serious problem as this took about half an hour. Often the complete experiment could be carried out in this period. If this was not possible, the surface could be cleaned by soaking the crystal in absolute alcohol.

The domains were observed using a Cook reflected light microscope at magnifications varying from 50X to 400X, although the most useful magnification was found to be 120X.

Photographs were taken with a Praktica LTL 35 mm camera which was coupled to the microscope by means of an adaptor with a focusing eye piece. The camera has through-the-lens metering so that exposure times could easily be determined. The films used were Ilford FP4 and HP4, chosen for their high contrast and small grain size. The FP4 was developed using a fine grain Paterson "Acutol" developer for seven and a half minutes

while HP4 needs about eleven minutes in the same developer. This solution was diluted one to ten parts of water and the developing temperature was 20°C. The film was then washed and fixed in Kodak "Unifix" fixer, diluted one to three parts of water for ten minutes. In order to calibrate the system, photographs were taken at various magnifications of a small scale with 1 μm divisions. The photographs were printed on high contrast Kodak paper of grade 4.

A suitable magnetic colloid had to be developed for the wet colloid studies. The colloid was prepared following the recipe of Elmore (1938). However, after preparation the magnetite was separated by filtration and washed carefully using secondary butyl alcohol. This has the advantage that it does not react with rare earth metals and has a freezing point of 184 K. It was therefore used as the suspending fluid. The colloid used by Bates and Spivey (1964) using methyl-cyclohexane stabilized by sodium oleate as a suspending liquid for observing domain in gadolinium was useful, but it easily evaporated and on this account it was found difficult to use. The colloid prepared in this study was agitated in a bath by an ultrasonic tranducer for about one hour and a suitable very finely dispersed colloid was produced. This colloid did not stain the surface very quickly since its rate of evaporation was very low.

The colloid was put on the specimen surface by a small pipette. Then the colloid on the specimen surface was covered by a microscope cover slide to retain a uniform amount of the colloid on the specimen

surface. This served to spread the colloid into a thin film of suitable thickness to show clear contrast under the microscope. A drop of secondary butyl alcohol was placed on the top of the slide to prevent the formation of fog and frost when the temperature was reduced. The colloid used moved freely in the liquid under the cover slide. A small magnetic field, applied either perpendicular or parallel to the specimen surface and of the order of 100 Oe was used to increase the contrast of the patterns. It was found that the lowest temperature at which this colloid could be used was 220K. On reducing the temperature below this value the colloid particles became very restricted in their movement and they adhered to the surface regardless of the effect of the stray fields on the surface before the liquid froze at 184K.

5.5.2 Apparatus for dry colloid technique

The Bitter technique cannot be applied at very low temperatures. The technique used for producing magnetic domain patterns at low temperatures was based on that developed by Hutchinson, Lavin and Moon (1965) and this has been applied in the present work. The technique developed consists basically of evaporating iron or nickel on to the specimen surface in a chamber containing a small pressure of helium. It was found that when the evaporation is carried out in an inert gas of low pressure the deposit consists of very fine magnetic particles. Consequently these particles will deposit preferentially

on the surface of a ferromagnetic crystal at those regions where the local magnetic field strength is a maximum. The patterns obtained in the deposit will therefore give information about the magnetic flux distribution at the surface of the specimen due to the domain structure. Subsidiary experiments showed that once the pattern was obtained, subsequent field or temperature changes did not modify the pattern.

A schematic diagram of the apparatus which was used for production of the small ferromagnetic particles is shown in figure (5.2), the apparatus consisted merely of a vacuum chamber containing an evaporation source. The chamber was evacuated by a pumping system capable of producing 10^{-3} torr in the chamber. This system consisted of a two stage Edward's (model ED 50, no.A4403 - 614) rotary pump and small oil diffusion pump (model 102A, no.1653). The pressure was measured by Pirani guage. It is important that the specimen and its surroundings be very nearly at the same temperature. The chamber consisted of a 80 cm long stainless steel tube of diameter 7 cm and wall thickness 0.1 cm. The tube was reinforced by rings of brass of 0.25 cm thickness and 1 cm width, soldered around the tube at distances of 10 cm between any two rings. The stainless steel tube was brazed, at its top end, to a brass plate to which was sealed a perspex disc of thickness 1.5 cm by means of an 'O' ring. Through the perspex were two vacuum-tight electrodes joined to two brass leads of diameter 0.5 cm and whose lengths could be varied. The current was supplied through these electrodes to the filament. A copper tube was joined to the perspex disc using an 'O' ring seal.

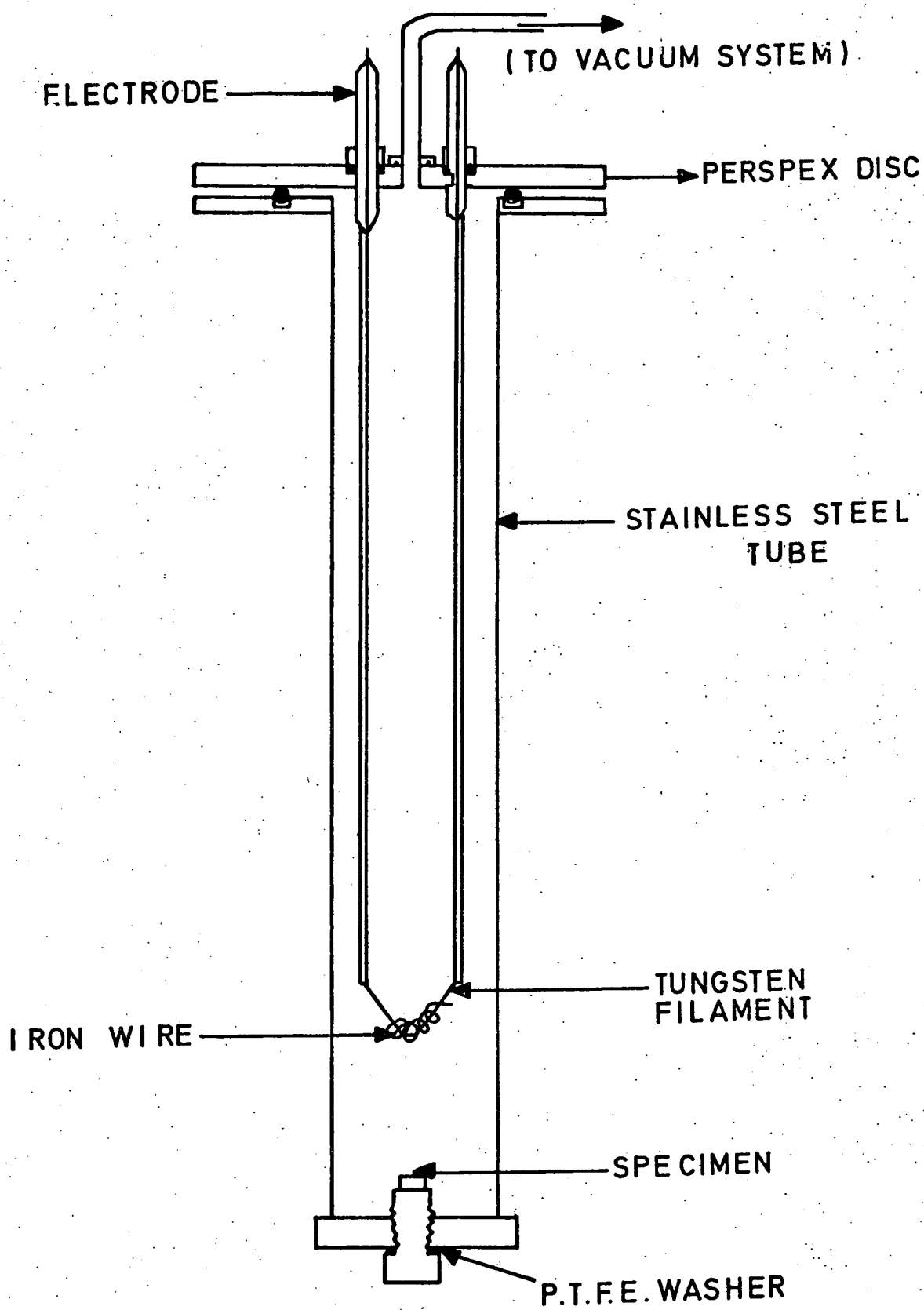

FIG. (5-2)

APPARATUS FOR DRY COLLOID TECHNIQUE

The copper tube was in turn joined to a vacuum system and a helium gas cylinder. The disc made of perspex was very useful since it is a transparent material which enabled the operator to see through and to control the amount of evaporation taking place. The evaporation heating source used consisted of a tungsten wire filament of diameter 0.1 cm bent into the form of a "V" shape. On this a very fine wire of iron of diameter 0.027 cm was wound. Iron was used throughout the experiment rather than nickel since the latter easily alloys with the tungsten filament. The "V" shaped filament was used to reduce the iron-tungsten contact area, thereby reducing alloying of the two metals. On heating the filament the iron melted and formed a bead. A large bead, corresponding to 7 cm length of iron wire, was used so that pure iron was evaporated from its surface. The quantity of iron evaporated was controlled by using standard evaporation times. For obtaining the best results the amount of iron evaporated must be optimized separately for each observation.

The high current supply consisted of a Variac connected to a large transformer with an input of 240 volts and an output of up to 130 amperes and 2 volts. It was found in this case that a current of 50amperes at 1 volt used at liquid nitrogen temperature gave the best results. For temperatures in the region of 25K the optimum current was larger and in the range of 70 amperes at 1.5 volts. The current was applied slowly to the heating source to ensure that the iron wire completely melted and formed a bead which slowly evaporated. The process was

terminated while the bead was still quite large to reduce the possibility of evaporating any alloy formed. It was also found that the optimum pressure of helium gas depended on the temperature. It is useful to flush the system with high purity helium before starting the evaporation of iron. If the helium was not of high purity iron oxide formed. In this work it was found that three stages of flushing helium gas were very satisfactory. The helium gas was inlet to the stainless steel tube through a needle valve, so it was easy to adjust the pressure of the helium gas to the desired value. It took between five and ten minutes for the iron particles to deposit on the surface of the specimen.

The specimen was placed on a brass rod which was screwed into the end of the stainless steel tube. This brass rod had a very large and heavy top to ensure temperature uniformity. A washer of PTFE of thickness 0.1 cm was used to ensure a tight vacuum seal. In a redesign of the apparatus to allow lower temperatures to be achieved it was decided to seal the bottom of the tube and put the specimen on another holder inserted through the top of the tube. This specimen holder consisted of a brass disc, of diameter 5 cm and thickness 0.5 cm, and three brass strips soldered to its circumference and joining it to a brass ring of the same diameter.

For low temperature observation of domains, the stainless steel tube was immersed in liquid nitrogen or dry ice. This ensured an equilibrium temperature between all the objects inside the stainless steel tube.

It is useful to leave the liquid surrounding the tube long enough to maintain steady state temperature and in the same time to allow the domain structure to stabilize. It was found that about twenty minutes are enough to obtain this condition.

After decoration, the specimen was warmed up to room temperature by directing stream of hot air onto the end of the tube. It took about half an hour to warm the tube. Then the crystal was removed from the apparatus and the domain patterns examined by the optical microscope. Photographs were taken as before and it was noticed that the patterns were clearer in this case than with wet colloid.

5.5.3 Temperature measurement

Throughout the major part of this study, temperatures are measured using a copper/constantan thermo-couple. Both thermo-couple wires are insulated with PTFE sleeving, and the junctions are soldered. For the wet colloid work temperatures were measured using a Noronix direct reading temperature meter. For the dry colloid observations the thermo-couple e.m.f. was measured either by means of Pye portable potentiometer or by a Solartron digital voltmeter, and temperature then obtained from a calibration chart. The direct reading meter will measure down to 77K, but the other methods give results down to 4K.

The reference junction was placed in a dewar containing a mixture of water and ice or liquid nitrogen, dependent on the measuring range of temperature. The other sensing junction is held as close to the specimen

as possible in order to prevent temperature lag. This is achieved by threading both thermo-couple wires down inside the stainless steel tube and attaching the junction to the base of the specimen holder. The thermo-couple wires were passed through home-made vacuum seals in the perspex disc. These permitted the use of continuous runs of wire and avoided spurious e.m.f.'s due to joints.

5.5.4 System for observing domains below 77K

The apparatus was modified so that it could be used at lower temperatures than that of liquid nitrogen. This was done, as in figure (5.3), by surrounding the tube by two double-walled Pyrex glass dewars. The inner dewar vessel contained the liquid helium, around this was a dewar vessel full of liquid nitrogen. Both the two dewars were silvered and clear slits ran vertically. The evaporation tube was joined at its top end to a brass disc. This disc lay on another large disc which formed the top of a housing for the top of the dewar of liquid helium, the vacuum was sealed by an 'O' ring between the two discs. The liquid helium dewar was sealed to the housing by a rubber tube sleeve, its diameter being slightly less than the dewar diameter. The dewar was also sealed by being held against a flat surface ring inside the housing.

The housing was usually supported rigidly on a framework and the helium dewar hung from the housing. The supports on which the dewar hung were made of cotton cloth strips which do not conduct too much heat into the cryostat. The evaporation tube was mounted eccentrically

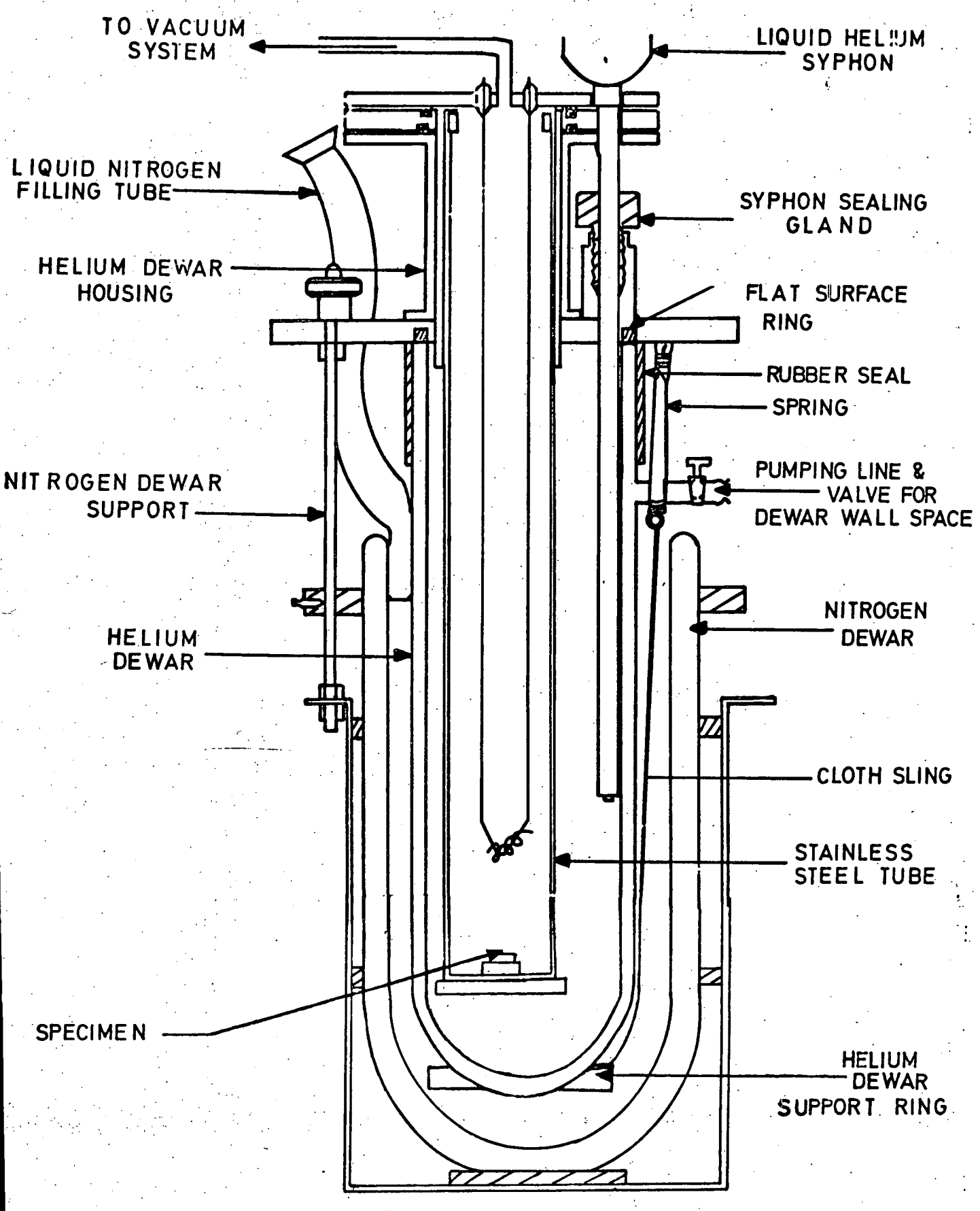

FIG (5-3)

APPARATUS FOR OBSERVING DOMAINS BELOW 77K

inside the dewar vessel with a clearance of about 0.5 cm on one side and 3 cm in the other. The tube could easily be removed by undoing the 'O' ring seal, between the disc and the housing, and withdrawing it.

The amount of liquid helium used depends on the dimension of the stainless steel tube. For the initial cooling of this from 77K it was estimated that two litres of liquid helium would be required. An additional two would be required to fill the inner dewar to a reasonable level. The cryostat was made fairly long, so that the top, which is at room temperature, is well separated from the level of the liquid helium. This reduced the rate at which the liquid helium evaporated.

The tube could be put back if necessary, while the cryostat contained liquid helium, though some gas would be lost during this process. Before inserting the tube, it should be pre-cooled by immersion in liquid nitrogen for some time.

The procedure for cooling down the tube was as following. The tube was first pumped out when the sample was inside, by joining the tube to the vacuum system. With the whole system at room temperature, space inside the helium dewar was then pumped out through an exhaust tube (not shown in figure 5.3) with a rotary pump. The inner dewar was then filled with helium gas from a gas cylinder. It was then re-evacuated and helium again admitted. This flushing out process could be repeated several times to be sure that no air remained in the dewar. The space between the walls of the helium vessel was evacuated with a rotary pump and then helium was admitted to this also.

Before syphoning in liquid helium, the system must be pre-cooled, and this was accomplished by filling the outer dewar with liquid nitrogen. The amount of helium left between the walls of the inner dewar conducted the heat away from the inside of the dewar, so that the contents cooled to the temperature of the liquid nitrogen. This cooling normally took two to three hours at least. After the inside of the inner dewar had cooled it was re-evacuated and fresh helium gas was admitted from the gas cylinder. The space between the walls of the inner dewar was then evacuated to ensure that no helium gas remained between the walls. A small pressure of helium would be enough to spoil the heat insulating properties of the inner dewar.

Liquid helium could then be transferred through a syphon which entered the dewar by way of a gland in the dewar housing (Figure 5.3). The syphon was a demountable one of stainless steel which was in place throughout the evacuation process with its outer end sealed by a rubber bung. In order to transfer liquid helium the bung was removed and the other half of the syphon, already in the helium transport dewar, was joined to the part attached to the cryostat. The section in the helium dewar passed through a tube with a football bladder and a release valve connected to the gas space in the transfer dewar. Transfer could be initiated by closing the valve and squeezing the bladder and stopped by releasing the valve. When enough helium had been transferred the syphon could be uncoupled and the rubber bung again used to close the part attached to the cryostat.

When the temperature reached the desired value evaporation

of the iron took place in the manner previously described. Then the tube was taken from the cryostat and warmed to room temperature while the sample was in it. Then the sample was removed and the surface of the crystal observed under the optical microscope.

5.6 Particle formation

To prepare fine particles, a metal must be evaporated not in vacuum but in an inactive gas at low pressure. The metal vapour thus produced is cooled in the gas and fine metal particles are formed like a smoke.

Investigation of the production of fine metal particles by this technique have been made by, amongst others, Tasaki and Wada (1965). However, it was necessary to carry out some preliminary experiments to discover the optimum conditions for the production of particles for the present purpose. The particle size in the experiments of Tasaki and Wada was controlled by changing the pressure of the helium gas. Particle diameter varied from about one hundred Angstroms at 1 torr to a few tenths of microns at 30 torr. Particles of ferromagnetic metals showed remarkable necklace-like arrangements at higher pressures of the inert gas. For decoration of domains single particles are required and investigation into appropriate conditions were carried out using electron microscopy to study the particles produced.

5.6.1 Experimental

Evaporation was carried out in the stainless tube

described before. After the air was evacuated from the work-chamber until a pressure of 10^{-3} torr was achieved, helium gas was introduced into it. The gas had a purity better than 99.9 per cent. The pressure of the gas in the chamber was varied between 0.07 torr and 3 torr. The metal evaporated was iron of 99.99% purity. The iron wire was of diameter 0.27 mm and of length 6 cm wound around the tungsten filament. The iron metal wire evaporated in about three seconds. As soon as the filament was heated, metal smoke was produced as shown in figure (5.4) provided that the gas pressure was higher than 0.05 torr. Some of the smoke went upwards due to the convection of the gas, while some moved downwards. Particles moved through only a limited distance below the filament and under the conditions of the present experiment, this distance was mainly determined by the gas pressure and the temperature of the gas and of the surrounding. It was found that at any fixed temperature this limited distance decreased as the pressure of the helium gas increased. At the same time it was observed that at a fixed value of the gas pressure this limited distance increased on decreasing the temperature of the helium gas and the surroundings. These effects are shown in figure (5.5) and figure (5.6). These were constructed by placing specimen grids carrying evaporated carbon films under the tungsten filament at different distances. The particles deposited on the grids were studied in an electron microscope. Most of the micrographs were taken at a magnification of X 20,000. For the grids

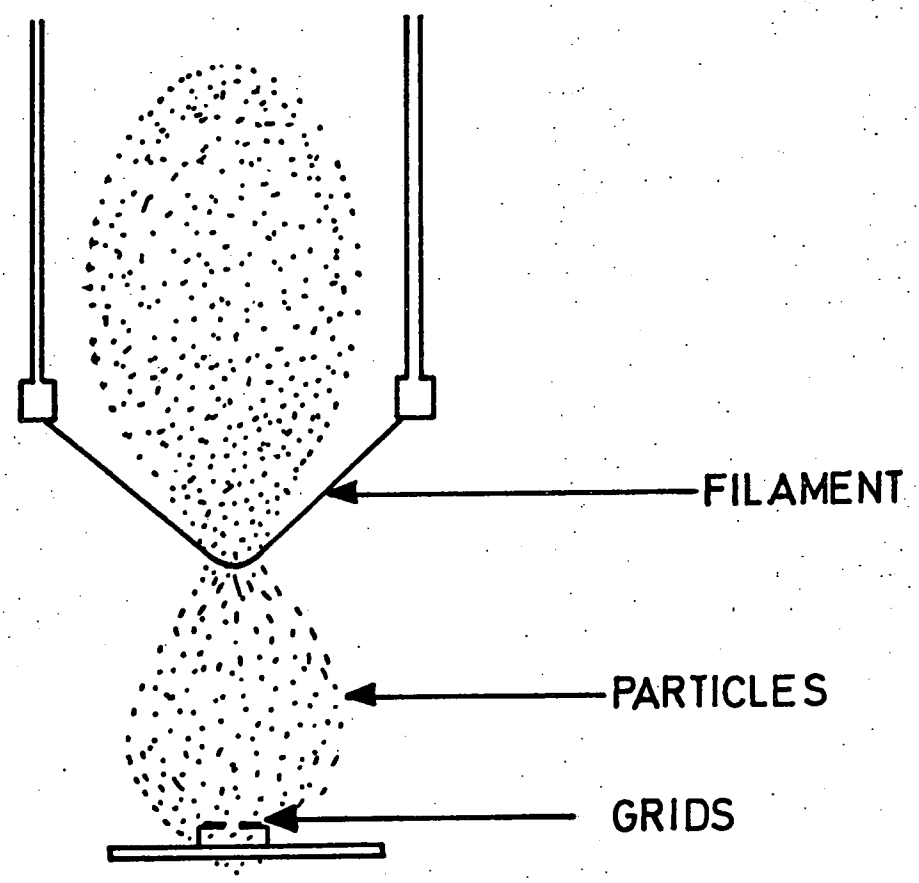

FIG. (5·4) PARTICLE FORMATION.
(AFTER KIMOTO et. al.)

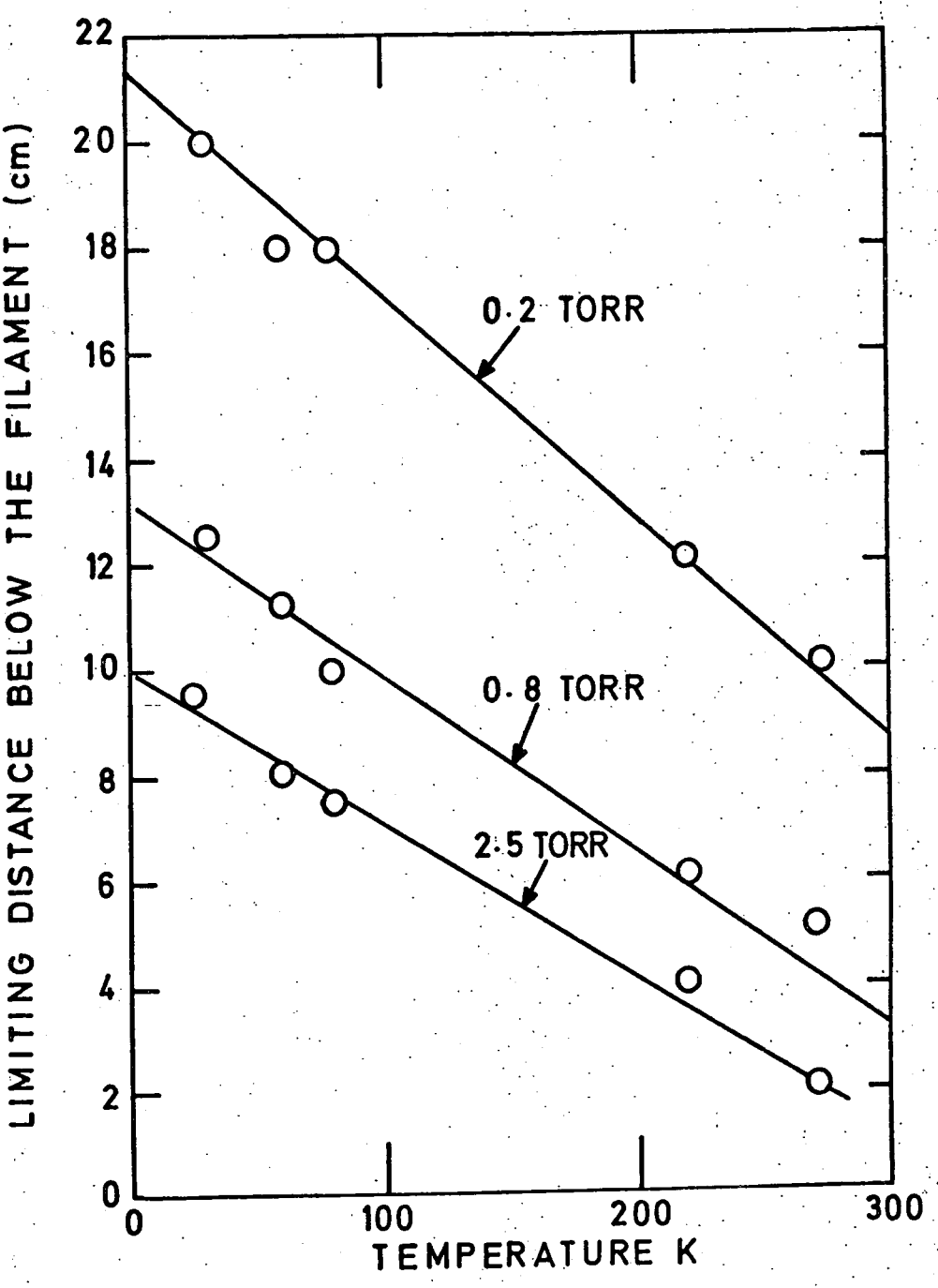

FIG.(5-5)

RELATION BETWEEN THE LIMITING DISTANCE BELOW THE FILAMENT AND THE TEMPERATURE

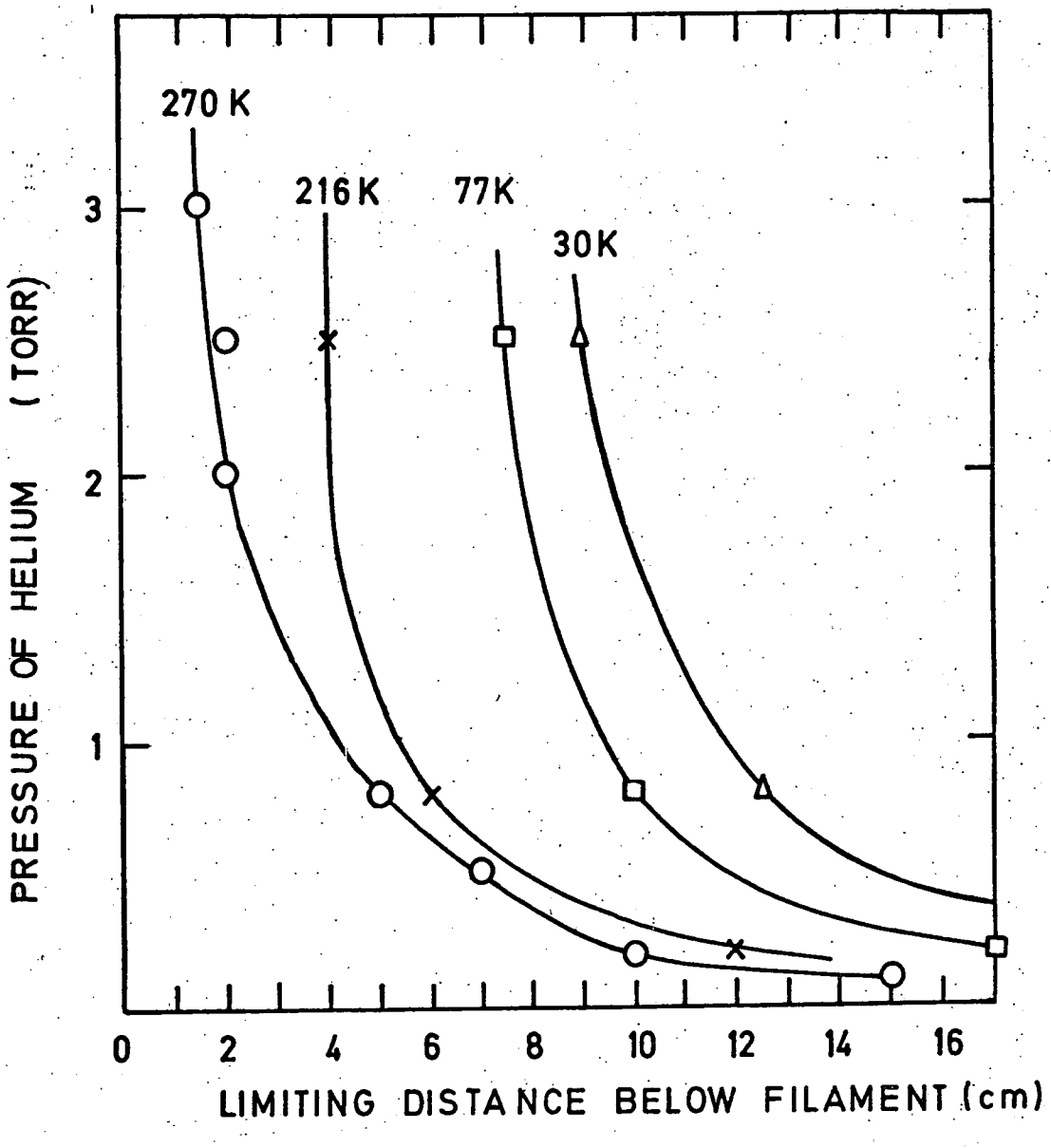

FIG.(5-6)

RELATION BETWEEN HELIUM PRESSURE AND THE LIMITING DISTANCE BELOW THE FILAMENT

outside the smoke, it was found that no particles deposited on them and only thin films were observed. A typical micrograph of a thin film is shown in figure (5.7), while figure (5.8) shows a deposit of iron particles. The results shown in figures (5.5) and (5.6) can be used to predict the most suitable location of the sample relative to the filament for a range of pressures and temperatures. The distance must not be much less than the limiting distance or a satisfactory deposit is not obtained.

Tasaki and Wada investigated the variation of particle size with pressure of the inert gas; their results are shown in table (5.1).

TABLE (5.1)

Helium Pressure torr	Particle diameter Å
0.5	80
3	300
35	2000

In a helium atmosphere the iron atoms coalesce to give small particles which have a resultant magnetic moment and experience a force in a field gradient. The smaller the particle the less domains it will contain and sufficiently small particles will be single domains, each behaving as a small permanent magnet.

Bergmann (1956) has pointed out that single domain particles in colloidal suspension are affected by two fields which influence their distribution on the surface

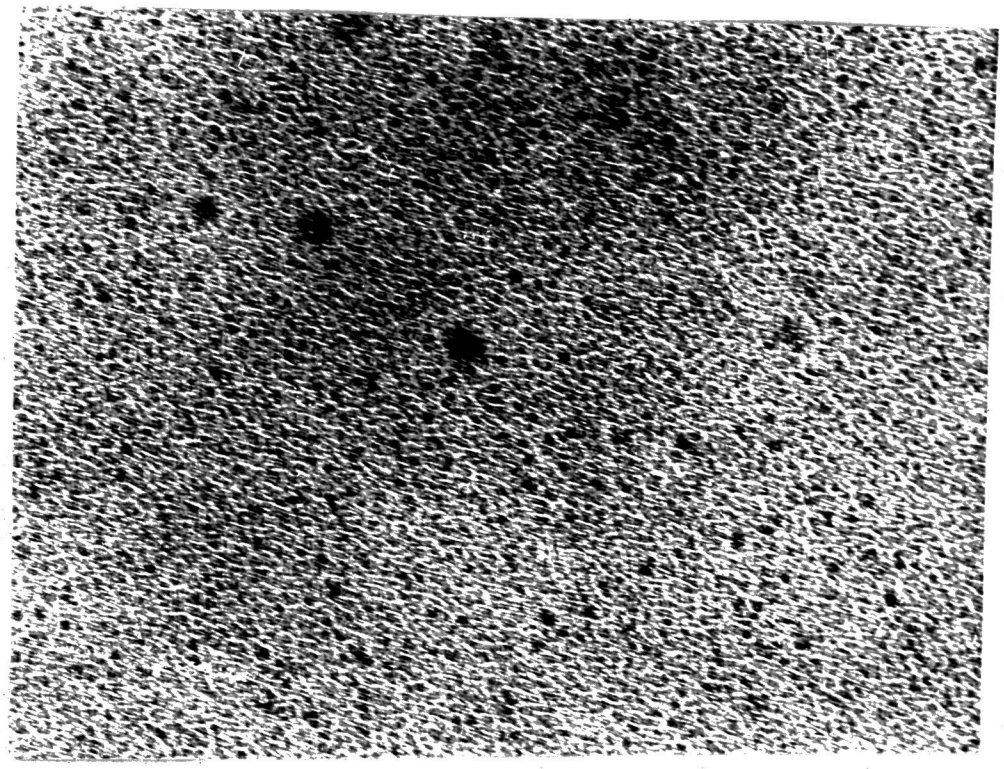

Figure (5.7) Micrograph of thin film

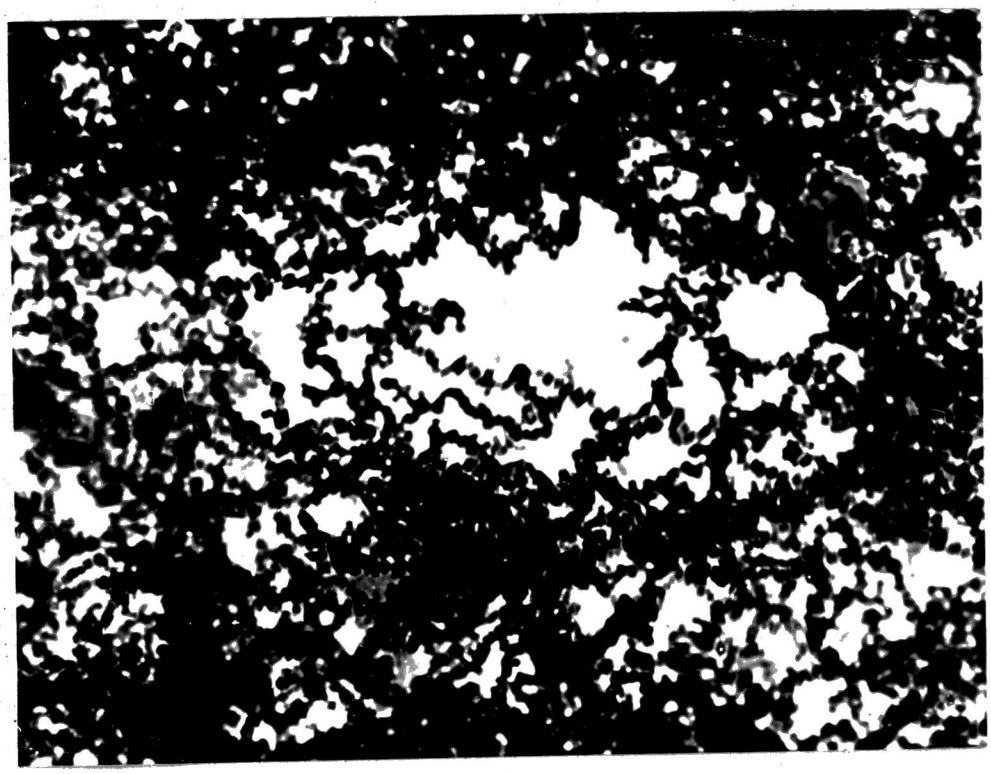

Figure (5.8) Deposit of iron particles

of a polished ferromagnetic specimen. These are the self field H_p of each particle and the stray fields H_w due to inhomogenities in the magnetization at the specimen surface.

For dry colloid the particle are not in suspension and they have a distribution of velocities. We suppose that the particles are in thermal equilibrium. We might use the same treatment as Bergmann when considering the interaction of magnetic particles as they fall onto the surface of a magnetic material. Thus to get patterns, it is required that the appropriate magnetic energy must be larger or smaller than the thermal energy. i.e.

$\mu H_w > 3\ kT$ for interaction between specimen and particles.

$\mu H_p < 3\ kT$ for interaction between particles.

The particle fields encourage the particles to aggregate, and thus reduce the magnetic moment. So that the aggregate plays no part in pattern formation. The magnetic moment of a spherical single domain particle of diameter d and magnetization I_s is given by

$$\mu = \frac{\pi d^3 I_s}{6}$$

The field H_p due to a spherical particle which acts on an adjacent particle is given approximately by

$$H_p = \frac{2\mu}{d^3}$$

The condition for particle aggregation is satisfied when $\mu H_p > 3\ kT$. This means that particles with diameter greater than d_e given by

$$d_e = 3\left(\frac{2\ kT}{\pi^2 I_s^2}\right)^{1/3} \qquad (5.1)$$

will form self closing aggregates and particles with

diameter less than d_e will be effective in formation of patterns.

There is a lower limit on the diameter of useful particles below which patterns cannot be formed for certain specimens. This is obtained from the condition $\mu H_w > 3 KT$.

Kittel (1949) estimated the magnitude of the stray field H_w at distance r above a 180° domain wall as

$$H_w = \frac{2 I_w \sigma_w}{r} \cdot \frac{2}{1 + \mu_w^*}$$

where $\mu_w^* = 1 + 2\frac{\pi I_w^2}{K_w}$ where I_w is the spontaneous magnetization of the specimen, σ_w the wall thickness and K_w the magneto crystalline anisotropy of the specimen. Bergmann deduced the lower limit of the particle diameter for pattern formation to be

$$d_w = 3\left(\frac{k\ T(1 + \mu_w^*)}{2\pi I_s I_w \sigma_w}\right)^{\frac{1}{2}} \qquad (5.2)$$

Thus clear patterns will be formed when $d_e > d_w$ and the particle size should lie between d_e and d_w. It is noticeable that the diameters (d_e or d_w) vary with the temperature. In Equations (5.1) and (5.2), for evaporation, inserting suitable values for the constants of iron particles on a gadolinium single crystal gives the following condition.

TABLE (5.2)

Temperature K	Range of particle diameter A°	Helium pressure torr
77	$26 < d < 27$	0.7
210	$30.6 < d < 37$	0.3
270	$40 < d < 41$	0.2

This narrow range of diameters was surprising, but it must be realised that the expressions used were only crude approximations and refer strictly only to the decoration of 180° walls.

The particle diameter at low temperatures was dependent on gas pressure. It appears that the diameter at a given pressure decreases on decreasing the temperature. This was found by varying the pressure to get the right diameter of particle for domain observations. The experimentally observed pressures are shown in the final column of Table (5.2). Sarma and Moon (1967) found that the mode of particle diameter was 40 A°, at pressure of helium of 1 Torr, at temperature 4.2 K.

CHAPTER SIX

EXPERIMENTAL RESULTS

The domain structure of gadolinium was first observed on a sample in which a large amount of oxide inclusion was present. Then successive samples were used, of considerably higher purity and containing little or no oxide. Clear domain patterns have been observed on all prepared surfaces. As explained before gadolinium is essentially different from the other rare earths in that it exhibits normal ferromagnetism over its entire ordering range. The easy direction is the c-axis between the Curie temperature 292 K and 240 K. Below 240 K the easy direction lies on a cone about the c-axis. Also the basal plane magneto-crystalline anisotropy constant K_4 has been determined by Darby et al (1964) and Graham (1967). It is found to be small and of order 10^3 erg/cm^3, at 90 K and does not contribute appreciably to the anisotropy energy above 160 K.

The present work will provide indirect evidence of the internal magnetic domain structure as well as the nature of the superficial domain at the surface. It includes studies of domain patterns in both the region of temperature in which the c-axis is the easy direction and that in which an easy cone applies. Also the results of a study of the effects of magnetic fields as well as variations of temperature are presented. The variation of the structure with the thickness of the specimen has also been investigated.

The sample was first mounted in the plastic as

mentioned in the previous chapter; after polishing the colloid was put on the surface at different temperatures. A typical domain pattern obtained at 273 K with a field of 300 Oe applied parallel to the surface is shown in figure (6.1). This shows the influence of inclusions on the domain structure. At very low temperature the difference between the elastic constants of gadolinium and of the oxide inclusions is thought to prevent the observation of domain structure. Work was therefore started on other samples which had been previously treated by solid state electrolysis and were nearly free from oxide inclusion.

6.1 Domain structure on surface containing the c-axis at 273 K.

Observations on this surface were made at a temperature where the anisotropy constant K_1 has nearly its maximum value. The magnetization at this temperature has a value of about 950 e.m.u. cm^{-3}. Clear domain patterns were observed at this temperature and there was no difference between the patterns observed on $(11\bar{2}0)$ and $(10\bar{1}0)$ surfaces, which are respectively a and b surfaces. This is not surprising since the material is nearly isotropic in the basal plane at this temperature.

The structure is shown in figure (6.2) on b surface, here the pattern consists of 180° parallel walls and the spacing was different at different regions on the surface. In figure (6.3) the pattern shown consists of 180° parallel walls, and in part of the figure domain contrast is seen. Due to applying a magnetic field which was

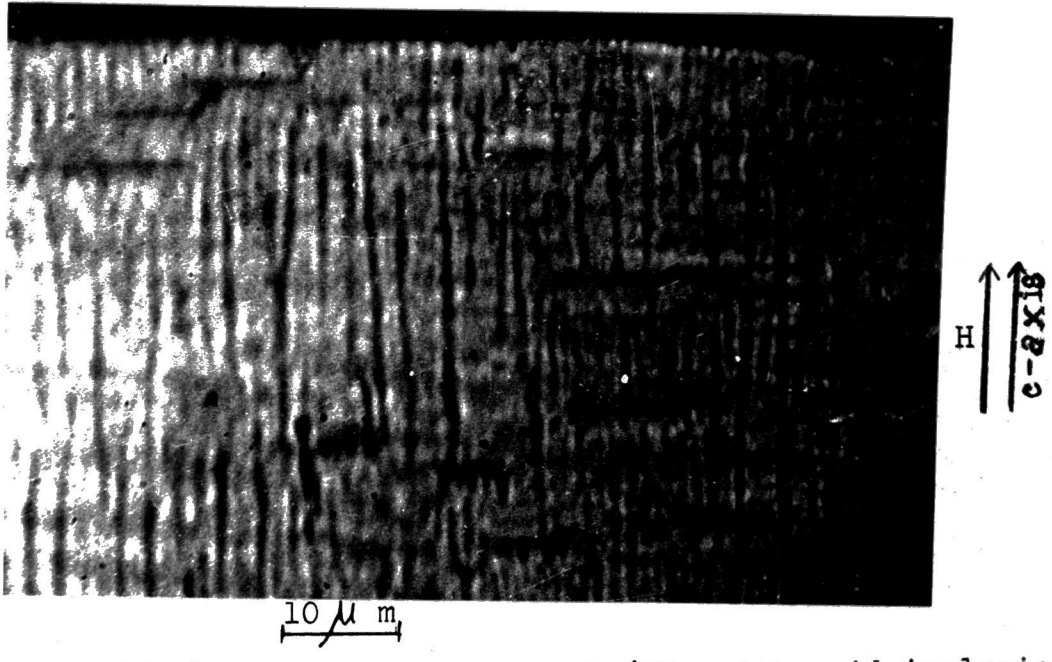

Figure (6.1) Wet colloid at 273 K (XI. with oxid inclusion) on b-surface specimen E.

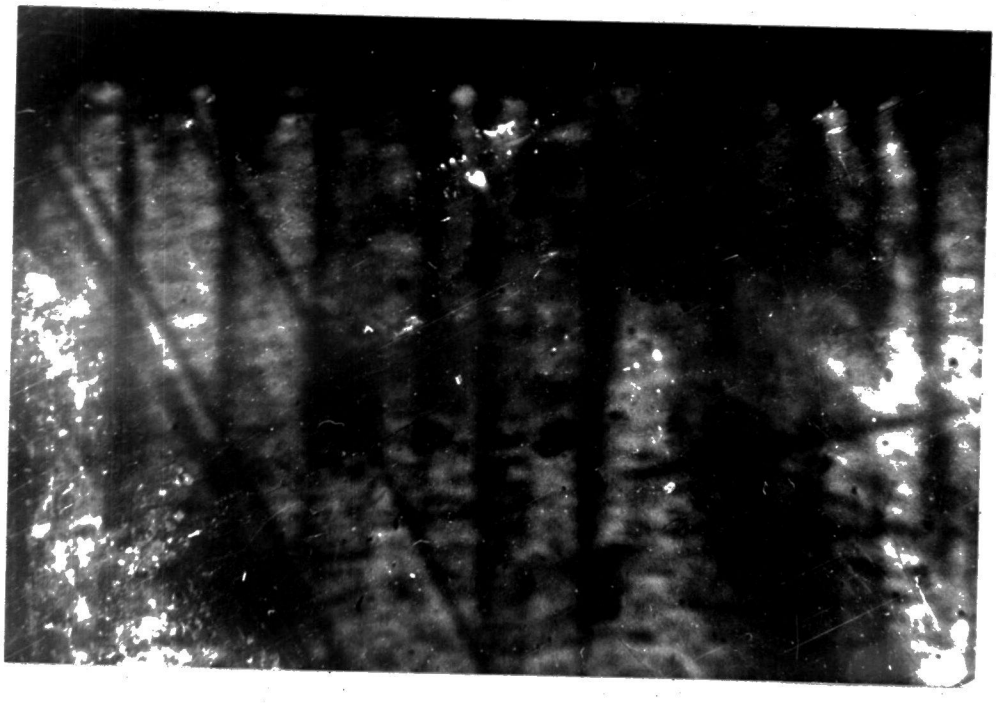

Figure (6.2) Wet colloid at 273 K on b-surface
H = 300 Oe specimen D

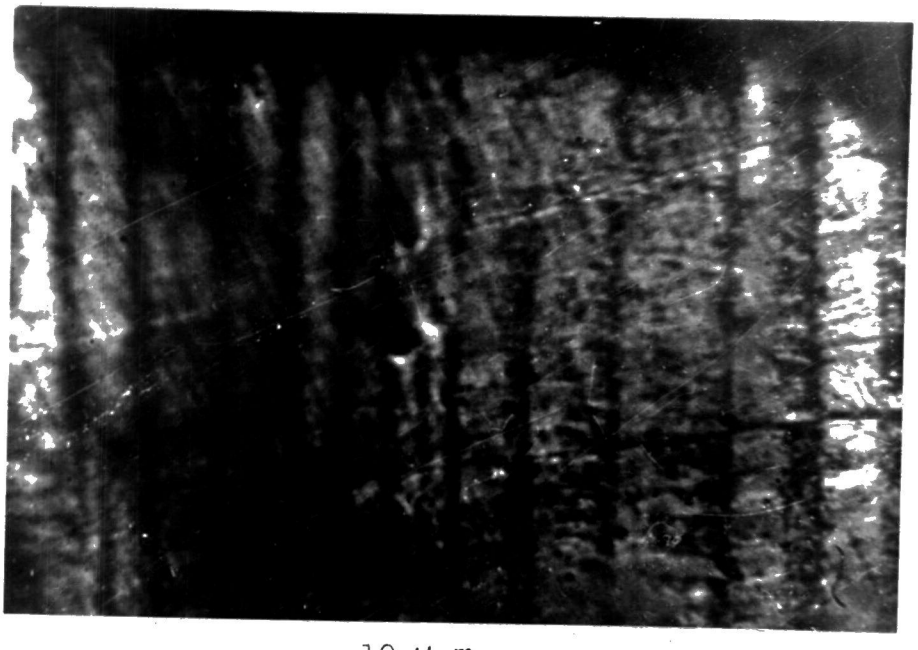

10 μ m

Figure (6.3) Wet colloid at 273 K on b-surface

H = 300 Oe specimen D

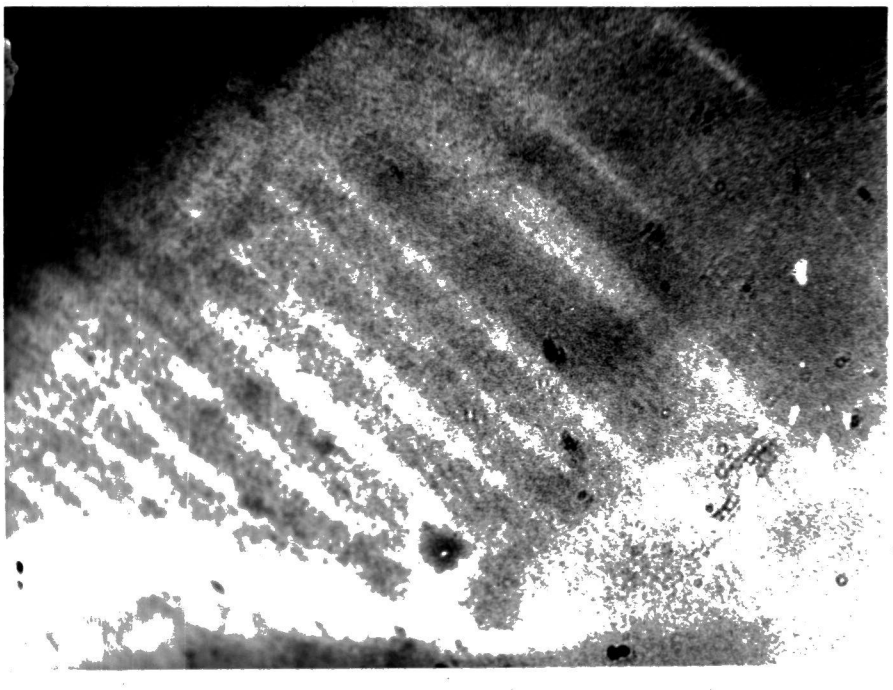

10 μ m

Figure (6.4) Dry colloid at 273K on a-surface

specimen A

not parallel to the surface but had a small normal component, the colloid was polarized and domains rather than walls could be seen. The magnetic field was in the c-axis direction of value 300 Oe. The spacing was greatly different at different parts on the surface, dependent on the presence of inclusions, and the inclination of the magnetic field to the surface. Figure (6.3) is near the edge of the surface, the formation of closure structure not clearly seen. There does not appear to be complete flux closure, but there are areas of free pole on the basal plane surface. From this figure there is no evidence for the formation of reverse dagger or closure domains.

Figure (6.4) shows some closure structure on a surface not containing inclusion, by using Dry colloid, near the edge of a - surface. Using another crystal the domain structure shown in figure (6.5), shows wall multiplication in the b-surface using wet colloid. The spacing of domain walls is seen to be much less near the free (0001) surface than in the interior of the crystal.

Figure (6.6) shows the effect of reducing the temperature on the patterns, using the wet colloid and a magnetic field of 300 Oe in the c-axis direction. This shows disappearance of domain walls as T→ 240 K. Below this temperature a new type of structure would be expected, but this is not clear at temperature 220 K. This was the lowest temperature at which the wet colloid could be used.

6.2 Domain structure on basal plane surface at 273 K

As may be expected of any uniaxial ferromagnetic

Figure (6.5) Wet colloid at 273 K on b-surface

H = 300 Oe specimen C

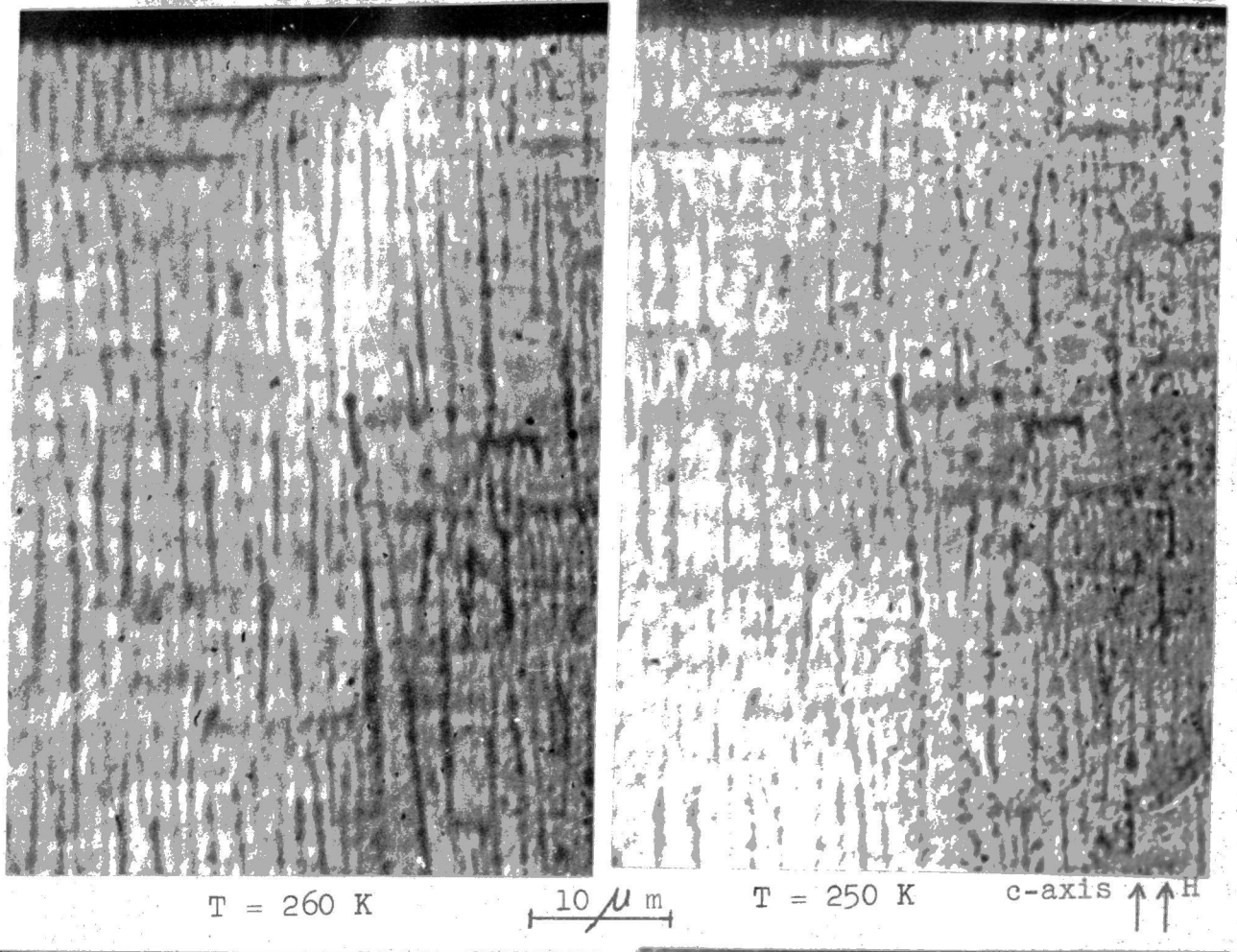

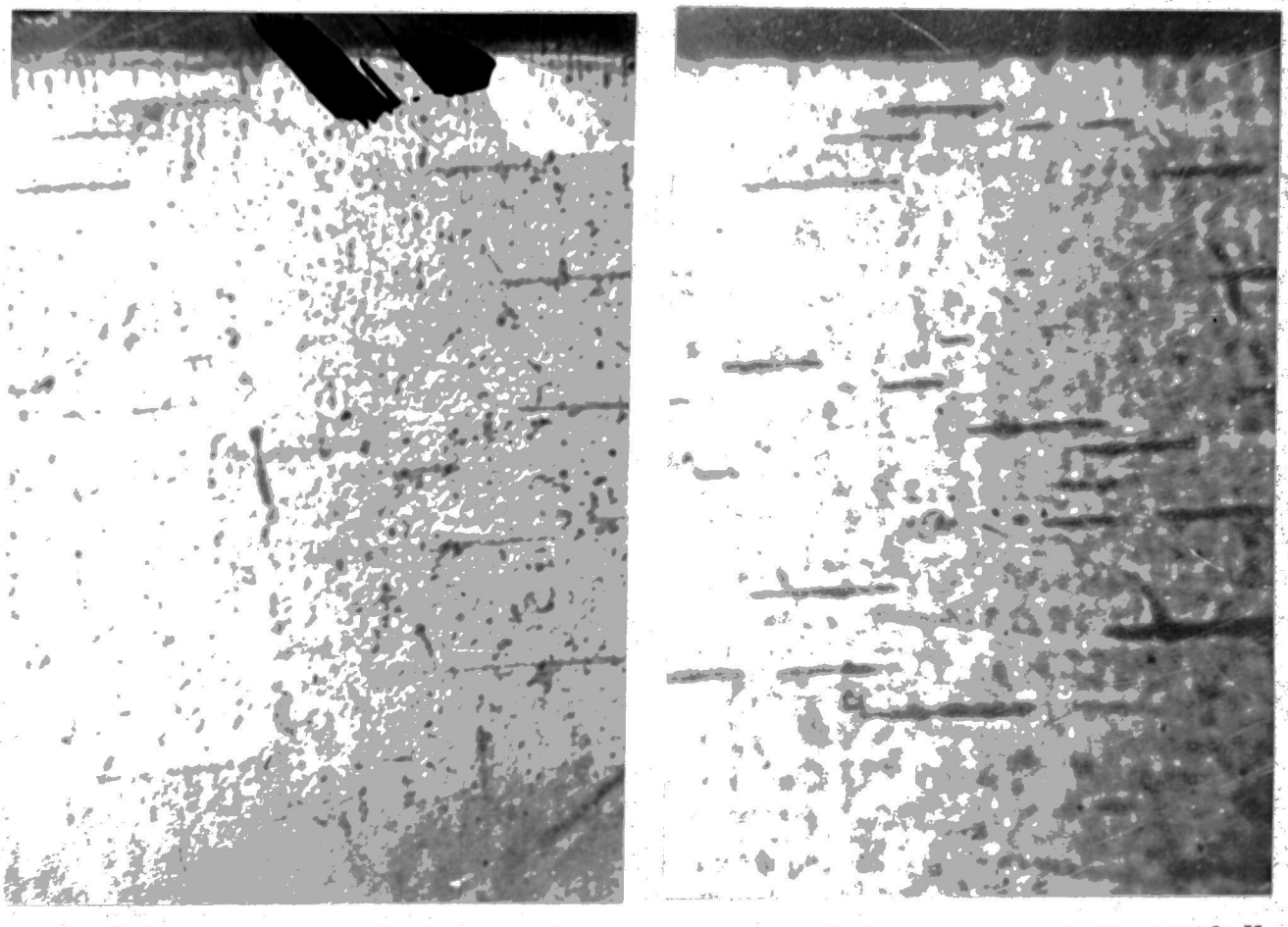

Figure (6.6) Effect of reducing the temperature b-surface
H = 300 Oe specimen E

material the pattern observed on this surface is complex, and there is no preferred direction of wall alignment, confirming the isotropy of magnetic properties in the basal plane at this temperature. Figure (6.7a) shows a pattern on the basal plane surface with magnetic field normal to the surface and of value 200 Oe, using dry colloid. The pattern is of honey-comb type with a general, but not complete, six-fold symmetry. This structure changes in a consistent fashion with the sample thickness as shown in figure (6.7b). This is consistent with other evidence that the size of domains depends on the crystal size. For thin crystals the domain configuration is small in size and as the thickness is increased the size of the pattern increases.

The surface structure observed is such as would result from a distribution of free poles and with little magnetization parallel to the surface. It is suggested that it is due to reverse domains on the ends of long thin domains of hexagonal cross-section. The effect of the change in crystal thickness on domain width will be discussed in detail later.

6.3 Domain structures on inclined planes to a b-surface at 273 K

The domain structure on a surface inclined to a simple crystallographic plane is expected to be somewhat complicated and to depend on the inclination of the surface. Figure (6.8 a - d) shows different types of domain at different places of a surface inclined at 10° to the b-surface with a magnetic field of 300 Oe applied in the direction of

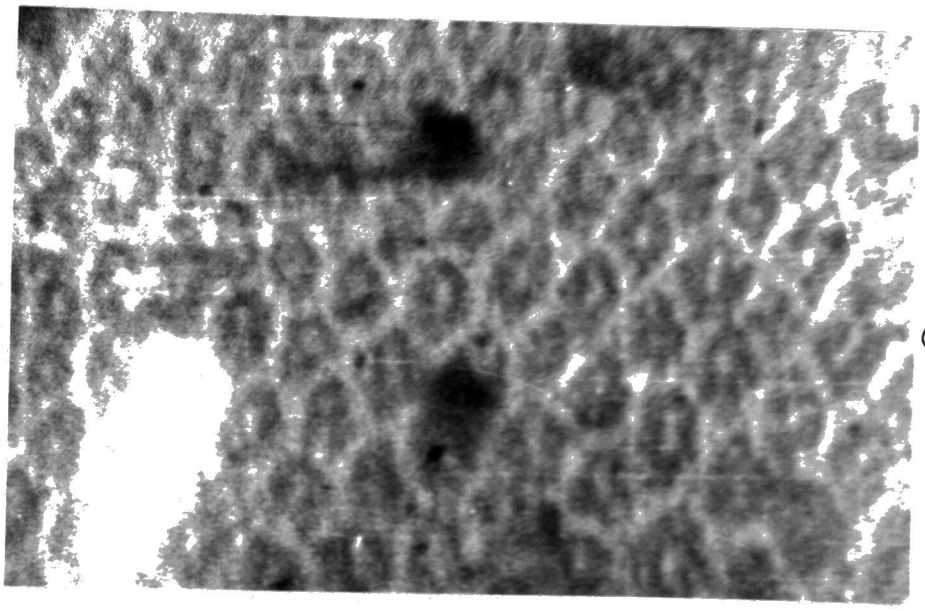

(a)
Crystal thickness
= 2 mm

10 μ m

H ⊗

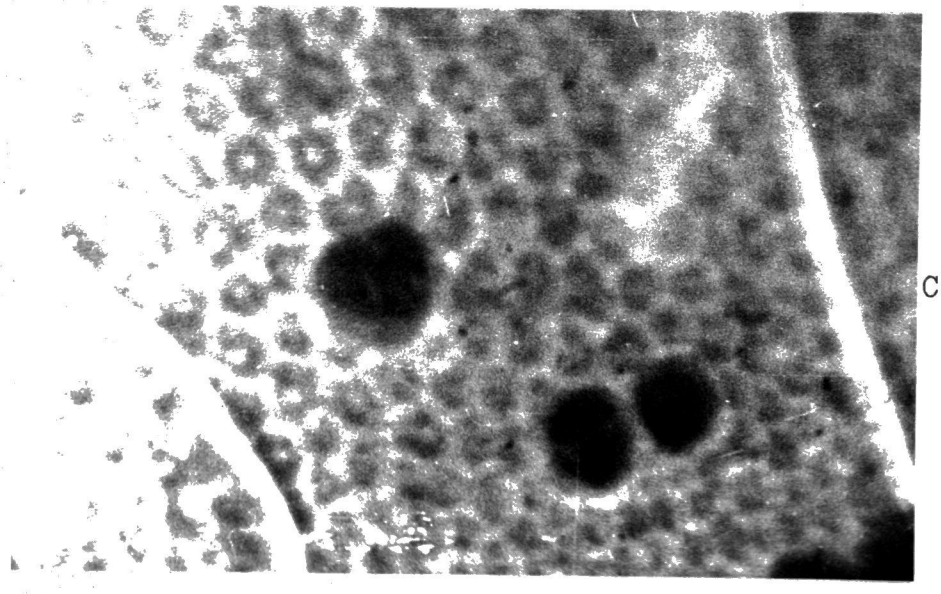

(b)
Crystal thickness
= 1 mm

Figure (6.7) Dry colloid at 273 K on basal plane

H = 200 Oe specimen A

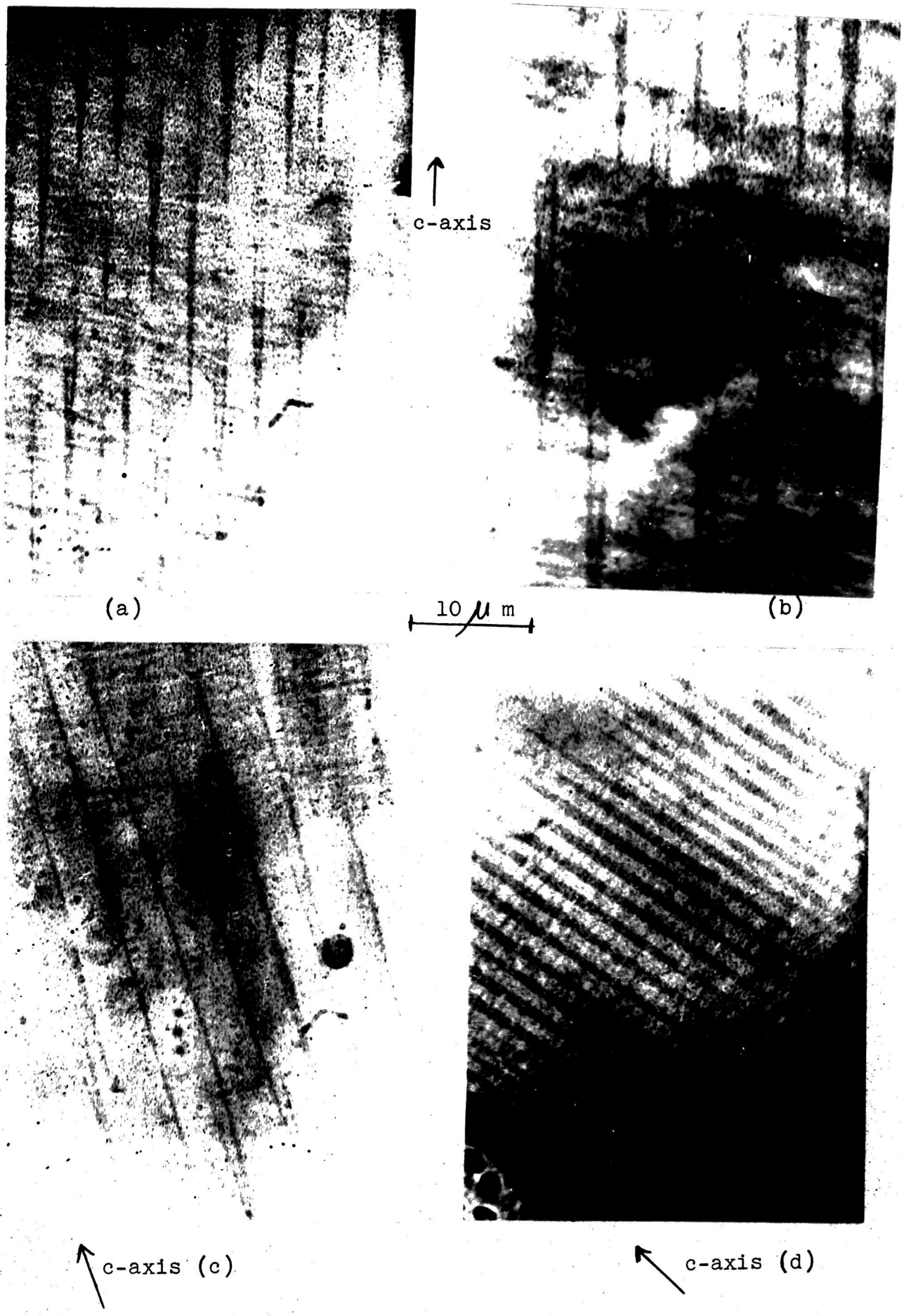

Figure (6.8) Dry colloid at 273 K on plane inclined to b-plane specimen B

the projection of the c-axis on the surface. These show clearly the existence of different sizes of dagger domain. Figure (6.8d) shows a structure near to a basal plane surface. The appearance of domain rather than wall contrast shows that there is a component of magnetization normal to the surface.

Figure (6.9) shows more complicated domain structures at different points on another crystal surface inclined with a larger angle 30^{o} to the b-surface. The applied magnetic field of order 300 Oe was parallel to the projection of the c-axis on the surface. It shows different types and sizes of domain including loops and daggers.

6.4 Domain structure on planes inclined to basal plane at 273 K

The domain on a surface inclined to the basal plane gave rise to a fairly regular but very complicated pattern. Figure (6.10a) shows domain on a surface inclined at 15^{o} to the basal plane. A magnetic field of order 200 Oe was applied normal to the surface. This shows a basic large scale structure of roughly hexagonal symmetry containing a complicated smaller scale structure. It appears that this is derived from the honeycomb structure seen on the basal plane, but including more complicated arrangements for the reduction of magnetostatic energy. Figure (6.10b) shows domains on the same surface of this wedge-shaped sample at a thicker part of the wedge. The effect of changing of the crystal thickness on domain structure is clearly seen, the domain structure

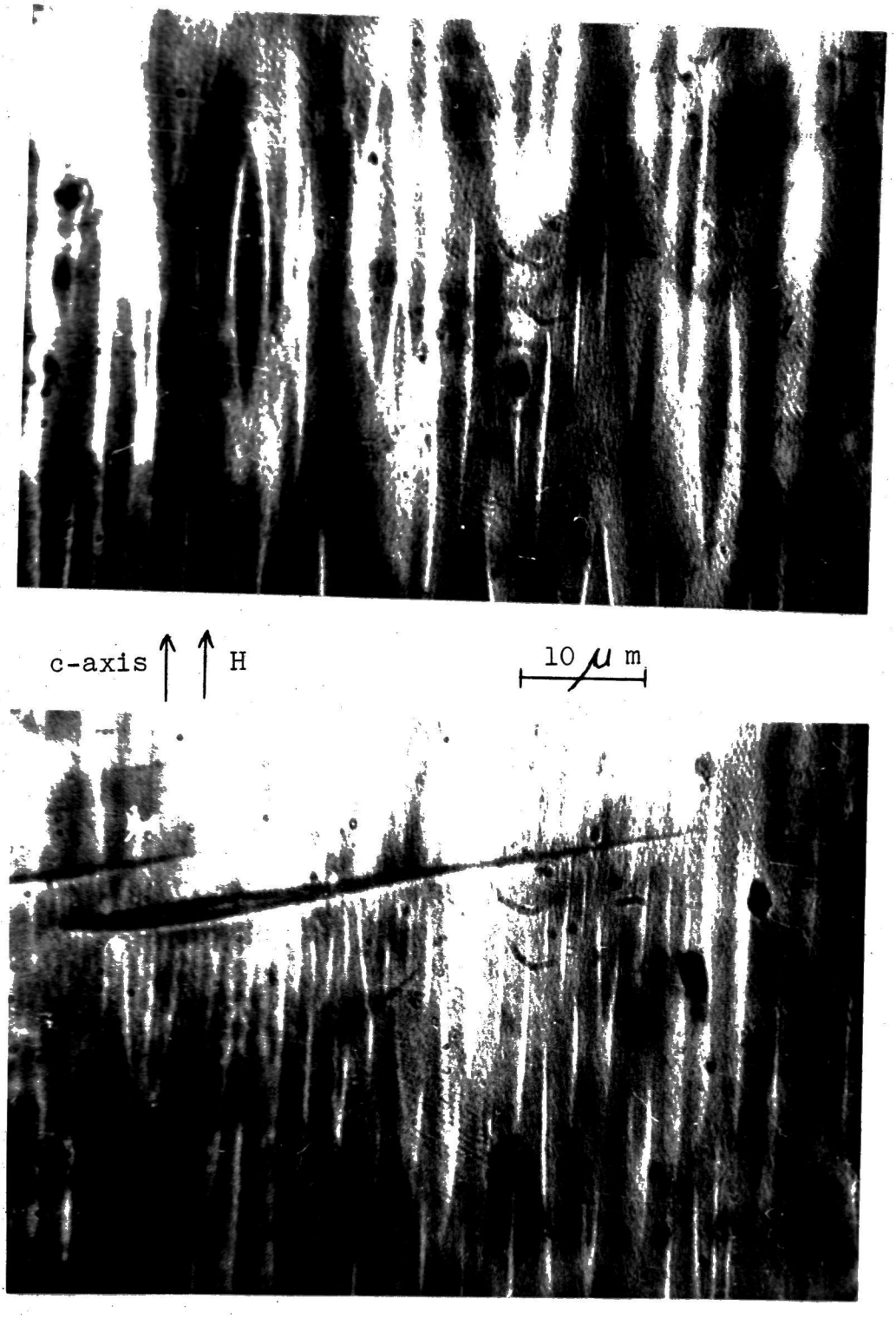

Figure (6.9) Dry colloid technique at 273 K on inclined plane to b-surface H = 300 Oe
specimen C

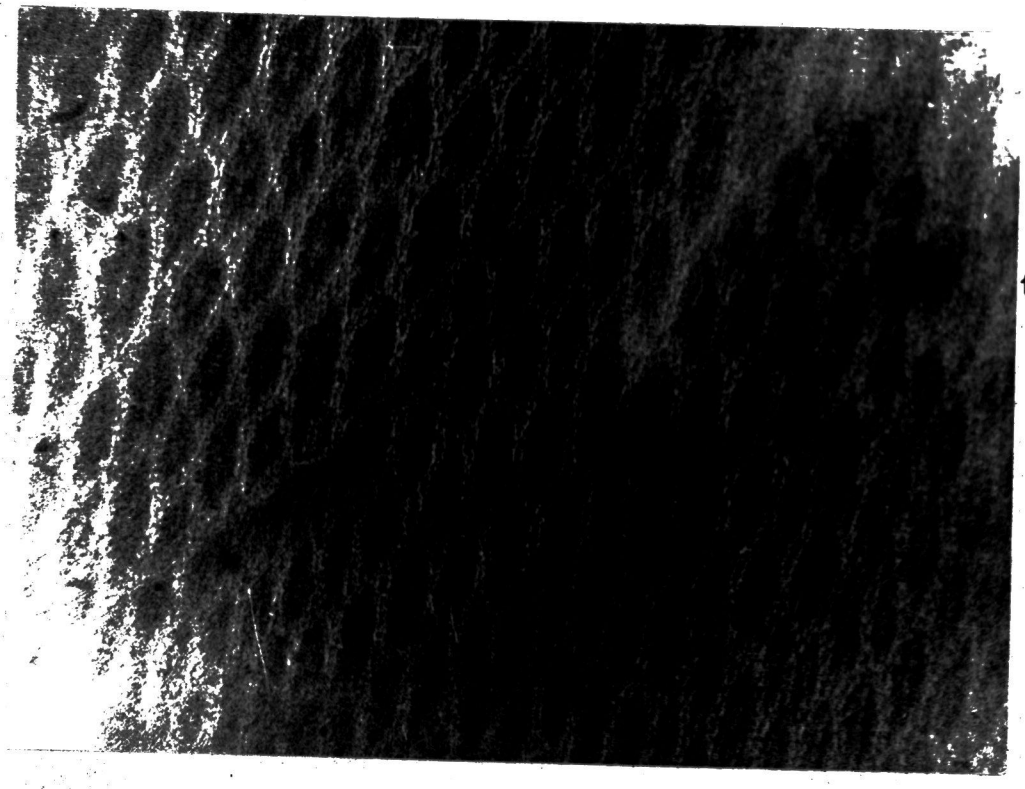

(a)
crystal
thickness =
1 mm

H ⊙ 10 μm

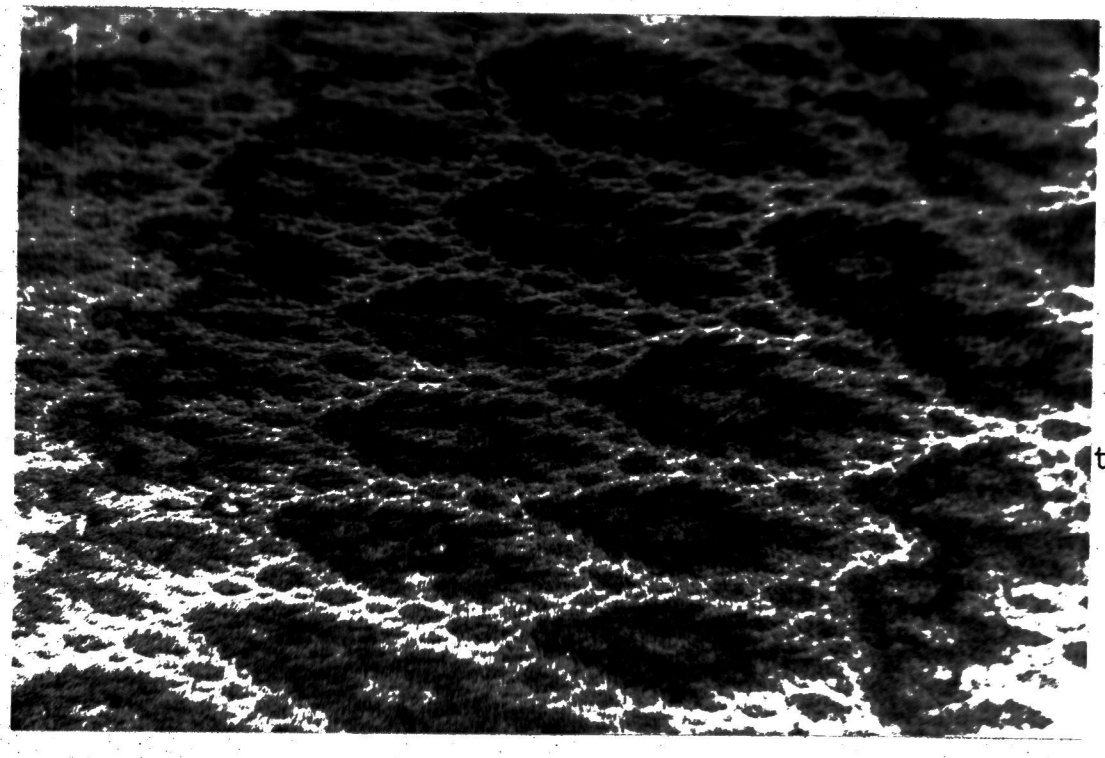

(b)
crystal
thickness =
4mm

Figure (6.10) Dry colloid at 273 K on surface inclined to basal plane H = 200 Oe
specimen A

remaining the same type but growing larger in size as the thickness of the crystal increases. Figure (6.11) shows another type of complex domain structure on a surface inclined by 30° to basal plane, and it is clear that it is different from that observed on the surface inclined at 15°.

6.5 Domain structure on b-plane at 77 K

Patterns were observed on both a-planes $(11\bar{2}0)$ and b-planes $(10\bar{1}0)$ but no differences were evident. Therefore only the detailed results on the b-plane will be presented here. At 77K as explained before the easy direction is on a cone with angle θ around the c-axis equal to 37°, according to Corner and Tanner (1976) figure (4.10) . Because of this the domain structure was expected to be different from that for the case of the c-axis being the easy direction. Figure (6.12) shows the domain structure observed on the surface containing the c-axis, with a magnetic field applied parallel to the surface and in the c-axis direction. These patterns show domain contrast rather than wall contrast with reverse or closure domains near the edge of the surface. Experiments with stronger fields showed a narrowing of alternate domains, but above 600 Oe contrast became so low that the patterns were no longer visible. The domain structure shown in figure (6.13) was observed on the same surface; in this case the magnetic field was applied normal to the c-axis direction but parallel to the plane of the surface. The domain structure is the same but

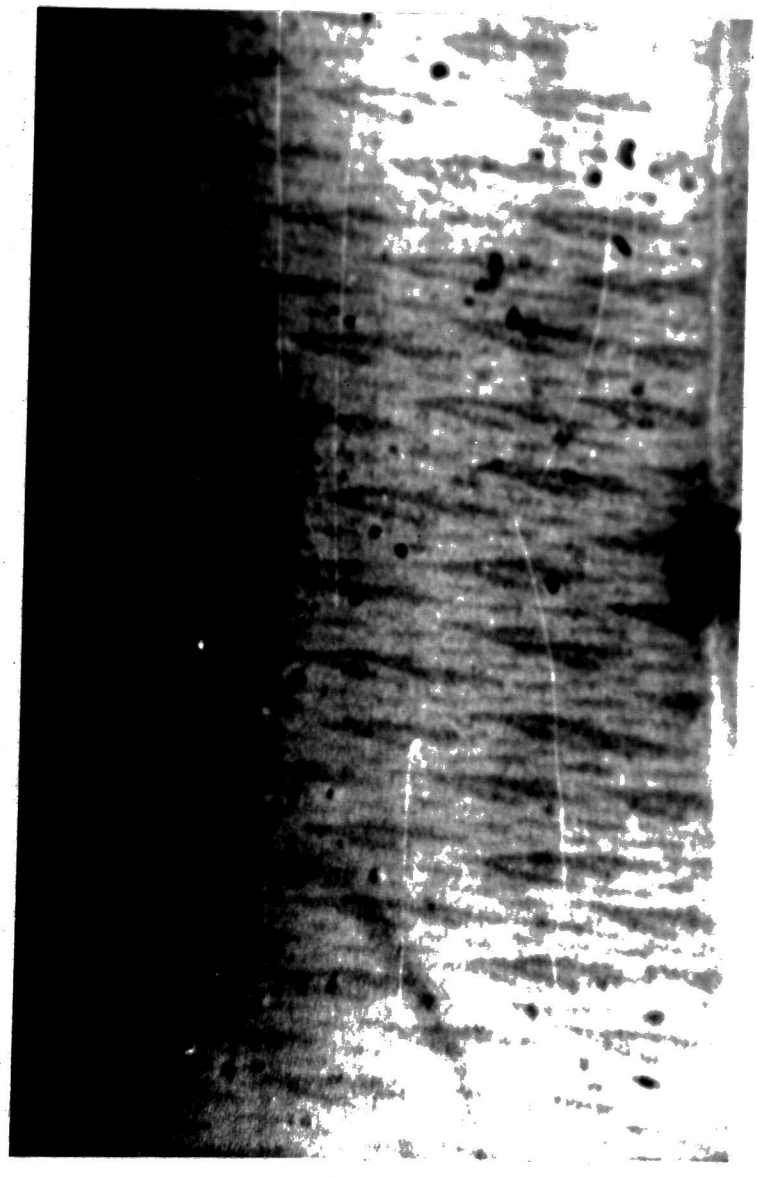

Figure (6.11) Dry colloid at 273 K on inclined plane to basal plane
H = 300 Oe specimen A

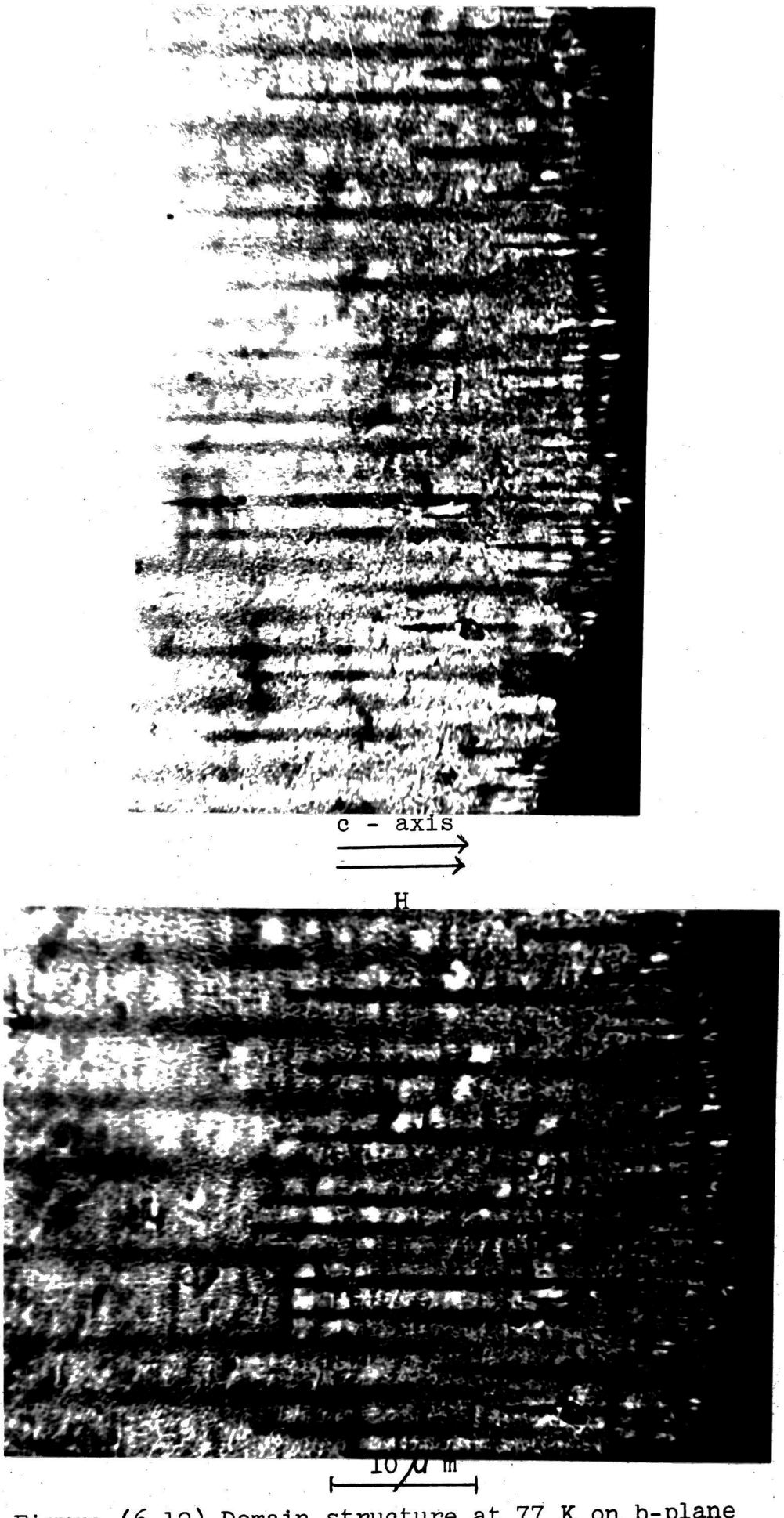

Figure (6.12) Domain structure at 77 K on b-plane
H = 200 Oe specimen B

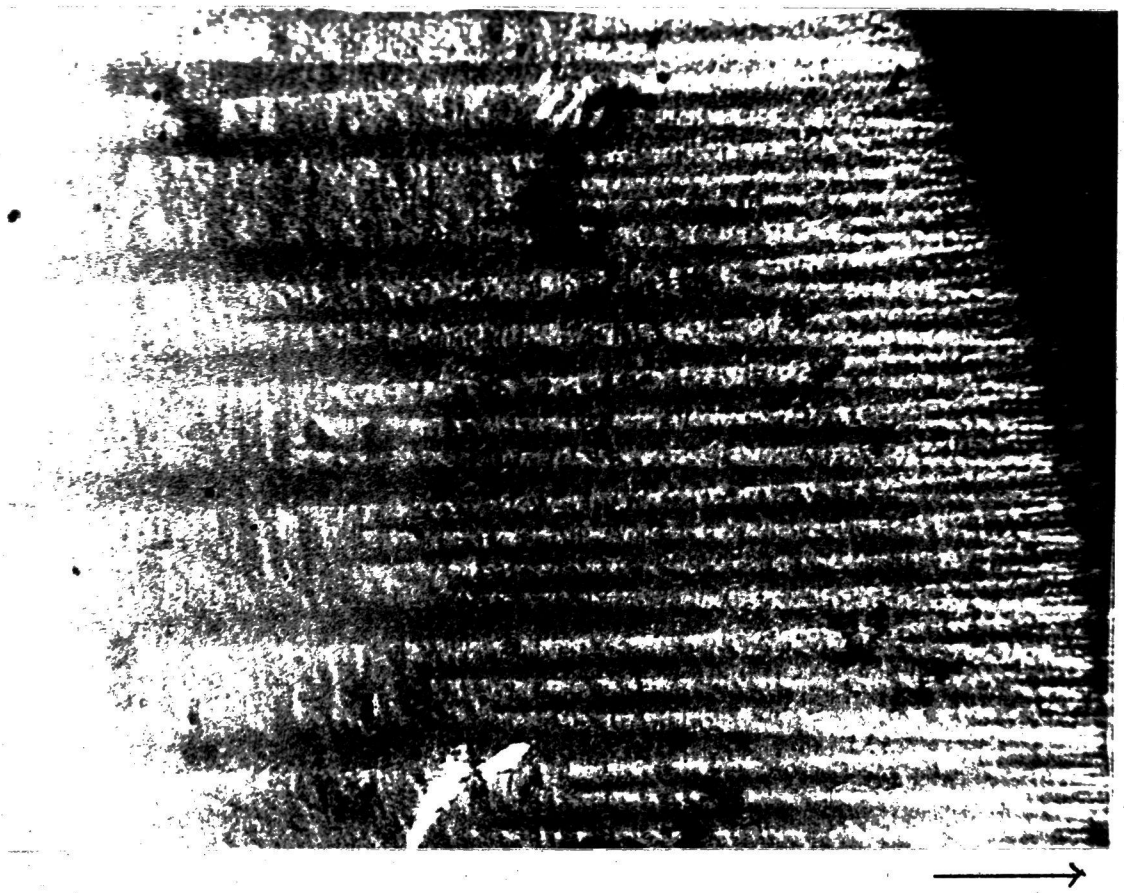

Figure (6.13) Domain structure at 77 K on b-plane
H = 200 Oe

specimen B

the domains are clearer and the reverse domains become much longer than in the previous case. The domains in these two cases look like a loops along the c-axis direction, running over the crystal surface and few of them reach the other edge of the sample. The magnetic field was applied in these two cases by using a permanent horseshoe magnet giving a field of 200 Oe. The principal domain structure in the previous two cases was parallel to the c-axis, but there are traces of regions of domains or walls running normal to the c-axis. These lie inside the principal domains and show opposite polarity.

Figure (6.14a) shows the domain structure with an applied magnetic field of 75 Oe normal to the surface of this plane. Here the domain structure is very clear and runs over the whole surface to the other edge of the sample as shown in figure (6.14b). There is still the same type of structure of reverse domains near the edge. The principal domains running in the c-axis direction and the transverse structures both become clearer than in the previous figures. On increasing the magnetic field applied normal to the surface to a value of 100 Oe, the domain structures observed are as shown in figure (6.15). The transverse structures have developed into a cell structure and the principal domains are now represented by wavy walls; the reverse domains near the edge have nearly disappeared. In figure (6.16) obtained on increasing the field normal to the surface to the value of 300 Oe, the cell structure has developed faster and the boundaries of the principal domains are now no longer exactly parallel

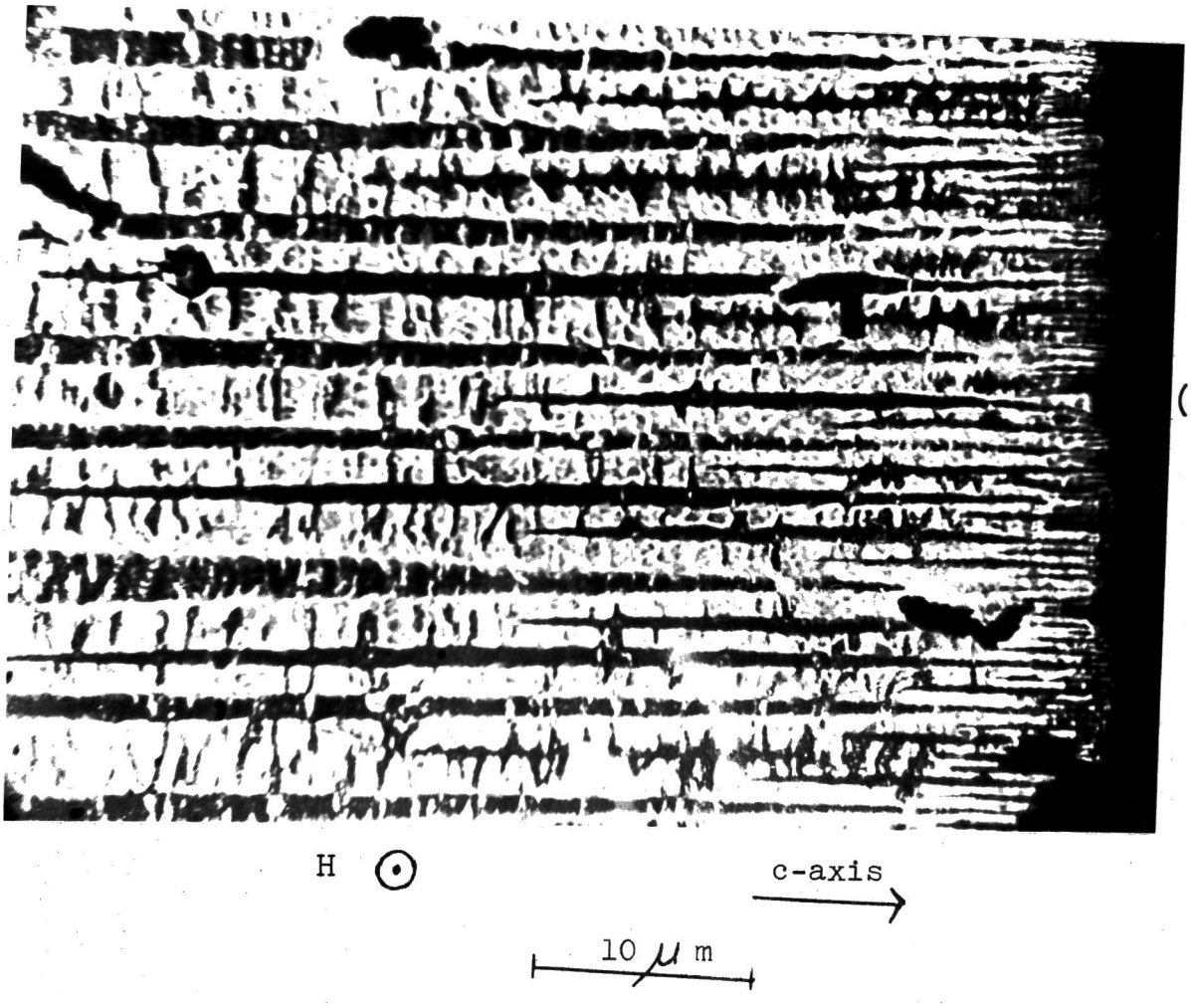

Figure (6.14) Domain structure at 77 K on b-plane
H = 75 Oe
specimen B

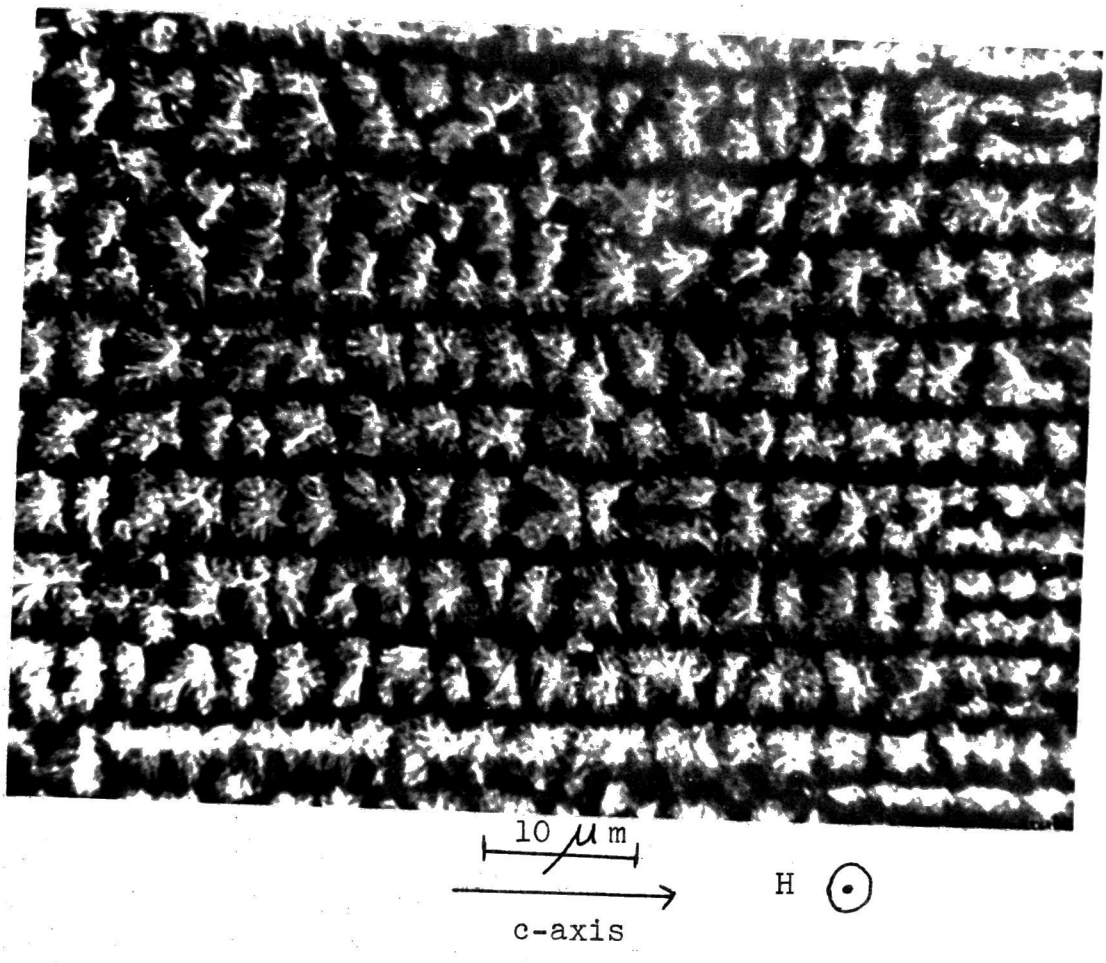

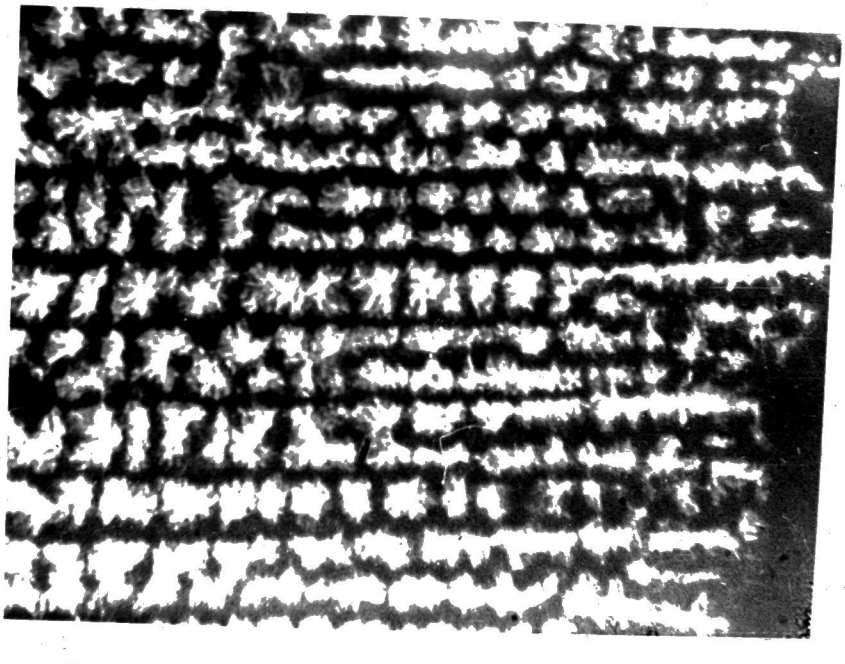

Figure (6.15) Domain structure at 77 K on b-plane
H = 100 Oe
specimen B

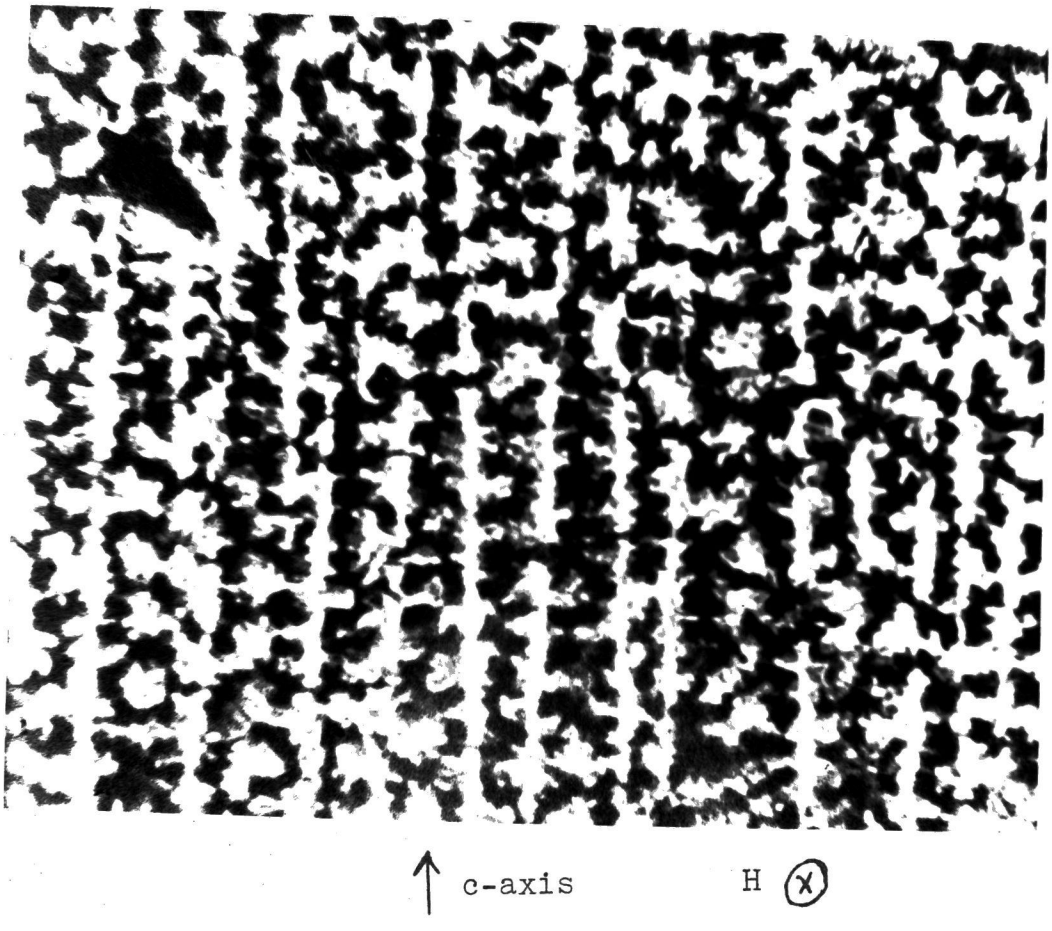

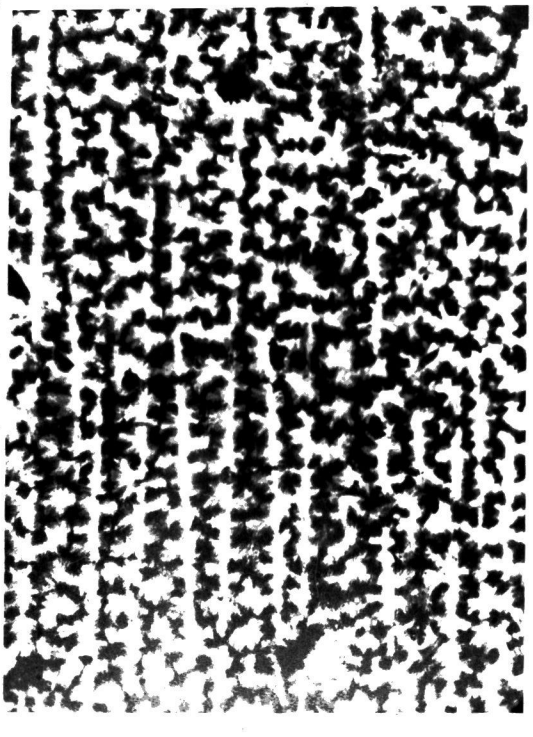

Figure (6.16) Domain structure at 77 K on b - plane
H = 300 Oe
specimen B

to the c-axis. It should be noted that the field for this figure is in the reverse sense to that in figures (6.14) and (6.15).

With no magnetic field applied to this surface, walls rather than domains should be seen. Figure (6.17a) shows the domain pattern on the b-plane without applying magnetic fields, the walls appeared clear and some reverse or closure structures are observed near the edge of the surface as in figure (6.17b). There are in this domain pattern some weak walls running normal to the main walls which take the c-axis direction.

Figure (6.18, a, b, c and d) show the domain structure in the middle parts of the crystal surfaces, with higher magnification corresponding to each of the photographs in Figures (6.12), (6.13), (6.14) and (6.15) respectively.

Figure (6.19) shows the effect of increasing the value of the helium gas pressure at the time of evaporation, the particles joined together in chains before depositing on the domain structure. This had a detrimental effect on the clarity of the patterns.

6.6 Domain structure on basal plane at 77 K

6.6.1 Thin Crystal

The domain structure observed at 77K on this plane is very complicated as in figure (6.20), when deposition took place in the absence of a magnetic field. The domain pattern showed a wall structure of very complicated pattern looking like small stars of different sizes. Applying a magnetic field normal to the surface of order 15 Oe, begins to simplify the pattern which becomes more

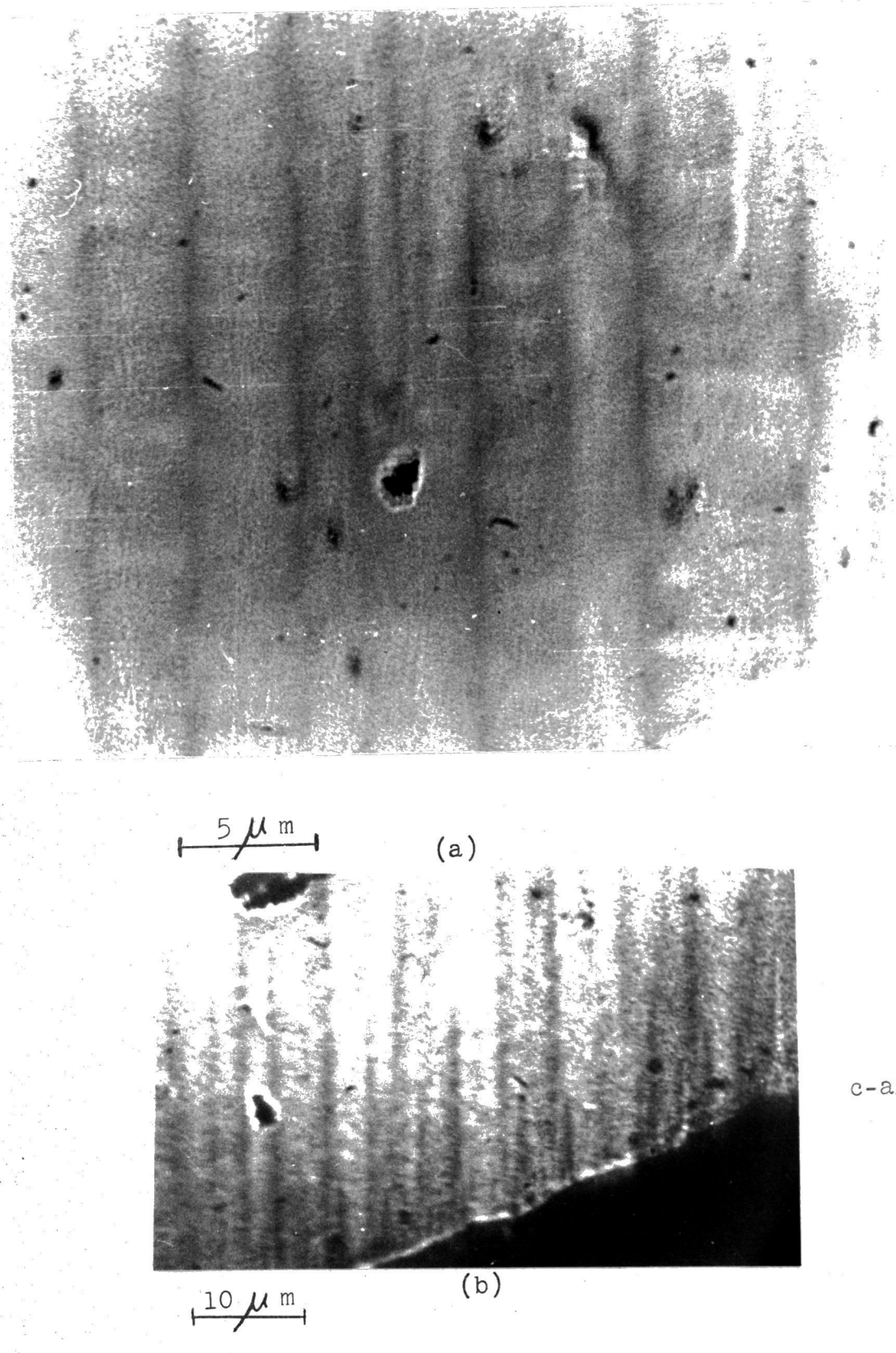

Figure (6.17 Domain structure at 77 K on b-surface
H = zero
specimen B

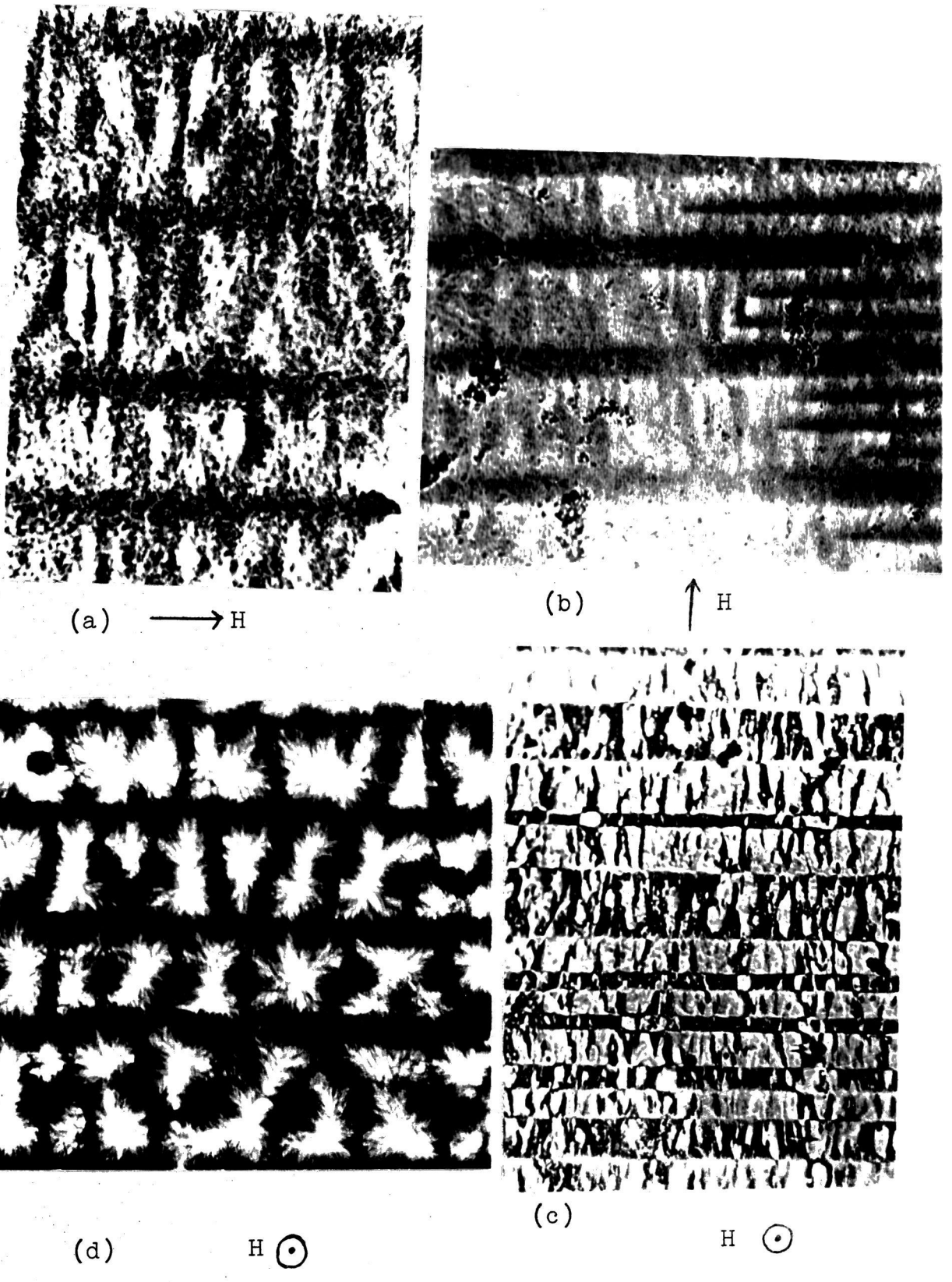

Figure (6.18) Domain structure at 77 K on b-plane
(a) H = 200 Oe (b) H = 200 Oe
(c) H = 75 Oe (d) H = 100 Oe
specimen B

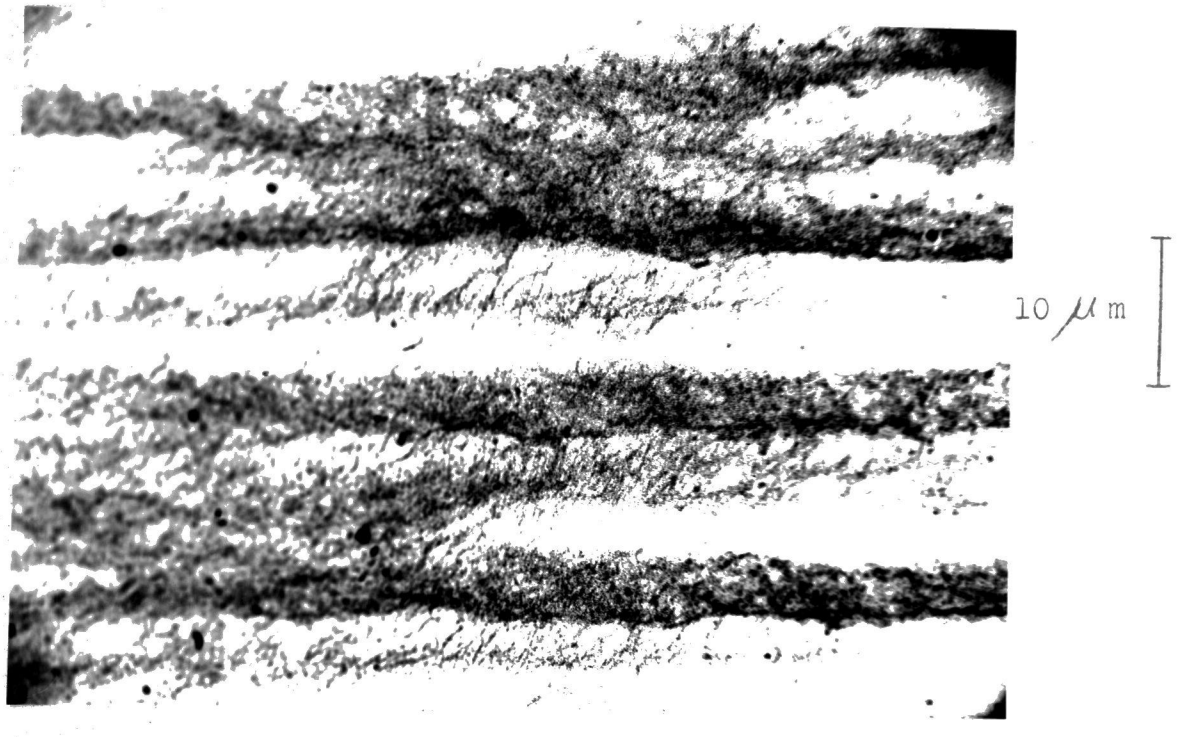

Figure (6.19) Domain structure on b-plane at 77 K
Helium gas pressure = 2 Torr
H = 300 Oe
specimen B

regular as in figure (6.21). In this case it shows domains of different polarity on the surface as expected. Figure (6.22) shows a regular domain structure on this surface abtained by increasing the normal applied field to a value of 30 Oe. The magnetic field used in all these cases was from a small cylindrical shape permanent magnet, giving a homogeneous magnetic field.

Figure (6.23) shows the pattern observed on the basal surface by applying a field of 70 Oe normal to the surface. The patterns are not very different from that in figure (6.22) but the black area, which has a magnetization in the same sense as the magnetic field, increases.

Figure (6.24) shows a further change in the domain structure on increasing the field to a value of 120 Oe. It has not changed completely, but the white area with magnetization in opposite sense to that of the magnetic field has increased. The cells are separated by sections of nearly straight boundaries with small circular domains inside both cells and boundaries.

On increasing the field normal to the surface in the same sense, the domains become more circular in section as in figure (6.25) and the black boundaries between these become very clear. The boundaries contain clear regions of opposite polarity and there are remnants of the structures seen inside the cells at lower magnetic field strengths.

At this point the question could be asked as to why an electromagnet was not used in observing the domain

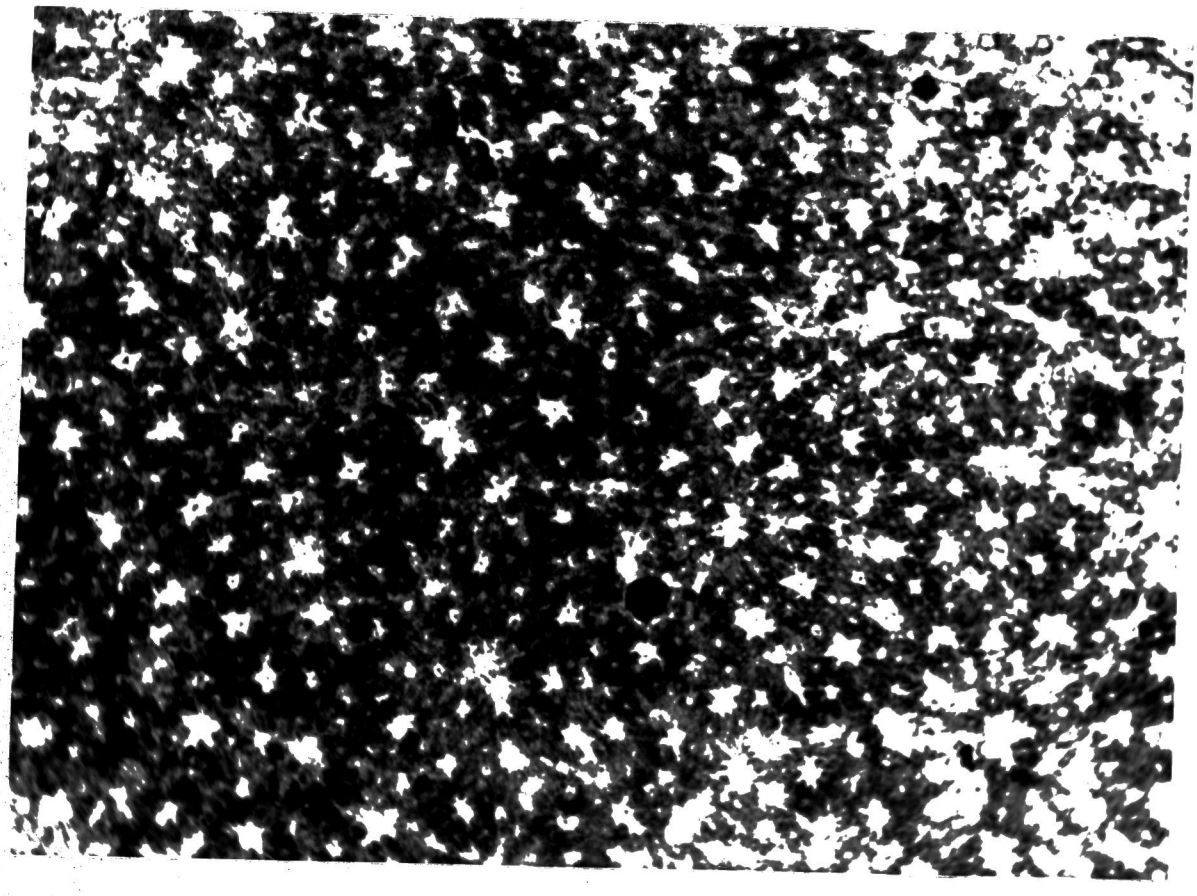

Figure (6.20) Domain structure on basal plane at 77 K
H = zero specimen C

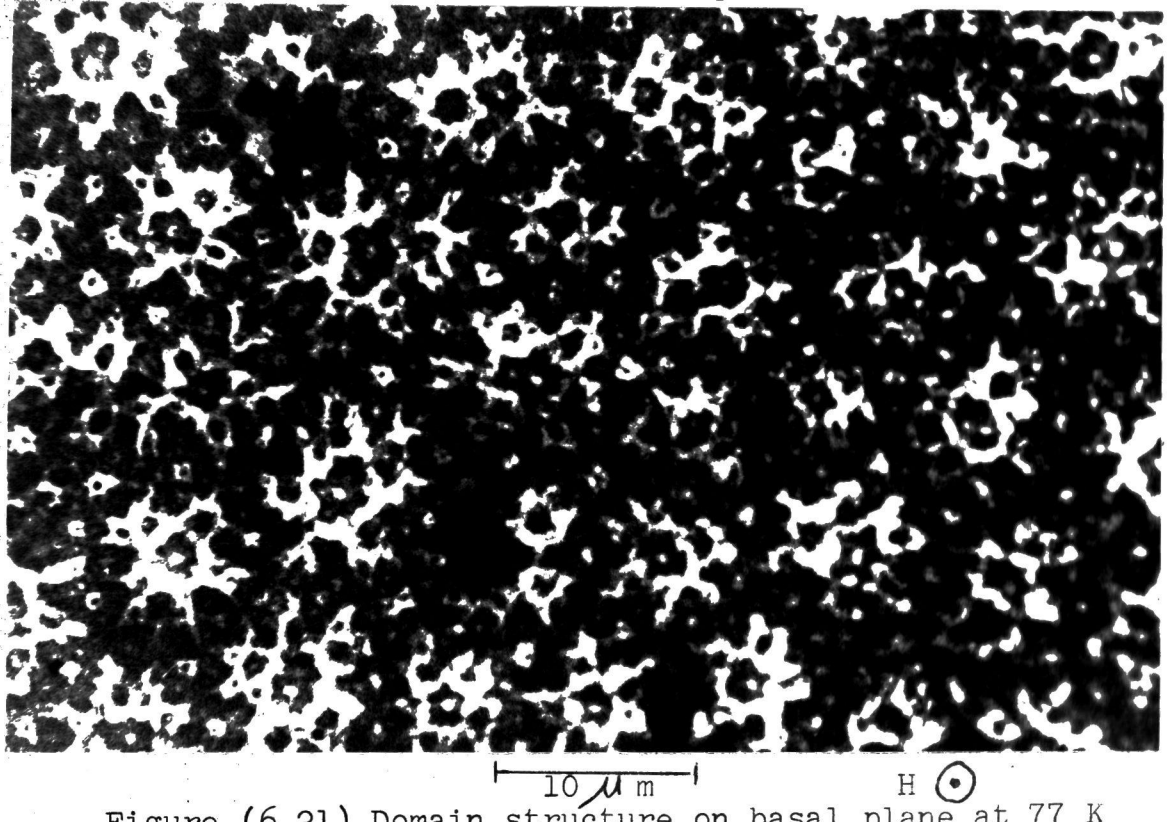

Figure (6.21) Domain structure on basal plane at 77 K
H = 15 Oe specimen C

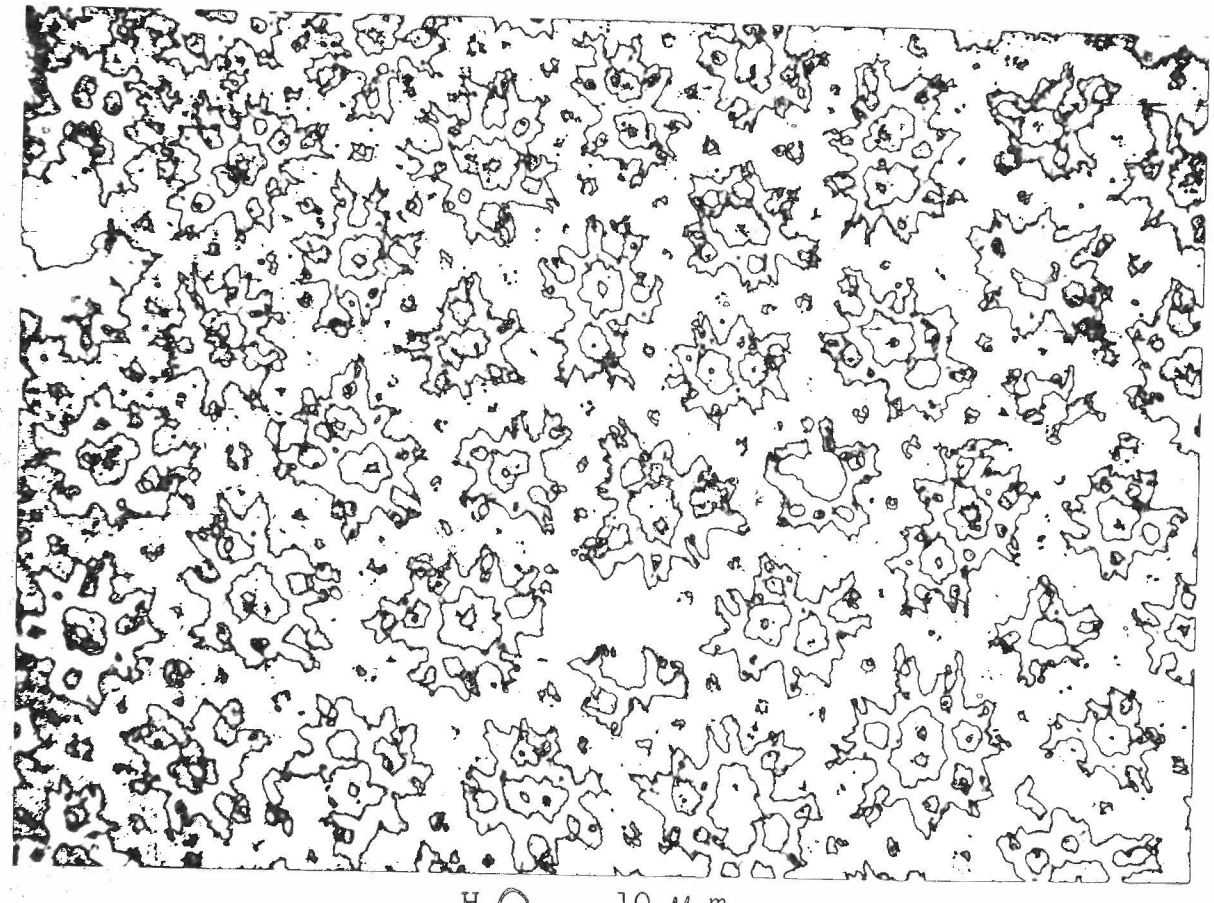

Figure (6.22) Domain structure on basal plane at 77 K
H = 30 Oe normal to the surface specimen C

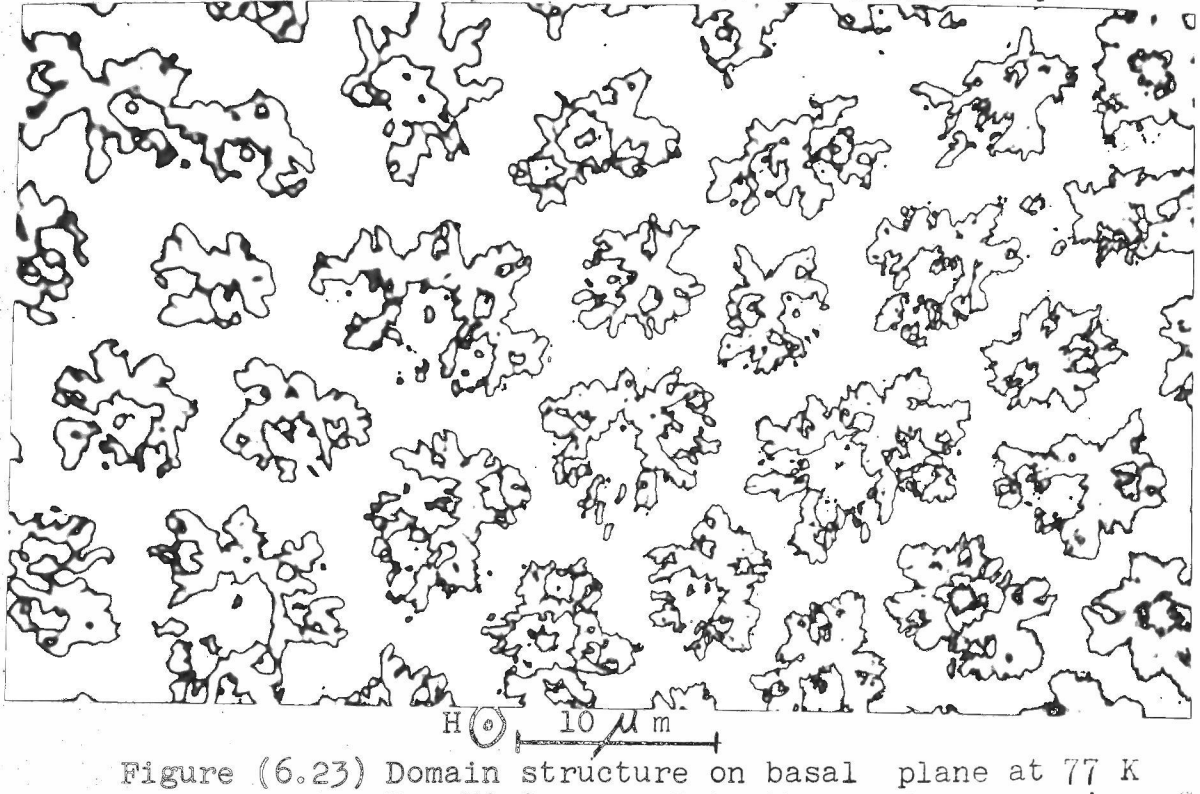

Figure (6.23) Domain structure on basal plane at 77 K
H = 70 Oe normal to the surface specimen C

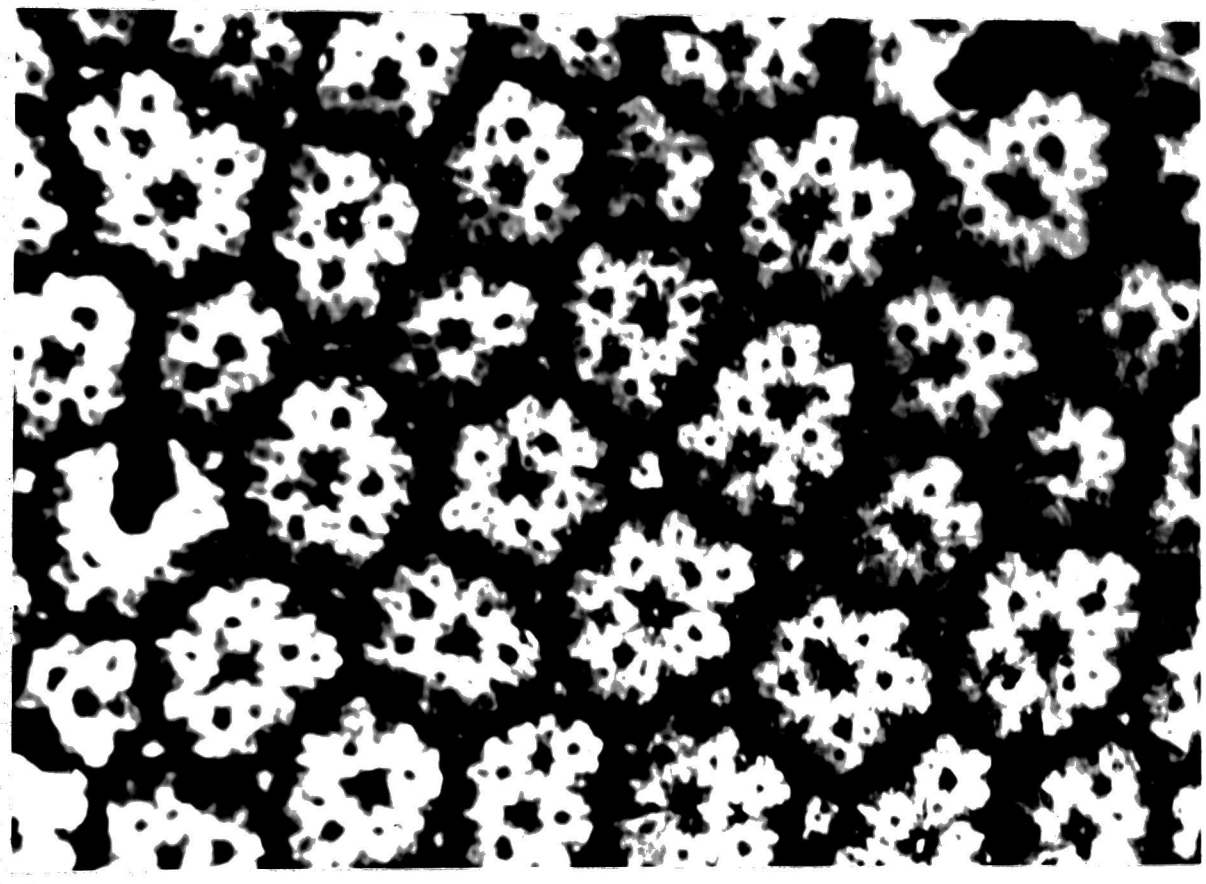

Figure (6.24) Domain structure on basal plane at 77 K
H = 120 Oe specimen C

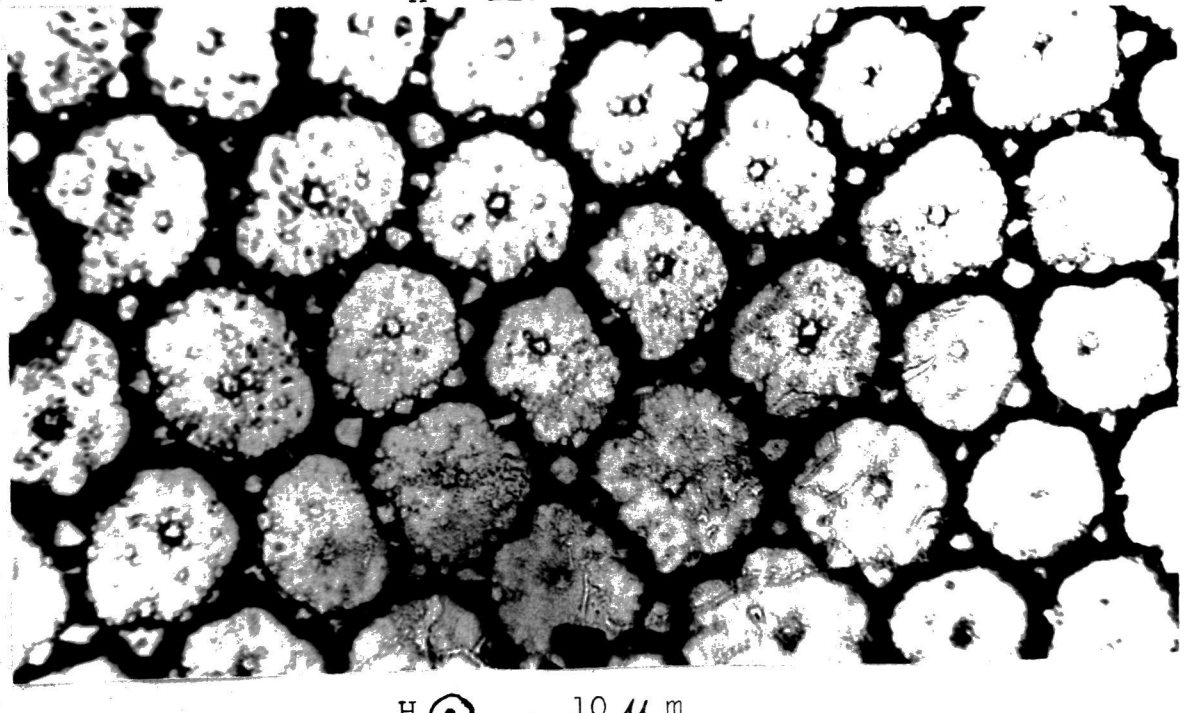

Figure (6.25) Domain structure on basal plane at 77 K
H = 300 Oe specimen C

structure. It might be possible that the observed structure shows the remains of a structure at higher temperature as the field is being applied throughout the cooling of the crystal. The experiment was repeated therefore at 77 K by applying the magnetic field after the crystal has been cooled. Figure (6.26) shows the domain structure observed on applying a field of 30 Oe from an electromagnet. It is clear that the same type of pattern has been found, but here finer detail is visible.

Figures (6.27a) and (6.27b) show the effect of reversing the field, a permanent magnet being employed in each case to give a field of 30 Oe. It is clear that the patterns are complementary, the black areas in one becoming white ones in the other. The fine detail in the two photographs is also reversed. Figure (6.28) shows the domain structure near the edges of the crystal. There is no change in the general pattern due to the proximity to the edge except for very minor variations probably due to slight irregularities.

Figures (6.29a - f) and (6.30a - f) show how the domain spacing is affected by changing the crystal thickness. These photographs taken at different points on the surface of a wedge shaped specimen. Figures (6.29) and (6.30) were taken with normal magnetic fields of 200 Oe, from a permanent magnet but in opposite senses.

6.6.2 Thick Crystal

For a crystal of thickness 6mm the domain structure observed is the same as in a thin crystal at low field.

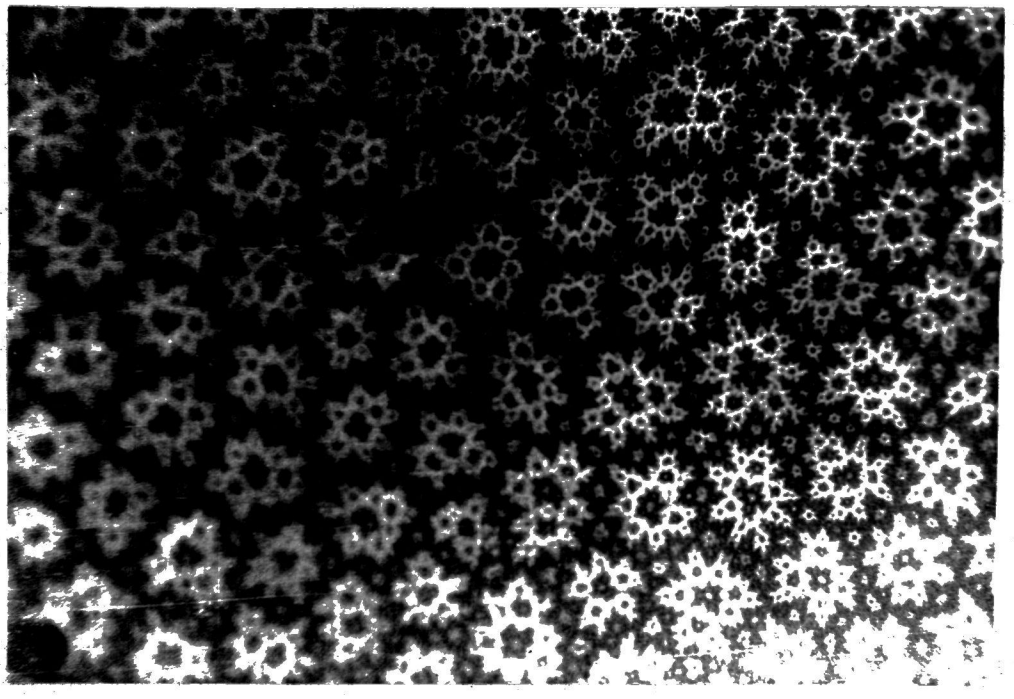

Figure (6.26) Domain structure on basal plane at 77 K
H = 30 Oe From electro magnet
specimen C

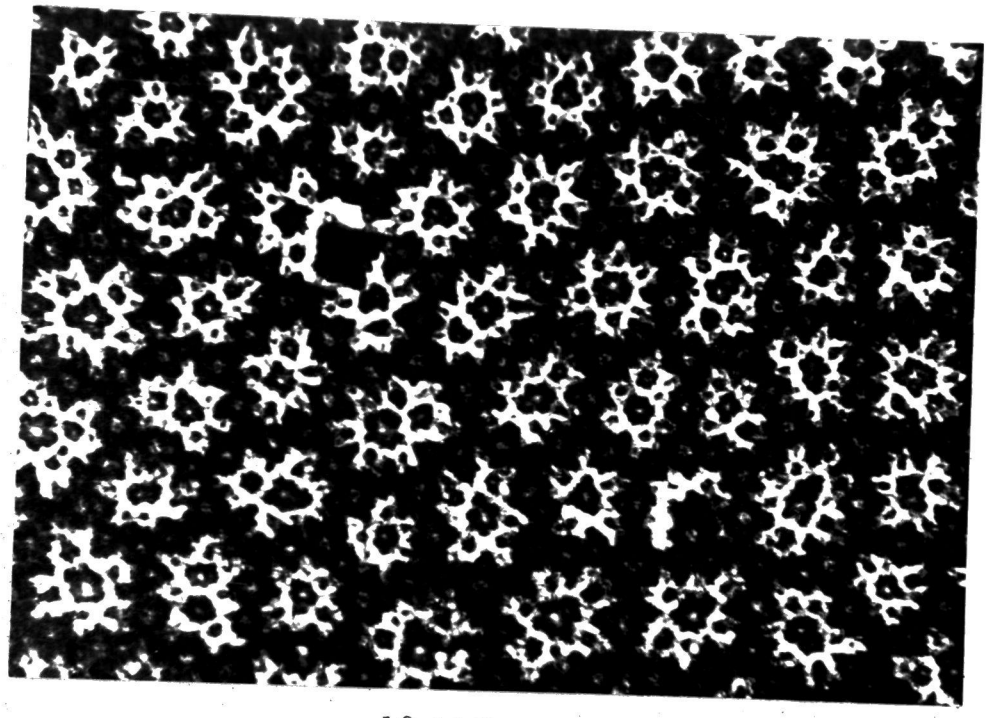

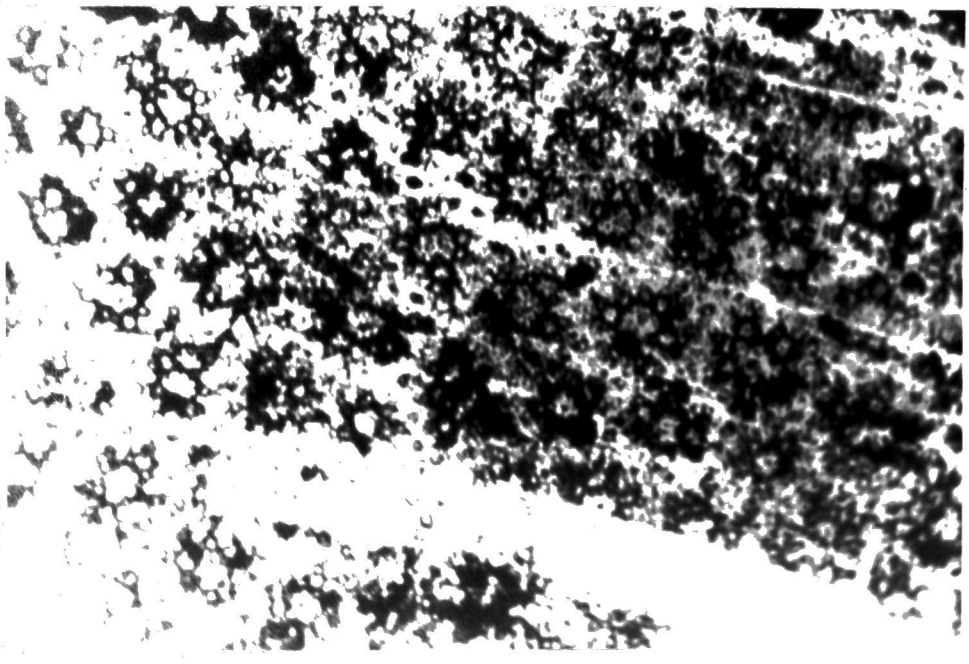

Figure (6.27) Domain structure on basal plane at 77 K
The direction of the field reversed
H = 30 Oe
specimen C

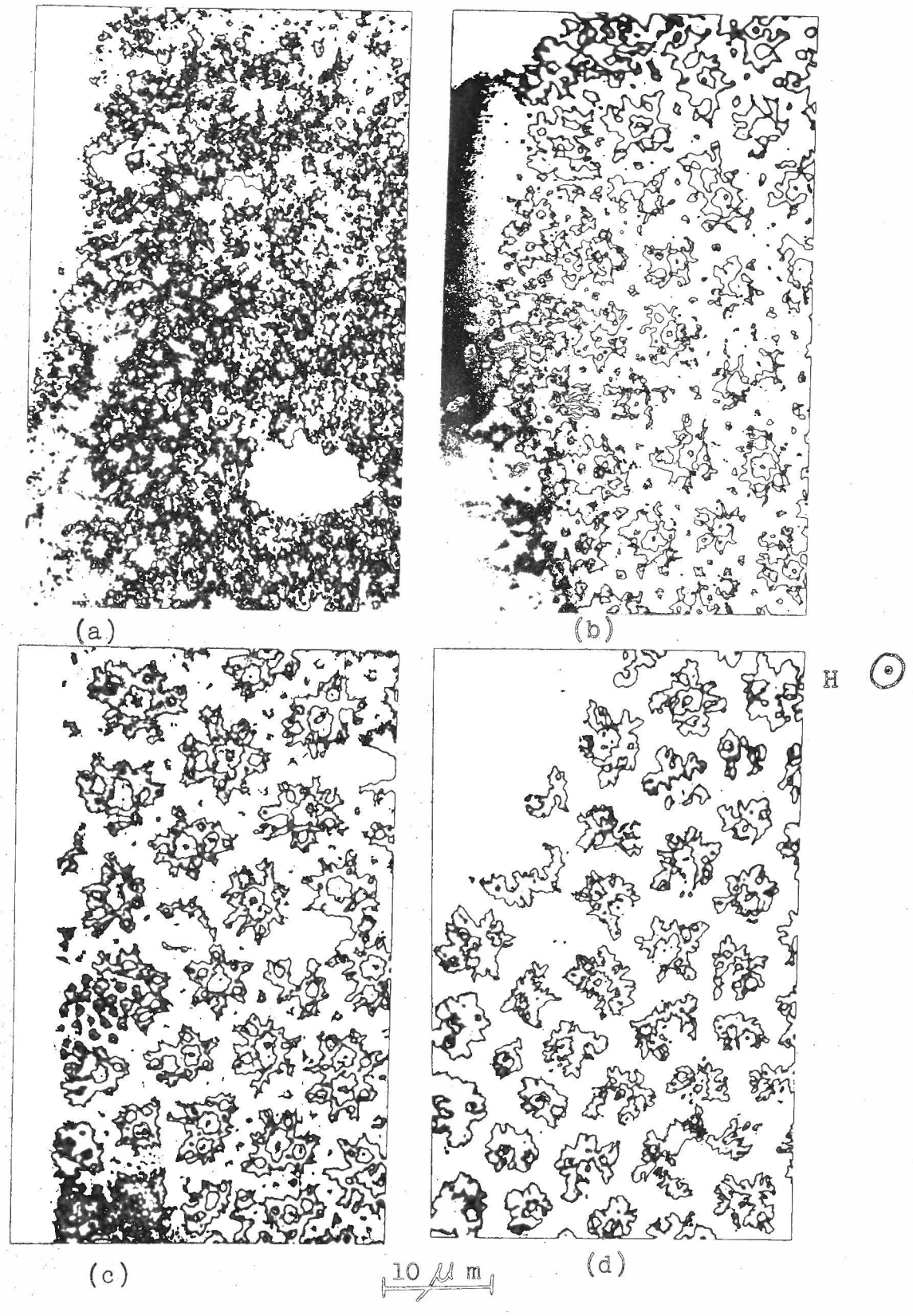

Figure (6.28) Domain structure on basal plane at 77 K
H (a) = zero H (b) = 15 Oe
H (c) = 30 Oe H (d) = 70 Oe
specimen C

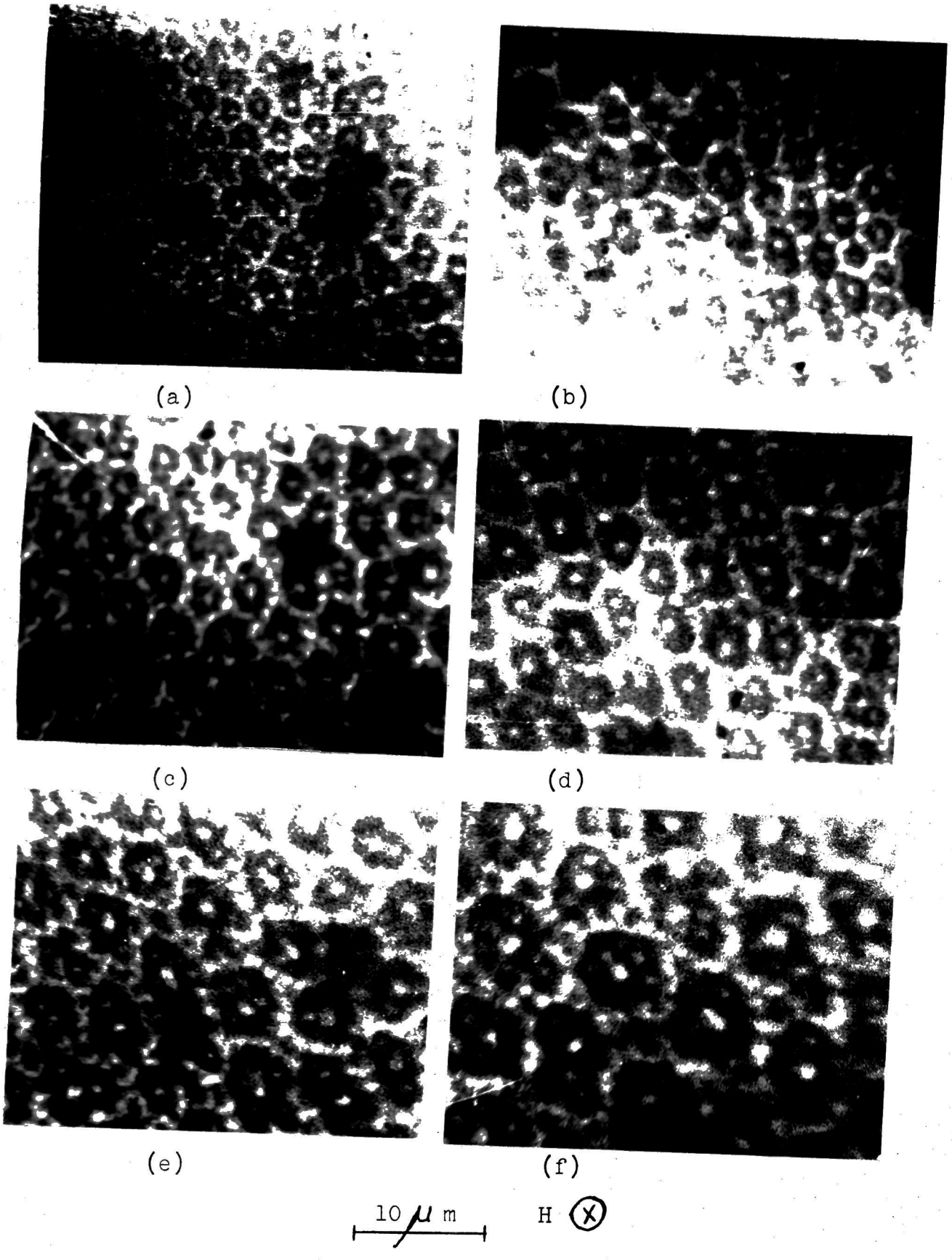

Figure (6.29) Domain structure at 77 K on basal plane thickness T as following

T(a) = 1 mm T(b) = 1.5 mm T(c) = 2 mm

T(d) = 3 mm T(e) = 3.5 mm T(f) = 4 mm

specimen A

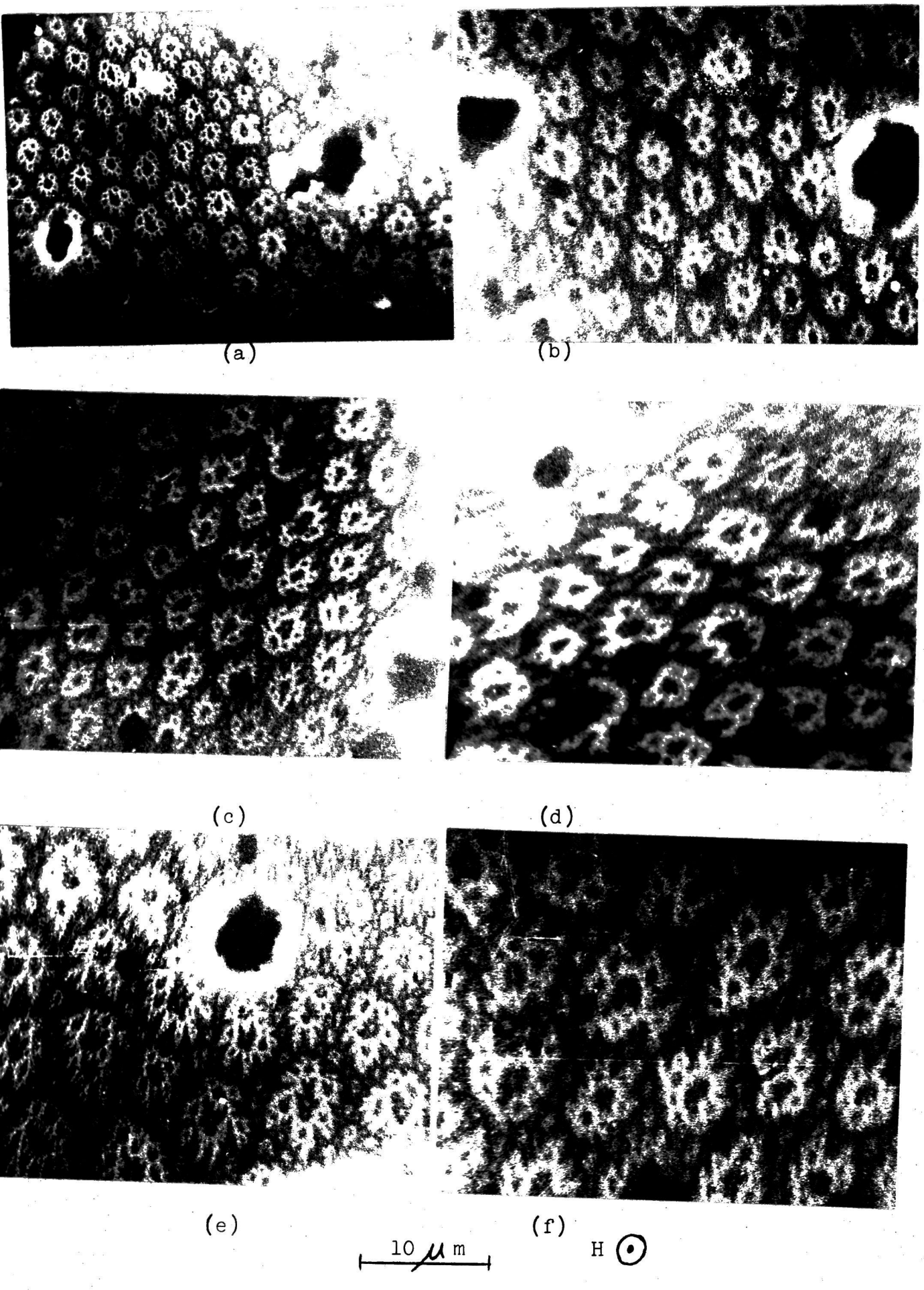

Figure (6.30) Domain structure on basal plane at 77 K thickness T

T(a) = 1 mm T(b) = 2 mm T(c) = 2.5 mm
T(d) = 3 mm T(e) = 3.5 mm T(f) = 4 mm
specimen A

By increasing the field in this case the domain structure was not changed in type but the pattern became more complicated.

Figure (6.31) shows the domain structure on a basal plane with a field applied by the electromagnet of value 380 Oe normal to the surface. The domain pattern is similar to that of a thin crystal, but consists of stars of black and white joining together in lines in some places on the surface.

Figure (6.32a - f) shows the effect of increasing the value of the normal magnetic field on the crystal surface domain structure by using the electromagnet, the value increasing from (a) to (f) till value of 400 Oe. Figure (6.33a - f) shows the effect of increasing the value of the normal magnetic field on basal plane domain using the permanent magnet on this crystal. The value of the magnetic field applied increases to value of 1000 Oe. After this value, it is not possible to observe domain structure on this surface. Here the pattern is more regular than using the electromagnet, and the stars are not joined together in lines on most of the surface.

In the above two cases, it is clear that the domains retain the same type of structure on increasing the field, but there is a change in the size of the domain stars and the pattern becomes more complicated. Figure (6.34) shows the effect of reversing the field on this crystal, using the electromagnet. The patterns are nearly complementary.

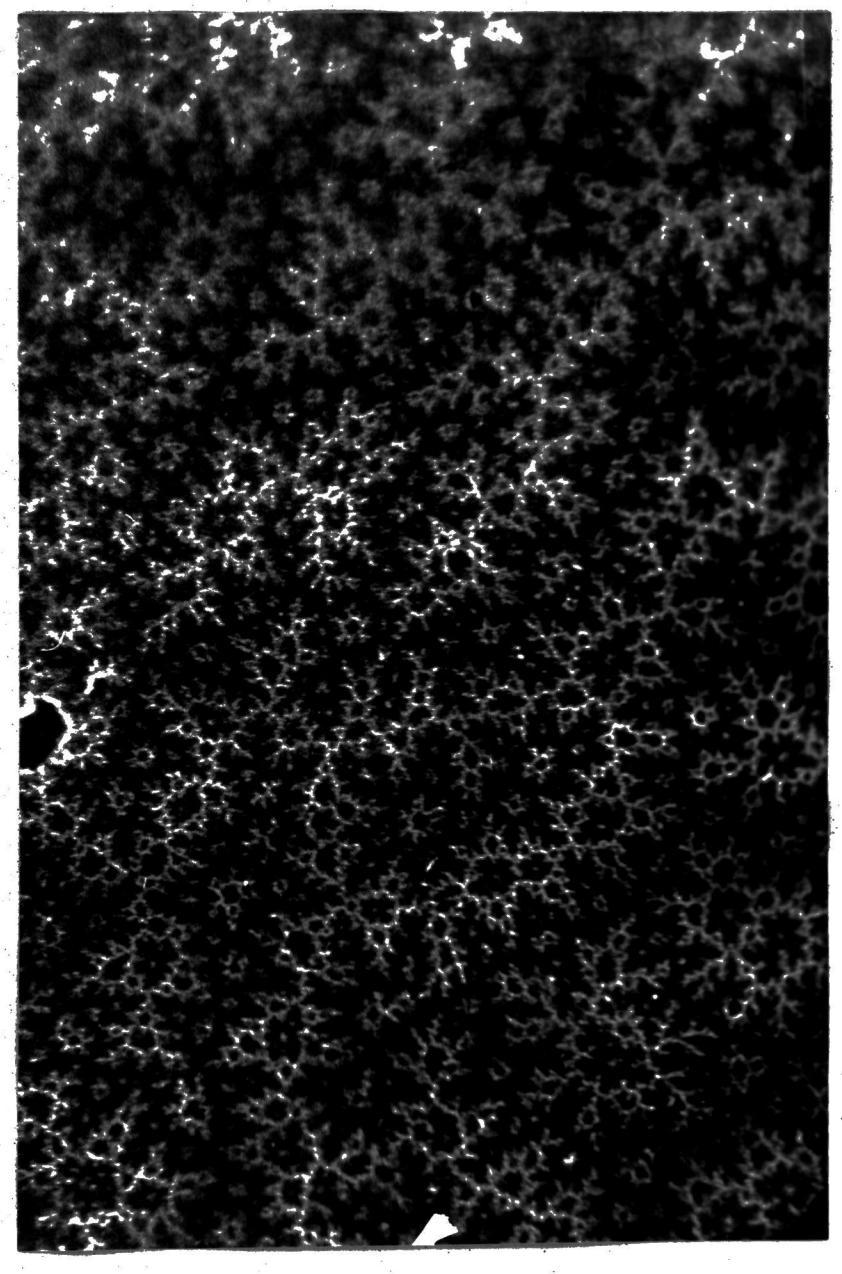

Figure (6.31) Domain structure on basal plane at 77 K
H = 380 Oe Using electromagnet
specimen B

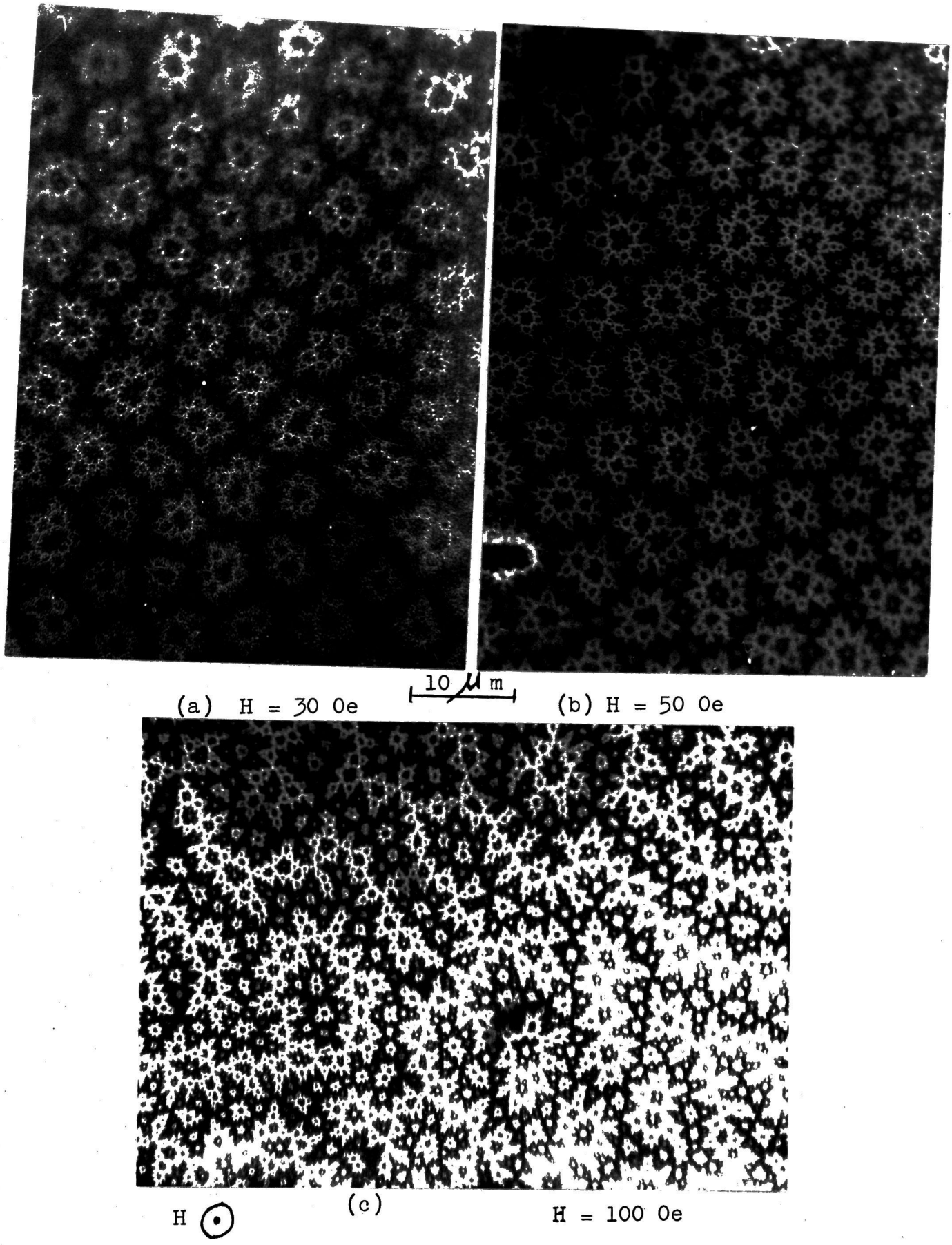

Figure (6.32 a, b, c) Domain structure on basal plane at 77 K Using electromagnet

specimen B

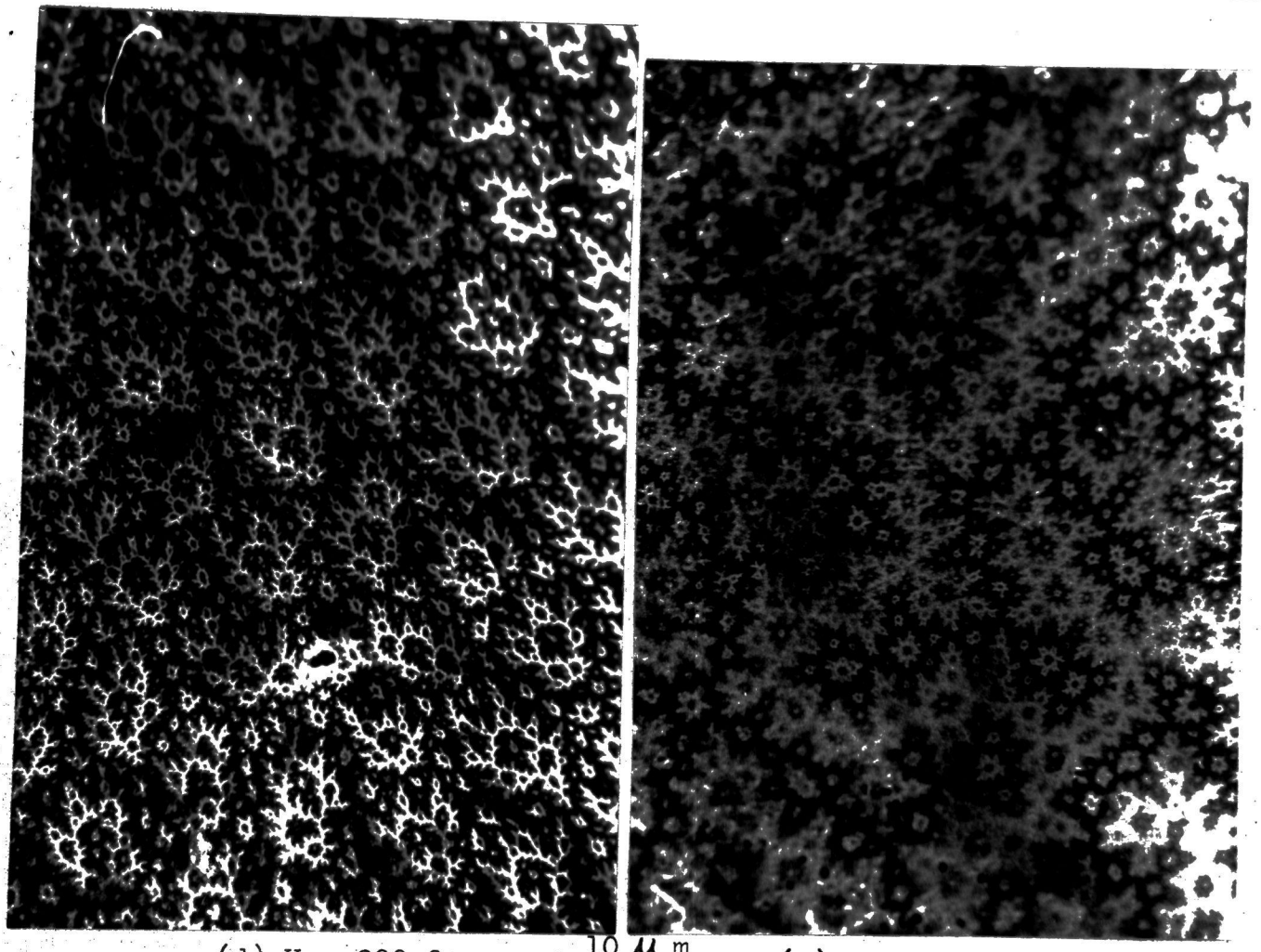

(d) H = 200 Oe (e) H = 300 Oe

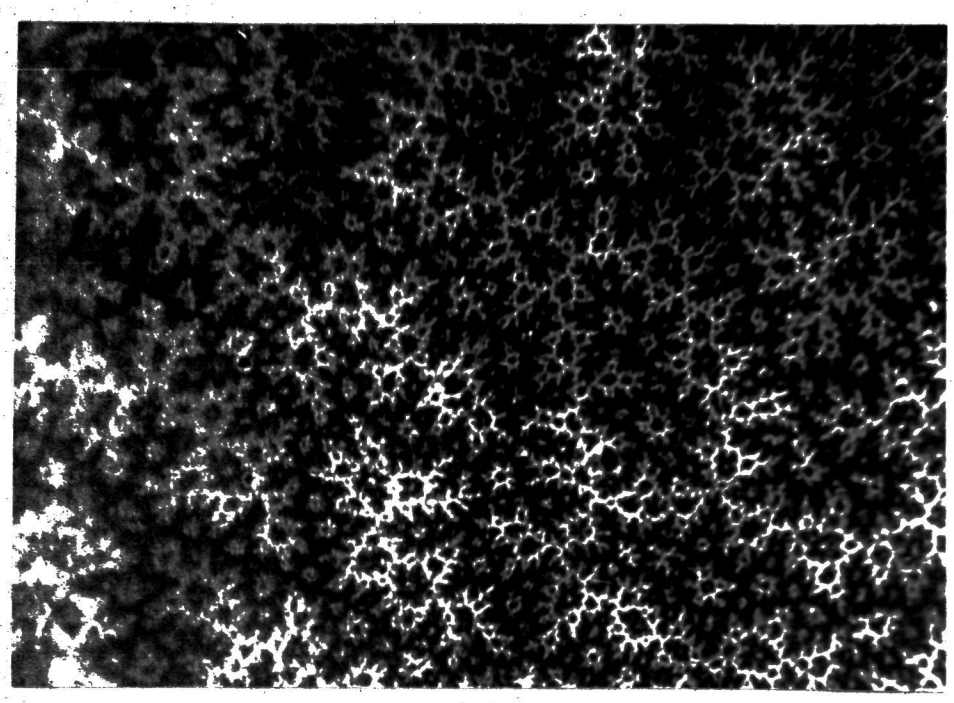

(f) H = 400 Oe

Figure (6.32 d, e, f) Domain structure on basal plane at 77 K Using electromagnet specimen B

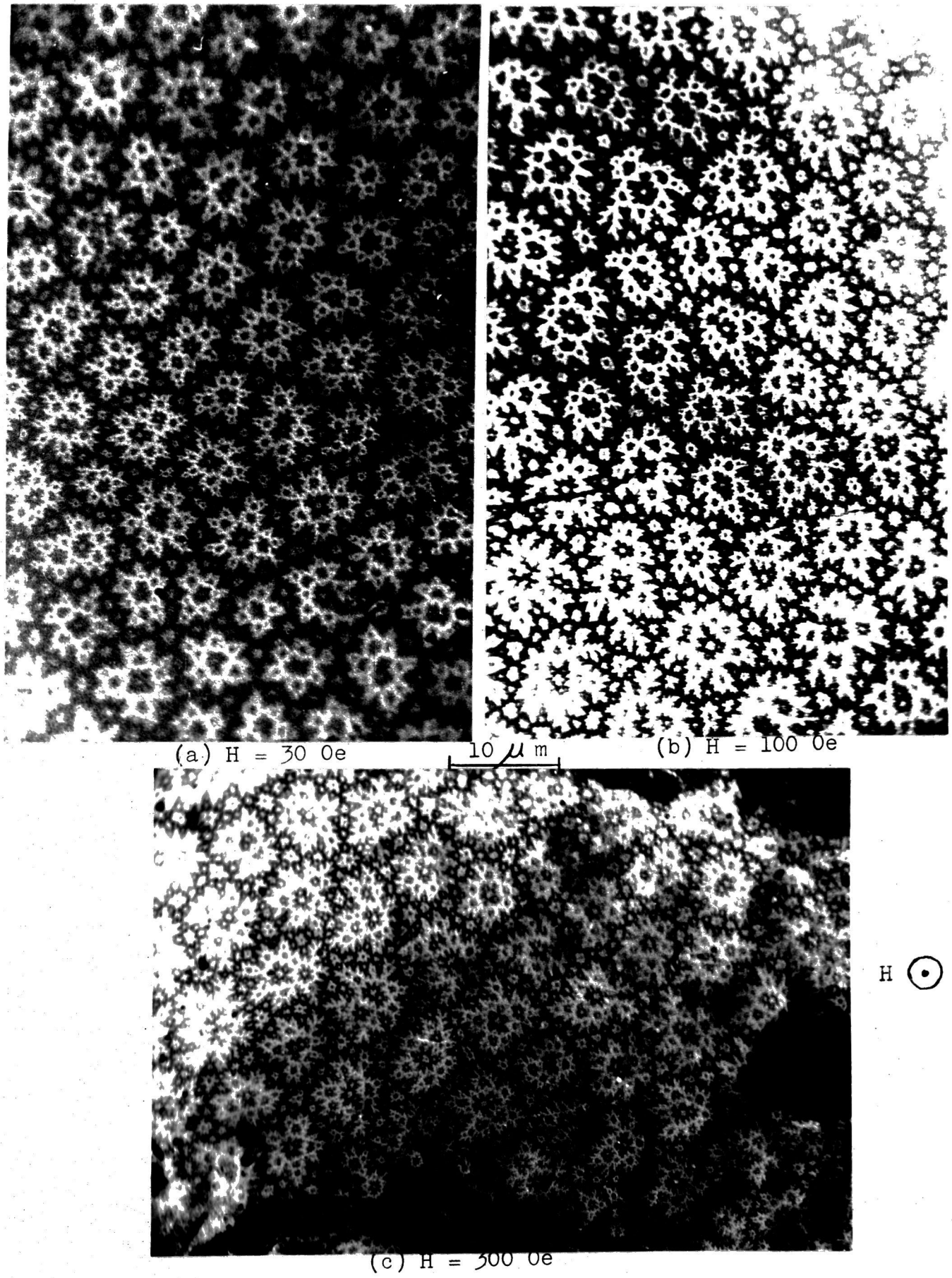

Figure (6.33 a, b, c) Domain structure on basal plane at 77 K using permanent magnet specimen B

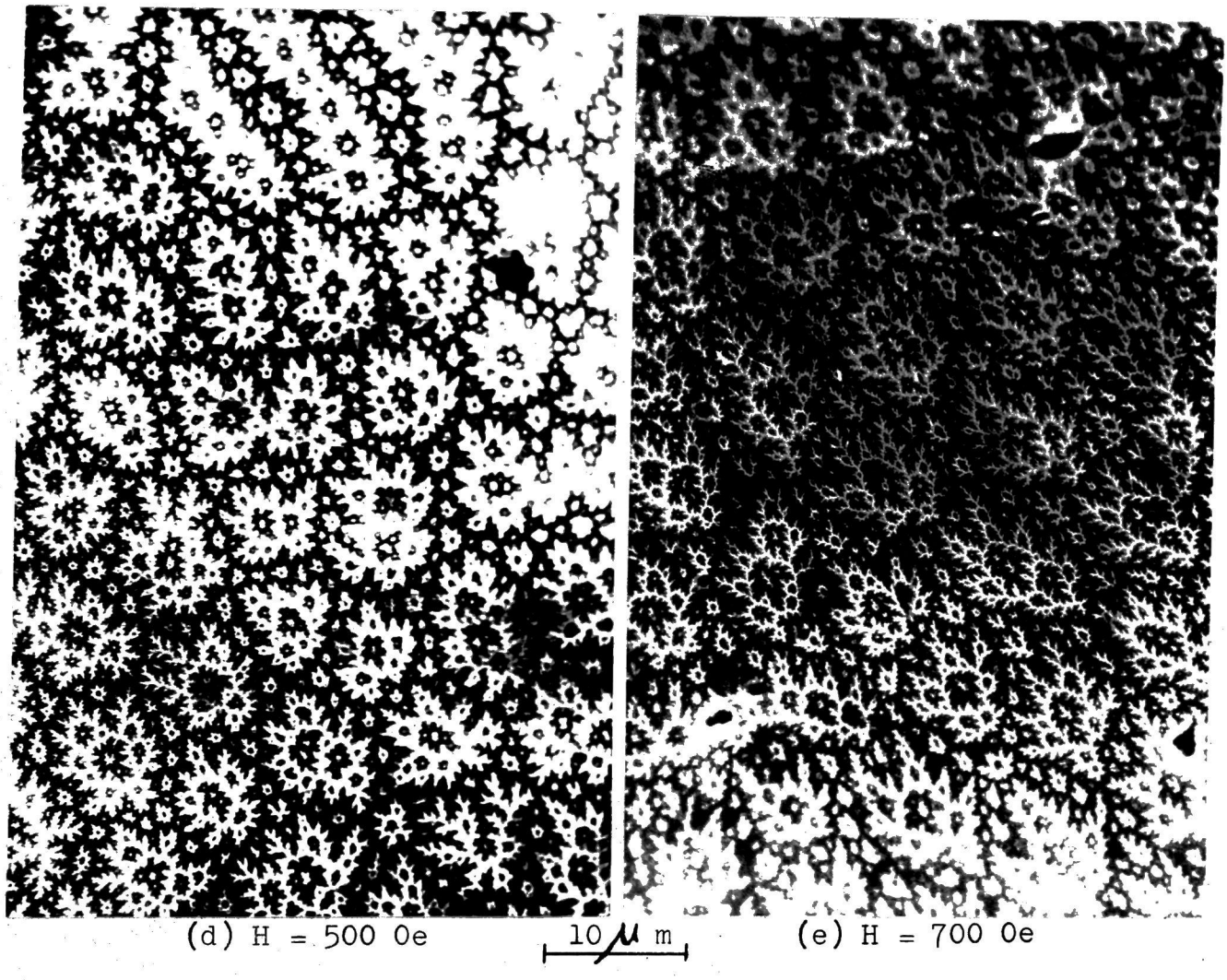

(d) H = 500 Oe

(e) H = 700 Oe

(f) H = 1000 Oe

Figure (6.33 d, e, f) Domain structure on basal plane at 77 K using permanent magnet specimen B

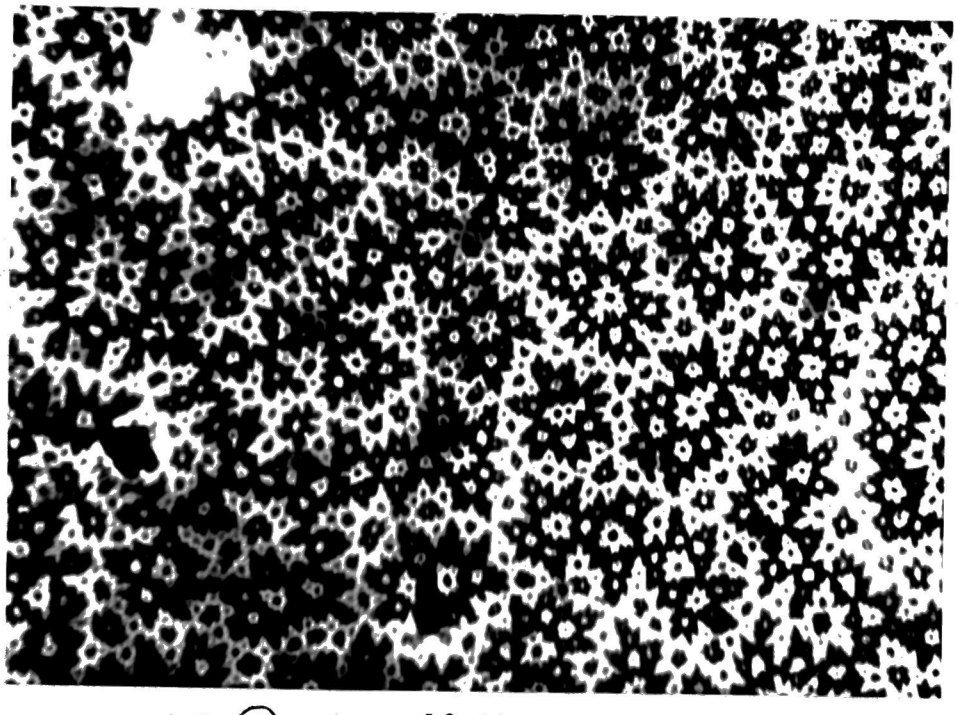

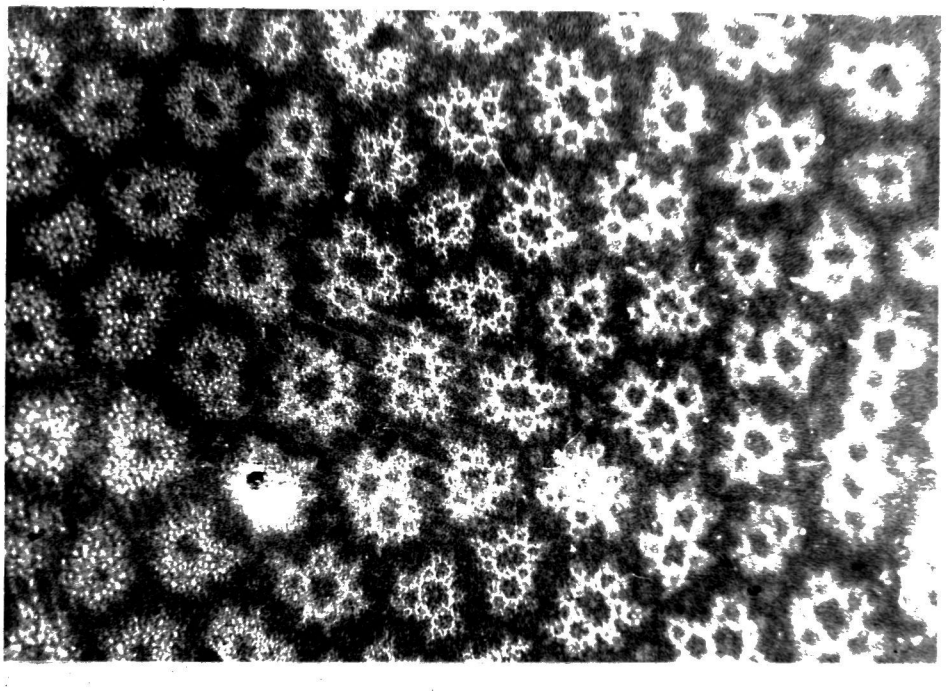

Figure (6.34) Effect of reversing the magnetic field on basal plane domain structure at 77 K using electromagnet H = 100 Oe specimen B

6.7 Domain structure on surface inclined to b-plane at 216 and 77 K

On cutting the crystal with planes inclined by small angles, of order 10° and 15°, to the b-plane the domain pattern was found to consist of complex shaped daggers. The domain structure depended on the angle of inclination.

Figure (6.35a) shows the domain structure at 216 K for a plane inclined at 10° to b-plane, the applied magnetic field was in the plane parallel to the surface. Figure (6.35b) shows the domain structure at another point on the surface.

Figures (6.36a - e) shows the domain pattern at different points on the same surface inclined by 10° to the b-plane at 77 K, and it is clear that it consisted of a combination of different types of loops and daggers.

Figures (6.37a - c) show the domain structure at different points of a surface inclined by 15° to the b-plane at 77 K, using a different crystal. It is quite different from that on the 10° inclined surface, but it contains the same type of structures. This is because the two crystals differ in size as well as in the angle of inclination of the surface.

6.8 Domain structure on surfaces inclined to the basal plane at 77 K

The domain structure on a surface inclined to the basal plane would be expected to differ from that already described for a temperature of 273K.

Figure (6.38a) shows the domain structure on a

(a)

10 μm

c-axis

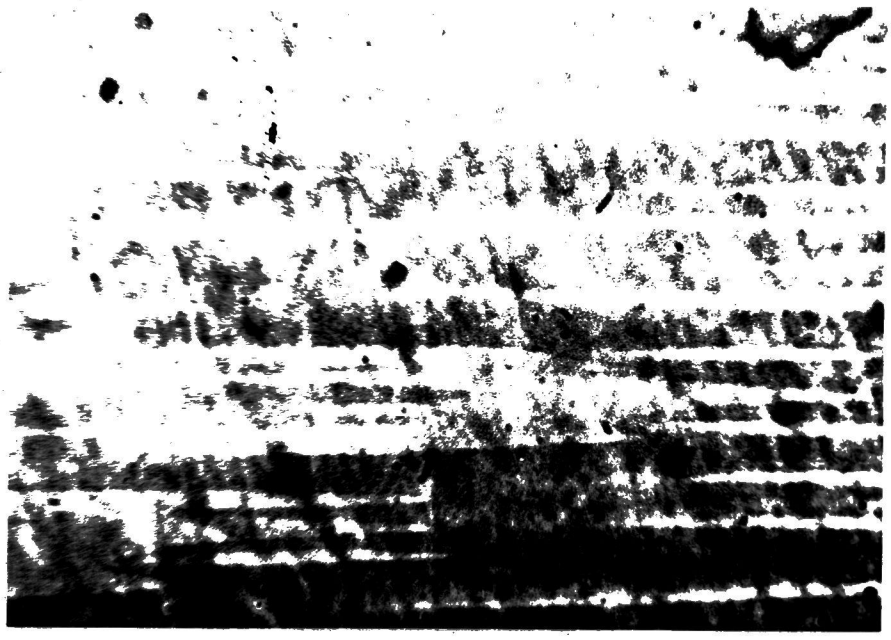

(b)

Figure (6.35) Domain structure on surface inclined at 10° to b-plane at 216 K
specimen B

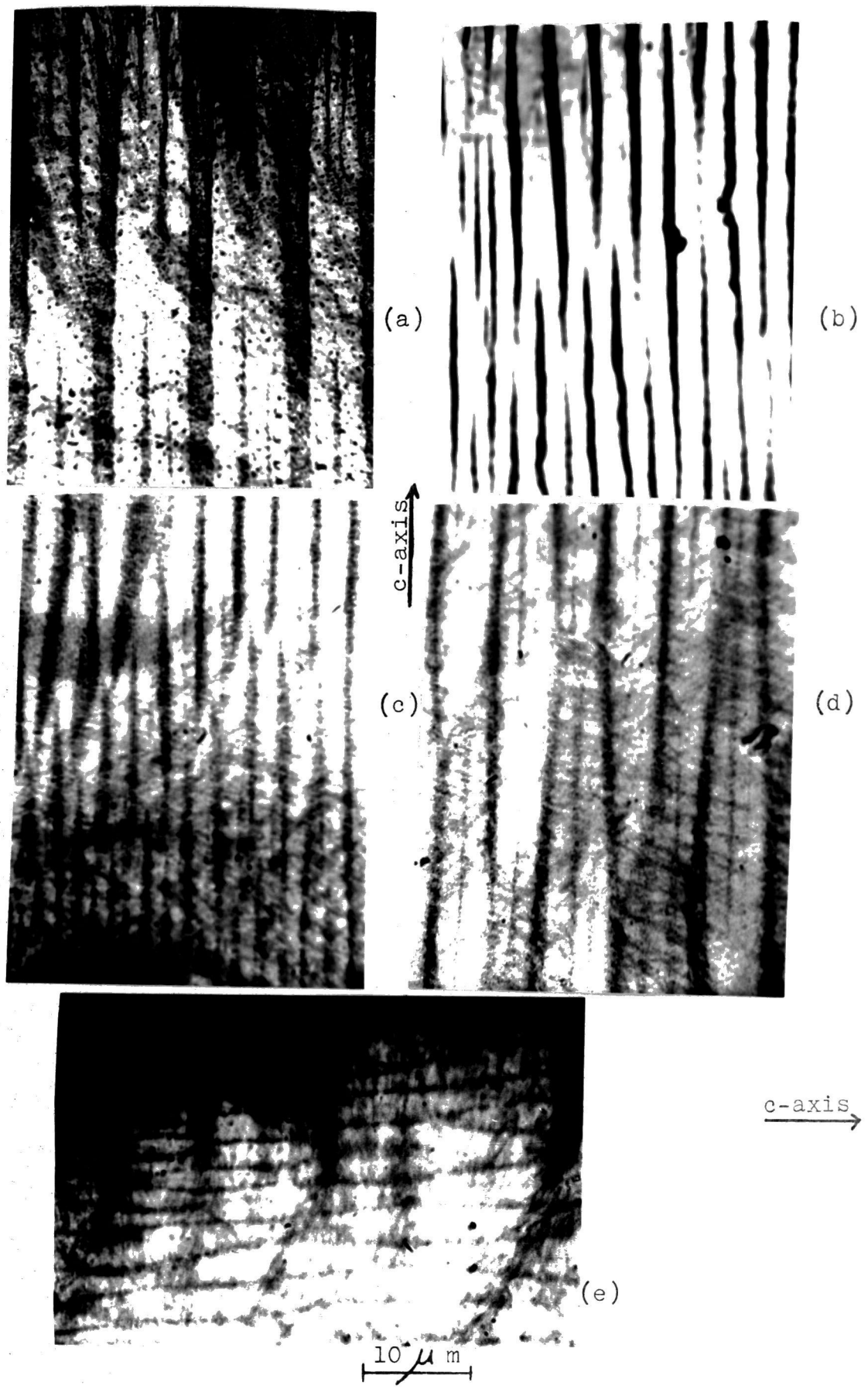

Figure (6.36) Domain structure on surface inclined at 10° to b-plane at 77 K

specimen B

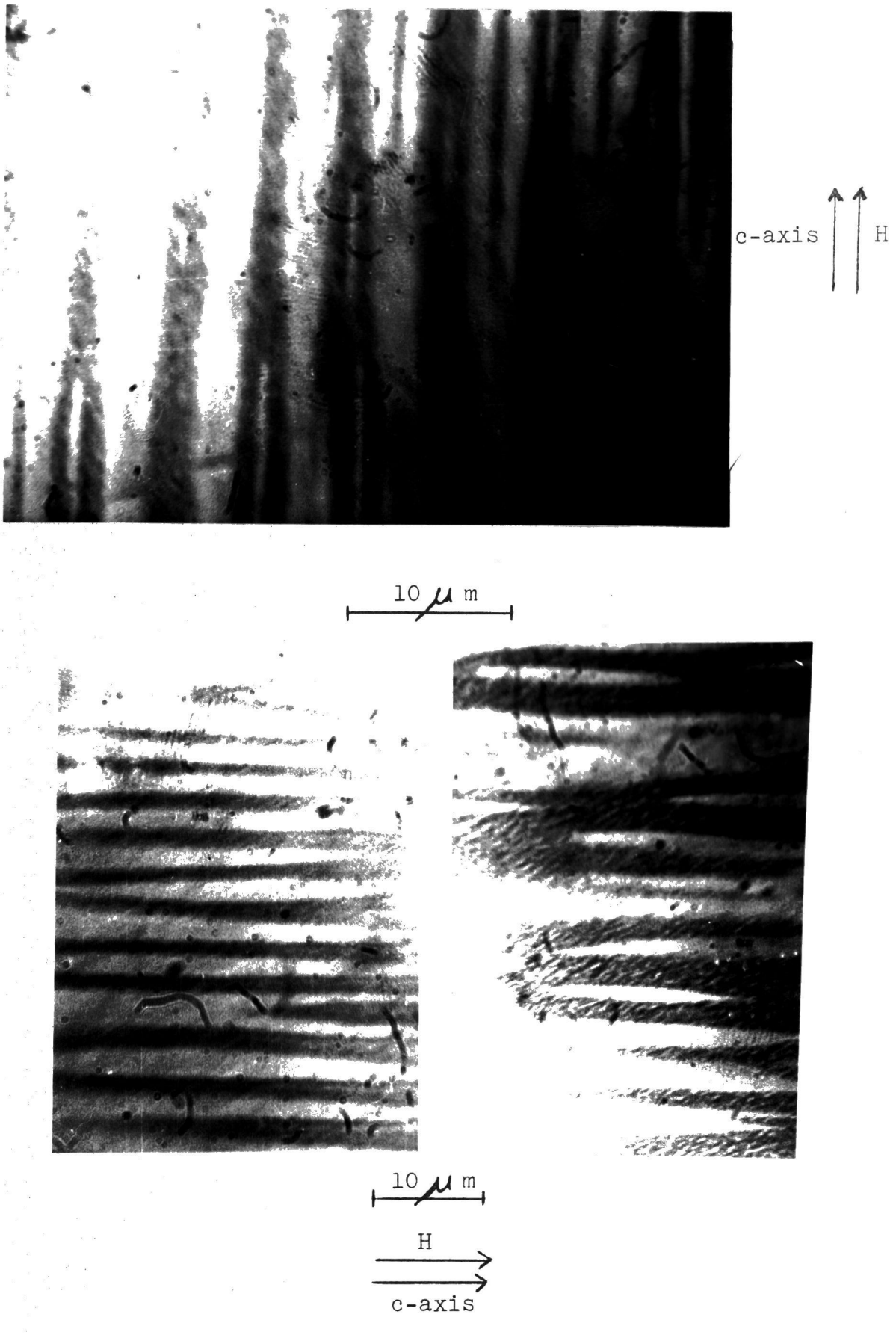

Figure (6.37) Domain structure on inclined surface to b-plane by 15° at 77 K H = 300 Oe

specimen C

surface inclined by 15° to basal plane, magnetic field was applied normal to the surface. Figure (6.38b) shows the domain structure at another part of the surface, with the same conditions. As expected the domain structure at this temperature is different; the honeycomb patterns do not join in cells of hexagonal symmetry and are less complicated than the patterns observed before at 273 K. Also here the domain structure pattern is not so clear as at 273 K, and the contrast is observed to be weak.

6.9 Domain structure at 25 K

In trying to observe domain pattern at temperatures lower than 77 K, we face the difficulties of retaining a constant temperature for the time of evaporation and for the time during which the particles deposit on the surface. However, domain structure was observed on the two surfaces, the plane containing the c-axis and the basal plane, at temperature of 25K.

Figure (6.39a) shows the domain structure on the basal plane at this temperature, the applied field was from the permanent magnet, applied normal to the surface and its value was 70 Oe. It shows domains of wavy types joined in patterns like trees or fingers. Figure (6.39b) shows a similar domain pattern near the central part of the surface, while Figure (6.39a) shows the pattern near the edge. It is noticed that the domain size is smaller than the size at 77 K, and the pattern observed shows considerable differences from that at the

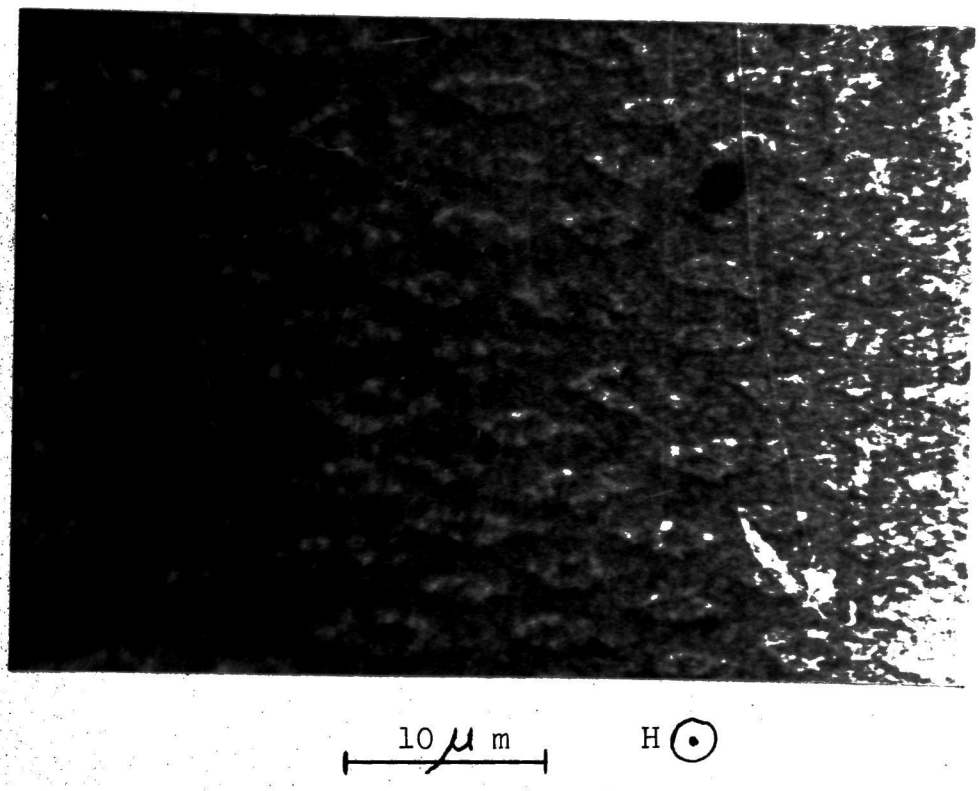

Figure (6.38) Domain structure on surface incline at 15° to the basal plane at 77 K
H = 200 Oe
specimen A

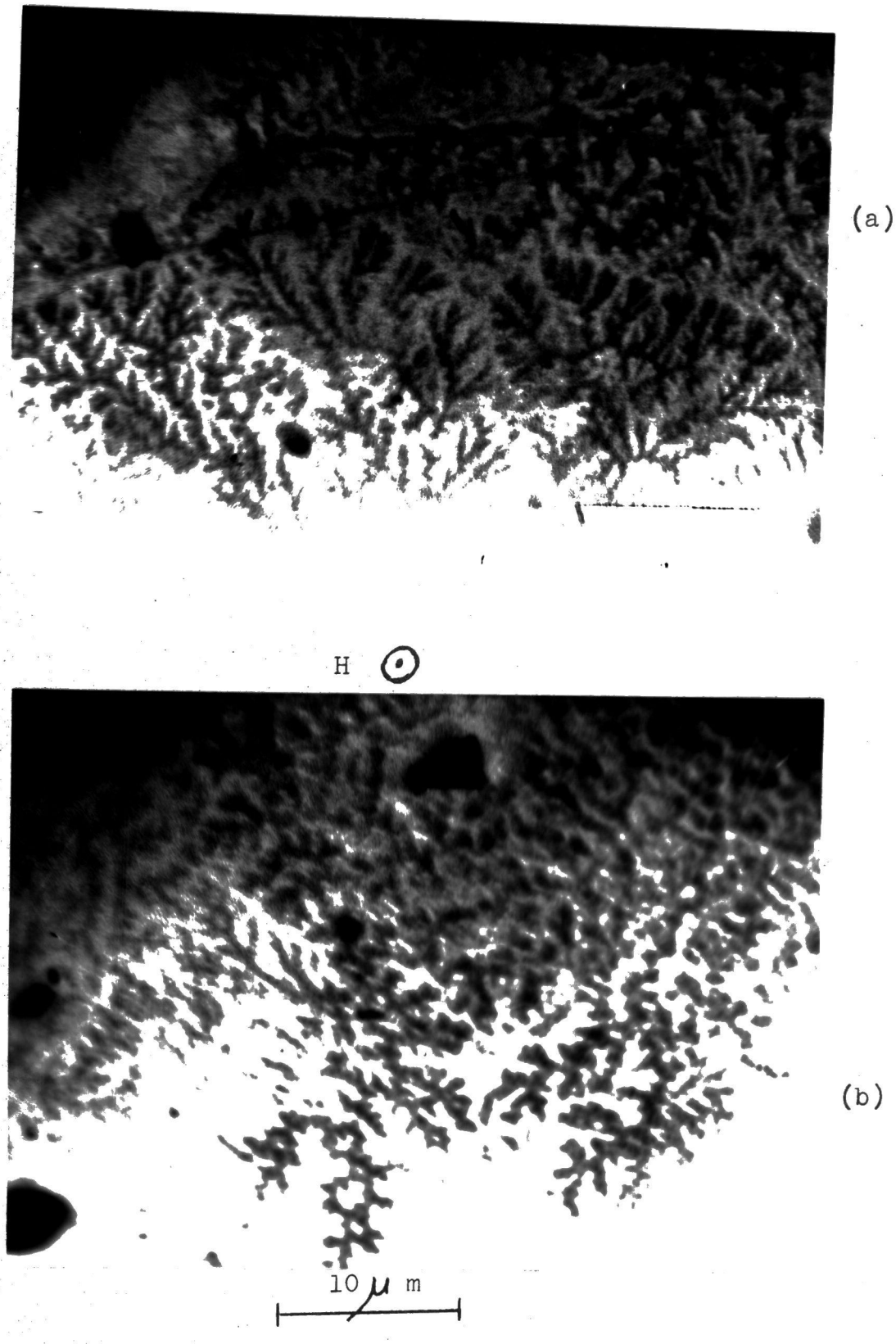

Figure (6.39) Domain structure on basal plane at 25 K
H = 70 Oe Specimen B

higher temperature.

On a b-surface the observed domain structure is shown in Figure (6.40a). Despite the low contrast evidence of domain structure may be clearly seen, but it is difficult to decide whether wall contrast or domain contrast is responsible. Figure (6.40b) shows the domain structure at a different part on the surface.

6.10 Effect of crystal thickness on size of domain structure at 273 K

The complexity and the width of the domain structure in gadolinium is a function of the specimen thickness, as in the case of other uniaxial ferromagnetic materials. Measurement of the thickness dependence of domain structure is one of the ways of verifying the existing theories on domain structure. Kaczer and Gemperle (1959) measured the dependence of the domain width D on the thickness T of a crystal of cobalt. They obtained a power law relationship of the form $D = \text{const. } T^{2/3}$. As explained in Chapter III a theory of the domain structure of a ferromagnetic with the easy axis normal to the surface was first proposed by Kittel (1949) who showed that the relation between domain width and crystal thickness was given by

$$D = (\gamma T / 1.7 I_s^2)^{\frac{1}{2}} \qquad (6.1)$$

where γ is the wall energy and I_s is the saturation magnetization. This was derived for the ideal case of an infinite sheet. Kaczer et al.(1959) showed that a dependence of the surface domain width on the thickness

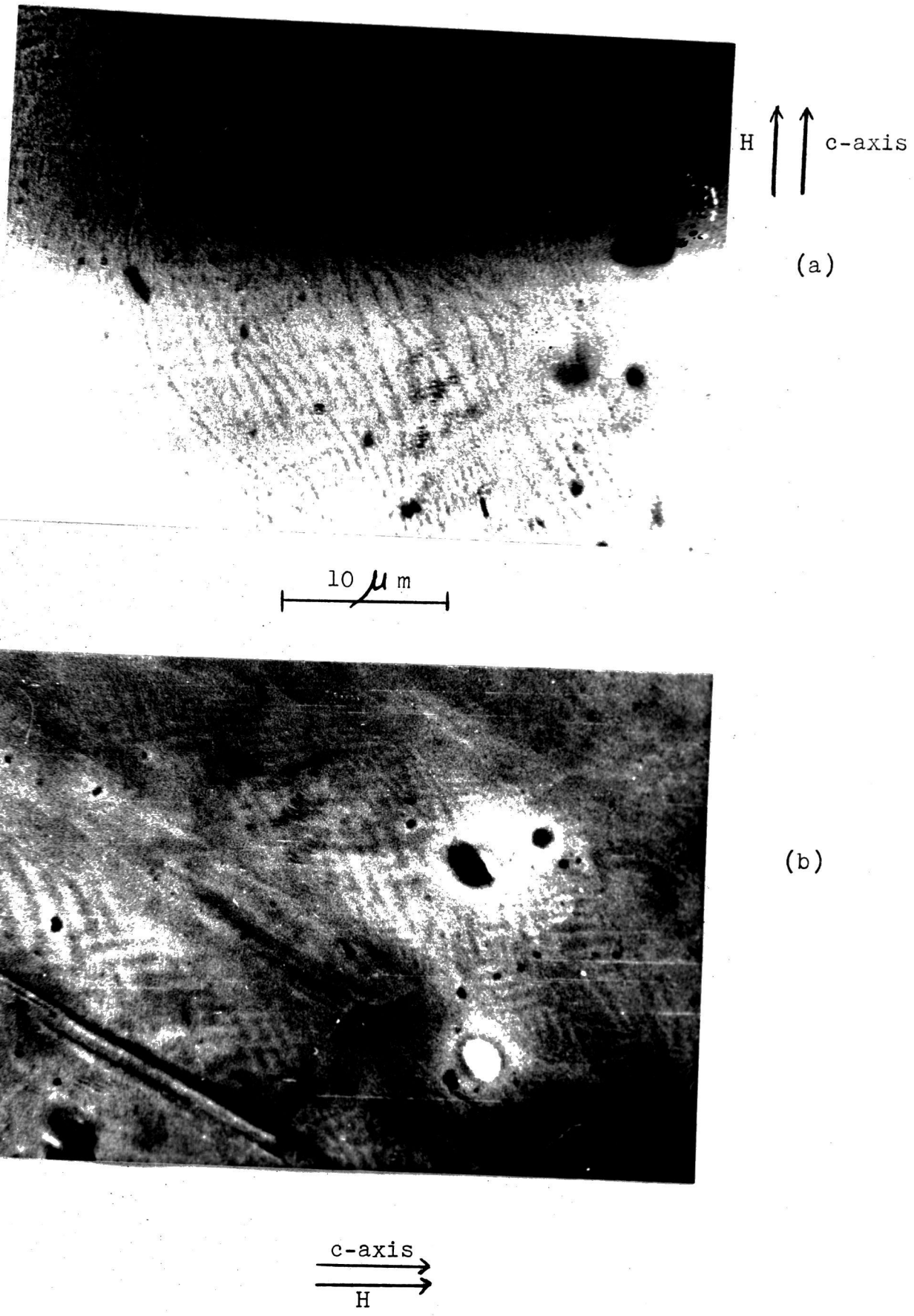

Figure (6.40) Domain structure on b-surface at 25 K
H = 200 Oe Specimen B

of the form $D \propto T^{2/3}$ would be expected above a certain critical thickness. Their treatment took into account the existence of a surface domain structure.

The present work involves a study of the variation of domain structure with thickness of the gadolinium crystal on the basal plane for a wedge-shaped crystal. Measurements of the domain width have been carried out on the same type of domain structure over as wide a crystal thickness range as possible. The regular surface domain structures in gadolinium are simple and complex honeycomb structures.

The accuracy in measuring the domain width was $\pm$ 0.1 μm. The domain structures were obtained by using a homogeneous magnetic field of 200 Oe in the c-axis direction. Under these conditions the domain structures appear to be regular. Domain structures were produced and the sizes of individual units of the honeycomb were measured. This was repeated many times to ensure a better average. The observation were extended over the basal surface of the sample. The sample thickness was measured at several points of the crystal surface using a metallurgical travelling microscope. The average domain width was measured from the micrographs of 1000 x magnification.

Figure (6.41) shows examples of the patterns on the basal crystal surface that represent the domain structure obtained at places of different thickness on the surface. In all of them the magnetic field is perpendicular to the plane and of value 200 Oe. Figures (6.41a) and

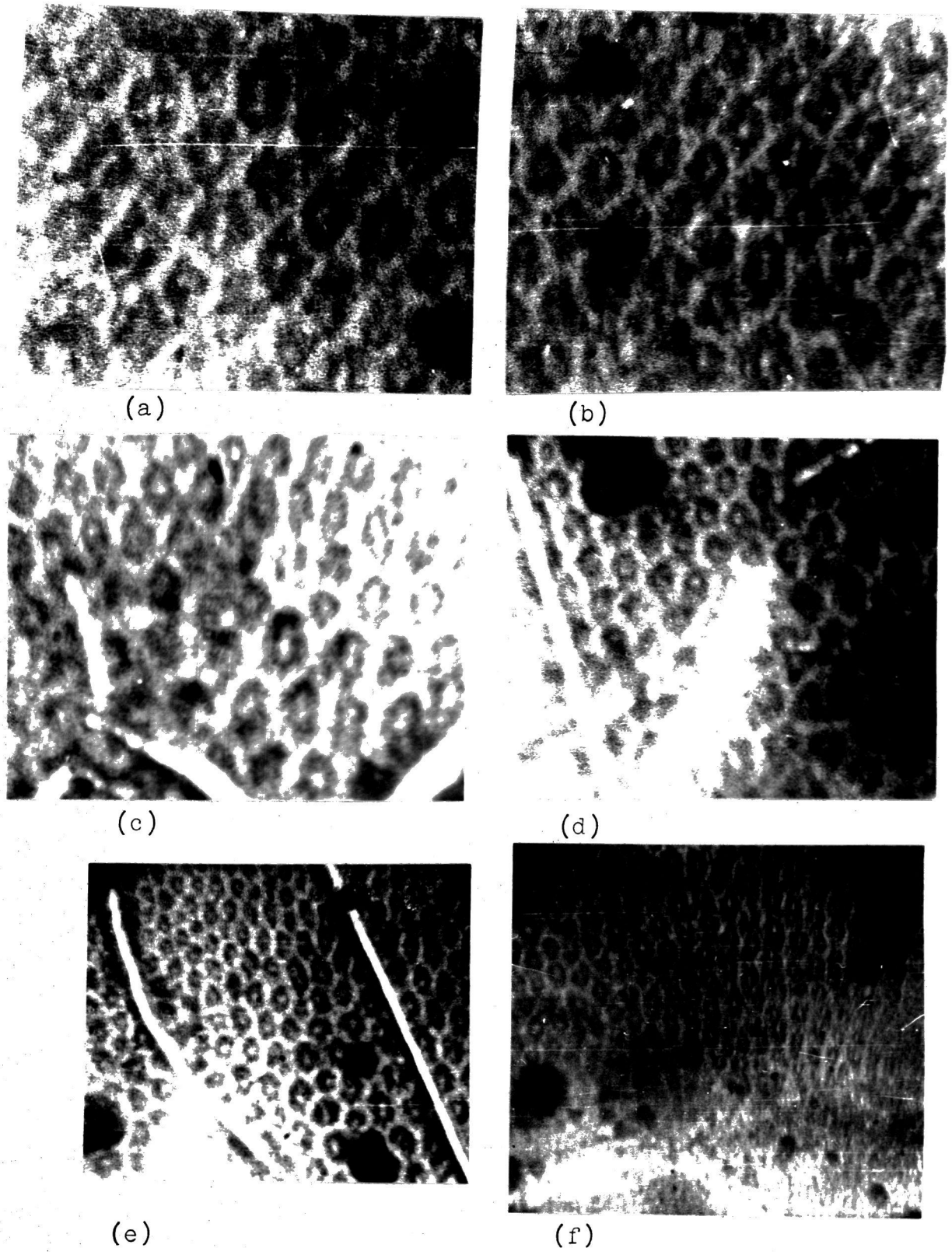

Figure (6.41) Domain structure on basal plane at 273 K
Effect of crystal thickness on domain width
H = 200 Oe Specimen A

(6.41f) correspond respectively to crystal thickness 4000 μm and 100 μm. Figure (6.41f) shows pattern at the sharp end of the wedge-shaped sample. The domain patterns for thickness from 100 μm to 4000 μm were similar, the size of the domains gradually increasing with thickness.

For crystal thickness larger than 100 μm the surface domain structure for H parallel with c-axis is basically of simple-honeycomb type. Accordingly as discussed in Chapter III we expect that the critical thickness for gadolinium must be less than 100 μm, but this has not been previously determined.

Experimental curves of the domain width as a function of the crystal thickness in the magnetically preferred direction [0001], at 273 K is plotted in figure (6.42). It shows the slope of the line was determined to be 0.64 $\pm$ 0.05. These results are in good agreement with Kaczer's theory. From the thickness dependence of the domain width results, the domain wall energy has been determined by using Kaczer's formula, as follows,

$$D = \left(\frac{3}{8I_s}\sqrt{\frac{\gamma\mu}{\pi}}\right)^{2/3} T^{2/3} \qquad (6.2)$$

where γ is the wall energy and $\mu = 1 + 2\pi (I_s^2/K_1)$. The domain wall energy may thus be calculated from the experimental data and correlated with the wall energy calculated from a theoretical model.

On the basis of the above relation (6.2), it is possible to determine the energy density of the Bloch wall for separate points on the wedge-shaped specimen, by knowing the value of Is the saturation magnetization and K_1 the anisotropy constant. Then the wall energy is

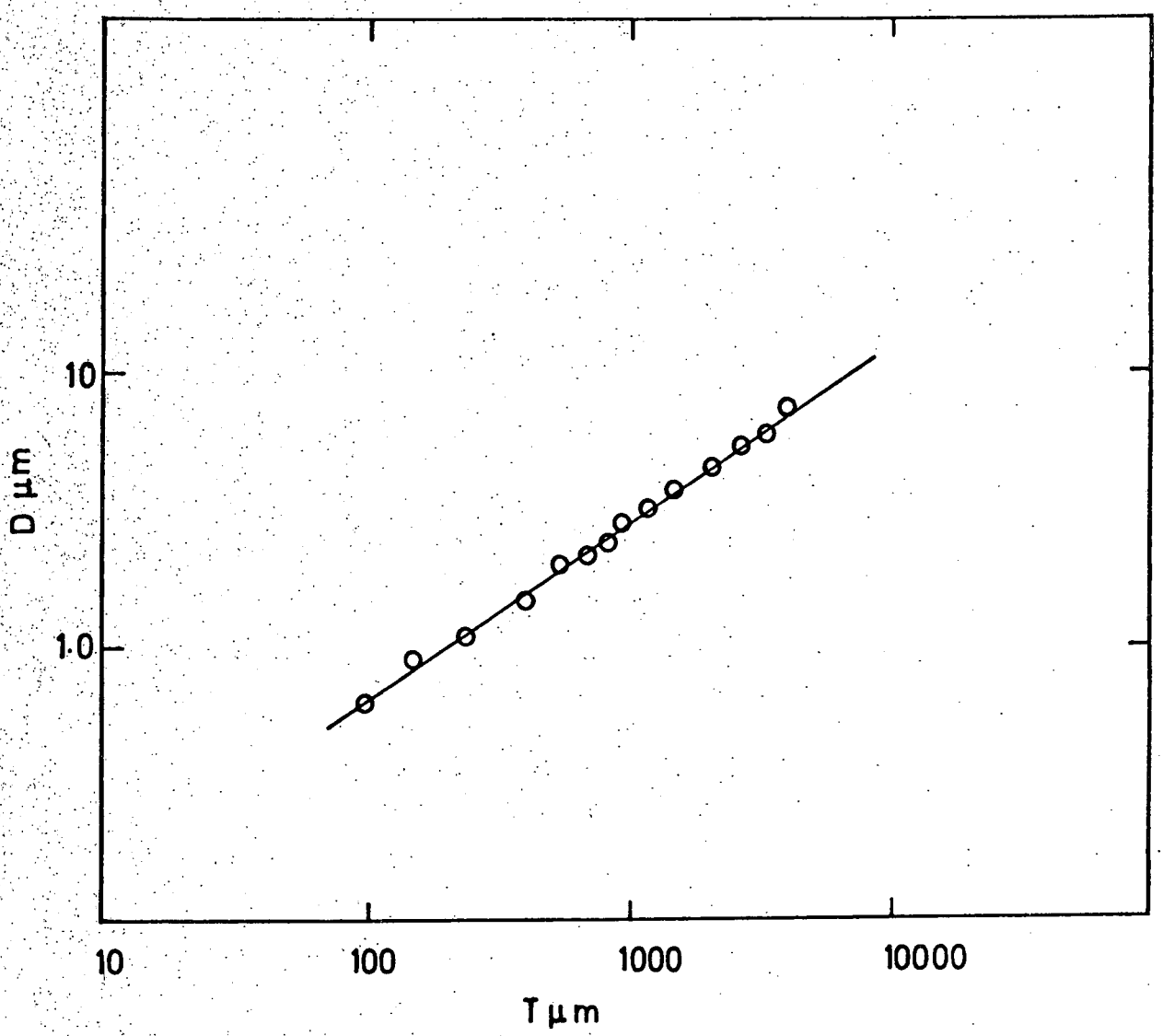

DEPENDENCE OF DOMAIN WIDTH D ON SPECIMEN THICKNESS T

FIG. (6·42)

given by the following value.

$$\gamma = 1.96 \pm 0.02 \text{ erg cm}^{-2} \qquad (6.3)$$

This value of the wall energy may be compared with the value calculated in Chapter III also for a temperature of 273 K,

$$\gamma = 1.94 \text{ erg cm}^{-2} \qquad (6.4)$$

The values of (6.3) and (6.4) correlated well.

6.11 Domain structure at non-magnetic inclusion

When a crystal possesses an imperfection such as a cavity or inclusion within the domain, surface poles will be present. The magnetostatic energy associated with these poles is reduced by a secondary domain structure, for the poles to distribute over a larger area. Néel (1944) has shown that the total energy is reduced, even though the wall energy of these domains is added to the total energy. Such structures have been observed, and there is experimental evidence of domain nucleation at inclusions in cubic crystals with many directions of easy magnetization.

Goodenough (1954) considered the conditions which bring about a reverse domain at a non-magnetic inclusion. Carey and Isaac (1964) examined the conditions under which the reverse spikes will form around a non-magnetic inclusion in a uniaxial material. Their calculation was based on the assumption that the total energy associated with the inclusion was reduced by the formation of reverse domains. The two previous papers suggested that the formation of domains of reverse magnetization depends on both the

size of the inclusion and the applied magnetic field.

For gadolinium, a uniaxial material, there has been previously no experimental evidence for the existence of reverse spikes based on inclusions. Using the dry colloid technique it has been possible to observe daggers at a non-magnetic inclusion.

Figure (6.43) was obtained at 77 K on the b-surface with an external applied field of 200 Oe in the c-axis direction parallel to the surface. As can be seen from the photograph these domains of reverse magnetization appear on both surfaces of the inclusion. This would obviously be expected since different polarities appear at opposite sides of the inclusion. In figures (6.44a, b), observed at 216 K on a plane inclined by 10° to a b-plane, one side of the inclusion has no reverse spikes. In figure (6.44a) the spikes are dark while in figure (6.44b) they are light. This is due to the formation of free poles of opposite polarity. In all the cases the reverse daggersare parallel to the c-axis.

Figure (6.45) shows a series of different types of reverse dagger at different condition of temperature and applied magnetic field and also on different planes of different inclination. The condition are given adjacent to the photograph in each case.

A series of measurements are made of the length l and base d of daggers observed in the curve of the investigation at various temperatures. Figure (6.46) shows the relationship between these two quantities for samples at two temperatures. It may be concluded that

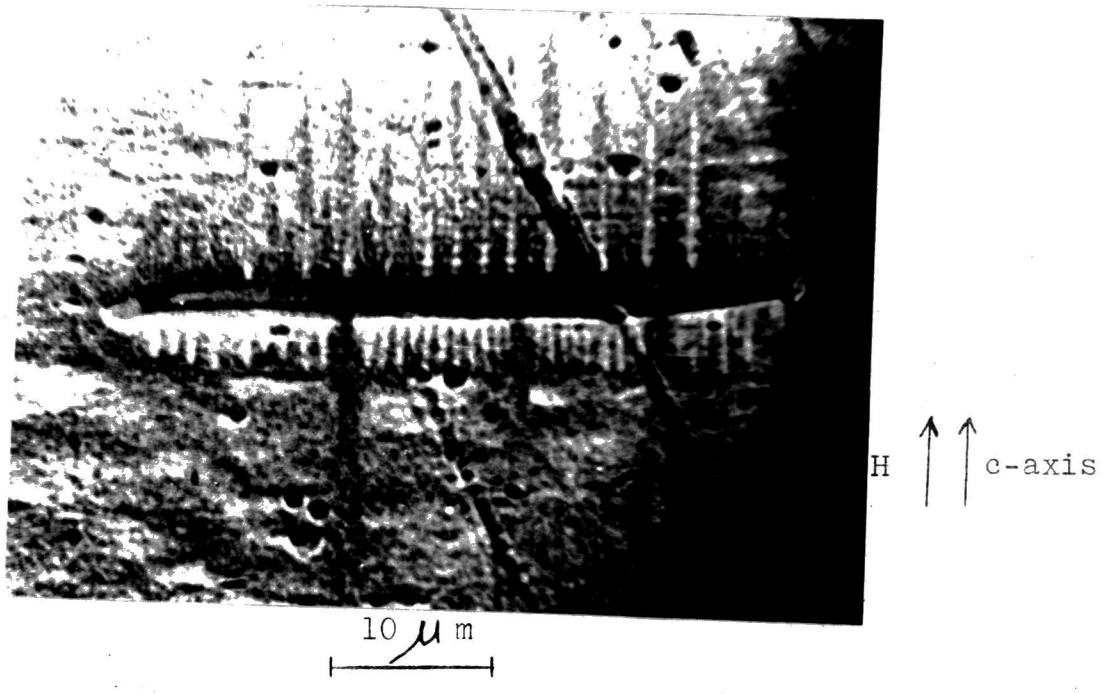

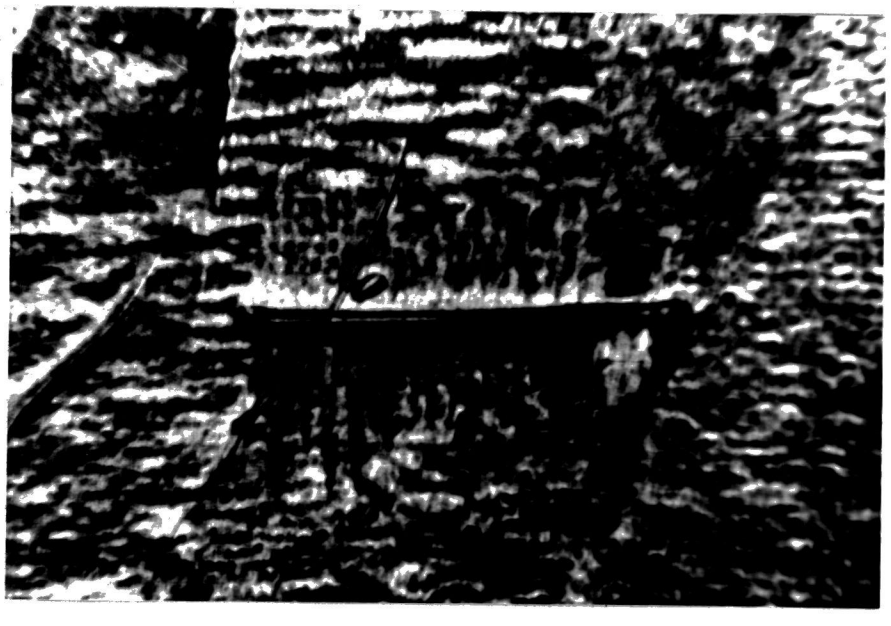

Figure (6.43) Reverse domain on b-surface at 77 K
H = 200 Oe Specimen B

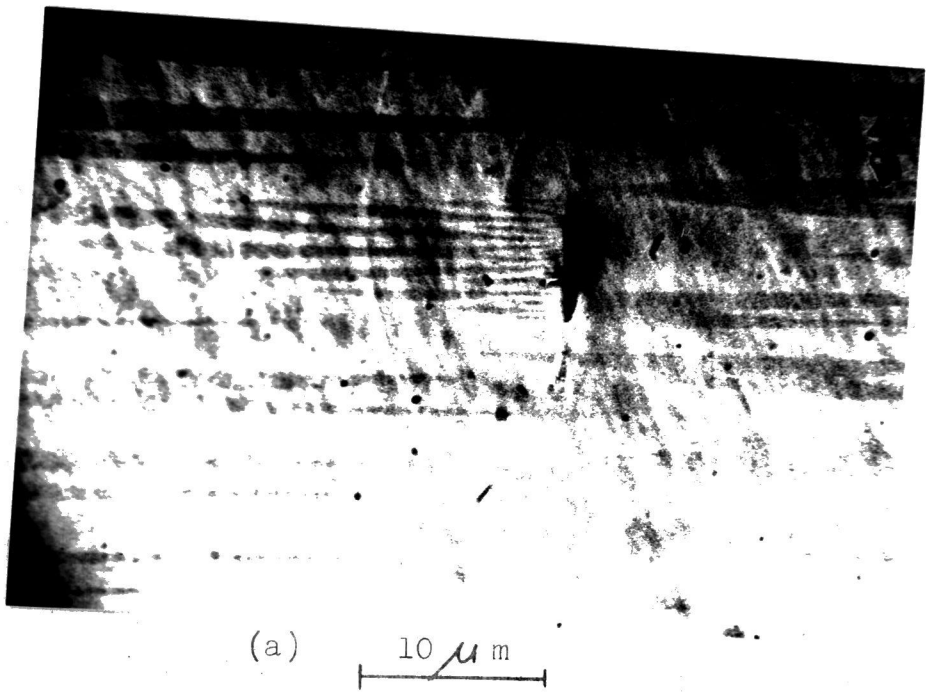

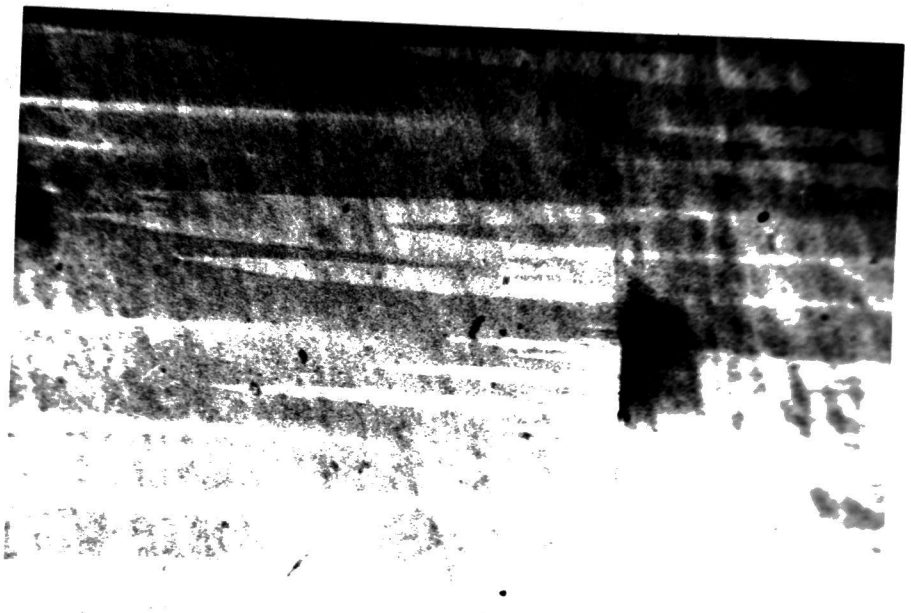

Figure (6.44) Domain of reverse magnetization on inclined surface to b-plane at 216K
Specimen B

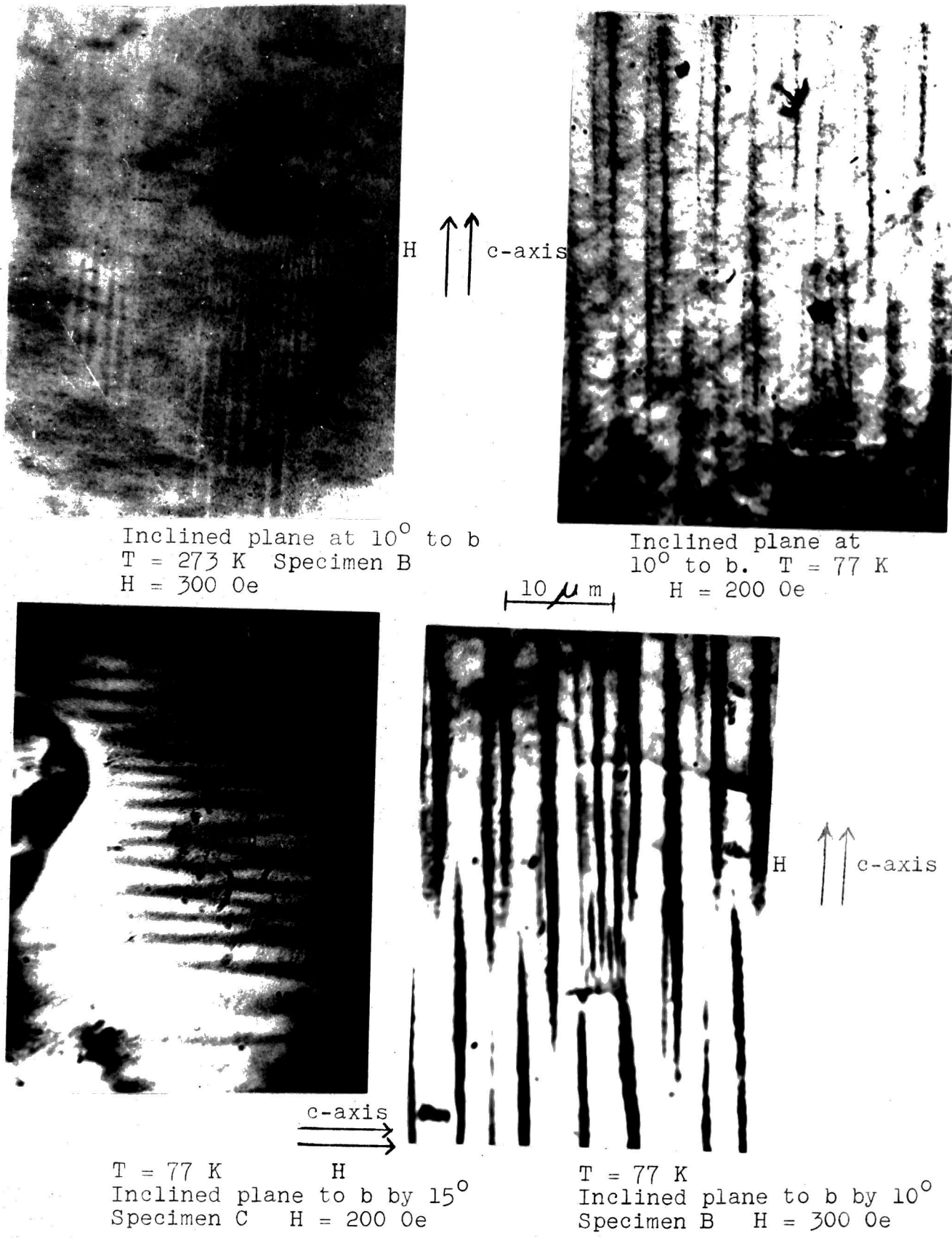

Figure (6.45) Domain structure of reverse magnetization

FIG. (6·46)

VARIATION OF DAGGER LENGTH (l) WITH ITS BASE (d)

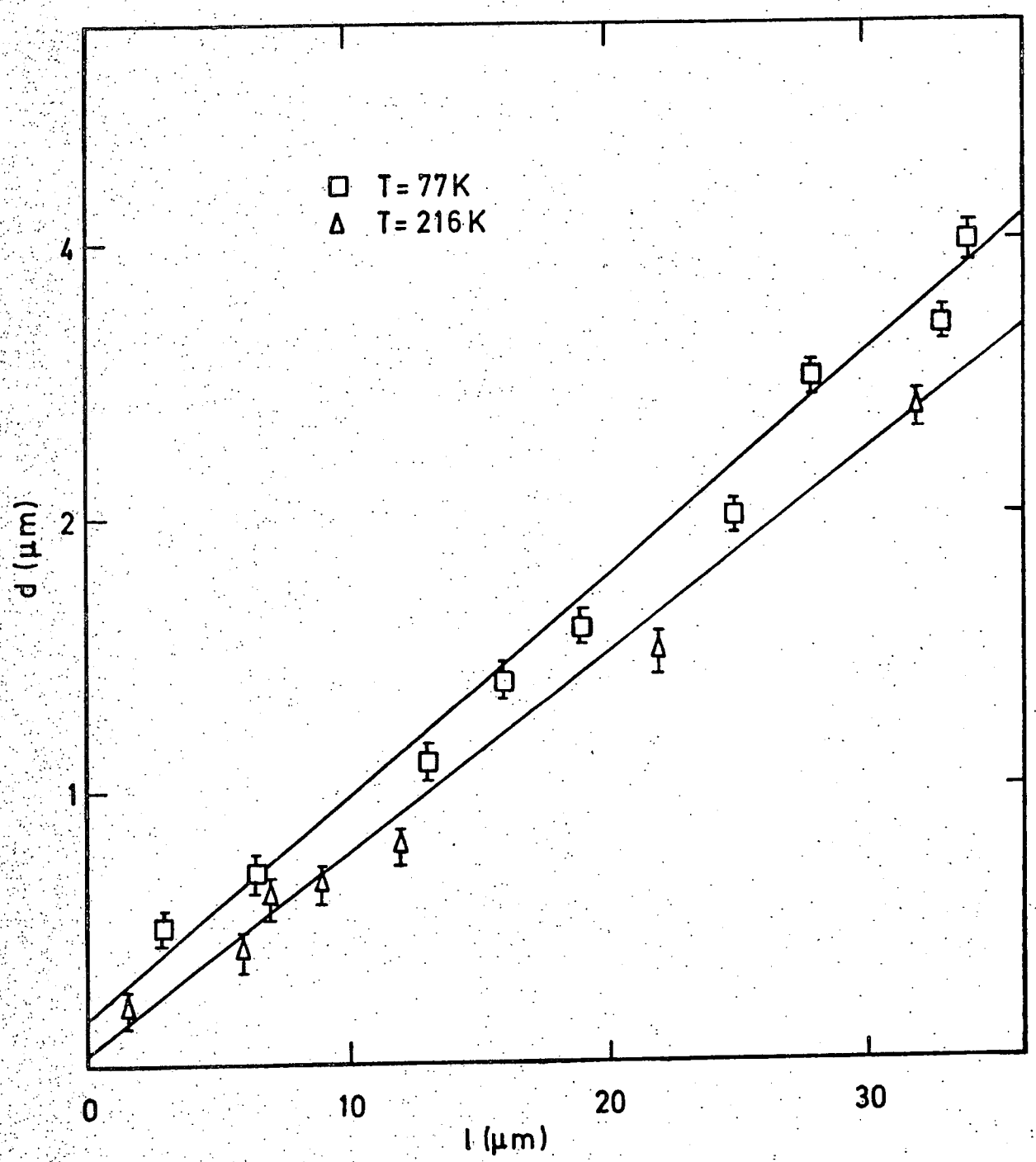

at each temperature l and d are in a direct proportion. By using a method of least squares the best straight line fits to the points for each temperature have been obtained and are shown in Figure(6.46). Both lines intersect the d-axis at a positive value. For the lower temperature it appears that for values of d less than 0.16μm the formation of a dagger is unfavourable. The corresponding value for 216 K is 0.03μm but this is not significantly different from zero within the accuracy of the measurements.

Domain structures are affected by irregularities, such as internal stresses and crystal grain boundaries. The size of the domain structure is influenced by the presence of inhomogeneities in the materials. Figure (6.47) shows reverse spikes grown around a grain boundary, observed at 77 K on a b-surface, while Figure (6.48) shows the effect of the internal stress on the domain at 77 K.

6.12 Effect of the magnetic field on the easy direction

Since many of the domain patterns were obtained with a magnetic field applied to the sample it is important to know what effect this might have on the easy directions. By calculating the total energy at different values of the effective magnetic field, it is possible to investigate how the anisotropy energy surface is distorted near to the liquid nitrogen temperature. The total energy consists of the sum of the magnetic energy and the anisotropy energy. The anisotropy energy E_A is given by the following equation:

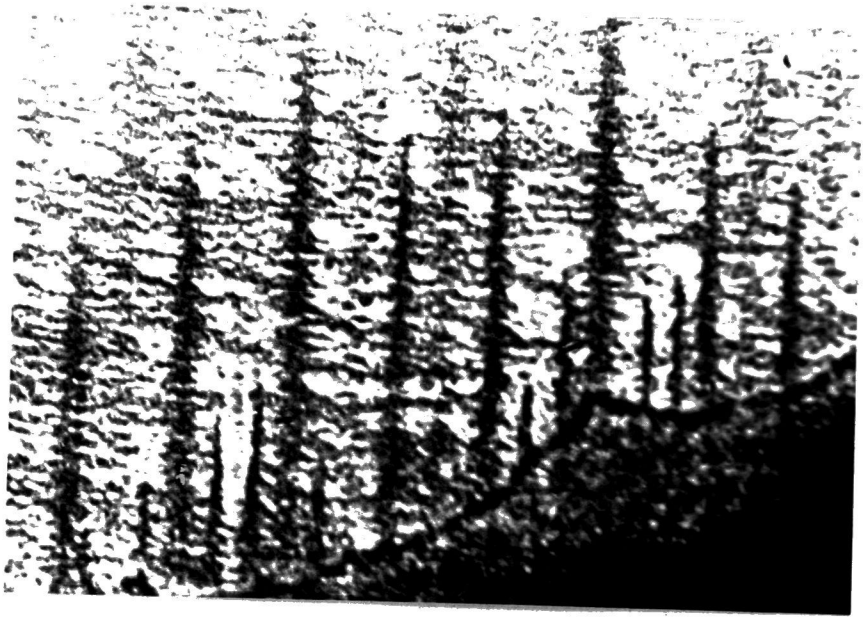

Figure (6.47) Domain structure on b-surface at 77 K
around the grain boundary
H = 200 Oe Specimen B

Figure (6.48) Domain structure on b-plane at 77K
effect of internal stress
H = 200 Oe Specimen B

$$E_A = K_o + K_1 \sin^2\theta + K_2 \sin^4\theta + K_3 \sin^6\theta . \qquad (6.5)$$

where the K's are anisotropy constants. When the field H is normal to the c-axis the magnetic energy E_M is given by,

$$E_M = - I_s \; H \sin\theta \qquad (6.6)$$

where θ is the angle between the magnetization and the c-axis. In case of a magnetic field parallel to the c-axis, the magnetic energy is given by

$$E_M = - I_s \; H \cos\theta \qquad (6.7)$$

Then from the graphs of the anisotropy constants figure (4.8), it is possible to determine the values of K_1, K_2 and K_3 at the temperature 80 K. Their values are as follows:

$$K_1 = - 0.76 \times 10^6 \quad \text{erg} \quad \text{cm}^{-3}$$
$$K_2 = 0.84 \times 10^6 \quad \text{erg} \quad \text{cm}^{-3}$$
$$K_3 = 0.25 \times 10^6 \quad \text{erg} \quad \text{cm}^{-3}$$

The saturation magnetization of gadolinium is given by

$$I_s = 2010 \quad \text{Gauss}$$

By taking different values of the magnetic field, and then calculating the total energy at different values of the angle θ. It is possible to find how the total energy depends on angle θ. Values of the magnetic field were taken from zero to 1000 Oe, for both directions of the field, i.e. one parallel to the c-axis and the other perpendicular to the c-axis.

Figure (6.49) shows the variation of the total energy with angle θ, for different values of the field H parallel to the c-axis. The easy directions of magnetization correspond to the positions of the minima in

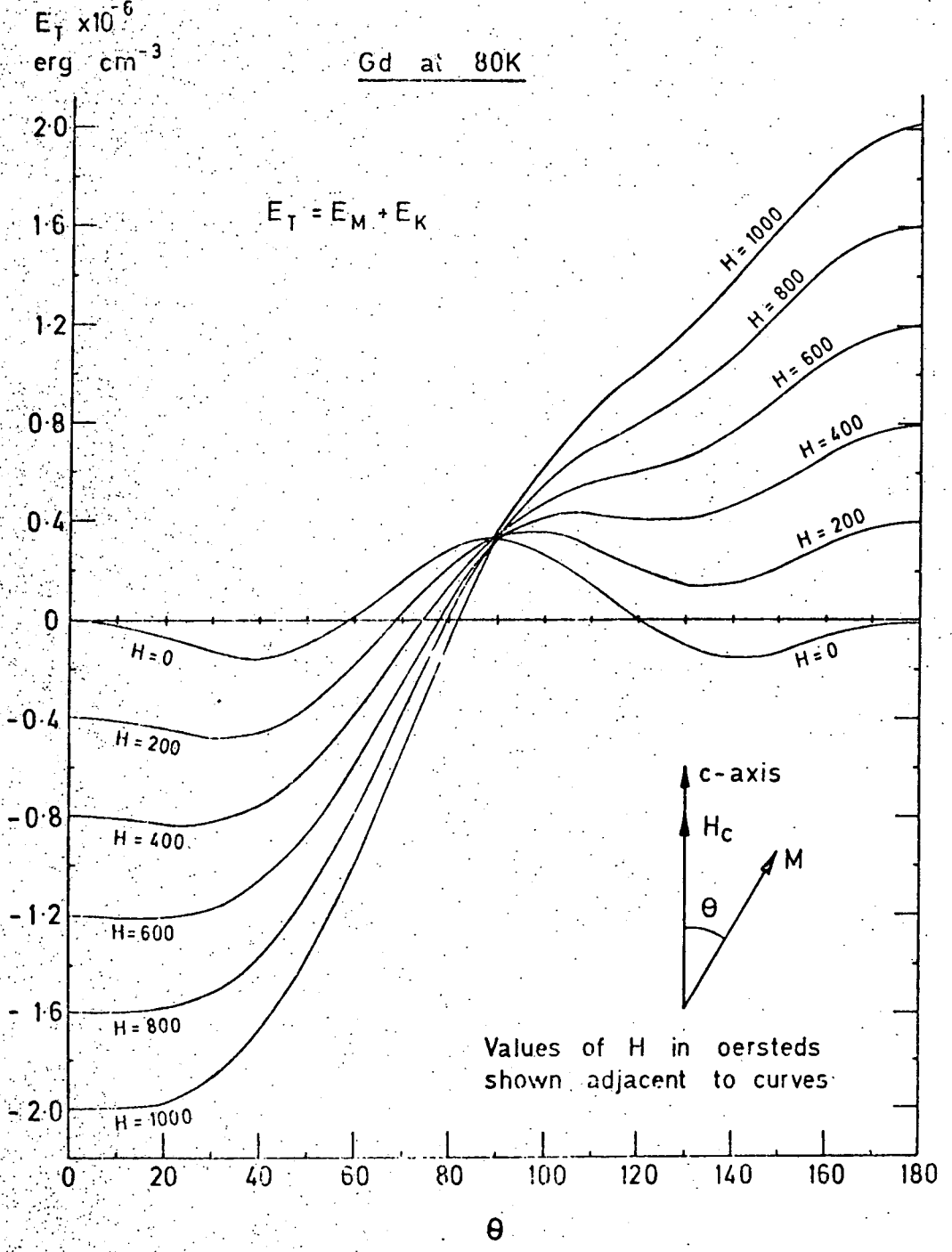

Figure (6.49) Variation of the total energy for value of θ

this curve. It is noticeable that the effect on the forward directed cone is different from that on the reverse cone. A field of 800 Oe is required before the forward minimum moves to the c-axis ($\theta = 0^{\circ}$), while a field of about 500 Oe is enough to destroy the reverse cone minimum.

Figure (6.50) shows the variation of the total energy with angle θ, for different values of H normal to the c-axis. Here the minima are again moved in position as the field is increased, but they move symmetrically towards the basal plane ($\theta = 90^{\circ}$). A field of 1000 Oe is however not strong enough to destroy the easy cone. Figure (6.51) and figure (6.52) show the change of the easy cone angle with field for the direction of the field parallel and perpendicular to the c-axis respectively.

For most of the patterns described the applied field did not exceed 300 Oe. From the graphs it can be seen that at this field in the direction of the c-axis the cone will not be destroyed, but the easy direction will lie closer to the c-axis than in zero field. With H = 30 Oe the easy direction lies on a cone with angle only slightly different from the angle with zero field.

If the field is perpendicular to the c-axis and of strength 300 Oe, from figure (6.52), it is clear that a slight increase of cone angle from 39° to 46° takes place.

The above measurements all relate to the applied field on the surface of the crystal and without calculating the value of the demagnetizing field. Because of difficulty in calculating realistic values of demagnetizing

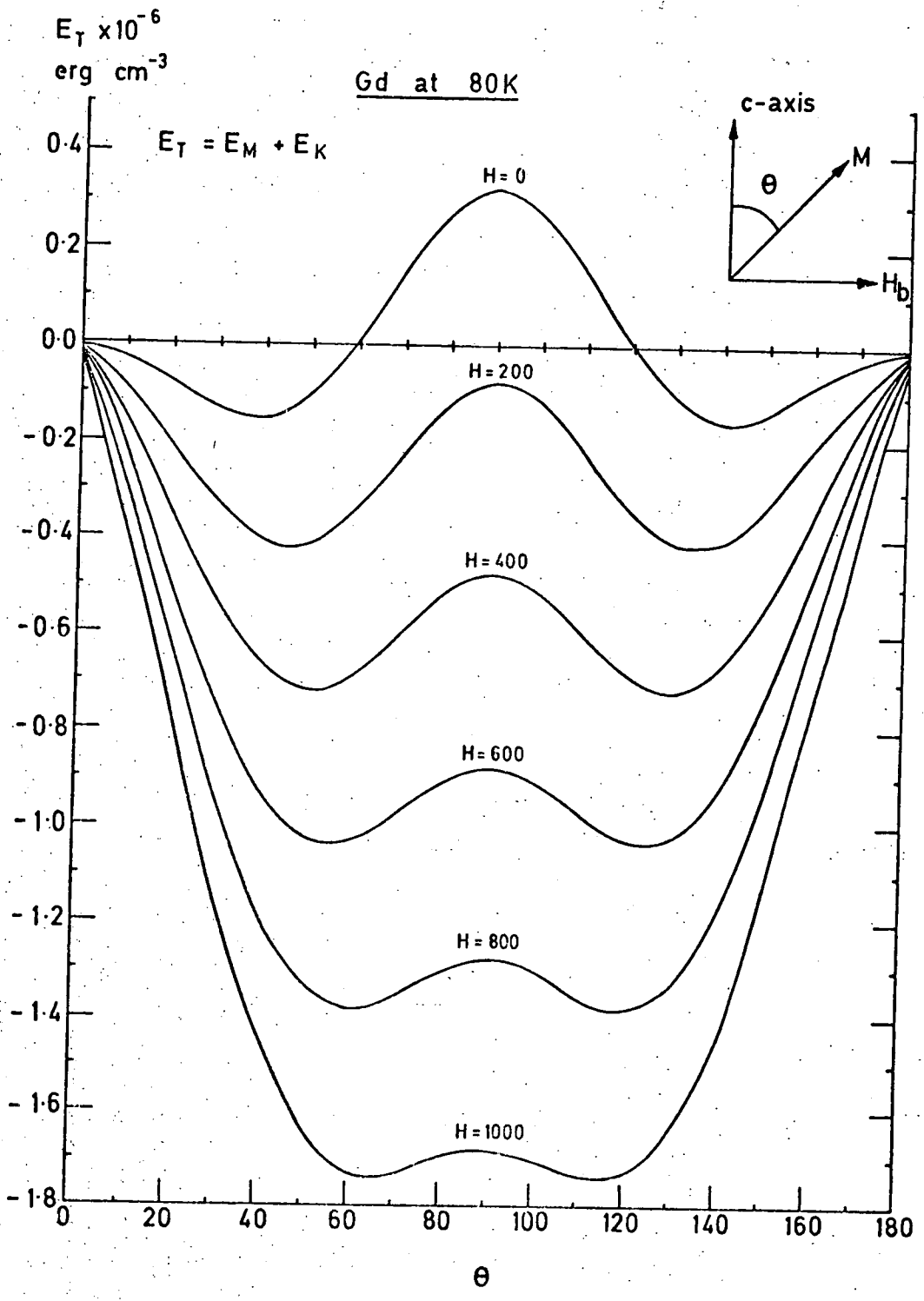

Figure (6.50) Variation of the total energy for values of θ

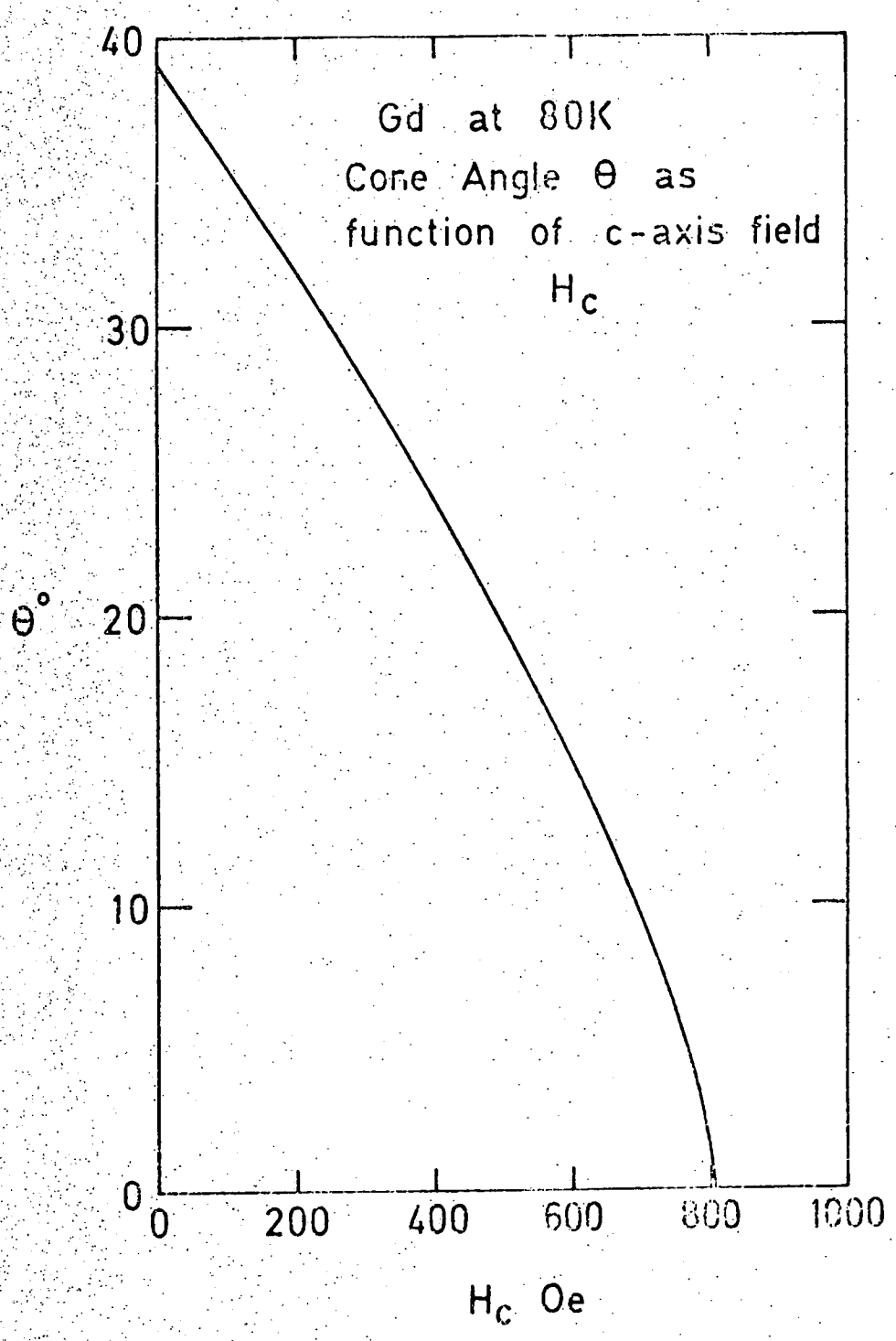

Figure (6.51) Relation between forward cone angle and the magnetic field

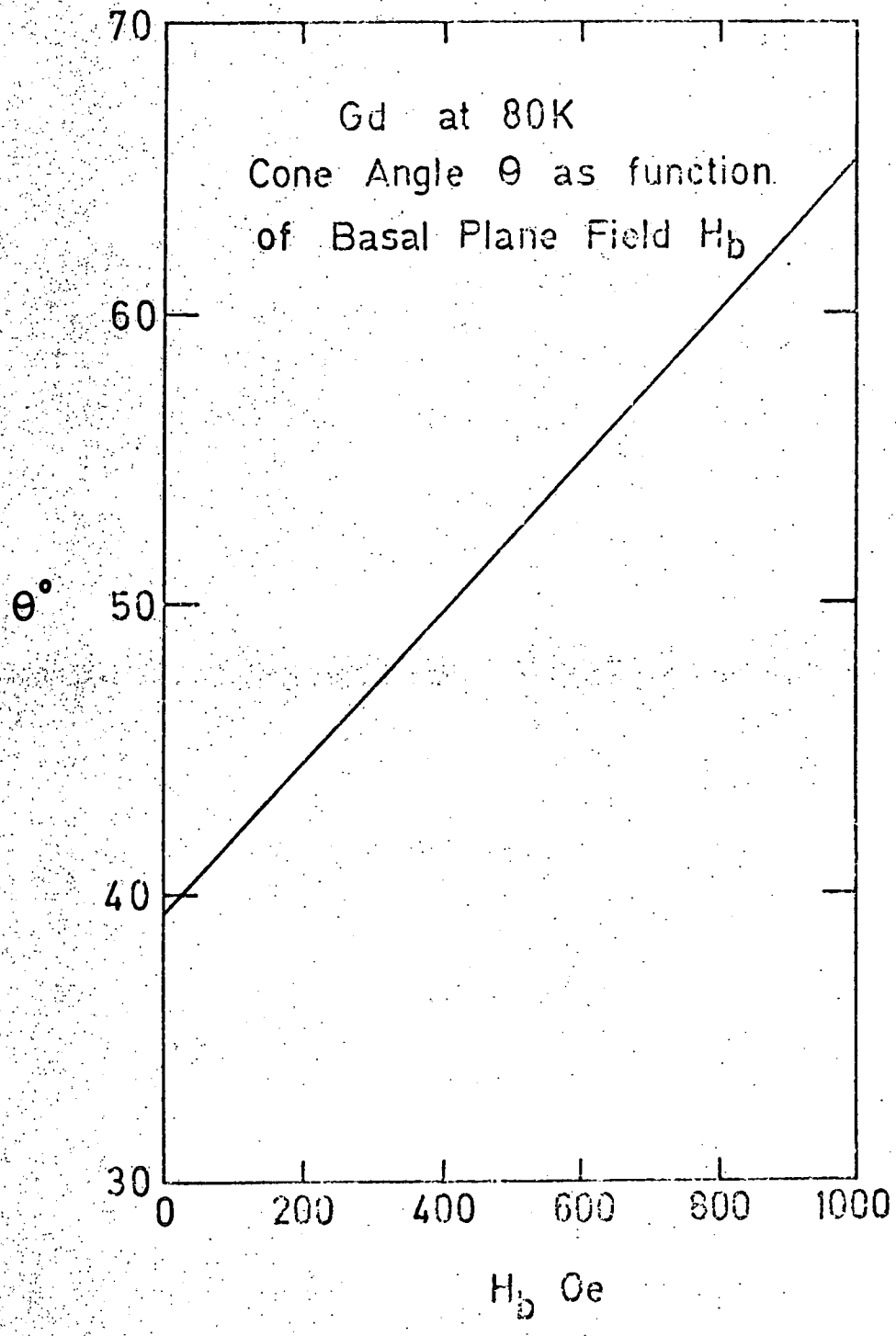

Figure (6.52) Relation between cone angle and the magnetic field

factor the effective field cannot easily be estimated. However, it must always be somewhat less than the applied field and the effects on the cone angle discussed above must be if anything, exaggerations. It is clear that with the fields employed the basic magnetic structure is not profoundly changed.

CHAPTER SEVEN

INTERPRETATION AND DISCUSSION

7.1 Model of domain structure at 273 K

The easy direction is the c-axis at this temperature and in consequence the pattern consists mainly of 180^{o} parallel walls. It was observed that when two surfaces of a single crystal, each containing the c-axis, were cut perpendicular to each other, both surfaces exhibited similar structures of walls running along the c-axis direction and the internal structure must therefore consist of domains separated by arrays of 180^{o} walls. These domains may be in the form of hexagonal prisms with some reverse magnetization domains near the surfaces. The domain structure on the basal plane was predominantly one of alternating free pole, the ends of the prismatic domains being sub-divided into smaller regions of different polarity. These represent the ends of spikes of reverse magnetization which form in order to reduce the magneto-static energy.

The model given by Privorotskii (1972) is a good example of this domain structure, and he calls it branching structure for uniaxial ferromagnets as in figure (7.1). He shows that at sufficiently large values of l (the crystal thickness), the domain structure begins to branch. In the limit $l/\delta \rightarrow \infty$ an infinitely branched structure is formed, δ is the wall width. Comparing this model with figure (6.5), observed for the domain structure in gadolinium, they are seen to be clearly similar. Privorotskii has shown that the

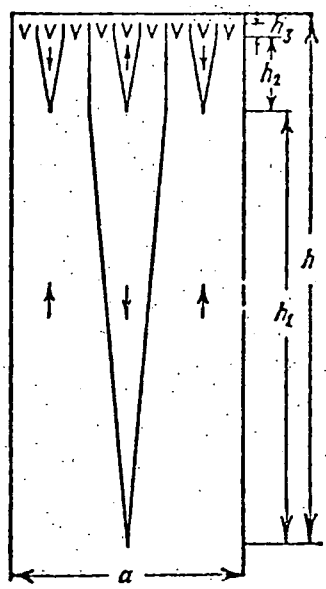

FIGURE (7.1).
(after Privorotskii 1972).

following relations would be expected to apply, irrespective of the properties of the material.

$$h = 0.117\ l \qquad (7.1)$$

and

$$\frac{h_1}{h} = (1 - 1/3\sqrt{3}) \quad \text{etc.} \qquad (7.2)$$
$$= 0.807$$

where h is the length of the maximum reverse dagger domains and h_1 is as shown in figure (7.1). Figure (6.5) shows three regions, the apparent spacing of lines on the pattern changing as the surface of the sample is approached. The changes took place at reasonably well defined distances from the surface which were taken as representing the positions from which h and h_1 should be measured. Measurements gave average values of $h = .23 \pm .02$ and $h_1 = .17 \pm .02$ mm. for a sample of thickness $l = 2.0 \pm .05$mm. This leads to

$$h = (0.116 \pm 0.001)\ l$$

and

$$\frac{h_1}{h} = (0.76 \pm 0.2)$$

which is in good agreement of the above equations (7.1) and (7.2). So an appropriate model for interpreting the domain pattern observed on b and a-surfaces for a thick crystal is that of figure (7.1), the branching structure. This, of course, carries implications for the structure on the basal plane of thick crystals, but these were not studied in the present work.

For thin crystals of gadolinium the surface structure on the basal plane consists of honey-comb patterns at 273 K. The honey-comb structure is observed by the application of a normal field produced by a permanent

magnet to the basal plane.

Kandaurova et al (1973) presented a discussion of the behaviour of a complex honey-comb domain structure in Mn Al Ge crystals. They suggested a model for this structure and for the changes they observed in it on applying a magnetic field parallel to the easy direction. This model is shown in figure (7.2). The crystal represented a matrix which was magnetized in one direction (light background in figure 7.2) and which surrounded oppositely directed domains (dark regions in figure 7.2). These domains were in the shape of regular cylinders with reverse domains in the form of additional mainly dagger shaped regions with magnetization directed in the same way as the matrix. A section of this structure is shown schematically in figure (7.2). The magnetic field employed in the present investigations was also parallel to the easy direction and did not exceed 300 Oe. Following Kandaurova it is possible to calculate the reduced field $h = \frac{H}{4\pi I_s}$ and this yeilds a value of 0.025 at 273 K. From figure (7.2a) it can be seen that this field could not be expected to cause any large change from the zero-field pattern.

The domain structure observed may be interpreted using a combination of the above models. These do not differ greatly for small effective fields, h. An attempt was made on the b surface to observe any closure structure (as distinct from the reverse dagger structure) existing on the edge of the specimen near the basal plane. The patternsin figure (6.3) and (6.2) show clearly the

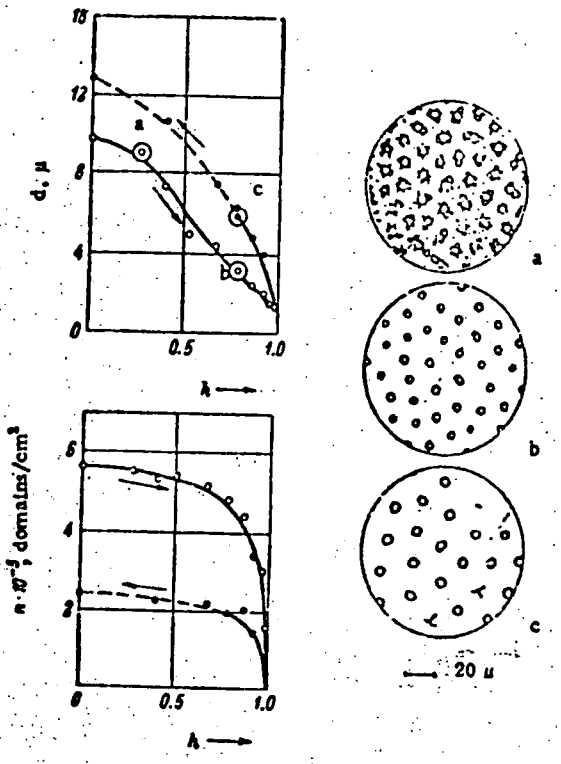

(a)

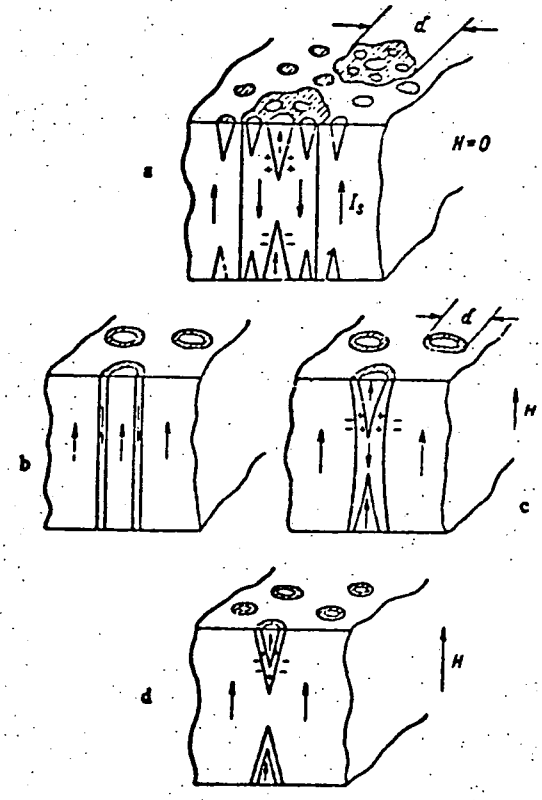

(b)

FIGURE (7.2)

(After Kandaurova et al 1973).

absence of any secondary structure of true closure domains near the surface. The walls are straight and meet the basal plane at 90^{o}. All structures could be interpreted in terms of domains of reverse magnetization as explained before.

The variation of domain width on the basal plane surface of a wedge-shaped crystal with thickness has been discussed in Chapter Six. Good agreement was found when comparison was made with the work of Kazcer (1959).

7.2 Interpretation of domain structure at 77 K

7.2.1 Magnetization direction

The intensity of magnetization in a ferromagnetic is everywhere equal to the saturation intensity I_s, but the direction of the magnetization varies from place to place in such a way as to make the free energy of the sample a minimum. A domain is a region in which the magnetization is constant in magnitude and direction and knowing the possible directions of the magnetization in a sample, the possible magnetization directions in each domain may be inferred. The free energy is the sum of two terms, the magnetocrystalline anisotropy energy and the magnetostatic energy.

For gadolinium at 77 K the expected direction of the magnetization, without applying a field, should lie on the two cones which represent the easy directions. The small magnitude of the six-fold contribution to the anisotropy energy ($K_4 = 0.002 \times 10^6$ erg cm^{-3} at 77 K)

gives an infinite number of phases on the cone around the c-direction. The cone make an angle equal to 37° with the c-axis. In zero-field the two cones are directions of minimum energy of magnetization.

As soon as a small field is applied, the angle of the cone changes as discussed in Chapter Six, and the domain magnetizations will take up corresponding directions. When the field is increased, the magnetization will turn from the cone direction towards the field so as to keep the free energy a minimum. This turning will increase the component of magnetization in the field direction. The difficulties arise when the resultant direction of magnetization is not the same as that of the applied field. In this case the demagnetizing field may modify the magnitude and the direction of the field acting in the interior of the crystal.

Birss and Martin (1975) gave a number of modes for the possible directionsof the domain magnetizations at various stages of the magnetization process for a hexagonal crystal. They presented equations the solution of which yeilds the intensity and orientation of the mean sample magnetization. They discussed the various orientations of the saturation magnetization in the domains for a variety of magnitudes and orientations of the magnetic field. They applied this theory of phases to magnetic materials which have the full 6/mmm hexagonal symmetry. They observed that the directionsof magnetization in the domains depend on the direction of the internal magnetic field.

Situations relevant to the current work are shown in figure (7.3). These correspond to phases in which the easy directions nearest to that of the effective field are preferred. Figure (7.3a) shows easy directions lying on a cone when the effective field is parallel to the c-direction. Figure (7.3b) shows a similar mode for an effective field in the b-direction. For small values of K_4 all direction on the cone would have closely similar energies when the effective field lay in the c-direction The arrangement shown in figure (7.3b) would be modified in such a case to give only two directions of magnetization symmetrically placed with $\phi = 90^\circ$ or $\theta = \theta_0$ or $180 - \theta_0$.

In the calculations of Chapter Six it was found that the cone angle changed with the values of the field in the above two directions in a similar way to that in the model of Birss and Martin except that for Gd at 77 K K_4 is negligible. Taking the equations given by Birss and Martin for the modes IIC and IIB, it is possible to calculate the components of the magnetization at 77 K, I_p parallel to the applied field H_e and I_n perpendicular to it. If the direction of H_e is specified by polar and azimuthal angles $\textcircled{H}_e$ and Φ_e then: for Mode IIC

$$I_p = I_s \cos\theta \cos \textcircled{H}_e + \frac{H_e}{N} \sin^2 \textcircled{H}_e \qquad (7.3)$$

$$I_n = I_s \cos\theta \sin \textcircled{H}_e - \frac{H_e}{N} \cos \textcircled{H}_e \sin \textcircled{H}_e \qquad (7.4)$$

where N is the demagnetizing constant of the crystal.

for Mode IIB

$$I_p = I_s \sin\phi \sin\theta \sin \Phi_e + \frac{H_e}{N} \cos^2 \Phi_e \qquad (7.5)$$

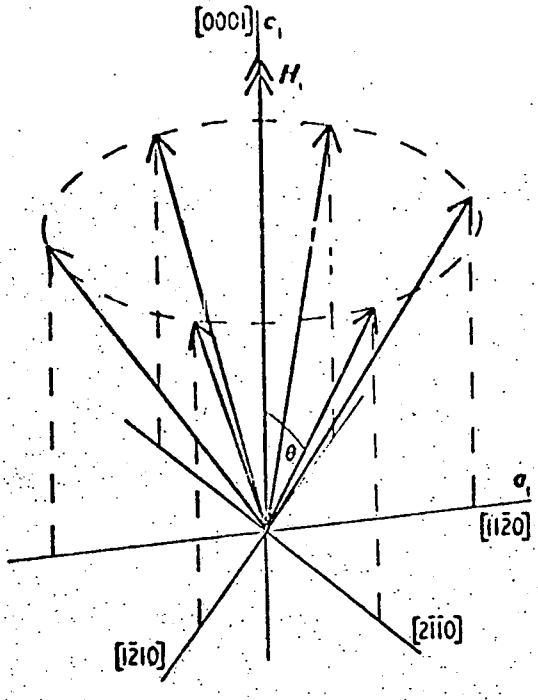

(a)

Mode IIC

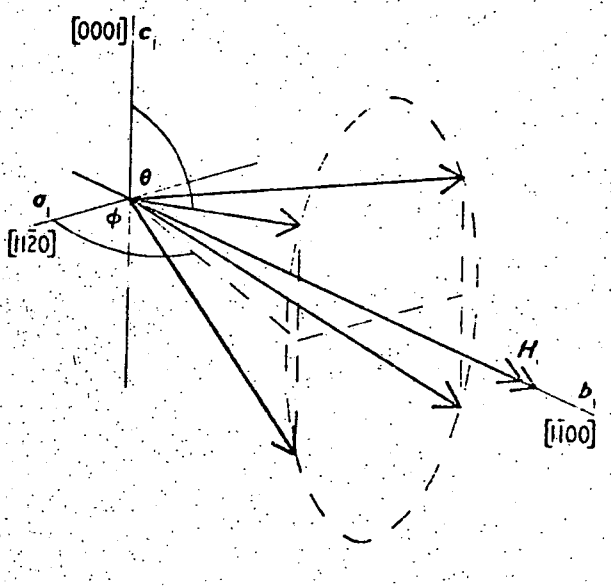

(b)

Mode IIB

FIGURE (7.3).

after Birss and Martin (1975).

$$I_n = -I_s \sin\phi \sin\theta \cos\Phi_e + \frac{H_e}{N} \cos\Phi_e \sin\Phi_e \quad (7.6)$$

By knowing the values of I_s, H_e, N and the different angles I_p and I_n can be found from these equations. For H parallel to the c-axis the equations simplify to $I_p = I_s \cos\theta$ and I_n = zero this becomes $(H)_e$ = zero. In case of H parallel to the b-axis and K_4 small, also both of Φ_e and ϕ equal to 90^o the equationsthen simplify to $I_p = I_s \sin\theta$ and I_n = zero. The applied field H_e and the effective field H_i have same direction because of symmetry.

7.2.2 Possible types of domain boundary wall

In most or all of the domain structures observed for gadolinium at 77 K, the main domain walls run parallel to the c-axis with traces of other less well defined walls normal to the c-axis.

Condition of zero or non-zero field determine possible magnetization directions. Walls must form to satisfy the condition that the normal component of the magnetization is continuous across the wall. The various possible walls satisfying this requirement are summarised in figure (7.4). This applies for the zero-field case i.e. mode I of Birss and Martin. When a field sufficient to proceed to Modes IIC or IIB is applied fewer walls are possible and this is indicated in the table.

In the first row of the table in figure (7.4) it can be seen that if the magnetization rotates from direction OA on the forward cone to OB on the reverse cone, the

FIGURE (7.4).

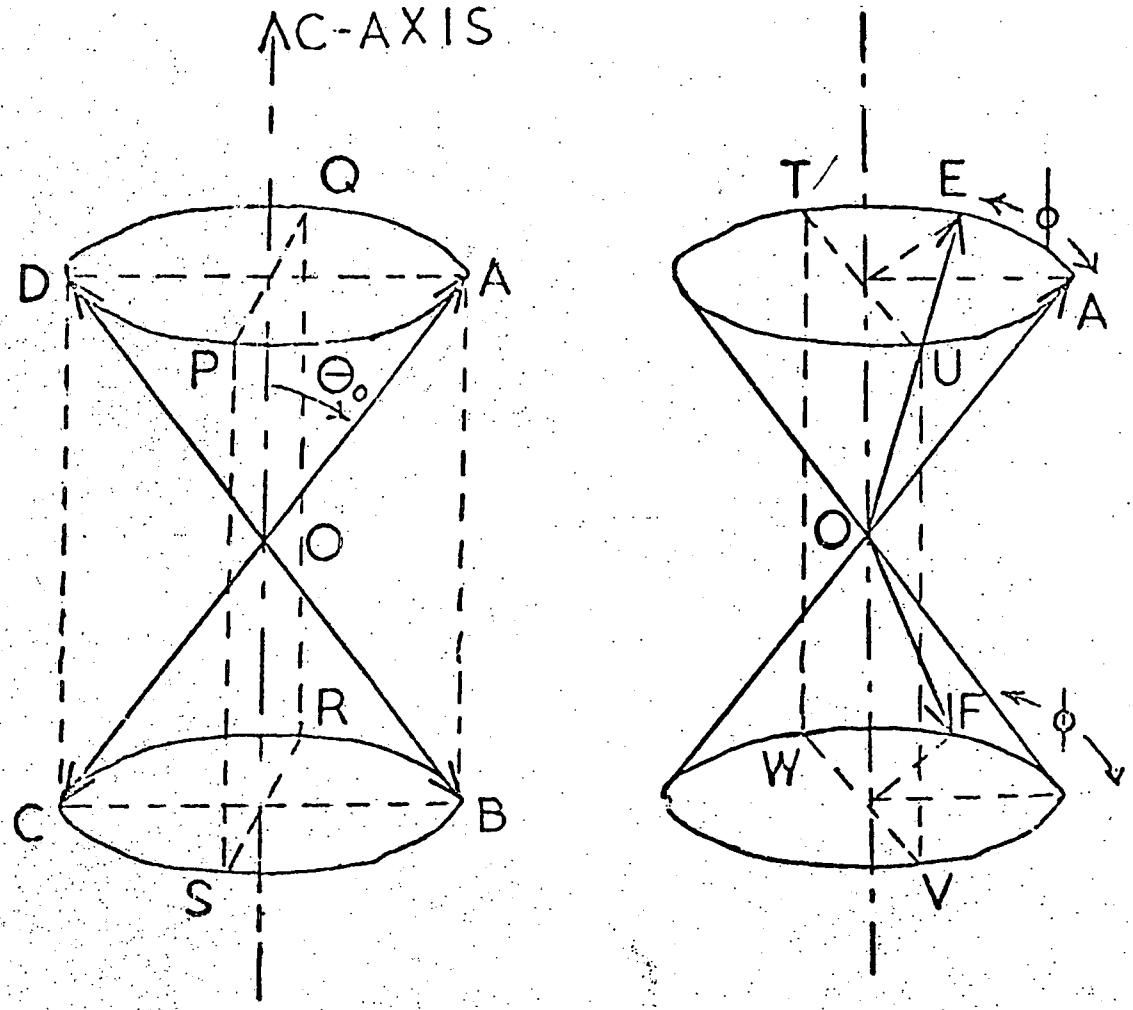

Wall Type	Possible Modes	Magnetization Directions	Angle of wall	Plane of wall	Normal Component of I_s	Anisotropy term x 10^6 erg cm^{-3}
1a	I, IIB	OA ⟶ OB	$\pi - 2\theta_o$	PQRS	$I_s \sin\theta_o$	$F_k(\pi/2)-F_k(\theta_o)= 0.523$
1b				ABCD	0	$F_k(\pi/2)-F_k(\theta_o)= 0.523$
2	I	OA ⟶ OC	π	ABCD	0	$F_k(\pi/2)-F_k(\theta_o)+ K_4=0.525$
3a	I, IIG	OA ⟶ OD	$2\theta_o$	ABCD	0	$K_4 = 0.002$
3b				Basal	$I_s \cos\theta_o$	$K_4 = 0.002$
4a	I, IIC	OA ⟶ OE	$o \rightarrow 2\theta_o$	TUVW	$I_s \sin\theta_o \cos\phi/2$	$K_4 = 0.002$
4b				Basal	$I_s \cos\theta_o$	$K_4 = 0.002$
5	I, IIB	OA ⟶ OF	$o \rightarrow \pi$	TUVW	$I_s \sin\theta_o \cos\phi/2$	$F_k(\pi/2)-F_k(\theta_o)+K_4=0.525$

normal component of the magnetization will be equal to $I_s \sin \theta_o$ and the corresponding anisotropy term $F_k (\pi/2) - F_k (\theta_o)$. The plane of the wall may be either PQRS or ABCD and its angle equal to $\pi - 2\theta_o$. Such a wall is possible in Modes I and IIB.

In considering a model for the domain structure in Gd at 77 K we must select from these possible walls ones which fit the observations. For the principal walls we may choose from those that lie in planes ABCD, PQRS or TUVW. The transverse walls must be either of the two which lie in the basal plane.

A further consideration is the wall energy. For a Bloch wall the total energy is made up of equal parts of exchange and anisotropy energy. The column headed "Anisotropy term" in the table in figure (7.4) therefore gives some idea of the relative energies of the different walls. Four types of wall have considerably lower energy (determined by K_4 alone) and may be found in Modes I and IIC. However, in Mode IIB only two types of wall are possible and these are of considerably greater energy. It must also be remembered that wall thickness is inversely related to wall energy and that thin walls give better wall contrast in colloid observations.

7.2.3 Model for the domain pattern at 77 K

With the decreasing of the temperature from 273 K, the anisotropy constant decreases rapidly and K_1 changes sign at about 245 K. The easy direction moves off the

c-axis and lies on a cone. As a result of this a re-orientation of domain structures takes place. As the temperature falls the walls become less well defined and disappear completely at 240 K. A new wall may be found at lower temperature besides the 180^{o} walls. When the temperature falls to a value 77 K, a new type of structure would be expected owing to the rotation of the easy direction.

It is clear that the observed patterns represent true magnetic domains. The usual difficulty of interpretation of such patterns is present i.e. the development of a three dimensional model from only surface information, but some progress may be made. A model as in figures (7.5) and (7.6) is suggested as an interpretation of the pattern observed at 77 K.

Most of the structures on the c-plane and that on the b-plane are viewed under different conditions of applied, and effective, field. The domains on the b-plane consist of "daggers" but the daggers become narrow towards the surface and smaller ones appear between.

The model in figure (7.5) is suggested for the pattern observed on basal plane. The magnetization in each domain may be considered as consisting of two components, one normal to the surface and the other in the basal plane. Since the basal plane anisotropy is small, the basal plane magnetization component will not be strongly bound to a particular direction and may vary in direction from point to point even in a single domain. The arrows in the

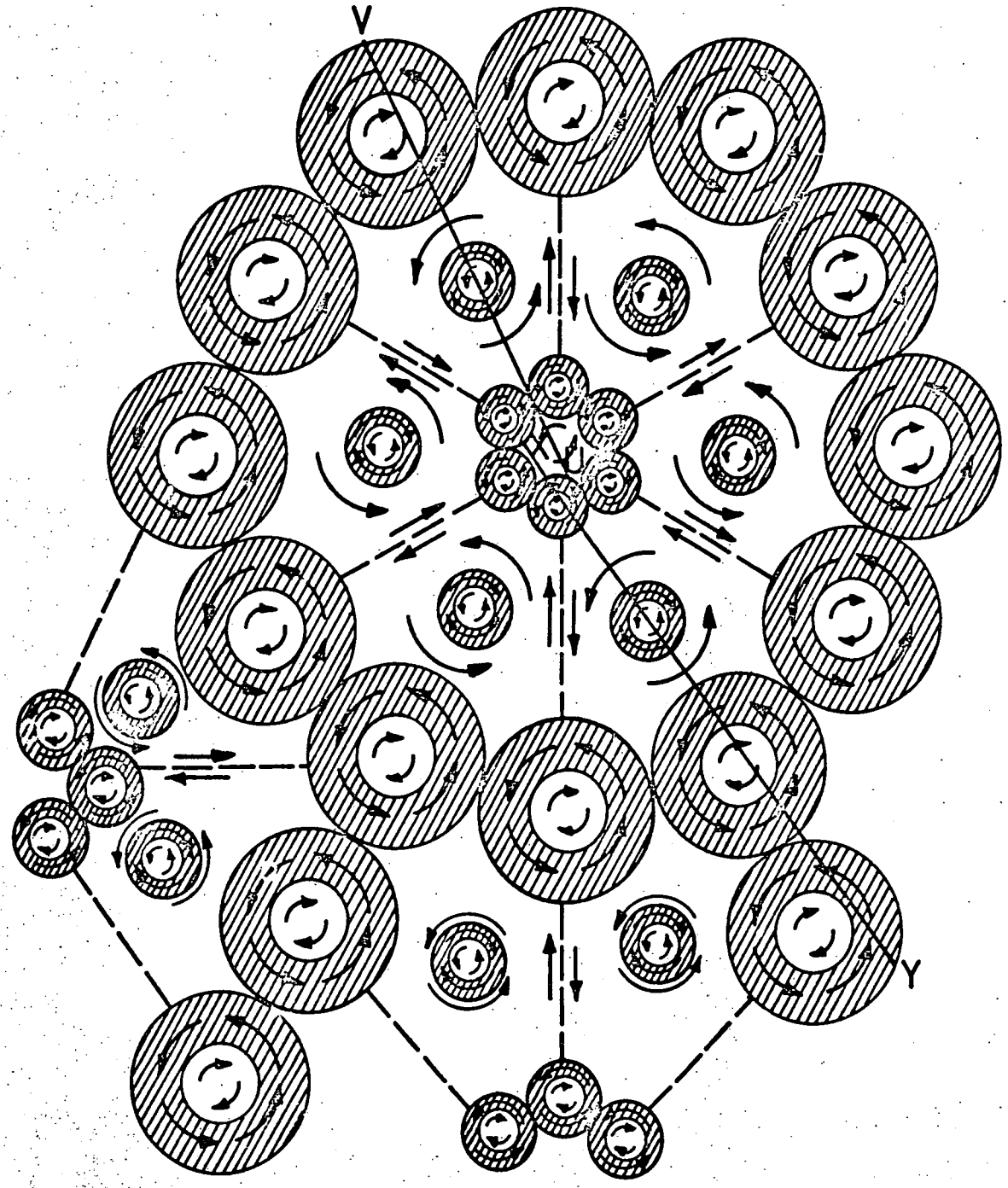

Fig. 7.5. Arrows represent direction of basal plane component of I_S, shading represents surface polarity $+I_S \cos \Theta_0$, unshaded areas have polarity $-I_S \cos \Theta_0$.

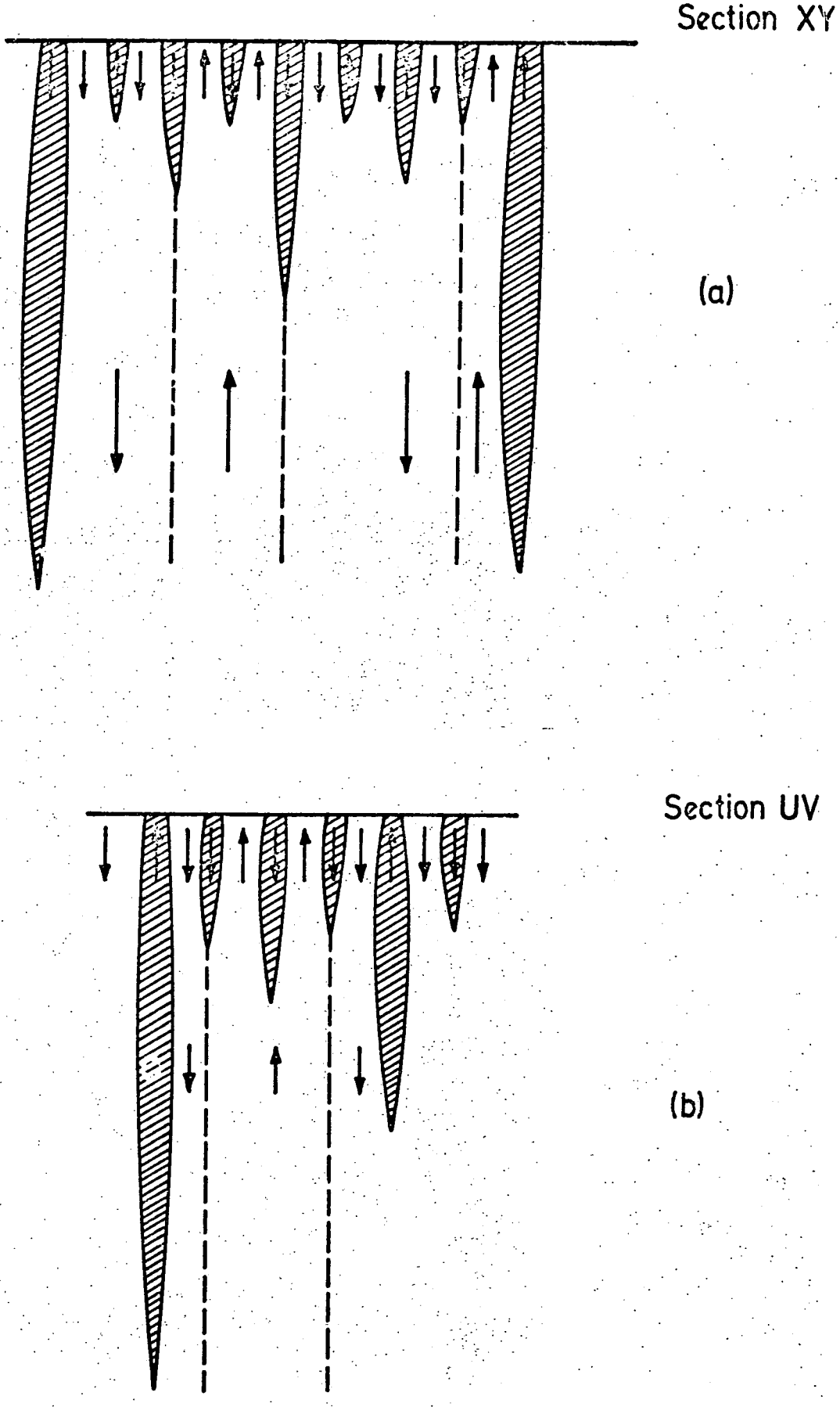

Fig. 7.6. Arrows represent direction of c-axis component of I_S, shaded areas have north polarity on b-plane, unshaded areas have south polarity on b-plane.

figure represent possible magnetization directions on the basal plane in each domain. The shaded areas are domains with the normal component of the magnetization out of the plane. The white areas are domains with this component of magnetization oppositely directed.

In any one domain the magnetization is considered to vary in direction but to lie on a conical surface. In an adjacent domain a similar variation takes place on the reverse cone. In figure (7.4) the change of direction across the boundary walls could be of the type (OA - OB), (OA - OC) or the general case (OA - OF). All these conditions are required for the model shown in figures (7.5) and (7.6). Thus we require walls as in figure (7.4) of types 1a, 1b, 2 or 5.

Figures (7.6a, b) are sections through the domain structure of figures (7.5); (7.6a) represents the section XY while (7.6b) represents section UV. These sections fit with the general observation of the domains observed on the b-plane. The condition of continuity of the normal component through the wall is satisfied in this model. The fact that the pattern shown in figure (7.6) for a section cut through the crystal agrees with the observations on the b-plane is not conclusive evidence for its validity. The cutting of a surface must necessarily affect the patterns because of the magneto-static energy involved. However, there is evidence from Figure (6.28) that the patterns continue with little change right to the edge of a basal plane.

Basal plane patterns must be still in Mode I because opposite polarity is seen up to fields of the order of 1000 Oe, but it may change to Mode IIC above this field. Patterns on the b-plane with H normal to the surface are also in Mode I as is evidenced by areas of alternating polarity, but the structure may change to Mode IIB at about 600 Oe. This means that the walls have comparitively high energy since rotation must take place over the basal plane energy hump.

The model in figures (7.5) and (7.6) is an ideal representation, but is clearly not exactly correct over the whole of the crystal surface. Patterns contain the basic elements of the model, but vary somewhat from point to point, presumably due to local influences such as surface irregularity and residual strain. The walls in figure (7.5) shown as broken lines would not be expected to be visible in a colloid pattern produced with a normal bias field since the component of the magnetization normal to the specimen surface is the same on both sides of the wall.

Various other models have been considered as giving rise to the patterns observed. None of these proved to be satisfactory for a material with conical easy directions owing to the difficulty of satisfying the condition of continuity of the normal component through the wall in all walls. A complete and unambiguous interpretation of the patterns is not possible on the evidence so far available and some suggestions are made in the following section for the types of experiments which could help to

resolve the remaining problems.

7.3 Suggestions for further work

The colloid technique has various limitations, particularly the fact that only the surface domain structure is observed. Also it is not possible to study the dynamic changes of the domain structure by the effect of applying a variable magnetic field or by changing the temperature of the sample in the low temperature range where the dry colloid method is used.

The apparatus used in this work could operate only at a fixed values of the temperature, and a range of small values of the applied field. The modification of the apparatus for use at liquid helium temperature was not completely successful owing to the need to use the same sample tube and an existing dewar for liquid helium. A complete redesign of the system would be desirable if helium temperatures are to be reliably achieved. This is particularly important since in further work on the domain structure of gadolinium, it will be of interest to study between 77K and 4K where the basal plane anisotropy constant K_4 has a much higher value. Further information on the domain structure when the basal plane anisotropy is not negligible would be of great assistance in interpreting the patterns at 77 K as there is not a large change in the magnetization over this temperature range and the anisotropy change could be expected to be a controlling factor.

It would be valuable too to incorporate a small

heater in the cryostat to permit the observation of domain structures at various values of temperatures so that the progressive effect of increase in K_4 could be observed.

The application of a large normal field to the basal plane, capable of being increased until saturation was approached would enable studies to be carried out to determine whether in fact the magnetization changes from Mode I to Mode IIC. This might give more detailed information about the nature of the pattern observed.

Further attention could usefully be given to the design of a low temperature Kerr effect apparatus. This would require improvements in surface preparation techniques and the possible inclusion of the objective inside a redesigned cryostat. Attention could also be given to the enhancement of the affect by applying a suitable dielectric layer to the surface of the crystal. This might also be used to protect the sample from contamination. The equipment could then be used to study the behaviour of the domain structure with both temperature and magnetic field without removing the specimen from the apparatus.

The domain structure of gadolinium might be studied by using the scanning electron microscope if the surface of the crystal was prepared carefully and not allowed to contaminate. Alternatively, the use of high voltage electrons of greater penetration might reduce the effect of surface contamination and permit the observation of domains. The technique is also capable of giving more

detailed information about magnetization directions in the domains.

REFERENCES

References for Chapter One:

1. Barkhausen, H. (1919). Physik.Z. 20, 401.

2. Becker, R. (1930). Z.Phys., 62, 253.

3. Bitter, F. (1931). Phys. Rev., 38, 1903.

4. Block, F. (1930). Z.Phys., 61, 206.

5. Elmore, W.C. (1938). Phys. Rev., 53, 757.

6. Heisenberg, W. (1928). Z.Phys., 49, 619.

7. Honda, K. and S.Kaya (1926). Sci. Rept. Tohoku. Imp. Univ., 15, 721.

8. Kaya, S. (1934). Z.Physik, 89, 706.

9. Landau, L.D and E.M.Lifshitz (1935). Phys. Z.Sowj., 8, 153.

10. Shubin, S.P. and S.V. Vonsovskii (1934). Proc.Roy. Soc. A145, 159.

11. Slater, J.C. (1936). Phys. Rev., 49, 537.

12. Stoner, E.C. (1936). Proc. Roy.Soc. A154, 656.

13. Van Vleck, J.H. (1945). Rev. Mod. Phys., 17, 27.

14. Von Hamos, L. and Thiessen, P.A., (1932), Z.Physik, 71, 442.

15. Vonsovskii, S.V. (1946). Zhurn Ekxp.Teor.Fiz., 16, 981.

16. Weiss, P. (1907). J.Phys.et Radium, 6, 661.

17. Williams, H.J., R.M.Bozorth and W.Shockley (1949). Phys.Rev., 75, 155.

References for Chapter Two.

1. Akulov, N.S. (1931). Z.Physik. 69, 78.

2. Becker, R. (1930). Z.Phys., 62, 253.

3. Becker, R. and W.Doring (1939), Ferro., J.Springer, 277, Berlin.

4. Bloch, F. (1930). Z.Phys. 61, 206.

5. Brooks, H. (1940). Phys. Rev. 58, 909.

6. Brown, W.F., (1953)., Rev. Mod. Physics. 25, 131.

7. Landau, L.D., and E.M.Lifshitz (1935). Phys.Z.Sowj., 8, 153.

8. Néel, L. (1944). Cahiers Phys., 25, 1, 221.

9. Osborn, J.A. (1945). Phys. Rev. 67, 351.

10. Rhodes, S.P. and G.Rowlands, (1954) Proc. Leeds Phil Lit. Soc., 6, 181.

11. Seavey, M.H., and P.E. Tannenwald (1959). Phys. Rev. Letters. 1, 168.

12. Sommerfeld, A., and H.A. Bethe (1933) Handbuck der physik, 24, part 2. J.Springer, Berlin, 596.

13. Stoner, E.C., (1945). Phil Mag. 36, 803.

14. Van Vleck, J.H., (1945). Rev. Mod. Phys. 17, 27.

15. Van Vleck, J.H., (1947). Annales de l'Institut Henri Poin-Caré. 10, 57.

16. Williams, H.J., R.M.Bozorth and W.Shockley (1949) Phys. Rev. 75, 155.

References for Chapter Three:

1. Andra, W. (1956). Ann. Phys. Lpz. 17, 233.

2. Banbury, J.R. and W.C.Nixon (1967). J.Sci.Instr. 44, 889.

3. Bates, L.F. and S.Spivey (1964). Brit.J.Appl.Phys., 15, 705.

4. Birss, R.R. and P.M.Wallis (1963). Phys.Letters 4, 313.

5. Bitter, F. (1931). Phys. Rev., 38, 1903.

6. Bloch. F. (1932). Phys. Z. 74, 295.

7. Corner. W.D. and T.Al-Bassam (1969) Les Elementes des Terres Rares (C.N.R.S. No. 180) P.47.

8. Craik, D.J. and P.M.Griffiths (1958). Brit.J.Appl. Phys. 9, 279.

9. Elmore, W.C. (1934). Phys.Rev. 46, 226.

10. Fowler, C.A. and E.M.Fryer. (1952). Phys. Rev. 86, 426.

11. Garood, J.R. (1962). Proc.Phys.Soc. 79, 1252.

12. Goodenough, S.B. (1956). Phys. Rev. 102, 356.

13. Hale, M.E., H.W.Fuller and H.Rubinstein (1959), J.Appl.Phys. 30, 789.

14. Hutchinson, R.H. et al (1965). J.Scient.Instr. 42, 885.

15. Joy, D.C. and J.P.Jakubovics (1968). Phil.Mag., 17, 61.

16. Kittel, C.(1949). Rev. Mod. Phys. 21, 541.

17. Landau, L. and E.Lifshitz (1935). Physik, Z.Sowjet 8, 153.

18. Lifshitz, E. (1944). J.Appl.U.S.S.R., 8, 337.

19. Polcarova, M. and A.R.Lang (1962). Appl.Phys.Letters 1, 13.

20. Schaffer; Helmut (1965) Dissertation Tech.Univ.Berlin.

21. Williams, H.J., F.C.Foster and E.A.Woods (1951) Phys. Rev. 82, 119.

References for Chapter Four:

1. Belov, K.P. and Pedko, A.V. (1962). Sov. Phys. JETP, 15, 62.

2. Bjerrum Møller H. et al (1966) Phys.Rev.Letters, 16, 737.

3. Cable, J.W. et al (1964) Phys. Rev. Letters, 12, 553.

4. Cable, J.W. and E.O.Wollan (1968). Phys. Rev., 165, 733.

5. Callen, E. and H.B.Callen (1965). Phys.Rev., 139, A455.

6. Callen, E. and H.B.Callen (1966). J.Phys.Chem.Solids, 27, 1271.

7. Clark, A.E. et al (1962). Phys. Letters, 5, 100.

8. Cohen, R.L. et al (1969). Phys. Letters, 28A, 582.

9. Corner, W.D. and F.Hutchinson (1960) Proc.Phys.Soc. 75, 781.

10. Corner, W.D. et al (1962). Proc.Phys.Soc.London, 80, 927.

11. Corner, W.D. and B.K.Tanner (1976). J.Phys.C, 9, 627.

12. Evenson, W.E. and S.H.Liu (1969). Phys.Rev., 178, 783.

13. Graham, C.D. (1962) J.Phys.Soc.Japan, 16, 1310.

14. Graham, C.D. (1963) J.Appl.Phys., 34, 1341.

15. Graham, C.D. (1967) J.Appl.Phys., 38, 1375.

16. Jordan, R.G. and E.W.Lee (1967) Proc.Phys.Soc., 92, 1074.

17. Kasuya, T. (1956) Progr.Theor.Phys. (Kyoto), 14, 45.

18. Keeton, S.C. and T.L.Loucks (1968) Phys.Rev., 168, 783.

19. Koehler, W.C. (1965) J.Appl.Phys., 36, 1078.

20. Koehler, W.C. et al (1970) Phys.Rev.Letters, 24, 16.

21. Koehler, W.C. et al (1972), in AIP Conf.Proc.Series.

22. Kuchin, V.M. et al (1969). Soc.Phys.JETP, 28, 649.

23. Lebech, B. and B.D.Rainford (1971) J.Phy. (Paris), 32, 370.

24. Lock, J.M. (1957). Proc.Phys.Soc. (London), B70, 566.

25. Moon, R.M. etal (1964) J.Appl.Phys.Suppl., 35, 1041.

26. Nicklow, R.M. et al (1971). Phys.Rev.Letters, 26, 140.

27. Nigh, H.E., S.Legvold and F.H.Spedding (1963) Phys. Rev., 132, 1092.

28. P.de.V.Du Plessis and L.Alberts (1965) Solid State Comm., 3, 251.

29. Rudermann, A. and C.Kittel (1954) Phys.Rev., 96, 99.

30. Schieber, M. et al (1968). J.Appl.Phys., 39, 885.

31. Taylor, K.N.R. and M.I.Darby (1964) Proc.Int: Conf. Magnetism Nottingham P. 742.

32. Yosida, K. (1957) Phys.Rev., 106, 893.

33. Watson, R.L., A.J.Freeman and J.P.Dimmock (1968) Phys.Rev., 167, 497.

34. Weinstein, S. et al (1963) J.Appl.Phys., 34, 1354.

35. Will, G., R.Nathans and H.A.J.Alperin (1964) J.Appl. Phys. 35, 1045.

36. Woods, A.D.B., et al (1967) Phys.Rev.Letters, 19, 908.

References for Chapter Five:

1. Bates, L.F. and S.Spivey (1964). Brit.J.Appl.Phys., 15, 705.

2. Bergman, W.H. (1956). Z.Angew.Phys., 11, 559.

3. Elmore, W.C. (1938). Phys.Rev., 54, 1092.

4. Hutchinson, R.I., P.A.Lavin and J.R.Moon (1965) J.Sci. Inst., 42, 885.

5. Jordan, R.G. et al (1974). J.Less.Common Metals, 34, 25.

6. Kittel, C. (1949). Rev.Mod.Phys., 21, 541.

7. Mackeehan, L.W. and Elmore, W.W. (1934). Phys.Rev., 46, 226.

8. Sarma, N.V. and J.R.Moon (1967). Phil.Mag., 16, 433.

9. Tasaki, A. et al (1965) Japan.J.Appl.Phys., 4, 707.

References for Chapter Six:

1. Carrey, R. and Isaac, F.D.C. (1964) Brit.J.Appl.Phys., 15, 551.

2. Corner, W.D. and B.K. Tanner (1976) J.Phys.C, 9, 627.

3. Darby, M.I. et al. (1964) Proc.Int.Conf. on Magnetism, Nottingham P. 742.

4. Goodneough, J.B. (1954) Phys.Rev., 95, 917.

5. Graham, C.D. (1967) J.Appl.Phys., 38, 1375.

6. Kaczer, J. and R.Gemperle (1959) Czech.J.Phys., 9, 605.

7. Kittel, C. (1949) Rev. Mod.Phys., 21, 541.

8. Néel, L. (1944) Cahiers de Phys., 25, 21.

References for Chapter Seven:

1. Birss, R.R. and D.J. Martin (1975) J.Phys.C., 8, 189.

2. Kandaurova, G.S. et al (1973). Sov.Phys.Solid State, 15, 38.

3. Privorotskii, I.A. (1972). Rep.Prog.Phys., 35, 115.